

Structure Elucidation and Biosynthetic Enzyme Characterization of Bacteriocins

by

Jeella Zara Acedo

A thesis submitted in partial fulfillment of the requirements for the degree of

Doctor of Philosophy

Department of Chemistry  
University of Alberta

© Jeella Zara Acedo, 2017

## Abstract

Acidocin B (AcdB), a bacteriocin from *Lactobacillus acidophilus* M46 that was initially reported to be a linear peptide, was purified and shown to be circular based on MALDI-TOF MS and MS/MS sequencing. MS analysis further revealed that AcdB is comprised of 58 amino acid residues, instead of 59 residues as initially reported. The NMR solution structure of AcdB in sodium dodecyl sulfate micelles was solved, revealing that AcdB consists of four  $\alpha$ -helices that are folded to form a globular bundle with a central pore. This is the first reported three-dimensional structure (3D) for a subgroup II circular bacteriocin. Comparison of the structure of AcdB to that of carnocyclin A, a subgroup I circular bacteriocin, highlighted the differences between the two subgroups. At least seven putative subgroup II circular bacteriocins were identified using BLAST, and sequence analysis revealed a highly conserved asparagine residue at the leader peptide cleavage sites, suggesting that an asparagine endopeptidase might be involved in their biosynthesis. Lastly, the biosynthetic gene cluster of AcdB was sequenced and characterized.

Lacticin Q (LnqQ) and aureocin A53 (AucA) are leaderless bacteriocins (class IIc) from *Lactococcus lactis* QU 5 and *Staphylococcus aureus* A53, respectively. Their 3D NMR solution structures were determined, revealing that both peptides are composed of four  $\alpha$ -helices that assume a saposin-like fold with a highly cationic surface and a hydrophobic core. The observed structural motif is remarkably similar to the overall fold of the two-component leaderless bacteriocins, enterocin 7A and 7B. Homology modeling showed that the aforementioned motif may be shared among broad-spectrum leaderless bacteriocins despite the variations in their sequence identities and lengths. The structures

of LnqQ and AucA were also demonstrated to exhibit certain similarities to those of the circular bacteriocins. Activity assays showed that the two peptides, LnqQ and AucA, combined do not act synergistically and have different antimicrobial spectra and potency, suggesting that sequence disparities play a vital role in their modes of action.

Carnobacteriocin X (CbnX) was originally reported as a single-peptide bacteriocin (class IId). However, sequence analysis and synergy assays revealed that CbnX belongs to a two-peptide bacteriocin (class I Ib), with CbnY as its partner. CbnXY is the first two-peptide bacteriocin reported in carnobacteria. CbnX and CbnY are inactive individually, but elicit synergistic activity against closely related strains when combined. The NMR solution structures of CbnX and CbnY were elucidated and shown to strongly resemble the structures of other class I Ib bacteriocins (i.e. LcnG, PlnEF, PlnJK). CbnX consists of an extended, amphipathic  $\alpha$ -helix and a flexible C-terminus. CbnY has two  $\alpha$ -helices (one hydrophobic, one amphipathic) connected by a short loop, and a cationic C-terminus. Binding studies showed that CbnX and CbnY do not interact directly, suggesting that a membrane-bound receptor may be required to mediate the formation of the CbnXY complex.

Pneumococcin is a two-component lantibiotic, comprised of PneA1 and PneA2, from *Streptococcus pneumoniae* R6. Its biosynthetic machinery encodes a putative flavin-dependent reductase, named PneJ<sub>B</sub>, which is likely involved in the formation of D-Ala and D-Abu. The activity of PneJ<sub>B</sub> was investigated through the heterologous expression of pneumococcin biosynthetic proteins in *Escherichia coli*. Coexpression of the precursor peptides (PneA1 and PneA2) and the lantibiotic synthetase (PneM) with and without PneJ<sub>B</sub> produced a mixture of partially modified substrates that could not be separated by

RP-HPLC. To potentially address this issue, truncated precursor peptides were designed and cloned. The truncated peptides, however, could not be successfully expressed in *E. coli*. Hence, chemical synthesis of substrate analogues is currently being pursued. Other approaches to obtain the precursor peptides are presented herein. The PneJ<sub>B</sub> enzyme was expressed and purified as a SUMO fusion protein, wherein the SUMO tag could be readily cleaved. The substrate analogues and the PneJ<sub>B</sub> enzyme will consequently be used for *in vitro* PneJ<sub>B</sub> activity assays and future crystallization trials.

## Preface

The content of Chapter 2 was published as Acedo et al. *Appl. Environ. Microbiol.* **2015**, *81*, 2910-2918. I performed all the experiments with assistance from the other authors, specifically in the sequencing of the AcdB biosynthetic gene cluster and acquisition of NMR spectroscopic data. I wrote the manuscript except for the section on the gene cluster.

Studies described in Chapter 3 were published as Acedo et al. *Biochemistry.* **2016**, *55*, 4798-4806. I performed all the experiments with assistance from the other authors, specifically in the cloning of the expression plasmids, acquisition of NMR spectroscopic data, and activity assays. I wrote the manuscript.

The studies in Chapter 4 were published as Acedo et al. *FEBS Lett.* **2017**, *591*, 1349-1459. I performed the circular dichroism experiments, expression and purification of [<sup>13</sup>C,<sup>15</sup>N]-CbnX and CbnY, and the elucidation of their NMR solution structures. The other authors performed the activity assays, cloning of expression plasmids, binding studies, and assisted with the acquisition of NMR spectroscopic data. I performed approximately 75% of the work and assisted in writing the manuscript.

Chapter 5 is an unpublished work. I performed all the experiments described in this chapter.

## Acknowledgements

This thesis would not have been possible without the help, guidance, and support of several individuals. First and foremost, I am beyond grateful to my supervisor, Prof. John C. Vederas, for giving me the opportunity to do research in his lab. His insights, constant support, and encouragement kept me moving forward and honed my skills as a researcher. The lab environment and resources provided in the Vederas group have been ideal for learning and professional growth. I am thankful to all the people I worked with in the various projects presented in this thesis. I am also very grateful to the exceptional support staff members in the Department of Chemistry who are among the kindest and most approachable people I have worked with. In particular, I would like to thank Mark Miskolzie and Dr. Ryan McKay of the NMR facility, Jing Zheng, Dr. Randy Whittal and Bela Reiz of the MS facility, Wayne Moffat of the Analytical Instrumentation laboratory, and Gareth Lambkin of the Biological Services laboratory. I am also grateful to Pascal Mercier of NANUC for his help in CYANA. I am thankful to Dr. Marco van Belkum, Dr. Conrad Fischer, and Sorina Chiorean for proofreading this thesis, and all their inputs in improving this manuscript. I am thankful to the Alberta Innovates Health Solutions and the University of Alberta for funding my graduate studies.

I also would like to acknowledge special people who have been instrumental not only in the completion of this thesis, but also in the success of my graduate studies as a whole. On top of my thank you list is Dr. Marco van Belkum, who has been my mentor since day one. I am extremely grateful for all the things that you taught me, and it was much pleasure working with you. I am thankful to Dr. Christopher Lohans, who also helped me start up in the lab, and has since been a constant source of advice. Thank you

Chris for unselfishly sharing your time and ideas. To Dr. Shaun McKinnie, thank you for being supportive throughout my graduate studies. I found your inputs in my seminars, scholarship applications, and random research questions very helpful. You and Chris have been inspirational and I look up to both of you for your character and brilliance. To Dr. Kaitlyn Towle, thank you for always being willing to help and for all our fruitful discussions. To Dr. Leah Martin-Visscher, thank you for always being reachable by e-mail to answer my NMR questions, and for dropping by the lab whenever we need help. You have been a very good teacher. To Albert Remus, thank you for assisting with genome work and answering all my genome-related questions. It was wonderful having to work with you. To Randy Sanichar, thank you for being my go-to person for my organic chemistry questions and for being a good friend. To everyone in the Vederas group who offered me advice and assistance at certain points during the last five years, and with whom I have shared some good times with, thank you very much!

I am also extremely grateful to my family and friends for the encouragement and support. To my parents, thank you for all your sacrifices, love, and support that paved the way to several amazing opportunities for me, and led me to where I am today. To my husband, Kristian, words are not enough to say how grateful I am to have gone through grad school with you. As a research-partner, you have been an endless source of ideas and your passion for research is inspiring. As a life-partner, your love and support are definitely unmatched.

Above all, I am grateful to God for the gift of life and for bringing good people along the way throughout this journey. To God be the glory!

## Table of Contents

<b>Chapter 1 .....</b>	<b>1</b>
<b>BACTERIOCINS – a diverse group of antimicrobial peptides .....</b>	<b>1</b>
<b>1.1. Introduction.....</b>	<b>1</b>
1.1.1. Definition and general overview .....	1
1.1.2. Applications of bacteriocins .....	3
1.1.2.1. Biopreservation .....	3
1.1.2.2. Medical and agricultural applications.....	4
1.1.3. Classification of bacteriocins.....	5
1.1.3.1. Gram-negative bacteria .....	5
1.1.3.2. Gram-positive bacteria.....	6
<b>1.2. Circular Bacteriocins.....</b>	<b>9</b>
1.2.1. Overview .....	9
1.2.2. Biosynthesis.....	11
1.2.3. Three-dimensional structures .....	12
1.2.4. Mode of action.....	13
<b>1.3. Leaderless Bacteriocins .....</b>	<b>15</b>
1.3.1. Overview .....	15
1.3.2. Biosynthesis.....	18
1.3.3. Three-dimensional structures .....	19
1.3.4. Mode of action.....	21
<b>1.4. Two-Peptide Bacteriocins.....</b>	<b>22</b>
1.4.1. Overview .....	22

1.4.2. Biosynthesis.....	24
1.4.3. Three-dimensional structures .....	25
1.4.4. Mode of action.....	30
<b>1.5. Lanthipeptides.....</b>	<b>32</b>
1.5.1. Overview .....	32
1.5.2. Classification based on biosynthetic machinery.....	37
1.5.3. Mode of action.....	43
<b>1.6. Significance and Overview of Projects.....</b>	<b>44</b>
<b>Chapter 2.....</b>	<b>47</b>
<b>Solution Structure of the Circular Bacteriocin Acidocin B.....</b>	<b>47</b>
<b>2.1. Project Background.....</b>	<b>47</b>
2.1.1. Classification of circular bacteriocins .....	47
2.1.2. Acidocin B.....	47
2.1.3. Objectives .....	48
<b>2.2. Results and Discussion.....</b>	<b>49</b>
2.2.1. Isolation of acidocin B.....	49
2.2.2. Mass spectrometry.....	49
2.2.3. Circular dichroism spectroscopy .....	51
2.2.4. NMR solution structure of acidocin B.....	52
2.2.4.1. NMR data acquisition .....	52
2.2.4.2. Structure calculations.....	53
2.2.4.3. Structural features .....	54

2.2.4.4. Comparison to subgroup I circular bacteriocins .....	57
2.2.4.5. Homology modeling of the other subgroup II circular bacteriocins....	60
2.2.5. Gene cluster sequencing .....	63
2.2.6. Bioinformatics and phylogenetic analysis.....	64
<b>2.3. Conclusions and Future Directions .....</b>	<b>67</b>
<b>Chapter 3.....</b>	<b>69</b>
<b>Structures of Leaderless Bacteriocins Lacticin Q and Aureocin A53 ...</b>	<b>69</b>
<b>3.1. Project Background.....</b>	<b>69</b>
3.1.1. Lacticin Q and aureocin A53.....	69
3.1.2. Objectives .....	70
<b>3.2. Results and Discussion.....</b>	<b>71</b>
3.2.1. Attempted expression and purification of MBP-lacticin Q.....	71
3.2.2. Expression and purification of SUMO-lacticin Q and SUMO-aureocin A53.....	71
3.2.3. Circular dichroism spectroscopy .....	73
3.2.4. NMR solution structures of lacticin Q and aureocin A53 .....	74
3.2.4.1. Structure calculations.....	74
3.2.4.2. Structural features .....	78
3.2.4.3. Comparison to enterocin 7A and 7B.....	82
3.2.4.4. Homology modeling of broad-spectrum leaderless bacteriocins.....	84
3.2.4.5. Comparison to circular bacteriocins .....	86
3.2.5. Antimicrobial activity.....	88

3.3. Conclusions and Future Directions .....	90
<b>Chapter 4 .....</b>	<b>91</b>
<b>Identification and Structure of the Two-Peptide Bacteriocin CbnXY ..</b>	<b>91</b>
4.1. Project Background .....	91
4.1.1. Carnobacteriocin X and Y .....	91
4.1.2. Objectives .....	93
4.2. Results and Discussion.....	93
4.2.1. Antimicrobial activity.....	93
4.2.2. Circular dichroism spectroscopy .....	95
4.2.3. Expression of [ <sup>13</sup> C, <sup>15</sup> N]-labelled SUMO-CbnX and SUMO-CbnY .....	96
4.2.4. NMR solution structures of CbnX and CbnY .....	97
4.2.4.1. Structure calculations.....	97
4.2.4.2. Structural features .....	99
4.2.4.3. Structural comparison to other two-peptide bacteriocins .....	102
4.2.5. Binding studies .....	104
4.2.5.1. Isothermal titration calorimetry .....	104
4.2.5.2. Permeability experiments.....	105
4.3. Conclusions and Future Directions .....	106
<b>Chapter 5 .....</b>	<b>108</b>
<b>Characterization of Lanthipeptide Dehydrogenase, PneJ<sub>B</sub> .....</b>	<b>108</b>
5.1. Project Background .....	108

5.1.1. D-Amino acids in lanthipeptides .....	108
5.1.2. LanJ dehydrogenases .....	109
5.1.2.1. LanJ <sub>A</sub> enzymes .....	109
5.1.2.2. LanJ <sub>B</sub> enzymes .....	111
5.1.3. Pneumococcin and the putative PneJ <sub>B</sub> reductase.....	114
5.1.3.1. Biosynthetic gene cluster of pneumococcin .....	114
5.1.3.2. X-ray crystal structure of PneJ <sub>B</sub> .....	118
5.1.4. Objectives .....	120
<b>5.2. Results and Discussion.....</b>	<b>120</b>
5.2.1. Expression of pneumococcin in <i>Escherichia coli</i> .....	120
5.2.1.1. Cloning and expression of <i>pneM</i> , <i>pneJ<sub>B</sub></i> , <i>pneA1</i> , and <i>pneA2</i> .....	120
5.2.1.2. Cloning and expression of truncated PneA1 and PneA2 .....	124
5.2.2. Expression and purification of SUMO-PneJ <sub>B</sub> .....	125
<b>5.3. Conclusions and Future Directions .....</b>	<b>127</b>
 <b>Chapter 6 .....</b>	 <b>129</b>
 <b>Summary and Conclusions .....</b>	 <b>129</b>
 <b>Chapter 7 .....</b>	 <b>134</b>
 <b>Experimental Procedures.....</b>	 <b>134</b>
<b>7.1. General Experimental Details.....</b>	<b>134</b>
7.1.1. Media and bacterial strains .....	134
7.1.1.1. Media preparation .....	134

7.1.1.2. Glycerol stocks.....	134
7.1.1.3. Growth conditions for indicator strains .....	135
7.1.2. Antimicrobial activity assays.....	135
7.1.2.1. Deferred inhibition assay .....	135
7.1.2.2. Spot-on-lawn assay .....	136
7.1.3. General molecular biology techniques .....	136
7.1.3.1. Plasmid isolation.....	136
7.1.3.2. Polymerase chain reaction .....	137
7.1.3.3. Restriction enzyme digestion.....	137
7.1.3.4. Agarose gel electrophoresis .....	137
7.1.3.5. DNA quantification.....	138
7.1.3.6. Ligation reactions.....	138
7.1.3.7. Transformation of chemically competent <i>Escherichia coli</i> .....	138
7.1.3.8. DNA sequencing.....	139
7.1.4. Heterologous expression of proteins .....	139
7.1.4.1. Cell lysis.....	139
7.1.4.2. Tris-Glycine SDS-PAGE .....	140
7.1.4.3. Tris-Tricine SDS-PAGE .....	140
7.1.5. Purification of peptides and proteins .....	141
7.1.5.1. Amberlite XAD-16 .....	141
7.1.5.2. C8 and C18 solid-phase extraction .....	141
7.1.5.3. RP-HPLC .....	141
7.1.5.4. Ni-NTA affinity chromatography .....	142

7.1.6. SUMO protease digestion.....	142
7.1.7. Protein quantification .....	142
7.1.7.1. Spectrophotometric quantification.....	142
7.1.7.2. BCA colorimetric analysis.....	143
7.1.8. Circular dichroism spectroscopy .....	143
7.1.9. Mass spectrometry.....	144
7.1.9.1. MALDI-TOF MS.....	144
7.1.9.2. LC-MS/MS .....	144
7.1.10. NMR spectroscopy .....	145
7.1.11. Bioinformatics and structural programs .....	145
<b>7.2. Experimental Procedures for the Structural Studies of Acidocin B.....</b>	<b>146</b>
7.2.1. Bacterial strains and culture conditions.....	146
7.2.2. Plasmid isolation and sequencing.....	146
7.2.3. Isolation of acidocin B.....	146
7.2.4. LC-MS/MS .....	147
7.2.5. Circular dichroism spectroscopy .....	148
7.2.6. NMR spectroscopy .....	148
7.2.7. Structure calculations .....	149
7.2.8. Topology prediction, homology modeling, and phylogenetic tree construction.....	150
<b>7.3. Experimental Procedures for the Structural Studies of Lacticin Q &amp; .....</b>	<b>152</b>
<b>Aureocin A53 .....</b>	<b>152</b>
7.3.1. Construction of pET SUMO-lacticin Q and pET SUMO-aureocin A53.....	152

7.3.2. Expression of SUMO-lactacin Q and SUMO-aureocin A53 .....	152
7.3.3. Purification of SUMO-lactacin Q and SUMO-aureocin A53 .....	153
7.3.4. SUMO protease digestion.....	153
7.3.5. Purification of lactacin Q by RP-HPLC.....	154
7.3.6. Purification of aureocin A53 by RP-HPLC.....	154
7.3.7. Circular dichroism spectroscopy .....	155
7.3.8. NMR spectroscopy .....	155
7.3.9. Structure calculations .....	156
7.3.10. Homology modeling and secondary structure predictions .....	157
7.3.11. MIC testing.....	160
7.3.12. Synergy assay .....	160
<b>7.4. Experimental Procedures for the Structural Studies of CbnXY.....</b>	<b>161</b>
7.4.1. Unlabelled CbnX and CbnY.....	161
7.4.2. Antimicrobial activity assay .....	161
7.4.3. Circular dichroism spectroscopy .....	161
7.4.4. Construction of pET SUMO-CbnX and pET SUMO-CbnY.....	162
7.4.5. Expression of [ <sup>13</sup> C, <sup>15</sup> N]-labelled SUMO-CbnX and SUMO-CbnY.....	162
7.4.6. Purification of [ <sup>13</sup> C, <sup>15</sup> N]-labelled SUMO-CbnX and SUMO-CbnY.....	163
7.4.7. SUMO protease digestion.....	163
7.4.8. Purification of [ <sup>13</sup> C, <sup>15</sup> N]-labelled CbnX and CbnY.....	164
7.4.9. NMR spectroscopy .....	164
7.4.10. Structure calculations .....	170
7.4.11. Isothermal titration calorimetry .....	170

7.4.12. Permeability experiments .....	171
7.4.12.1. Vesicle preparation .....	171
7.4.12.2. Fluorescence spectroscopy.....	172
<b>7.5. Experimental Procedures for the Biosynthetic Studies of PneJ<sub>B</sub> .....</b>	<b>173</b>
7.5.1. Construction of pRSFDuet-PneM-PneA1 and pRSFDuet-PneM-PneA2 ...	173
7.5.2. Construction of pETDuet-PneJ <sub>B</sub> .....	174
7.5.3. Expression of PneMA1 and PneMA2 with and without PneJ <sub>B</sub> .....	175
7.5.4. Purification of expressed PneMA1 and PneMA2.....	175
7.5.5. Construction of truncated pRSFDuet-PneM-PneA1 and pRSFDuet-PneM- PneA2.....	176
7.5.6. Expression and purification of truncated PneMA1 and PneMA2 .....	177
7.5.7. Construction of pET SUMO-PneJ <sub>B</sub> .....	177
7.5.8. Expression of SUMO-PneJ <sub>B</sub> .....	178
7.5.9. Purification of SUMO-PneJ <sub>B</sub> .....	179
7.5.10. SUMO protease digestion.....	179
<b>References.....</b>	<b>180</b>

## List of Tables

Table 1.1. Classification of bacteriocins from Gram-positive bacteria .....	7
Table 1.2. List of circular bacteriocins .....	10
Table 1.3. Gene clusters of known circular bacteriocins .....	12
Table 1.4. List of unmodified leaderless bacteriocins .....	17
Table 1.5. List of unmodified two-peptide bacteriocins .....	23
Table 2.1. MS/MS sequencing result after trypsin-chymotrypsin digestion of AcdB.....	51
Table 2.2. Structure calculation statistics for AcdB.....	54
Table 2.3. Characteristics of predicted proteins encoded by the AcdB gene cluster.....	64
Table 3.1. Percentage $\alpha$ -helicity of LnqQ and AucA in various solvent systems .....	74
Table 3.2. Structure calculation statistics for LnqQ and AucA .....	75
Table 3.3. Antimicrobial activity of LnqQ and AucA against various strains.....	89
Table 4.1. Structure calculation statistics for CbnX and CbnY .....	99
Table 7.1. Indicator strains and corresponding growth conditions .....	135
Table 7.2. $^1\text{H}$ Chemical shift assignments for AcdB in 80 mM SDS .....	151
Table 7.3. NMR data acquisition parameters for LnqQ and AucA .....	156
Table 7.4. $^1\text{H}$ Chemical shift assignments for LnqQ in 25% trifluoroethanol.....	158
Table 7.5. $^1\text{H}$ Chemical shift assignments for AucA in water .....	159
Table 7.6. NMR data acquisition parameters for CbnX and CbnY .....	165
Table 7.7. $^1\text{H}$ Chemical shift assignments for CbnX in 50% trifluoroethanol.....	166
Table 7.8. Nitrogen and carbon chemical shift assignments for CbnX .....	167
Table 7.9. $^1\text{H}$ Chemical shift assignments for CbnY in 50% trifluoroethanol.....	168
Table 7.10. Nitrogen and carbon chemical shift assignments for CbnY .....	169

## List of Figures

Figure 1.1. Biosynthetic gene cluster of enterocin AS-48. ....	11
Figure 1.2. NMR solution structures of circular bacteriocins.....	13
Figure 1.3. Biosynthetic gene cluster of lacticin Q.....	18
Figure 1.4. Biosynthetic gene cluster of aureocin A53.....	19
Figure 1.5. NMR solution structures of leaderless bacteriocins enterocin 7A, enterocin 7B, LsbB, and enterocin K1; and X-ray crystal structure of laterosporulin. ....	20
Figure 1.6. Biosynthetic gene cluster of lactococcin G. ....	24
Figure 1.7. NMR solution structures of two-peptide bacteriocins lactococcin G (LcnG $\alpha$ and LcnG $\beta$ ), plantaricin EF (PlnE and PlnF), and plantaricin JK (PlnJ and PlnK). ....	26
Figure 1.8. Proposed structural model of lactococcin G (LcnG $\alpha$ -LcnG $\beta$ ) dimer. ....	28
Figure 1.9. Proposed structural model of plantaricin EF (PlnEF) dimer. ....	29
Figure 1.10. Formation of DL-lanthionine and DL-methylanthionine residues.....	33
Figure 1.11. Formation of LDL-labionin and methylabionin residues.....	34
Figure 1.12. LanJ-catalyzed reduction of D-Ala to Dha and D-Abu to Dhb.....	35
Figure 1.13. LanD-catalyzed formation of aminovinylcysteine. ....	36
Figure 1.14. Classification of lanthipeptides based on their biosynthetic machinery.....	37
Figure 1.15. Biosynthetic gene cluster of nisin.....	39
Figure 1.16. Biosynthetic scheme for nisin A maturation. ....	42
Figure 2.1. MALDI-TOF mass spectrum of AcdB.....	50
Figure 2.2. Bead structure of AcdB precursor peptide. ....	50
Figure 2.3. CD profile of AcdB in SDS (red) and DPC (green). ....	52
Figure 2.4. Superimposition of the 20 lowest energy conformers of AcdB. ....	53
Figure 2.5. NMR solution structure of AcdB (PDB: 2MWR). ....	55
Figure 2.6. Surface analysis of AcdB. ....	56
Figure 2.7. Amino acid sequence alignment of AcdB and carnocyclin A.....	59

Figure 2.8. Comparison of electrostatic potential maps of AcdB and carnocyclin A.....	60
Figure 2.9. Amino acid sequence alignment of known subgroup II circular bacteriocins. ....	61
Figure 2.10. Homology models of gassericin A and butyrvibriocin AR10.....	62
Figure 2.11. Biosynthetic gene cluster of AcdB. ....	63
Figure 2.12. Amino acid sequence alignment of known and putative subgroup II circular bacteriocins. ....	65
Figure 2.13. Phylogenetic tree of subgroup II circular bacteriocins.....	66
Figure 3.1. Amino acid sequence alignment of LnqQ and AucA.....	69
Figure 3.2. Tricine SDS-PAGE gels of the pilot cleavage trials for (A) SUMO-LnqQ and (B) SUMO-AucA fusion proteins. ....	72
Figure 3.3. MALDI-TOF MS spectra of (A) LnqQ and (B) AucA. ....	73
Figure 3.4. CD spectra of (A) LnqQ and (B) AucA in various solvent systems. ....	74
Figure 3.5. NMR solution structures of LnqQ (PDB: 2N8P) and AucA (PDB:2N8O).....	76
Figure 3.6. Structures of (A) AucA highlighting the interactions of Lys44 to Trp40 and Trp31, and (B) LnqQ highlighting the interactions of Lys44 to Trp41 and Trp32.....	77
Figure 3.7. Surface analysis of LnqQ and AucA. ....	79
Figure 3.8. 3D structures highlighting the tryptophan residues of (A) LnqQ and (B) AucA. ....	81
Figure 3.9. Alignment of the (A) 3D structures and (B) amino acid sequences of LnqQ, AucA, Ent7A (PDB: 2M5Z), and Ent7B (PDB: 2M60). ....	82
Figure 3.10. Synergy assay for LnqQ and AucA.....	83
Figure 3.11. Homology modeling of broad-spectrum leaderless bacteriocins. ....	85
Figure 3.12. Overlay of the structures of LnqQ and AucA with circular bacteriocins (A) carnocyclin A (PDB: 2KJF), (B) enterocin AS-48 (PDB: 1E68), and (C) acidocin B (PDB: 2MWR). ....	87
Figure 4.1. Biosynthetic gene cluster of CbnXY.....	91
Figure 4.2. Amino acid sequences of the precursor peptides of CbnX and CbnY. ....	92

Figure 4.3. Spot-on-lawn assay showing the synergistic activity of CbnX and CbnY at different concentrations against <i>C. maltaromaticum</i> A9b–.	94
Figure 4.4. CD profile of (A) CbnX and (B) CbnY	95
Figure 4.5. MALDI-TOF mass spectra of (A) [ <sup>13</sup> C, <sup>15</sup> N]-CbnX and (B) [ <sup>13</sup> C, <sup>15</sup> N]-CbnY.	96
Figure 4.6. <sup>1</sup> H, <sup>15</sup> N-HSQC spectra of (A) CbnX and (B) CbnY.	98
Figure 4.7. NMR solution structure and surface maps of CbnX (PDB: 5UJR).	100
Figure 4.8. NMR solution structure and surface maps of CbnY (PDB: 5UJQ).	101
Figure 4.9. Comparison of the 3D structures of CbnXY to PlnEF, PlnJK, and LcnG.	103
Figure 4.10. ITC data for the titration of 0.1 mM CbnY into 1 mM CbnX at 25 °C.	104
Figure 5.1. Peptides processed by LanJ <sub>A</sub> enzymes.	110
Figure 5.2. Two-component lantibiotics processed by LanJ <sub>B</sub> enzymes.	113
Figure 5.3. Biosynthetic gene cluster of pneumococcin.	114
Figure 5.4. Amino acid sequence alignment of PneJ <sub>B</sub> with LanD enzymes.	116
Figure 5.5. Amino acid sequence alignment of PneJ <sub>B</sub> and the LanJ <sub>B</sub> enzymes, CrnJ and BsjJ.	117
Figure 5.6. Amino acid sequence alignment of pneumococcin and carnolysin.	117
Figure 5.7. Crystal structure of SP_1951 dimer (PneJ <sub>B</sub> enzyme).	119
Figure 5.8. pRSFDuet-1 and pETDuet-1 vector maps.	122
Figure 5.9. SDS-PAGE gel of Ni-NTA affinity chromatography fractions from the purification of proteins from pRSFDuet-PneM-PneA1 expression.	123
Figure 5.10. MALDI-TOF mass spectra of PneA1.	124
Figure 5.11. PneA1 and PneA2 precursor peptides and their truncated versions.	125
Figure 5.12. SDS-PAGE gel of SUMO-PneJ <sub>B</sub> Ni-NTA affinity chromatography fractions.	126
Figure 5.13. SDS-PAGE gel of SUMO-PneJ <sub>B</sub> pilot cleavage trials.	127

## List of Abbreviations

<b>2D</b>	two-dimensional
<b>3D</b>	three-dimensional
<b>a.a.</b>	amino acid
<b>ABC</b>	ATP-binding cassette
<b>AcdB</b>	acidocin B
<b>Abu</b>	aminobutyrate
<b>APBS</b>	adaptive Poisson-Boltzmann solver
<b>APT</b>	all-purpose Tween
<b>ATCC</b>	American type culture collection
<b>ATP</b>	adenosine triphosphate
<b>AucA</b>	aureocin A53
<b>AviCys</b>	aminovinylcysteine
<b>BCA</b>	bicinchoninic acid
<b>BCECF</b>	2',7'-bis-(2-carboxyethyl)-5-(and-6)-carboxyfluorescein
<b>BHI</b>	brain heart infusion
<b>BLAST</b>	basic local alignment search tool
<b>bp</b>	base pairs
<b><sup>13</sup>C-HSQC</b>	<sup>13</sup> carbon-heteronuclear single quantum coherence
<b>CbnX</b>	carnobacteriocin X
<b>CbnY</b>	carnobacteriocin Y
<b>CD</b>	circular dichroism

<b>CrnA1</b>	carnolysin A1
<b>CrnA2</b>	carnolysin A2
<b>CTP</b>	cytidine triphosphate
<b>CYANA</b>	combined assignment and dynamics algorithm for NMR applications
<b>Dha</b>	2,3-dehydroalanine
<b>Dhb</b>	2,3-dehydrobutyryne
<b>DNA</b>	deoxyribonucleic acid
<b>dNTP</b>	deoxynucleotide triphosphate
<b>DOPE</b>	1,2-dioleoyl-sn-glycero-3-phosphoethanolamine
<b>DOPG</b>	1,2-dioleoyl-sn-glycero-3-phospho-(1'-rac-glycerol)
<b>DPC</b>	dodecylphosphocholine
<b>DSS</b>	2,2-dimethyl-2-silapentane-5-sulfonic acid
<b>EdcA</b>	epidermicin NI01
<b>EDTA</b>	ethylenediaminetetraacetic acid
<b>Ent7A</b>	enterocin 7A
<b>Ent7B</b>	enterocin 7B
<b>EntK1</b>	enterocin K1
<b>EntL50A</b>	enterocin L50A
<b>EntL50B</b>	enterocin L50B
<b>ETEC</b>	enterotoxigenic <i>Escherichia coli</i>
<b>FMN</b>	flavin mononucleotide
<b>gDQF-COSY</b>	gradient double-quantum-filter correlation spectroscopy

<b>GG-motif</b>	double glycine-motif
<b>GRAS</b>	generally regarded as safe
<b>GTP</b>	guanosine triphosphate
<b>IPA</b>	isopropanol
<b>IPTG</b>	isopropyl $\beta$ -D-1-thiogalactopyranoside
<b>ITC</b>	isothermal titration calorimetry
<b>LAB</b>	lactic acid bacteria
<b>Lab</b>	labionin
<b>Lan</b>	lanthionine
<b>LB</b>	Luria-Bertani broth
<b>LC</b>	liquid chromatography
<b>LC-MS/MS</b>	liquid chromatography-tandem mass spectrometry
<b>LcnG</b>	lactococcin G
<b>LnqQ</b>	lacticin Q
<b>LnqZ</b>	lacticin Z
<b>LsbB</b>	lactococcal small bacteriocin B
<b>MALDI-TOF MS</b>	matrix-assisted laser desorption ionization-time of flight mass spectrometry
<b>MBP</b>	maltose-binding protein
<b>MeLab</b>	methyllabionin
<b>MeLan</b>	methyllanthionine
<b>MIC</b>	minimum inhibitory concentration
<b>MRS</b>	de Man, Rogosa and Sharpe

<b>MRSA</b>	methicillin-resistant <i>Staphylococcus aureus</i>
<b>MS</b>	mass spectrometry
<b>MS/MS</b>	tandem mass spectrometry
<b>MW</b>	molecular weight
<b><sup>15</sup>N-HSQC</b>	<sup>15</sup> nitrogen-heteronuclear single quantum coherence
<b>NADH</b>	nicotinamide adenine dinucleotide
<b>NADPH</b>	nicotinamide adenine dinucleotide phosphate
<b>NESG</b>	Northeast Structural Genomics Consortium
<b>NIH</b>	National Institutes of Health
<b>Ni-NTA</b>	nickel-nitrilotriacetic acid
<b>NMR</b>	nuclear magnetic resonance
<b>NOE</b>	nuclear Overhauser effect
<b>NOESY</b>	nuclear Overhauser effect spectroscopy
<b>NTP</b>	nucleotide triphosphate
<b>OD<sub>600</sub></b>	optical density at 600 nm
<b>ORF</b>	open reading frame
<b>PCR</b>	polymerase chain reaction
<b>PDB</b>	Protein Data Bank
<b>pI</b>	isoelectric point
<b>PlnEF</b>	plantaricin EF
<b>PlnKJ</b>	plantaricin JK
<b>PSI</b>	Protein Structure Initiative
<b>PSM</b>	phenol-soluble modulin

<b>PTM</b>	post-translational modification
<b>RMSD</b>	root-mean-square deviation
<b>RP-HPLC</b>	reverse-phase high-performance liquid chromatography
<b>QPS</b>	qualified presumption of safety
<b>SDS</b>	sodium dodecyl sulfate
<b>SDS-PAGE</b>	sodium dodecyl sulfate-polyacrylamide gel electrophoresis
<b>STEC</b>	Shiga toxin-producing <i>Escherichia coli</i>
<b>SUMO</b>	small ubiquitin-like modifier
<b>TAE</b>	Tris-acetate-EDTA
<b>TALOS</b>	torsion angle likelihood obtained from shift and sequence similarity
<b>TBE</b>	Tris-borate-EDTA
<b>TFA</b>	trifluoroacetic acid
<b>TFE</b>	trifluoroethanol
<b>TM</b>	transmembrane
<b>TOCSY</b>	total correlation spectroscopy
<b>TSB</b>	tryptic soy broth
<b>TTP</b>	thymidine triphosphate
<b>UppP</b>	undecaprenyl pyrophosphate phosphatase
<b>VRE</b>	vancomycin-resistant enterococci
<b>WeIM</b>	weissellicin M
<b>WeIY</b>	weissellicin Y

# Chapter 1

## BACTERIOCINS – a diverse group of antimicrobial peptides

### 1.1. Introduction

#### 1.1.1. Definition and general overview

Bacteriocins are ribosomally synthesized antimicrobial peptides produced by bacteria that serve as an integral part of the producer strain's defense mechanism against competing bacteria.<sup>1</sup> It was suggested that nearly all bacteria are capable of producing at least one bacteriocin.<sup>2-4</sup> Moreover, strains that produce several types of bacteriocins are not uncommon. The bacteriocin biosynthetic machineries normally consist of a common set of genes, which are present in clusters either in the bacteria's chromosomal DNA or plasmid DNA. These gene clusters include the genetic determinants for the bacteriocin structural and immunity genes, and often also include genes for maturation, transport, and regulation.

The first bacteriocin, named colicin V, was reported in 1925. It was isolated from *Escherichia coli* V and was demonstrated to be antagonistic against other *E. coli* strains.<sup>5</sup> Similar to colicin V, bacteriocins were initially described to be active only against closely related organisms, but as more broad-spectrum bacteriocins were discovered, it became apparent that this description is no longer valid. While the first bacteriocin was isolated from a Gram-negative species, the majority of the reported bacteriocins to date are produced by Gram-positive bacteria. The open-access bacteriocin database,

BACTIBASE<sup>6</sup>, includes 230 bacteriocins as of this writing; 90% of which originate from Gram-positive bacteria. Among the different genera of Gram-positive bacteria, most of the discovered bacteriocins are derived from lactic acid bacteria (LAB). As can be inferred from their name, LAB are strains that produce lactic acid during carbohydrate fermentation. They are found in a variety of processed food such as meat and dairy products, in spoiled beer, fermented wine, decomposing plants, and different biological organs such as the mouth, gastrointestinal tract, and urogenital tract of humans and animals.<sup>7</sup> LAB consist of the species under the genera *Aerococcus*, *Bifidobacterium*, *Carnobacterium*, *Enterococcus*, *Lactobacillus*, *Lactococcus*, *Leuconostoc*, *Oenococcus*, *Pediococcus*, *Sporolactobacillus*, *Streptococcus*, *Tetragenococcus*, *Vagococcus*, and *Weissella*.<sup>8,9</sup> Next to LAB, the *Bacillus* genus is regarded as the second most important source of bacteriocins.<sup>10</sup> *Bacillus* strains are receiving additional attention because they are also rich sources of other bioactive compounds such as lipopeptides and polyketides.<sup>11-13</sup> The *Staphylococcus* genus is another non-LAB genus that offers much potential in bacteriocin production. In particular, bacteriocins from *S. aureus* and *S. epidermidis* were reported to be effective agents against methicillin-resistant *S. aureus* (MRSA) and human infection-associated coagulase-negative staphylococci.<sup>14</sup>

## 1.1.2. Applications of bacteriocins

### 1.1.2.1. Biopreservation

Several bacteriocin-producing LAB are used as probiotics and as starter cultures in cheese and other dairy products.<sup>1,4,15,16</sup> The use of LAB bacteriocins in food preservation is particularly appealing due to the Generally Regarded As Safe (GRAS) and Qualified Presumption of Safety (QPS) status of most LAB.<sup>9</sup> In addition to their potency against several foodborne pathogens, many bacteriocins are pH- and heat-stable, rendering them compatible to various food processing treatments.

The most widely used bacteriocin commercially is nisin from *Lactococcus lactis*. Nisin was approved for food applications by the World Health Organization in 1969, and by the US Food and Drug Agency in 1988.<sup>1,16,17</sup> It is currently being used in food and livestock industries in over 80 countries worldwide.<sup>18-20</sup> Nisin is marketed by various companies as a natural preservative against Gram-positive bacteria, and is recommended for all types of food applications and meat products. It is commercialized under a number of brand names such as Nisaplin<sup>®</sup> (Danisco, DuPont Nutrition & Health, Copenhagen, Denmark; Gillco Products Inc., San Marcos, CA, USA), Novasin<sup>™</sup> (Gillco Products Inc.), Chrisin<sup>®</sup> (Chr. Hansen, Hørsholm, Denmark), NisinA<sup>®</sup> and NisinZ<sup>®</sup> (Handary, Brussels, Belgium). Another bacteriocin that is commercially used for biopreservation is pediocin PA-1 from *Pediococcus acidilactici*. It was previously marketed by Quest International (Naarden, Netherlands) and Kerry BioScience (Carrigaline, County Cork, Ireland) under the brand name ALTA<sup>™</sup> 2431.<sup>21,22</sup> Currently, Chr. Hansen supplies it under the brand name Bactoform<sup>™</sup> F-LC as a starter culture for pediocin and bavaricin production. It is

intended to inhibit the growth of *Listeria monocytogenes*.<sup>23</sup> Several studies have shown the potential of many other bacteriocins in food protection applications. A few examples include the effective use of enterocin AS-48 in preventing the growth of unwanted bacteria in cider, fruit juices, and vegetable juices; and the use of enterocin CCM4231 and enterocin EJ97 in the preservation of soy milk and zucchini purée, respectively.<sup>24–26</sup> However, thus far, only nisin and pediocin PA-1 have reached the commercial market as purified bacteriocins.

#### **1.1.2.2. Medical and agricultural applications**

Although bacteriocins are primarily used for preservation of food products, there is also great interest in their applications in the agricultural sector, both in livestock and plant industries, as well as in human therapeutics. Bacteriocins have not only been shown to inhibit animal pathogens such as the Shiga toxin-producing *E. coli* (STEC), enterotoxigenic *E. coli* (ETEC), MRSA, and vancomycin-resistant enterococci (VRE), but also plant pathogens such as agrobacteria and brenneria.<sup>27,28</sup> In human health therapeutics, several reports have highlighted the use of bacteriocins in addressing hospital-acquired infections, respiratory tract infections, tuberculosis, skin diseases, skin infections, and vaginosis.<sup>15,23</sup> With the increasing global threat posed by the development of antimicrobial resistance, bacteriocins are being considered as one of the promising alternatives to conventional antibiotics. Apart from the abovementioned antimicrobial applications, the potential of bacteriocins as intestinal protectors, antiviral agents, contraceptives, and in cancer therapy has also been explored.<sup>15,23</sup>

Several bacteriocins, mostly belonging to a class of bacteriocins called lantibiotics, are considered for therapeutic applications. However, only nisin is currently used commercially. One of its commercial therapeutic applications is as the active ingredient in the Wipe Out<sup>®</sup> dairy wipes (Immucell, Portland, ME, USA), an FDA-approved udder disinfectant for the treatment of bovine mastitis, which is an intramammary infection caused by *S. aureus*, *Streptococcus uberis*, and *Streptococcus dysgalactiae*.<sup>29</sup> In the clinical setting, a number of lantibiotics are currently undergoing clinical trials including the semi-synthetic derivatives of actagardine (NVB302 and NVB333), mutacin 1140, bioengineered microbisporicin (NAI-107), and duramycin (Moli1901).<sup>30</sup> NVB302 has completed phase I clinical trials as a control agent for *Clostridium difficile*, while NVB333 is at the preclinical phase. Mutacin 1140 and NAI-107 are both at the late preclinical stages as anti-infective agents against multi-drug resistant Gram-positive bacteria. Moli1901 has completed phase II clinical trials against cystic fibrosis.<sup>31</sup>

### **1.1.3. Classification of bacteriocins**

#### **1.1.3.1. Gram-negative bacteria**

Bacteriocins from Gram-negative bacteria can be classified based on molecular size into three groups namely microcins, colicins, and tailocins. Microcins are small peptides of ~10 kDa molecular weight (MW); colicins range from 20 to 80 kDa; while the tailocins are multi-subunit, bacteriophage tail-like, large bacteriocins.<sup>32,33</sup> Microcins and colicins are mainly obtained from *E. coli*, with a few examples from other Gram-negative species.<sup>34</sup> On the other hand, the first tailocin was isolated in 2002 from *Pseudomonas* sp.,

and several other tailocins have been consequently discovered from the  $\gamma$ -proteobacteria genera.<sup>33,35-39</sup> It is to be noted that the Gram-positive *C. difficile* was also reported to produce a tailocin.<sup>40</sup>

### **1.1.3.2. Gram-positive bacteria**

The classification scheme for bacteriocins from Gram-positive bacteria is more complex, and has been a subject of debate and revisions. Bacteriocins, in general, exhibit extensive diversity in size, structure, biochemical properties, inhibition spectrum, and mode of action. Bacteriocin classification schemes continuously evolve especially with the advent of genome mining and refinement of research tools that drive the discovery of new bacteriocin classes. For Gram-positive bacteria, several classification schemes have been proposed since the release of the first recommended grouping in 1993.<sup>41</sup> Table 1.1 presents the most recent classification of bacteriocins derived from Gram-positive bacteria. It is an updated version of the scheme proposed in 2016 by Alvarez-Sieiro *et al.*<sup>9</sup>, wherein bacteriocins are categorized based on biosynthetic mechanism and biological activity.

Class I covers peptides that undergo various post-translational modifications (PTMs) yielding non-canonical amino acids and other unique structural features. The bacteriocin structural gene in most cases encodes an inactive precursor peptide that is comprised of an N-terminal leader peptide and a C-terminal core peptide. In order to transform the precursor peptide into the mature, active form, it undergoes PTMs (including leader peptide removal) that are catalyzed by various tailoring enzymes. The leader peptide assumes various roles among the different bacteriocin classes. The functions of the leader

peptide may include (a) serving as the recognition binding segment for PTM enzymes, (b) stabilizing and promoting proper folding of the precursor peptide, (c) securing that the precursor peptide is inactive inside the host cell, and (d) acting as a secretion signal.<sup>42</sup> Class II consists of bacteriocins that do not undergo any PTM other than the removal of the leader peptide. Class III encompasses large (>10 kDa) unmodified bacteriocins that can either be bacteriolytic or non-lytic.

**Table 1.1. Classification of bacteriocins from Gram-positive bacteria**

Group		Distinguishing feature	Example
<b>Class I</b> (Modified)  heat stable (<10 kDa)	Lantibiotics	Contain (methyl)lanthionine residues	Nisin
	Circular bacteriocins	Head-to-tail cyclization	Enterocin AS-48
	Linear azol(in)e-containing peptides (LAPS)	Contain heterocyclic rings of thiazole and methyl(oxazole)	Streptolysin S
	Sactibiotics	Contain sulfur-to- $\alpha$ -carbon linkages	Subtilisin A
	Glycocins	Contain S-linked glycopeptides	Sublancin 168
	Lasso peptides	Assume a lasso structure	Lariatins
	Thiopeptides	Contain heterocycles and a central pyridine, dihydropyridine, or piperidine ring	Thiostrepton
	Botromycins	Contain macrocyclic amidine, a decarboxylated carboxy-terminal thiazole, and carbon-methylated amino acids	Botromycin A2
	Linaridins	Linear peptides with dehydro residues	Cypemycin
	<b>Class II</b> (Unmodified)  heat stable (<10 kDa)	Ia: Pediocin-like bacteriocins	Posses a conserved YGNGV motif (where N = any amino acid)
Ib: Two-peptides		Two unmodified peptides required for optimal activity	Lactococcin G
Ic: Leaderless bacteriocins		Synthesized without a leader peptide	Enterocin L50
IId: Non-pediocin-like, single peptides		Unmodified, linear, non-pediocin-like, single peptide bacteriocins	Lactococcin A
<b>Class III</b>  thermo-labile (>10kDa)	Bacteriolysins	Degrade bacterial cell wall causing cell lysis	Lysostaphin
	Non-lytic proteins	Do not cause cell lysis, but instead, disrupt cell membrane potential leading to ATP efflux	Helveticin J

In this thesis, projects on four different classes of Gram-positive bacteriocins are presented. Chapter 2 is a structural work on a putative circular bacteriocin. Chapter 3 is a project on leaderless bacteriocins. Chapter 4 describes the identification and structure of a two-peptide bacteriocin. And lastly, Chapter 5 presents the characterization of a biosynthetic enzyme involved in a lantibiotic system. Hence, the succeeding sections of this chapter will provide a background on the above-mentioned bacteriocin classes in the same order as the projects are presented in this thesis.

## 1.2. Circular Bacteriocins

### 1.2.1. Overview

Circular bacteriocins are characterized by a PTM that releases the leader peptide and subsequently links the N- and C-termini of the core peptide through a peptide bond. The sequences and lengths of the leader peptides vary substantially, ranging from 2 to 35 amino acid residues, whereas the core peptides are comprised of 58 to 70 residues.<sup>43</sup> Circular bacteriocins are considered as promising alternatives to antimicrobial agents that are currently used in food and medical industries due to their broad inhibition spectra and increased stability against proteolysis and temperature/pH induced-denaturation.<sup>43-45</sup> They have been shown to be active against a wide range of organisms that include the foodborne pathogens *Listeria* spp. and *Clostridium* spp.<sup>44</sup> Circular bacteriocins are mostly active against Gram-positive organisms, although enterocin AS-48, lactocyclin Q, and leucocyclin Q were also shown to be active against Gram-negative strains, albeit at higher concentrations.<sup>46-48</sup> Carnocyclin A, on the other hand, was able to inhibit the growth of Gram-negative strains that were pre-treated with the metal-chelating ethylenediaminetetraacetic acid (EDTA), which compromised the cell wall integrity.<sup>49</sup>

The first member of the circular bacteriocins is enterocin AS-48, identified in 1994.<sup>50</sup> Currently, there are 14 known circular bacteriocins that are produced by a variety of species, and are presented in Table 1.2. The list excludes acidocin B<sup>51</sup>, which is described in Chapter 2 of this thesis.

The bacteriocin subtilisin A was initially classified under this class because it also exhibits N- to C- termini cyclization.<sup>52</sup> However, it was later recategorized to a new class referred to as sactipeptides, which are characterized by the presence of Cys sulfur to  $\alpha$ -carbon linkages.<sup>53,54</sup>

**Table 1.2. List of circular bacteriocins**

Bacteriocin name	Size (a.a) <sup>a</sup>		MW (Da)	Producer strain	Year discovered <sup>b</sup> [Reference]
	Leader	Bacteriocin			
Enterocin AS-48	35	70	7,150	<i>Enterococcus faecalis</i> S-48	1994 [50]
Gassericin A	33	58	5,654	<i>Lactobacillus gasseri</i> LA39	1998 [55]
Butyrivibriocin AR10	22	58	5,982	<i>Butyrivibrio fibrisolvens</i> AR10	2003 [56]
Circularin A	3	69	6,771	<i>Clostridium beijerinckii</i> ATCC 25752	2003 [57]
Uberolysin	6	70	7,048	<i>Streptococcus uberis</i> 42	2007 [58]
Carnocyclin A	4	60	5,862	<i>Carnobacterium maltaromaticum</i> UAL307	2008 [59]
Lactocyclin Q	2	61	6,060	<i>Lactococcus sp.</i> QU 12	2009 [46]
Garvicin ML	3	69	6,007	<i>Lactococcus garvieae</i> DCC43	2011 [60]
Leucocyclin Q	2	61	6,115	<i>Leuconostoc mesenteroides</i> TK41401	2011 [47]
Amylocyclin	48	64	6,382	<i>Bacillus amyloliquefaciens</i> FZB42	2014 [61]
Aureocyclin 4185 <sup>c</sup>	4	60	5,607 <sup>d</sup>	<i>Staphylococcus aureus</i> 4185	2014 [62]
Enterocin NKR-5-3B	23	64	6,317	<i>Enterococcus faecium</i> NKR-5-3	2015 [63]
Pneumocyclin <sup>c</sup>	34	64	6,156 <sup>d</sup>	<i>Streptococcus pneumoniae</i>	2015 [64]
Pumilarin	38	70	7,083	<i>Bacillus pumilus</i>	2017 [65]

<sup>a</sup> a.a., number of amino acid residues

<sup>b</sup> Year during which the peptide was confirmed to be a circular bacteriocin.

<sup>c</sup> Genetic and *in silico* analysis were done. The mature peptide has not yet been isolated.

<sup>d</sup> Calculated based on amino acid sequence minus 18 Da due to loss of water during N- to termini C-cyclization.

### 1.2.2. Biosynthesis

The biosynthetic gene clusters of circular bacteriocins consist of a minimum of 5 to 7 genes that are required for production and immunity. These include genes that encode the bacteriocin precursor peptide (e.g. AS-48A for enterocin AS-48), an immunity protein (e.g. AS-48D<sub>1</sub>), an ATPase (e.g. AS-48D), a DUF95 membrane protein (e.g. AS-48C), and one or more unknown hydrophobic proteins (e.g. AS-48B, AS-48C<sub>1</sub>).<sup>44</sup> The gene cluster for enterocin AS-48, the most studied among the circular bacteriocins, is shown in Figure 1.1. The cluster also contains an accessory operon (*as-48EFGH*) that forms a dedicated ATP-binding cassette (ABC) transporter complex that is implicated in immunity.<sup>66,67</sup> This operon is, however, not found in other circular bacteriocin gene clusters except for aureocyclicin 4185, carnocyclin A, circularin A, and garvicin ML (Table 1.3). A more recent work on the DUF95 membrane protein for the circular bacteriocin, leucocyclicin Q, indicated that the DUF95 protein serves as an immunity-associated transporter and secretion-aiding agent.<sup>68</sup>

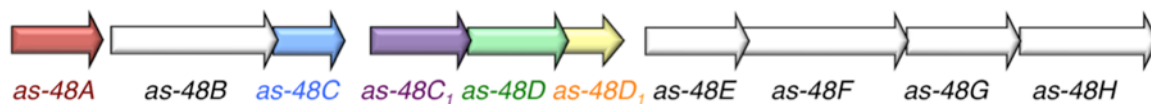


**Figure 1.1. Biosynthetic gene cluster of enterocin AS-48.**

The minimum set of genes required for production and immunity of enterocin AS-48 is shown in color. The red (*as-48A*), blue (*as-48C*), purple (*as-48C<sub>1</sub>*), green (*as-48D*), and yellow (*as-48D<sub>1</sub>*) genes encode the precursor peptide, a DUF95 membrane protein, an unknown protein, an ATPase, and an immunity protein, respectively. For the white genes, *as-48B* encodes a protein with unknown function; and the accessory operon *as-48EFGH* encodes an ABC transporter complex.

**Table 1.3. Gene clusters of known circular bacteriocins**

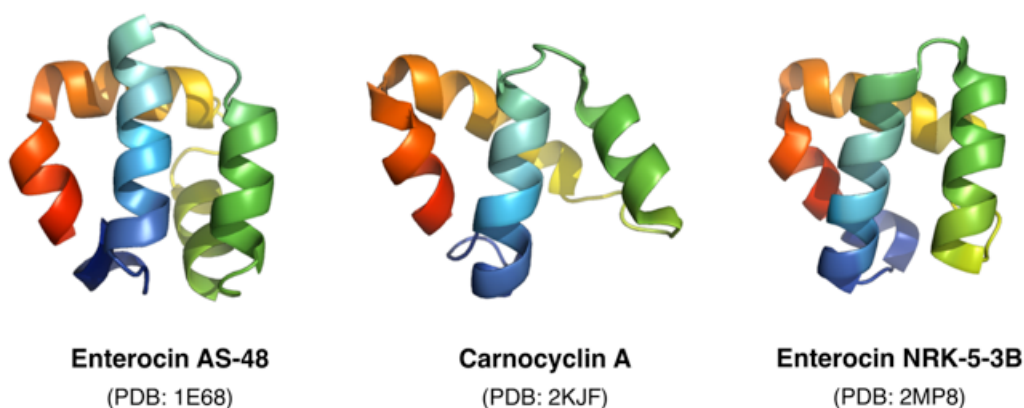
<b>Bacteriocin name</b>	<b>Gene cluster</b>	<b>Reference</b>
Amylocyclicin	<i>acnBACDEF</i>	[61]
Aureocyclicin 4185	<i>aclXBITCDAFGH</i>	[62]
Butyrvibriocin AR10	<i>bviBCDAE</i>	[56]
Carnocyclin A	<i>cclBITCDAEFGH</i>	[69]
Circularin A	<i>cirABCDEGHI</i>	[70]
Enterocin AS-48	<i>as-48ABCC<sub>1</sub>DD<sub>1</sub>EFGH</i>	[66]
Enterocin NKR-5-3B	<i>enkB1234 (enkABCDE)</i>	[71]
Garvicin ML	<i>garXABCDEFGH</i>	[72]
Gassericin A	<i>gaaBCADITE</i>	[73]
Lactocyclicin Q	unknown	N/A
Leucocyclicin Q	<i>lycRABCD</i>	[68]
Pneumocyclicin	<i>pcyABCDE</i>	[64]
Pumilarin	<i>pumABCC<sub>1</sub>D</i>	[65]
Uberolysin	<i>ublABCDE</i>	[58]

Table 1.3 lists the gene clusters of known circular bacteriocins. The gene clusters share substantial similarities suggesting that the mechanism by which these bacteriocins are biosynthesized may be similar as well. However, despite the various gene cluster functional analyses, the detailed mechanism by which the core peptide is cyclized and the leader peptide is cleaved remains to be determined.

### 1.2.3. Three-dimensional structures

The NMR solution structures of enterocin AS-48<sup>74</sup> (70 residues), carnocyclin A<sup>75</sup> (60 residues), and enterocin NRK-5-3B<sup>63</sup> (64 residues) have been elucidated (Figure 1.2). Enterocin AS-48 is comprised of five amphipathic  $\alpha$ -helices, while carnocyclin A and enterocin NKR-5-3B both contain four amphipathic  $\alpha$ -helices. These helices are folded such that majority of the hydrophobic residues are buried at the core, while cationic residues are exposed on the surface. Despite the extra  $\alpha$ -helix in enterocin AS-48, a common saposin-like fold is shared among the three peptides. Saposins are proteins

produced in humans that are associated in glycosphingolipid catabolism and are known to bind to lipids.<sup>76</sup> Their characteristic structural motif is composed of 4 to 5 adjacent  $\alpha$ -helices that are folded into two leaves.<sup>77</sup> The saposin-like structural motif observed in enterocin AS-48, carnocyclin A, and enterocin NKR-5-3B was proposed to be conserved among all other circular bacteriocins.<sup>75</sup> The cyclization of their termini and the compact folding of their structures are suggested to impart the superior thermal, pH, and proteolytic stability of circular bacteriocins.<sup>43</sup>



**Figure 1.2. NMR solution structures of circular bacteriocins enterocin AS-48, carnocyclin A, and enterocin NKR-5-3B.**

A rainbow color scheme is used with the N-terminus of the core peptide shown in blue, and the C-terminus shown in red. The site of cyclization is indicated by a gap between the N- and C- termini that is located within the C-terminal  $\alpha$ -helix.

#### 1.2.4. Mode of action

The conserved structural motif of circular bacteriocins suggests that they may operate via a common mode of action. Moreover, the highly cationic nature of these peptides implies that they initially interact with anionic bacterial membranes through electrostatic interactions. Detailed mode of action studies, however, indicate that target

cells are killed by various circular bacteriocins via different mechanisms. For enterocin AS-48, studies showed that it could form non-selective pores that cause the leakage of ions and low molecular weight substances.<sup>78</sup> X-ray crystallography, molecular dynamics, and sedimentation equilibrium experiments further indicated that enterocin AS-48 forms a dimer at pH 4.5 to 8.5, and transforms from a water-soluble to a membrane-bound conformation, wherein hydrophobic patches that are originally hidden become exposed in order to interact with the target membrane.<sup>79,80</sup> Carnocyclin A was also reported to exhibit the ability to form pores, however, the pores it creates particularly cause leakage of anions.<sup>81</sup> Gassericin A, on the other hand, was demonstrated to cause potassium ion efflux.<sup>82</sup> All of these early studies suggest that a target receptor is not required for activity. More recent work on garvicin ML also demonstrated nonspecific activity, but only at a concentration substantially higher than what is required for *in vivo* activity (the same concentration range used for the mode of action studies on enterocin AS-48, carnocyclin A, and gassericin A). At a lower concentration, it was shown that garvicin ML, in fact, recognizes a maltose ABC transporter complex as the target receptor, and docking into this receptor increases the target strain's sensitivity to garvicin ML.<sup>83</sup> The receptor was identified through generation of garvicin ML-resistant mutants and sequencing their genomes, wherein a deletion of the genes associated to the maltose ABC transporter (*malEFG*) was detected among all mutants, and reintroduction of the said genes restored sensitivity towards garvicin ML.

## 1.3. Leaderless Bacteriocins

### 1.3.1. Overview

In contrast to other bacteriocin classes, leaderless bacteriocins are synthesized without an N-terminal leader peptide and do not undergo any PTMs. Furthermore, most members of the group have a formylated N-terminal methionine, which is normally cleaved by peptide deformylases and methionine aminopeptidases during protein synthesis.<sup>84-86</sup> Enterocin L50A (EntL50A) and L50B (EntL50B) from *Enterococcus faecium* L50 were the first members of this class.<sup>87</sup> Since then, several other leaderless bacteriocins were discovered (Table 1.4). The production of a particular type of leaderless bacteriocin is usually not isolated to a specific species or strain. For instance, EntL50A and EntL50B have been isolated from various other *Enterococcus* spp., including the most recently reported *Enterococcus durans* 61A.<sup>88</sup> Unlike their original discovery where the isolated peptides were not formylated, *E. durans* 61A produces both formylated and nonformylated EntL50A and EntL50B. The formylation of EntL50A and EntL50B increased their activity by 8- and 2-fold, respectively.<sup>88</sup> Previous reports demonstrated that some two-component leaderless bacteriocins show synergistic activity (e.g. EntL50A and EntL50B), while others do not (e.g. weissellicin Y and M).<sup>87,89</sup> Interestingly, three- and four-peptide bacteriocin systems (e.g. aureocin A70) have also been identified in this class. These multiple-component bacteriocins require the presence of all individual peptides to exhibit full activity against a broad spectrum of organisms.<sup>90,91</sup>

The laterosporulins represent another emerging group of broad-spectrum bacteriocins that are also produced without a leader peptide sequence, but unlike the

leaderless bacteriocins listed in Table 1.4, these peptides contain disulfide bridges. In addition, the N-terminal methionine residue is cleaved off during their maturation. Currently, there are two peptides belonging to this group, namely laterosporulin<sup>92</sup> and laterosporulin10<sup>93</sup>, which are both produced by *Brevibacillus* spp.

**Table 1.4. List of unmodified leaderless bacteriocins**

Bacteriocin name	Size (a.a.)	MW <sup>a</sup> (Da)	Producer strain(s)	Year discovered <sup>b</sup> [Reference]
Enterocin L50				
EntL50A	44	5,190	<i>Enterococcus faecium</i> L50	1998 [87]
EntL50B	43	5,178		
Enterocin Q	34	3,980 (f) <sup>c</sup>	<i>E. faecium</i> L50	2000 [94]
Aureocin A70				
AurA	31	2,924	<i>Staphylococcus aureus</i> A70	2001 [91]
AurB	30	2,797		
AurC	31	2,955		
AurD	31	3,087		
Aureocin A53	51	6,013 (f)	<i>S. aureus</i> A53	2002 [95]
Enterocin EJ97	44	5,328	<i>Enterococcus faecalis</i> EJ97	2003 [96]
Lactococcal small bacteriocin B (LsbB)	30	3,410 <sup>d</sup>	<i>Lactococcus lactis</i> BGMN1-5	2003 [97]
BHT-B	44	5,195 (f)	<i>Streptococcus rattus</i> BHT	2005 [98]
<sup>e</sup> Enterocin MR10A/ Enterocin 7A/ Enterocin DD14A	44	5,200 (f)	<i>E. faecalis</i> MRR 10-3/ <i>E. faecalis</i> 710C/ <i>E. faecalis</i> 14	2006 [99]/ 2011 [100]/ 2017 [101]
Enterocin MR10B/ Enterocin 7B/ Enterocin DD14B	43	5,207 (f)		
Lacticin Q	53	5,927 (f)	<i>L. lactis</i> QU 5	2007 [102]
Lacticin Z	53	5,969 (f)	<i>L. lactis</i> QU 14	2007 [103]
Weissellicin Y	42	4,925 (f)	<i>Weissella hellenica</i> QU 13	2012 [89]
Weissellicin M	43	4,967 (f)		
Epidermicin NI01	51	6,075 (f)	<i>Staphylococcus epidermidis</i> 224	2012 [104]
Enterocin K1	37	4,565 <sup>d</sup>	<i>E. faecium</i> E1630	2014 [105]
Garvicin KS				
GakA	34	3,479(f)	<i>Lactococcus garvieae</i> KS1546	2016 [90]
GakB	34	3,187 (f)		
GakC	32	3,126 (f)		
<sup>f</sup> Cereucin V			<i>Bacillus cereus</i> VD148	
CevA	30	2,975		2016 [90]
CevB	30	2,828		
CevC	31	3,113		
<sup>f</sup> Cereucin H				
CehA	26	2,847	<i>B. cereus</i> HuA2-4	2016 [90]
CehB	30	3,141		
CehC	30	2,838		
CehD	30	2,989		
<sup>f</sup> Cereucin X				
CexA	27	2,943	<i>B. cereus</i> BAG1X1-1	2016 [90]
CexB	29	3,136		
CexC	30	2,796		
Dur 152A	44	5,226	<i>Enterococcus durans</i> 152	2017 [106]
Lactolisterin BU	43	5,161	<i>L. lactis</i> subsp. <i>lactis</i> by. diacetylactis BGBU1-4	2017 [107]

<sup>a</sup> Molecular weights (MW) are the experimental values detected, unless otherwise indicated.

<sup>b</sup> Year during which the peptide was confirmed to be a leaderless bacteriocin.

<sup>c</sup> (f), formylated N-terminal methionine

<sup>d</sup> MW was calculated from the primary sequence.

<sup>e</sup> Identical peptides were given different names.

<sup>f</sup> Identified through genome mining and consequently chemically synthesized to confirm activity.

### 1.3.2. Biosynthesis

The gene clusters of several leaderless bacteriocins have already been identified, including those of enterocin L50<sup>87</sup>, aureocin A70<sup>91</sup>, enterocin EJ97<sup>96</sup>, BHT-B<sup>98</sup>, enterocin Q<sup>108</sup>, aureocin A53 (AucA)<sup>109</sup>, epidermicin NI01<sup>104</sup>, and lactacin Q (LnqQ)<sup>110</sup>. The gene clusters of LnqQ and AucA, which are the peptides that were studied in Chapter 3 of this thesis, are presented herein.

Production of LnqQ requires the biosynthetic gene cluster *lnqRQBCDEF* (Figure 1.3).<sup>110</sup> The ABC transporter LnqEF, which exports the bacteriocin from the cell, was identified to be essential for immunity. In addition to LnqEF, full immunity was attained in the presence of LnqBCD. Based on sequence homology through BLAST search, LnqB is a putative ABC transporter permease, while LnqC and LnqD are putative membrane proteins.<sup>110</sup> More recently, LnqR was confirmed to be a transcriptional regulator that positively regulates production of LnqQ in a temperature-dependent manner.<sup>111</sup>

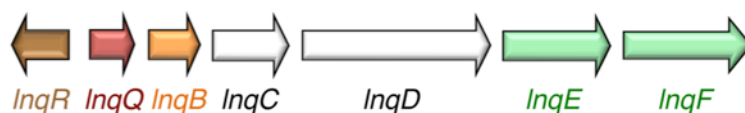


**Figure 1.3. Biosynthetic gene cluster of lactacin Q.**

The gene *lnqR* shown in brown encodes a transcriptional regulator; *lnqQ* in red is the structural bacteriocin gene; *lnqB* in orange encodes a putative ABC transporter permease; *lnqC* and *lnqD* in white are putative membrane protein genes; and *lnqE* and *lnqF* in green encode an ABC transporter complex.

The biosynthetic gene cluster proven to be responsible for AucA production and immunity is shown in Figure 1.4.<sup>109</sup> A three-component dedicated ABC transporter (AucEFG) was shown to be critical for immunity, and the presence of two putative

membrane proteins, AucIA and AucIA, further increased resistance towards AucA. An unidentified gene (*orf*) encodes a putative membrane protein that was experimentally proven to be essential for bacteriocin secretion.<sup>109</sup>

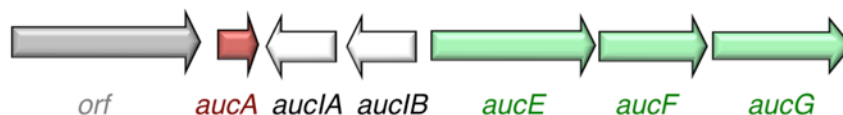


**Figure 1.4. Biosynthetic gene cluster of aureocin A53.**

The gene *aucA* shown in red is the structural bacteriocin gene; *aucIA* and *aucIB* in white encode unidentified proteins that play a role in immunity; *aucEFG* in green encode a putative ABC transporter; and the gene labelled as *orf* encodes for an unknown membrane protein that is suggested to be important in AucA secretion.

### 1.3.3. Three-dimensional structures

The three-dimensional (3D) structures of five leaderless bacteriocins have been elucidated thus far (Figure 1.5). These include the two-component bacteriocin system, enterocin 7, that is comprised of enterocin 7A (Ent7A; 44 residues) and 7B (Ent7B; 43 residues).<sup>100,112</sup> The NMR solution structures of Ent7A and Ent7B consist of amphipathic  $\alpha$ -helices that are folded to resemble the saposin-like motif observed in circular bacteriocins.<sup>112,113</sup> Like the circular bacteriocins, Ent7A and Ent7B have broad inhibition spectra. In contrast, the NMR solution structures of the leaderless bacteriocins, lactococcal small bacteriocin B (LsbB; 30 residues) and enterocin K1 (EntK1; 37 residues), are completely different from those of Ent7A and Ent7B (Figure 1.5). LsbB and EntK1 are both composed of an amphipathic  $\alpha$ -helical N-terminus and an unstructured C-terminus.<sup>105</sup> LsbB and EntK1 also differ from Ent7A and Ent7B in terms of activity, since LsbB and EntK1 have narrower inhibition spectra.<sup>97,105,114</sup> Moreover, circular dichroism (CD) data

showed that Ent7A and Ent7B are structured in water, whereas LsbB and EntK1 only assume a certain degree of helicity in structure-inducing conditions (i.e. with trifluoroethanol or dodecylphosphocholine).<sup>105,112,114</sup>

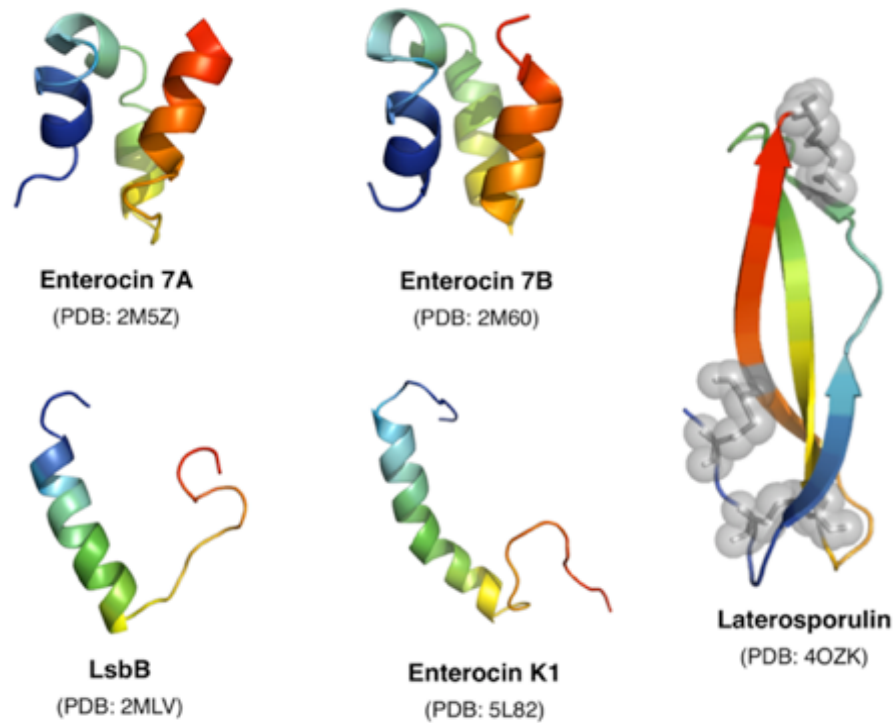


**Figure 1.5. NMR solution structures of leaderless bacteriocins enterocin 7A, enterocin 7B, LsbB, and enterocin K1; and X-ray crystal structure of laterosporulin.**

A rainbow color scheme is used with the N-terminus shown in blue, and the C-terminus shown in red. Disulfide bridges in laterosporulin are shown in gray spheres.

Lastly, the 3D structure of laterosporulin was solved by X-ray crystallography revealing that laterosporulin adopts a very different structure relative to the aforementioned leaderless bacteriocins.<sup>115</sup> Laterosporulin contains four  $\beta$ -strands that assume a twisted  $\beta$ -sheet conformation with 3 disulfide crosslinks. The overall architecture appears to resemble those of the mammalian  $\beta$ -defensins, an unprecedented

motif in bacteriocins.<sup>115</sup> Given the striking differences among the properties and structures of Ent7A, Ent7B, LsbB, EntK1, and laterosporulin, it may be assumed that leaderless bacteriocins can be subdivided into three subgroups, namely (1) saposin-like peptides, (2) LsbB-like peptides, and the (3) laterosporulins.

#### **1.3.4. Mode of action**

The most studied leaderless bacteriocins in terms of mode of action are AucA and LnqQ. A description of their modes of action is presented in Chapter 3. In general, both peptides have been suggested to permeate target membranes without docking into any receptor, and consequently allow efflux of vital metabolites.<sup>116-118</sup> The same general mechanism has been proposed for lacticin Z<sup>103</sup>, epidermicin NI01<sup>104</sup>, and BHT-B<sup>98</sup>.

On the other hand, LsbB and EntK1 were both demonstrated to interact with a Zn-dependent membrane metallopeptidase via the flexible C-terminus of both bacteriocins.<sup>105,114,119</sup> The same receptor was shown to be the target of another LsbB-like leaderless bacteriocin, named enterocin EJ97.<sup>114</sup> More recently, it was revealed through site-directed mutagenesis that Trp25 and Ala30 of LsbB are the critical residues for activity, and that these residues specifically interact with the third transmembrane helix of the receptor.<sup>120</sup> Further details on the subsequent processes after receptor docking have yet to be investigated. Similarly, much has to be learned on the mode of action of laterosporulin, although it has been demonstrated to compromise membrane integrity and reduce ATP levels in sensitive strains.<sup>93</sup>

## 1.4. Two-Peptide Bacteriocins

### 1.4.1. Overview

Two-peptide bacteriocins are comprised of two different unmodified peptides that exhibit optimal potency in the presence of equimolar amounts of both peptides.<sup>121</sup> Their structural genes are situated next to each other in the same operon, and the encoded precursor peptides contain double glycine (GG)-type N-terminal leaders of 15 to 30 amino acid residues in length. The leader peptide is cleaved at the C-terminus of the second glycine residue by a specific ABC transporter that subsequently extrudes the mature peptide across the cell membrane.<sup>121</sup> Two-peptide bacteriocins are also characterized by the presence of GXXXG (where X can be any other amino acid) and GXXXG-like motifs (where Gly is replaced by either Ala or Ser) that are known to be involved in helix-helix interactions in membrane proteins.<sup>122,123</sup> Altogether, two-peptide bacteriocins differ from two-component bacteriocins that belong to other classes (e.g. two-component leaderless bacteriocins, two-component lantibiotics) in terms of the presence of leader peptides, unmodified core peptides, and GXXXG motifs that serve as dimerization interface.

The first bacteriocin of this group, lactococcin G (LcnG), was discovered in 1992.<sup>124</sup> Since then, at least 18 additional members have been identified (Table 1.5), most of which are produced by lactobacilli. The other producer strains belong to the genera *Lactococcus*, *Brochothrix*, *Enterococcus*, and *Streptococcus*. Other two-peptide bacteriocins that have only been partially characterized, such as leucocin H<sup>125</sup>, lactococcin MN<sup>126</sup>, and lactococcin MMT24<sup>127</sup>, are not included in Table 1.5.

**Table 1.5. List of unmodified two-peptide bacteriocins**

<b>Bacteriocin name</b>		<b>Size (a.a.)</b>	<b>MW (Da)</b>	<b>Producer strain</b>	<b>Year discovered [Reference(s)]</b>
Lactococcin G	LcnG $\alpha$	39	4,346	<i>Lactococcus lactis</i>	1992 [124]
	LcnG $\beta$	35	4,110	LMG 2081	
Lactacin F	LafA	57	5,601	<i>Lactobacillus johnsonii</i>	1993 [128]
	LafX	48	4,736	VPI11088	
Plantaricin S	Pls $\alpha$	27	2,922	<i>Lactobacillus plantarum</i>	1995 [129,130]
	Pls $\beta$	26	2,873	LPC010	
Thermophilin 13	ThmA	62	5,776	<i>Streptococcus</i>	1997 [131]
	ThmB	43	3,910	<i>thermophilus</i> SFi13	
Brochocin-C	BrcA	59	5,245	<i>Brochothrix campertris</i>	1998 [132]
	BrcB	43	3,944	ATCC 43754	
Plantaricin EF	PlnE	33	3,545	<i>L. plantarum</i> C11	1998 [133]
	PneF	34	3,703		
Plantaricin JK	PlnJ	25	2,929	<i>L. plantarum</i> C11	1998 [133]
	PlnK	32	3,503		
Enterocin 1071	Ent $\alpha$	39	4,285	<i>Enterococcus faecalis</i>	2000 [134]
	Ent $\beta$	35	3,899	BFE 1071	
Lactocin 705	705 $\alpha$	33	3,578	<i>Lactobacillus casei</i>	2000 [135]
	705 $\beta$	33	3,309	CRL 705	
Mutacin IV	NlmA	44	4,172	<i>Streptococcus mutans</i>	2001 [136]
	NlmB	49	4,828	UA140	
ABP-118	Abp118 $\alpha$	45	4,087	<i>Lactobacillus salivarius</i>	2002 [137]
	Abp119 $\beta$	46	4,334	subsp. <i>salivarius</i> UCC118	
Plantaricin NC8	PLNC8 $\alpha$	29	3,587	<i>L. plantarum</i> NC8	2003 [138]
	PLNC8 $\beta$	34	4,000		
Lactococcin Q	LcnQ $\alpha$	39	4,260	<i>L. lactis</i> QU 4	2006 [139]
	LcnQ $\beta$	35	4,018		
Salivaricin P	Sln1	45	4,097	<i>L. salivarius</i> DPC6005	2007 [140]
	Sln2	46	4,285		
Enterocin C	EntC1	39	4,284	<i>E. faecalis</i> C901	2009 [141]
	EntC2	35	3,867		
Enterocin X	X $\alpha$	40	4,420	<i>Enterococcus faecium</i>	2010 [142]
	X $\beta$	37	4,069	KU-B5	
Salivaricin T	SalT $\alpha$	61	5,655	<i>L. salivarius</i> DPC6488	2011 [143]
	SalT $\beta$	52	5,269		
Brevicin 174A	174A $\alpha$	53	5,190	<i>Lactobacillus brevis</i> 174A	2015 [144]
	174A $\beta$	55	5,300		
SpbMN	SpbM	52	4,928	<i>Streptococcus pyrogenes</i>	2016 [145]
	SpbN	48	4,561	MGAS8232	

Two-peptide bacteriocins act as one unit. In certain cases, the antimicrobial activity is only observed when the two component peptides are used in combination (e.g. LcnG<sup>146</sup>). In other instances, the individual peptides are active by themselves, although optimal activity is achieved in the presence of both peptides (e.g. thermophilin 13<sup>131</sup>). It has also been demonstrated that individual peptides from one bacteriocin unit can be combined with the complementary peptide from another homologous two-peptide bacteriocin.<sup>146</sup> A number of two-peptide bacteriocins are only active against a closely related species, while others can kill a wide array of organisms.<sup>85,121</sup>

#### 1.4.2. Biosynthesis

Several of the two-peptide bacteriocins listed in Table 1.5 have been genetically characterized. It has been recognized that at least five genes are necessary for production and immunity of two-peptide bacteriocins. These include genes encoding the two precursor peptides (e.g. *lagA* and *lagB* for LcnG), an immunity protein (e.g. *lagC*), a dedicated ABC transporter (e.g. *lagD*), and an accessory protein that might be associated with immunity and/or secretion of the bacteriocin (e.g. *lagE*).<sup>147</sup> As an example, the gene cluster of LcnG, the founding member of this class, is shown in Figure 1.6.<sup>146</sup>

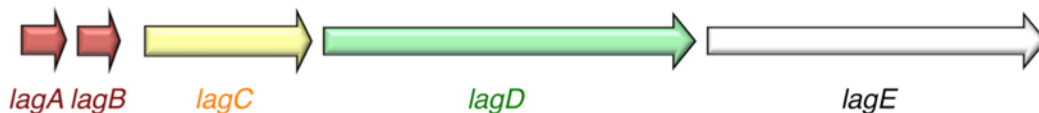


**Figure 1.6. Biosynthetic gene cluster of lactococcin G.**

The genes *lagAB* shown in red are the two structural bacteriocin genes; *lagC* in yellow encodes an immunity protein; *lagD* in green encodes an ABC transporter; and *lagE* in white encodes a putative secretion protein.

The structural genes in all of the two-peptide bacteriocins identified so far are always located next to each other in the same operon, suggesting that they are always produced in equal quantities.<sup>121</sup> After ribosomal synthesis of the precursor peptides, the leader peptide is cleaved and the core peptide is exported by the dedicated ABC transporter. The ABC transporter contains an additional peptidase domain of ~150 amino acid residues at its N-terminus that is normally not present in other ABC transporters. This N-terminal extension recognizes and cuts the leader peptide at the C-terminal side of the GG-motif.<sup>148</sup> The ABC transporter then releases the cleaved peptide across the cell membrane, while the immunity protein prevents re-entry of the bacteriocin to protect the producer from its own bacteriocin.<sup>146,149,150</sup>

Bacteriocin production of two-peptide systems is sometimes transcriptionally regulated by a three-component regulatory system comprised of an induction factor (peptide pheromone), a membrane-associated histidine kinase, and a response regulator.<sup>151</sup> The induction factor binds to the kinase, thereby initiating the phosphorylation of the intracellular response regulator, which consequently activates the operon for bacteriocin biosynthesis.<sup>151</sup> For instance, plantaricin A was discovered to be the induction factor of the two-peptide bacteriocins, plantaricin EF (PlnEF) and plantaricin JK (PlnJK), that are both produced by *Lactobacillus plantarum* C11.<sup>152</sup>

### **1.4.3. Three-dimensional structures**

The 3D NMR solution structures of LcnG<sup>153</sup>, PlnEF<sup>154</sup>, and PlnJK<sup>155</sup> (Figure 1.7) have been solved in structure-inducing solvents or membrane-mimicking conditions. CD studies showed that all these peptides are unstructured in aqueous conditions, but become

helical in the presence of trifluoroethanol or dodecylphosphocholine micelles.<sup>153–157</sup> The structures of LcnG $\alpha$  of LcnG, PlnE of PlnEF, and PlnJ of PlnJK appear to be similar, all of which are comprised of two distinct hydrophobic or amphipathic helices that are separated by a short loop. On the other hand, LcnG $\beta$ , PlnF, and PlnK have similar structures that are comprised of an extended amphipathic  $\alpha$ -helix, although a central kink is observed in the structure of LcnG $\beta$ .

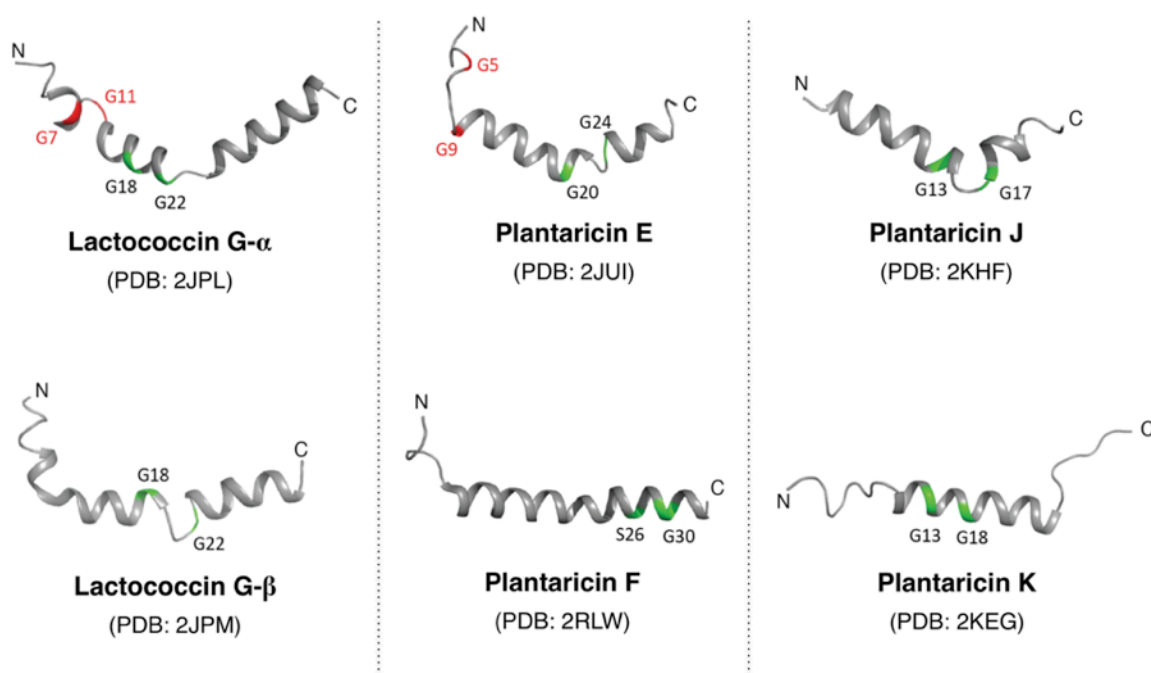


**Figure 1.7. NMR solution structures of two-peptide bacteriocins lactococcin G (LcnG $\alpha$  and LcnG $\beta$ ), plantaricin EF (PlnE and PlnF), and plantaricin JK (PlnJ and PlnK).**

Residues involved in the GXXXG (or GXXXG-like) motifs are labelled and highlighted in green. For PlnE and LcnG $\alpha$ , additional GXXXG motifs that are considered to be critical for activity are highlighted in red. The N- and C-termini of the peptides are indicated.

An increase in structural content was previously observed when complementary peptides were mixed and exposed to liposomes, implicating that a membrane-mimicking

environment allows complementary peptides to interact.<sup>153–157</sup> However, exposure to micelles did not result in any additional structuring of the combined peptides, suggesting that a reasonably flat surface, as in the case of liposomes and bicelles, is required to mediate the interaction.<sup>121</sup> The GXXXG and GXXXG-like motifs on both peptide components are specifically postulated to facilitate the mentioned interaction. The Gly/Ala/Ser residues of this motif are located on the same side of the  $\alpha$ -helix providing a flat surface for inter-helical contacts to form transmembrane-like helix-helix structures that penetrate target bacterial membranes.<sup>122,123,158</sup> The structural and functional importance of the GXXXG and GXXXG-like motifs have been demonstrated through mutational analysis in various two-peptide bacteriocins including LcnG<sup>159</sup>, PlnJK<sup>155</sup>, PlnEF<sup>160</sup>, PlnS<sup>161</sup>, and brevicin 174A<sup>144</sup>. Molecular dynamic simulations were also used to dissect the importance of these residues for membrane disruption in PlnS<sup>161</sup> and PlnEF<sup>160,162</sup>.

A structural model (Figure 1.8) has been proposed for LcnG based on the elucidated 3D structures of the  $\alpha$  and  $\beta$  peptides, and the site-directed mutagenesis studies that probed the importance of the GXXXG motifs and Trp residues in LcnG.<sup>153,159,163</sup> The model suggests that the  $\alpha$  and  $\beta$  peptides are situated parallel to each other, with the G<sub>7</sub>XXXG<sub>11</sub> motif of LcnG $\alpha$  interacting with G<sub>18</sub>XXXG<sub>22</sub> of LcnG $\beta$ . Furthermore, the authors proposed that the helix-helix interaction would turn the segments that contain the GXXXG motifs into well-defined helices, in contrast to the elucidated structures where these segments appear to be disrupted (Figure 1.7). It was postulated that the highly cationic C-terminus of LcnG $\alpha$  would facilitate the insertion of the complex across the membrane,

while the Trp-rich N-terminus of LcnG $\beta$  would be located at the outer membrane interface.<sup>121</sup>

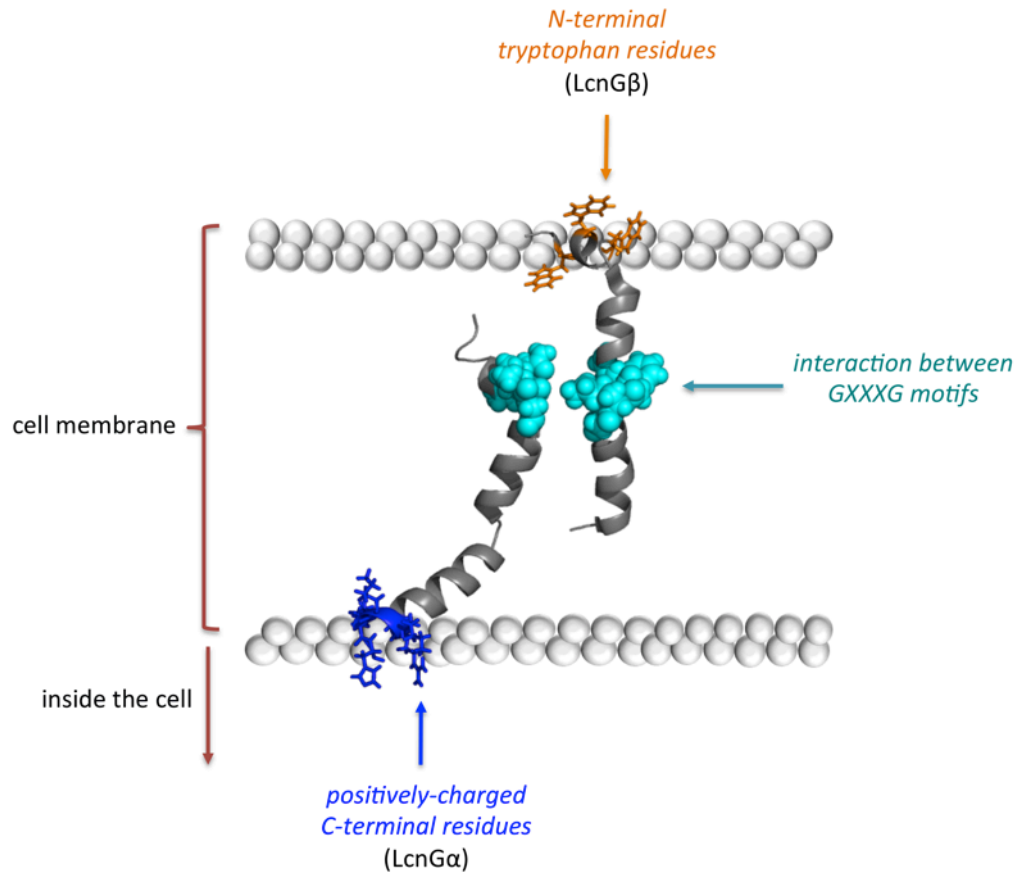


**Figure 1.8. Proposed structural model of lactococcin G (LcnG $\alpha$ -LcnG $\beta$ ) dimer.<sup>121</sup>**

The G<sub>7</sub>XXXG<sub>11</sub> motif of LcnG $\alpha$  interacts with G<sub>18</sub>XXXG<sub>22</sub> of LcnG $\beta$  (shown in cyan). The highly cationic C-terminus of LcnG $\alpha$  (shown in blue) facilitates insertion of the complex through the membrane, while the Trp-rich N-terminus of LcnG $\beta$  (shown in orange) is anchored at the outer membrane interface. Cell membrane phospholipid head groups are represented by gray spheres.

On the contrary, a different model was proposed for the PlnEF dimer (Figure 1.9) that was derived from molecular dynamics experiments coupled with mutational analysis of the GXXXG (and GXXXG-like) motifs and aromatic residues. In this model, PlnE and PlnF are oriented antiparallel to each other, with G<sub>5</sub>XXXG<sub>9</sub> of PlnE interacting with

S<sub>26</sub>XXXG<sub>30</sub> of PlnF.<sup>160</sup> The helix-helix interaction resulted in increased structuring at the N-terminus of PlnE, which was initially unstructured based on the 3D structure that was published earlier (Figure 1.7).<sup>154</sup>

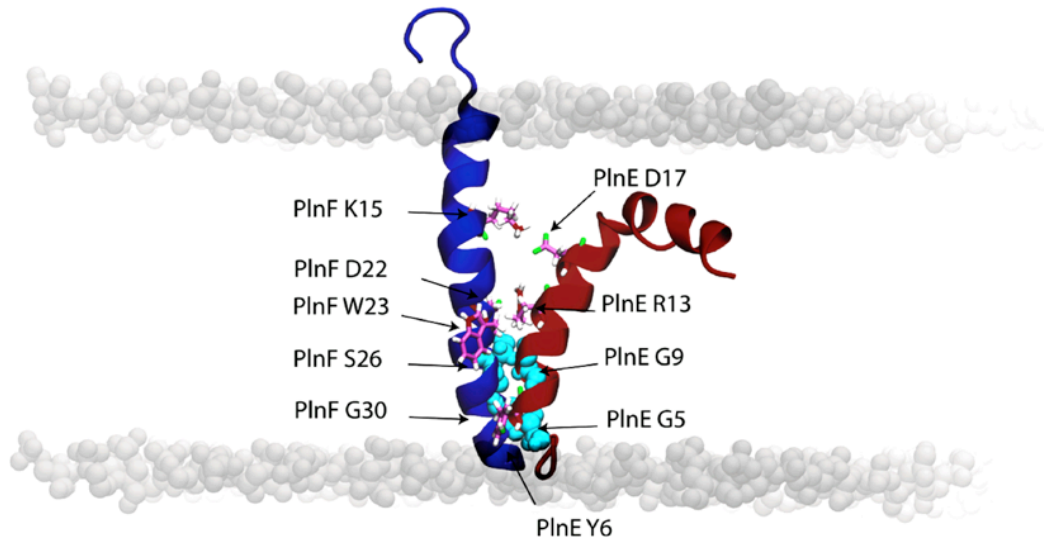


**Figure 1.9. Proposed structural model of plantaricin EF (PlnEF) dimer.**

(Adapted from Ekblad *et al.*, 2016)<sup>160</sup> The G<sub>5</sub>XXXG<sub>9</sub> motif of PlnE interacts with S<sub>26</sub>XXXG<sub>30</sub> (GXXXG-like motif) of PlnF (shown in cyan). Other residues that were determined to be important in forming the dimer are shown in pink using stick representation. Cell membrane phospholipid head groups are represented by gray spheres.

The PlnEF dimer is further stabilized by electrostatic interactions between Asp17 and Arg13 of PlnE with Lys15 and Asp22 of PlnF, respectively (Figure 1.9). Other residues that were shown to be important for facilitating this interaction are the aromatic amino acids, Trp23 of PlnF and Tyr6 of PlnE (Figure 1.9).<sup>160</sup>

#### 1.4.4. Mode of action

Investigations on the mode of action of various two-peptide bacteriocins including LcnG<sup>164,165</sup>, PlnEF<sup>166,167</sup>, PlnJK<sup>166,168</sup>, lactacin F<sup>169</sup>, thermophilin 13<sup>131</sup>, and lactocin 705<sup>170,171</sup> have shown that all these peptides induce cell death by causing pore formation and subsequent membrane leakage of ions. The nature of these ions varies depending on the specific bacteriocin. LcnG allows efflux of monovalent cations (e.g. Na<sup>+</sup>, K<sup>+</sup>, Li<sup>+</sup>, Cs<sup>+</sup>, Rb<sup>+</sup>, and choline), but not H<sup>+</sup>, divalent cations (e.g. Mg<sup>2+</sup>), and anions (e.g. phosphates).<sup>164,165</sup> PlnEF and PlnJK, on the other hand, leak monovalent ions, including H<sup>+</sup>. Moreover, it was determined that PlnEF conducts cations at a higher efficiency than PlnJK, while PlnJK conducts anions more efficiently than PlnEF.<sup>166</sup> Lactacin F and lactocin 705 were both able to cause leakage of K<sup>+</sup> and phosphate.<sup>169,170</sup> Thermophilin 13, on the other hand, was demonstrated to compromise membrane electrical potential and pH gradient, although the specific molecules that leak out through the membrane have not yet been identified.<sup>131</sup>

With the advancement of next-generation sequencing technology, mode of action research has been recently directed towards receptor identification through generation of resistant mutants and sequencing of the entire genomes. Upon comparison of the genome sequence with the wild-type organism, mutated genes encoding membrane-bound proteins may serve as candidate receptors, since their mutation may have possibly led to resistance. The putative bacteriocin receptors are then further evaluated through various approaches, including the heterologous expression of the gene in a bacteriocin-insensitive host and monitoring whether the incorporation of the gene confers sensitivity towards the bacteriocin.<sup>172</sup> The first receptor identified via this approach or a related procedure was

reported in 2012. It was the maltose ABC transporter, which serves as the receptor of the circular bacteriocin garvicin ML.<sup>83</sup> A year later, a membrane-associated zinc-dependent metallopeptidase was determined to serve as receptor of the leaderless bacteriocin LsbB.<sup>119</sup> More recently, receptors of various two-peptide bacteriocins were uncovered. These include the membrane-embedded undecaprenyl pyrophosphate phosphatase (UppP), which was identified by genome sequencing of resistant mutants and confirmed via heterologous expression to be the receptor of LcnG and enterocin 1071.<sup>173</sup> It was further suggested that a closely related two-peptide bacteriocin, lactococcin Q, also recognizes the same receptor. UppP is involved in cell wall synthesis, particularly in catalyzing the dephosphorylation of undecaprenyl pyrophosphate to undecaprenyl phosphate.<sup>174</sup> For another two-peptide bacteriocin, PlnJK, a different receptor was identified. A membrane-bound amino acid-polyamine-organocation transporter was pointed out as its putative receptor based on genome sequences of PlnJK-resistant mutants. However, heterologous expression or *in vitro* expression of the gene encoding this transporter still has to be pursued to prove its function.<sup>175</sup> In the same study, the generated PlnJK-resistant mutants were found to be sensitive towards PlnEF, signifying that the receptor for PlnJK is not the same for PlnEF. This result corroborates with earlier studies, which showed that PlnJK causes efflux of anions more efficiently, while PlnEF prefers cations.<sup>166,175</sup> More recently, a 3D structural model of the PlnJK putative receptor was obtained through template-based modeling.<sup>168</sup> In this study, the mutational hotspot regions were found to be localized at the C-terminus involving transmembrane helices 10 to 12 of the transporter, representing the potential docking site for PlnJK.

## 1.5. Lanthipeptides

### 1.5.1. Overview

Lanthipeptides comprise a diverse and large family of ribosomally synthesized peptides that undergo extensive PTMs, specifically characterized by the presence of lanthionine (Lan) and methyllanthionine (MeLan) residues.<sup>1,176</sup> On the basis of identified gene clusters in the genome database, lanthipeptides are considered the largest group of ribosomally synthesized and post-translationally modified peptides.<sup>177–181</sup> They are produced by several genera under the phyla firmicutes, actinobacteria, proteobacteria, bacteroidetes, and cyanobacteria.<sup>177,182,183</sup> Lanthipeptides have diverse biological activities, and those with antibacterial effects are specifically referred to as “lantibiotics”. Other lanthipeptides serve as antiviral<sup>184</sup>, antifungal<sup>185</sup>, antinociceptive<sup>186</sup>, morphogenetic<sup>187,188</sup>, and antiallodynic<sup>189</sup> agents.

Lan and MeLan residues are formed through enzyme-catalyzed dehydration and cyclization reactions. Ser and Thr residues are initially dehydrated to produce 2,3-dehydroalanine (Dha) and 2,3-dehydrobutyrine (Dhb), respectively. The dehydrated residue is subsequently attacked by a nearby cysteinyl thiol group via a Michael-type addition reaction to form Lan from Dha, and MeLan from Dhb (Figure 1.10). Lan and MeLan residues have been found to be essential for bioactivity and stability of lanthipeptides.<sup>1,176</sup> In certain cases, some of the Dha and Dhb residues are not modified further and are found in the mature peptides.

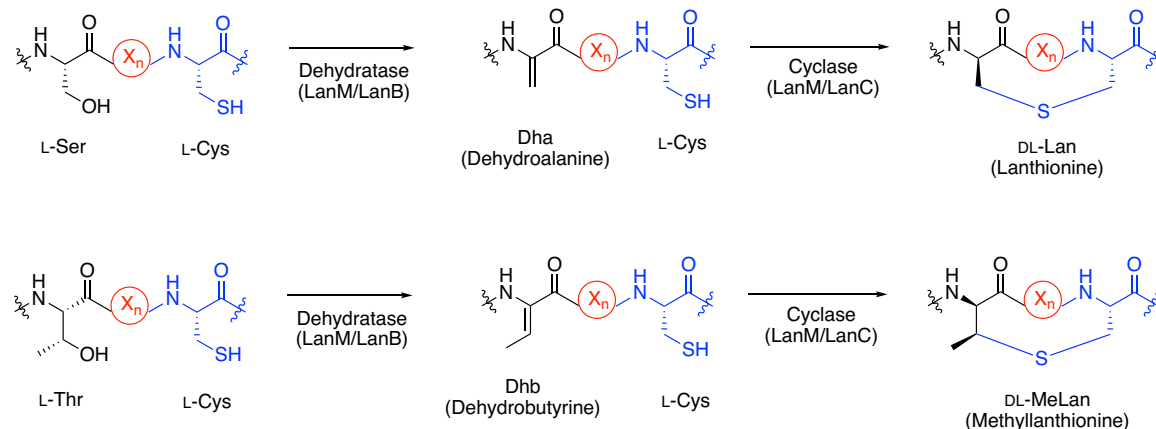


**Figure 1.10. Formation of DL-lanthionine and DL-methyllanthionine residues.**

The LL-stereoisomers have also been recently observed. X<sub>n</sub> = peptide of n amino acids.

The lanthipeptide family also includes variants that contain labionin (Lab) or methyllabionin (MeLab) residues. To form these functionalities, the Cys thiol group also attacks a dehydro residue, but instead of protonating the resulting enolate to form Lan or MeLan, the enolate subsequently attacks another dehydro residue to produce a carbon-carbon linkage (Figure 1.11).<sup>189</sup> Lab formation involves one Cys and two Dha residues, while MeLab synthesis initially utilizes a Cys and Dhb, followed by a second conjugate addition to a Dha.<sup>186,189</sup> Thus far, there are no examples where the second addition reaction involves a Dhb. Previously, the stereochemistry of Lan and MeLan residues had been exclusively assigned as DL-Lan and DL-MeLan. It was only in 2013, when LL-stereoisomers were first identified in the enterococcal cytolysin<sup>190</sup>, and were consequently also observed in carnolysin<sup>191</sup>. For labionins, only the LDL-Lab has been observed.<sup>177,189</sup> The stereochemistry of MeLab has not yet been identified.<sup>186</sup>

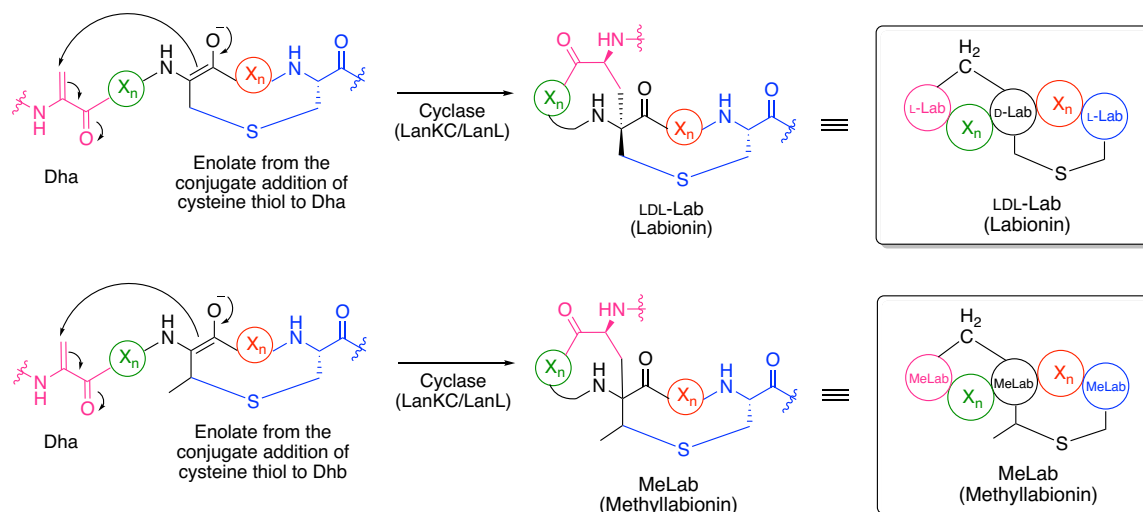


**Figure 1.11. Formation of LDL-labionin and methylabionin residues.**

The stereochemistry of methylabionin has not been identified. X<sub>n</sub> = peptide of n amino acids.

Apart from Dha, Dhb, Lan, MeLan, Lab, and MeLab, several other unusual amino acids have been found in lanthipeptides, including D-Ala (Figure 1.12), D-aminobutyrate (D-Abu) (Figure 1.12), and S-[(Z)-2-aminovinyl]-D-cysteine (AviCys) (Figure 1.13), among many others.<sup>191–193</sup> The presence of D-amino acids was first observed in 1994 in the lantibiotic lactocin S from *Lactobacillus sakei* L45.<sup>193</sup> Lactocin S specifically contains three D-Ala residues. Lacticin 3147, a two-component lantibiotic comprised of Ltn $\alpha$  and Ltn $\beta$ , was subsequently isolated from *L. lactis* DPC3147, and was shown to contain one D-Ala in Ltn $\alpha$ , and two D-Ala residues in Ltn $\beta$ . The LtnJ dehydrogenase of the lacticin 3147 biosynthetic machinery was the first enzyme to be characterized and confirmed as the enzyme responsible for the installation of D-Ala residues.<sup>194,195</sup> “LanJ” has since been assigned as the generic name for lantibiotic dehydrogenases. LtnJ stereoselectively reduces Dha to D-Ala, thereby inverting the stereocenter from L-Ser to D-Ala (Figure 1.12). The D-Ala residues were demonstrated to be critical for the bioactivity of lacticin

3147, since replacing the D-Ala residues with L-Ala or Dha substantially reduced antimicrobial activity.<sup>194</sup> It was further shown that LtnJ reduces Dha but not Dhb.<sup>194</sup> Only recently, a dehydrogenase that can reduce both Dha and Dhb to produce D-Ala and D-Abu, respectively, was identified (Figures 1.12). The said enzyme is referred to as CrnJ, which is involved in the biosynthesis of carnolysin, a two-component lantibiotic comprised of carnolysin A1 and A2, from *Carnobacterium maltaromaticum* C2.<sup>191</sup> To date, the only other identified lanthipeptide enzyme that can catalyze the aforementioned transformations is BsjJ of the two-component lantibiotic, bicereucin (Bsj $\alpha$  and Bsj $\beta$ ), from *Bacillus cereus* SJ1.<sup>196</sup> More details on these reducing enzymes are discussed in Chapter 5.

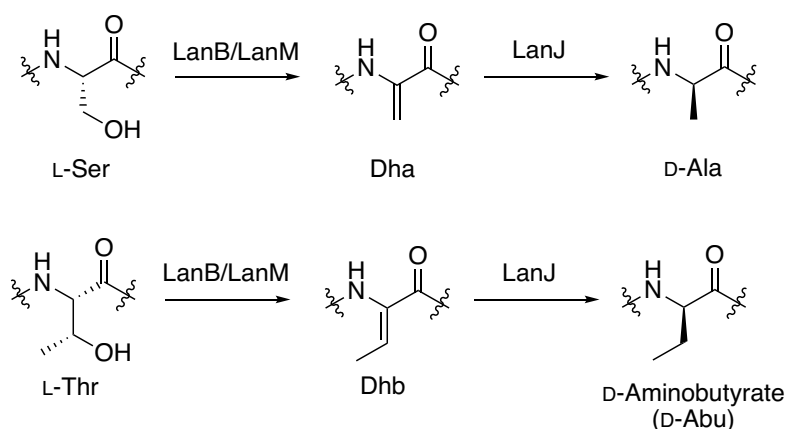


**Figure 1.12. LanJ-catalyzed reduction of D-Ala to Dha and D-Abu to Dhb.**

A C-terminal AviCys (Figure 1.13) is another non-canonical amino acid observed in several lanthipeptides including epidermin, gallidermin, microbisporicin, and mutacin 1140.<sup>177</sup> The AviCys residue was first identified in epidermin from *S. epidermidis* Tü3298.<sup>192</sup> Subsequent heterologous expression of the *epiD* gene confirmed the role of the EpiD enzyme (generally referred to as “LanD”) in the biosynthesis of the AviCys

moiety.<sup>197</sup> LanD, with flavin mononucleotide (FMN) as cofactor, catalyzes the leader-independent oxidative decarboxylation of a C-terminal Cys residue. Results of mutational analysis<sup>198</sup> and the cocrystal of EpiD bound with a peptide substrate<sup>199</sup> indicate that the terminal Cys is first oxidized by the FMN cofactor into a thioaldehyde, and a spontaneous decarboxylation then occurs to produce a (Z)-enethiolate (Figure 1.13).<sup>198,199</sup> The nucleophilic sulfur of the enethiolate then attacks the  $\beta$ -carbon of Dha or Dhb, likely through the catalysis of LanC, to form AviCys or AviMeCys, respectively.<sup>177</sup>

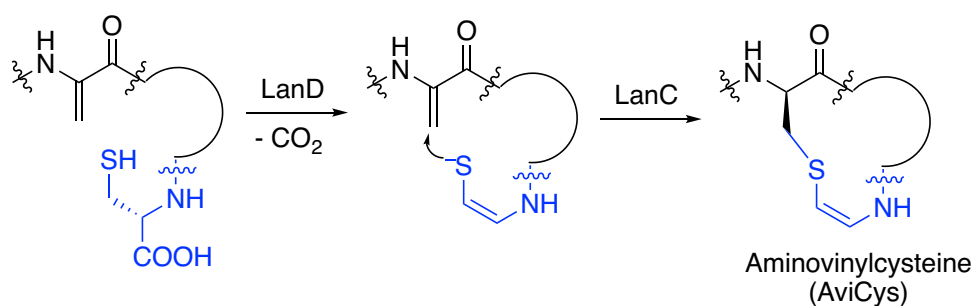


**Figure 1.13. LanD-catalyzed formation of aminovinylcysteine.**

### 1.5.2. Classification based on biosynthetic machinery

Lanthipeptides can be categorized into four classes (Figure 1.14) based on the biosynthetic machinery involved in their production.

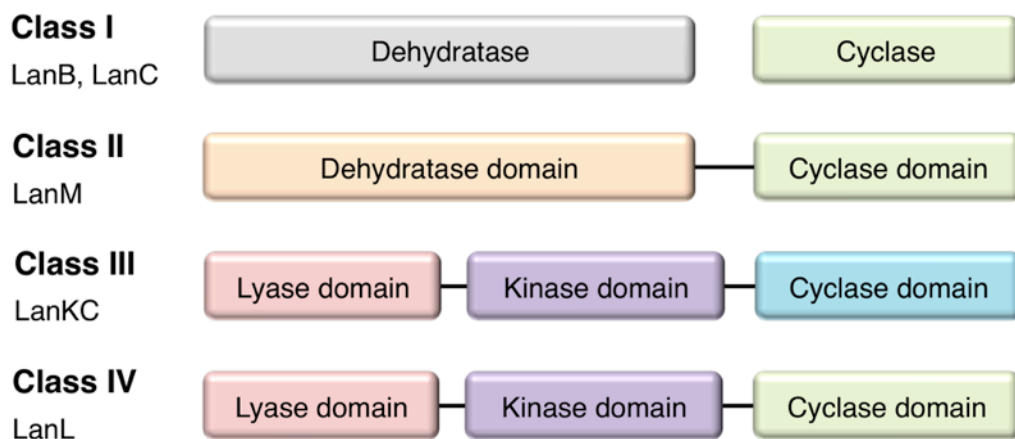


**Figure 1.14. Classification of lanthipeptides based on their biosynthetic machinery.**

Class I involves a dedicated lanthipeptide dehydratase (LanB) and cyclase (LanC). Class II systems utilize a bifunctional synthetase (LanM) comprised of an N-terminal dehydratase domain and a C-terminal cyclase domain. Class III enzymes are labionin synthetases (LanKC) with an N-terminal lyase domain, central kinase domain, and a C-terminal cyclase domain. Class IV enzymes (LanL) have homologous domains to those of LanKC except for the cyclase domain. LanKC (class III) lacks the zinc-binding ligands that are conserved in LanC (class I), LanM (class II), and LanL (class IV).

Class I lanthipeptides are modified by two separate enzymes. First, LanB dehydratase converts L-Ser and L-Thr to Dha and Dhb, respectively. This is followed by LanC cyclase-catalyzed addition of a Cys thiol to the  $\beta$ -carbon of Dha or Dhb.<sup>176</sup> For class II lanthipeptides, bifunctional synthetases (generically named as LanM) catalyze both the dehydration and cyclization steps. LanM has an N-terminal dehydratase domain and a C-terminal LanC-like cyclase domain.<sup>176</sup> The new classes of lanthipeptides, classes III and

IV, are the peptide variants that exhibit Lab/MeLab residues in addition to Lan/MeLan residues. Both classes utilize trifunctional synthetases comprised of an N-terminal lyase domain, a central Ser/Thr kinase domain, and a C-terminal cyclase domain.<sup>189</sup> The lyase and kinase domains are involved in the dehydration step, while the cyclase carries out the ring closure reaction. The enzymes for class III lanthipeptides are conventionally referred to as LanKC, while those of the class IV systems are denoted as LanL. LanKC vary from LanL in the cyclase domain, wherein LanKC does not contain the active site zinc-binding residues that are observed in LanL cyclases, as well as in LanC and LanM cyclases.<sup>189,200,201</sup>

To illustrate the genetic determinants for lanthipeptide biosynthesis, the biosynthetic gene cluster of nisin, a class I lantibiotic from *L. lactis*, is presented in Figure 1.15. Nisin is considered the prototype lantibiotic, being the founding member of the family of lanthipeptides and the most studied lantibiotic to date. As mentioned previously, nisin has been used as a natural preservative in food and livestock for around 50 years in over 80 countries worldwide.<sup>18-20</sup> In the nisin gene cluster, *nisA* encodes the structural bacteriocin gene, while modifying enzymes are encoded by *nisB* (dehydratase), *nisC* (cyclase), and *nisP* (serine protease). The gene *nisT* encodes an ABC transporter, *nisRK* encode transcriptional regulators, and genes *nisI* and *nisFEG* are involved in immunity.<sup>19</sup>

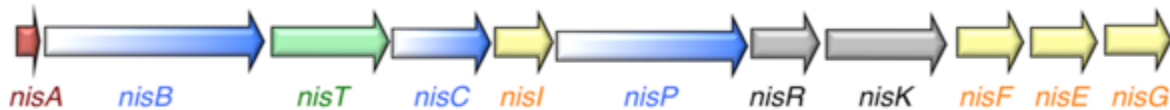


**Figure 1.15. Biosynthetic gene cluster of nisin.**

The gene *nisA* shown in red encodes the structural bacteriocin gene; genes in blue are modifying enzymes, where *nisB* encodes the dehydratase, *nisC* encodes the cyclase, and *nisP* encodes a serine protease involved in leader peptide cleavage; *nisT* in green encodes an ABC transporter; *nisRK* encode transcriptional regulators; and genes *nisI* and *nisFEG* in yellow are involved in immunity.

Structural genes for lanthipeptides (e.g. *nisA* for nisin) encode precursor peptides that bear an N-terminal leader peptide. The leader peptide normally functions as the recognition handle of the biosynthetic enzymes.<sup>42</sup> It may also be involved in the secretion of the mature peptide and in conferring immunity to the producer strain against its own lantibiotic.<sup>42</sup> Once NisA is synthesized by the ribosome, NisB dehydrates Ser and Thr residues using glutamyl-tRNA<sup>Glu</sup> as cosubstrate via a transesterification reaction from glutamyl-tRNA<sup>Glu</sup> to the Ser/Thr side chain. This is followed by  $\beta$ -elimination to yield the dehydro residues.<sup>202,203</sup> The NisC cyclase, with zinc as its cofactor, then catalyzes the addition of a Cys thiol to the dehydro residue.<sup>19,204</sup> Unlike the dehydration step catalyzed by the class I LanB dehydratases, as exemplified by NisB, the class II LanM dehydratase domain activates the Ser and Thr residues through phosphorylation with the use of ATP and Mg<sup>2+</sup>.<sup>205,206</sup> This is then followed by the elimination of the phosphate ester to yield Dha and Dhb.<sup>205,206</sup> It has been shown that for most two-component lanthipeptides, two separate LanM enzymes are required for each of the component peptide. As an example, for the lantibiotic lactacin 3147, LtnM1 carries out the modifications for Ltn $\alpha$ , while LtnM2 for Ltn $\beta$ .<sup>207</sup> The enterococcal cytolyisin is an exception, since it only utilizes one CylM synthetase to modify both precursor peptides, CylL<sub>S</sub> and CylL<sub>L</sub>.<sup>208</sup> As of this

writing, all the known two-component lanthipeptides are class II lanthipeptides.<sup>177</sup> For the class III and IV lanthipeptide synthetases, the dehydration occurs in two separate active sites. Phosphorylation takes place in the central kinase domain, while phosphate elimination is carried out by the N-terminal lyase domain.<sup>177</sup> Unlike LanM enzymes that require ATP for phosphorylation, LanKC enzymes appear to have different nucleotide specificity, with some enzymes favoring one nucleotide over the others (e.g. LanKC of the labyrinthopeptin biosynthesis requires GTP or deoxy-GTP<sup>209</sup>), while others can utilize any of the nucleotides (e.g. CurKC of curvopeptin accepts all NTPs/dNTPs<sup>210</sup>). Information regarding the nucleotide cosubstrate preference of LanL enzymes is not yet known. The mechanism of the cyclization step, particularly the installation of labionin residues, is also still unclear.<sup>177</sup>

Once the modifications have been installed, the leader peptide is cleaved off, and the mature peptide is exported. For nisin, the cleavage and transport are carried out by the membrane-associated proteins NisP and NisT, respectively.<sup>19,20,211</sup> In certain systems, the leader peptide cleavage is carried out by a bifunctional ABC transporter/protease.<sup>177</sup> In other cases, the removal of the leader peptide is accomplished by an unknown protease that is not associated with the lanthipeptide gene cluster.<sup>9,212</sup> The biosynthetic scheme for nisin is summarized in Figure 1.16.

Immunity proteins are used to protect the organism from the toxicity of the mature peptide. There are two general mechanisms by which these proteins operate, both of which are demonstrated in the nisin biosynthetic machinery. The first approach utilizes the lipoprotein NisI, which is located at the extracellular surface and binds to active nisin, thereby preventing pore formation on the cell membrane.<sup>213</sup> The second means is the active extrusion of nisin by the ABC transporter NisFEG.<sup>214</sup>



### 1.5.3. Mode of action

This section focuses on the antimicrobial activity of lanthipeptides, and only covers classes I and II lanthipeptides, since none of the reported members of classes III and IV exhibit antimicrobial activity.<sup>177</sup> Most lantibiotics elicit their antimicrobial effects by binding to lipid II, which is a precursor in the biosynthesis of cell wall peptidoglycan. The NMR solution structure of the nisin-lipid II complex showed that the N-terminal region of nisin docks to the pyrophosphate moiety of lipid II.<sup>215</sup> The potency of nisin, being active at the nanomolar range, has been attributed to its ability to inhibit cell wall synthesis by sequestering lipid II, and the formation of pores on target membranes.<sup>216</sup> It has been suggested based on fluorescence and circular dichroism experiments that the nisin-lipid II pore complexes are composed of eight nisin and four lipid II molecules.<sup>217</sup> Another lantibiotic named mersacidin was shown to target lipid II. Unlike nisin, mersacidin binds to the disaccharide unit of lipid II.<sup>218–220</sup> The two-component lantibiotic, lactacin 3147, also targets lipid II. In particular, Ltn $\alpha$  is suggested to bind to lipid II, sequentially recruiting Ltn $\beta$ , and the resulting complex then forms pores and causes potassium efflux.<sup>221</sup> Haloduracin is another two-component lantibiotic that is suggested to have a similar mode of action to that of lactacin 3147 despite the differences in their structures.<sup>222</sup> For other lantibiotics, their ability to form pores is limited by the membrane composition and thickness of sensitive strains.<sup>223</sup>

## 1.6. Significance and Overview of Projects

Despite the numerous bacteriocins that have been identified to date, only a few (e.g. nisin, pediocin PA-1) are currently used commercially.<sup>224</sup> From the initial bacteriocin discovery to reaching commercial applications, several studies have to be done to establish the properties, safety, efficacy, structure, and modes of action of these antimicrobial peptides. Elucidation of the structure of antimicrobial peptides is of paramount importance in acquiring a deeper understanding of their properties and mechanism of action. Structural information also serves as basis for the rational design of analogues with improved properties, including solubility, stability, and potency. Biosynthetic enzyme characterization is an equally important research endeavor, since a detailed understanding of the mechanism by which enzymes install various modifications in bacteriocins will provide the basis for bioengineering of bacteriocin variants with better properties. Altogether, these studies will ultimately guide the optimization of the various applications of bacteriocins in biotechnology, food and animal feed preservation, and as potential drug candidates.

The projects in this thesis focused on the characterization of bacteriocins, particularly on NMR solution structure elucidation of bacteriocins belonging to different classes, and examining their modes of action through structural analysis. This thesis also includes work on the investigation of biosynthetic machineries involved in bacteriocin production.

Chapter 2 describes the isolation, purification, and structural characterization of the bacteriocin acidocin B (AcdB), which was originally reported to be a linear bacteriocin.<sup>51</sup> Through mass spectrometry, AcdB was shown to be a circular peptide that is one amino

acid shorter than the earlier report. Its NMR solution structure was solved, and is reported as the first representative structure for its subclass. The gene cluster associated with the biosynthesis of AcdB was also sequenced and characterized.

Chapter 3 deals with the heterologous expression of leaderless bacteriocins, lacticin Q and aureocin A53, and the subsequent elucidation of their NMR solution structures.<sup>225</sup> The calculated structures resemble the saposin-like fold observed in circular bacteriocins, and homology modeling suggests that the motif is conserved among many other broad-spectrum leaderless bacteriocins. Activity assays showed that despite having a similar overall fold, there are some deviations in their modes of action.

Chapter 4 describes the identification and structure of a two-peptide bacteriocin, carnobacteriocin XY (CbnXY).<sup>226</sup> CbnX was previously reported to be a single-peptide bacteriocin, but sequence analysis and synergy assay demonstrated that it comprises a two-peptide system, with CbnY as its partner. CbnXY is the first two-peptide bacteriocin reported in carnobacteria. The NMR solution structures of both CbnX and CbnY were elucidated. Binding assays showed that CbnX and CbnY do not directly interact suggesting that a receptor is required to mediate interaction.

Chapter 5 discusses the investigation of the putative reductase, PneJ, of the two-component lantibiotic pneumococcin, comprised of PneA1 and PneA2. Attempts to heterologously express the precursor peptides, PneA1 and PneA2, are described. PneJ was successfully expressed as a stand-alone enzyme for future *in vitro* assays and crystallographic trials.

Chapter 6 presents a summary and the conclusions of the different projects described in Chapters 2 to 5. Lastly, Chapter 7 contains the materials and methods for these research projects.

## Chapter 2

### Solution Structure of the Circular Bacteriocin Acidocin B

#### 2.1. Project Background

##### 2.1.1. Classification of circular bacteriocins

Circular bacteriocins are categorized into two distinct subgroups that are mainly distinguished by their isoelectric point (pI).<sup>43</sup> The pI values of subgroup I circular bacteriocins are ~10, while those of subgroup II range from 4 to 7. The majority of known circular bacteriocins belong to subgroup I, and only two peptides are classified under subgroup II, namely gassericin A and butyrivibriocin AR10. As discussed in Chapter 1, the solution structures of enterocin AS-48, carnocyclin A, and enterocin NKR-5-3B have been solved.<sup>63,74,75</sup> These three peptides belong to subgroup I, and there are no 3D structures reported for any member of the subgroup II prior to this work.

##### 2.1.2. Acidocin B

Acidocin B (AcdB) is encoded by plasmid pCV461 from *Lactobacillus acidophilus* M46.<sup>227,228</sup> Unlike most bacteriocins, which are usually more active against species that are closely related to the producer of the bacteriocin, AcdB is more potent against *Clostridium* spp. than lactic acid bacteria.<sup>229</sup> Moreover, AcdB was shown to inhibit a broad range of Gram-positive bacteria including *Listeria monocytogenes* L2, *Clostridium sporogenes* C22/10, and *Brochothrix thermosphacta* 39.<sup>229</sup> Previously, it was

reported that the 91-mer precursor peptide of AcdB undergoes leader peptide cleavage to release a 59-mer active, linear bacteriocin.<sup>227</sup> However, the subsequent discovery of the circular bacteriocin from *Lactobacillus gasseri* LA39 named gassericin A<sup>55</sup>, to which AcdB shares 98% amino acid sequence identity with, led us to postulate that AcdB is in fact a circular peptide containing 58 residues instead of 59. In addition, previous attempts to determine the N-terminal amino acid residue of AcdB by Edman degradation were unsuccessful, further indicating that the N-terminal residue of the core peptide is blocked and may be involved in a peptide bond, likely with the C-terminal amino acid residue.<sup>227</sup> AcdB was also shown to be highly stable at extreme pH and temperature conditions, which are typical properties of circular peptides.<sup>229</sup>

### **2.1.3. Objectives**

This project aimed to confirm the circular nature of AcdB by mass spectrometry, and demonstrate that the mature peptide is composed of 58 amino acid residues instead of 59. Project goals also included the elucidation of the 3D solution structure of AcdB by NMR analysis, and homology modeling of other subgroup II circular bacteriocins based on the AcdB structure. The identification of putative members of subgroup II circular bacteriocins and construction of a phylogenetic tree are also described herein. Lastly, it was an aim of this work to determine the complete sequence of the AcdB gene cluster.

## **2.2. Results and Discussion**

### **2.2.1. Isolation of acidocin B**

AcdB was purified from an overnight culture of *L. acidophilus* M46 using hydrophobic interaction chromatographic techniques. The culture supernatant was first loaded into an Amberlite XAD-16 resin (Sigma-Aldrich), which was washed with increasing amounts of isopropanol (IPA). Spot-on-lawn assay showed that AcdB eluted in 80% IPA containing 0.1% trifluoroacetic acid. The AcdB fraction was further purified using a Bond Elut C8 solid phase extraction cartridge (Agilent), followed by RP-HPLC. A yield of ~2.5 mg of AcdB was obtained per liter of culture.

### **2.2.2. Mass spectrometry**

The molecular weight of AcdB was determined by MALDI-TOF mass spectrometry. The observed peak at 5,622.5 m/z (Figure 2.1) is consistent with the expected molecular weight for the 58-mer circular peptide, which is 18 Da lower than the linear peptide due to the loss of a water molecule during cyclization. Moreover, the molecular weight confirms that the previously reported length of 59 residues is incorrect.<sup>227</sup>

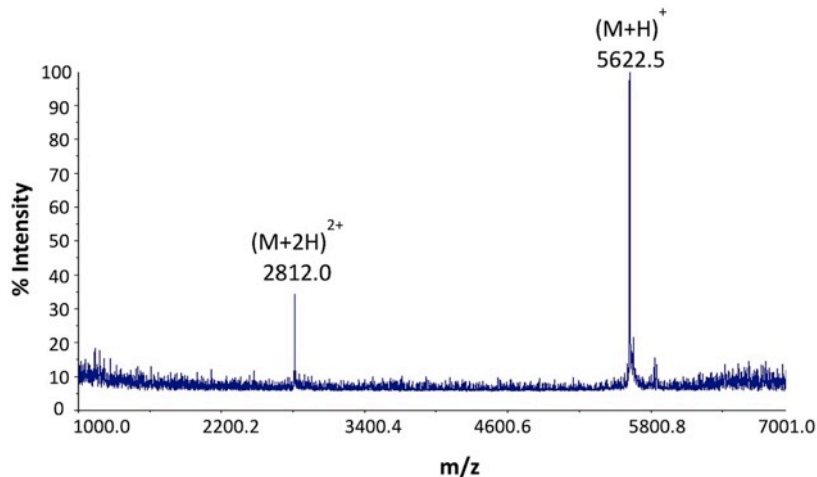


**Figure 2.1. MALDI-TOF mass spectrum of AcdB.**

Singly and doubly charged species are indicated.

To further ascertain the cyclic nature of AcdB, it was digested with trypsin and chymotrypsin, and subjected to liquid chromatography-tandem mass spectrometry (LC-MS/MS) sequencing. A high sequence coverage of 94.8% was obtained, and the detected fragments are summarized in Table 2.1. Fragment 9 indicates that Ile34 and Ala91 of the precursor peptide are linked. This confirms that the cleavage site during the maturation of the precursor peptide is between Asn33 and Ile34, consequently releasing a 58-mer mature circular peptide (Figure 2.2).

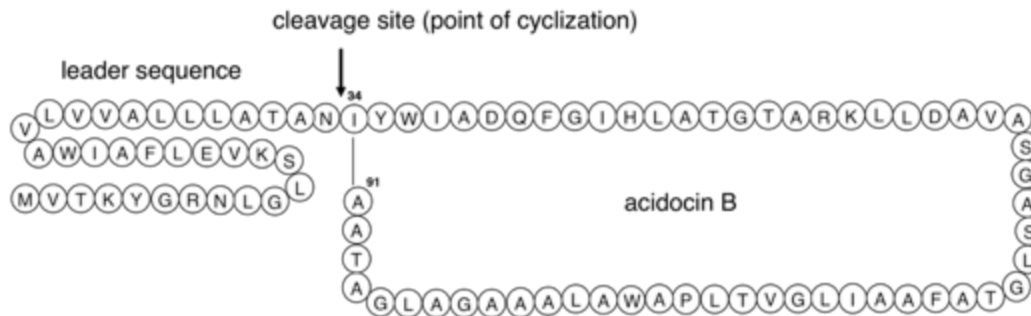


**Figure 2.2. Bead structure of AcdB precursor peptide.**

**Table 2.1. MS/MS sequencing result after trypsin-chymotrypsin digestion of AcdB**

Linear Sequence	Observed m/z	Charge	Calculated m/z
(1) --WIADQF	779.388	1	779.365
(2) ---IADQFGI HL	507.276	2	1013.534
(3) ---IADQFGI HLATGT	672.360	2	1343.688
(4) -----K L L D A V A S G A S L G T A F	760.929	2	1520.825
(5) -----L L D A V A S G A S L G T A F	696.886	2	1392.730
(6) -----A I L G V	472.290	1	472.306
(7) -----G V T L P A W	743.447	1	743.401
(8) -----A L A A A G A L	657.446	1	657.386
(9) I Y -----A A A G A L G A T A A	1120.619	1	1120.592
I Y W I A D Q F G I H L A T G T A R K L L D A V A S G A S L G T A F A A I L G V T L P A W A L A A A G A L G A T A A ← Complete linear sequence			

\*Ala17, Arg18, Ala35 were inferred from the deduced amino acid sequence from DNA sequence analysis.

### 2.2.3. Circular dichroism spectroscopy

A prerequisite to structure elucidation by NMR spectroscopy is the determination of an appropriate solvent system for dissolution of the peptide. This requires that the peptide be highly soluble and structured in a given solvent. Different solvent systems were screened for AcdB and circular dichroism (CD) spectroscopy was used to estimate the secondary structure content of AcdB in the various solvent systems tested. Previously, gassericin A was shown to be insoluble in aqueous conditions due to its high hydrophobic character.<sup>82</sup> This was also observed for AcdB in buffered aqueous solutions and organic solvents. AcdB was either completely insoluble or had a solubility that was below the concentration required for NMR studies. Hence, detergent micelles were considered, specifically with the use of sodium dodecyl sulfate (SDS) or dodecylphosphocholine (DPC), which are the most commonly used detergents in protein NMR. AcdB was completely soluble in both systems and CD analysis showed that AcdB in SDS and DPC

was 56% and 57%  $\alpha$ -helical, respectively (Figure 2.3). The anionic character of SDS mimics the negatively charged phospholipids in bacterial membranes, while the zwitterionic property of DPC resembles the neutral mammalian membranes.<sup>230</sup> Since there was no substantial difference in the structural content of AcdB in SDS and DPC, SDS was chosen for NMR analysis to better mimic bacterial membranes.

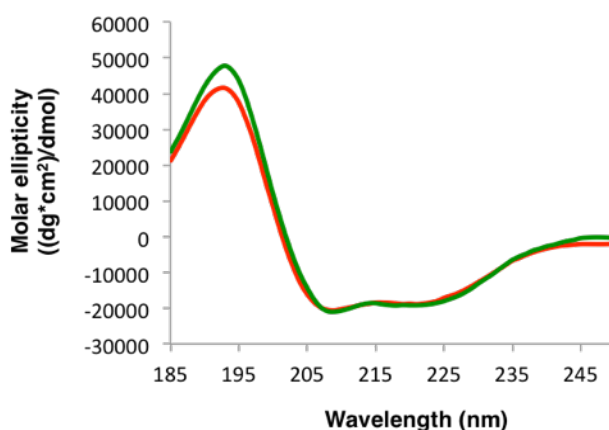


**Figure 2.3. CD profile of AcdB in SDS (red) and DPC (green).**

## 2.2.4. NMR solution structure of acidocin B

### 2.2.4.1. NMR data acquisition

In order to produce <sup>13</sup>C,<sup>15</sup>N-Ac dB, *L. acidophilus* M46 was grown in various <sup>13</sup>C,<sup>15</sup>N-enriched media, including Celtone Complete medium (Cambridge Isotope Laboratories Inc.), Bioexpress-1000 (Cambridge Isotope Laboratories Inc.), and a manually prepared labelling medium that was previously used for another *Lactobacillus* strain.<sup>231</sup> *L. acidophilus* M46, however, could not be cultured in any of the tested media. Hence, two-dimensional homonuclear <sup>1</sup>H,<sup>1</sup>H-TOCSY and <sup>1</sup>H,<sup>1</sup>H-NOESY experiments were performed using unlabelled Ac dB in deuterated SDS micelles. The well-dispersed

resonances and substantial number of nuclear Overhauser effect (NOE) crosspeaks facilitated the elucidation of the 3D solution structure of AcdB.

#### 2.2.4.2. Structure calculations

The TOCSY and NOESY spectra were processed using NMRPipe<sup>232</sup>, and were overlaid in NMRView<sup>233</sup>. Resonances were assigned sequentially based on the  $H^N$ - $H^{\alpha}$  crosspeaks. Structural calculations were performed using the assigned chemical shifts, and a combination of manually and automatically assigned NOEs. These data were inputted into CYANA 2.1<sup>234</sup>, wherein a family of 20 calculated structures was obtained (Figure 2.4).

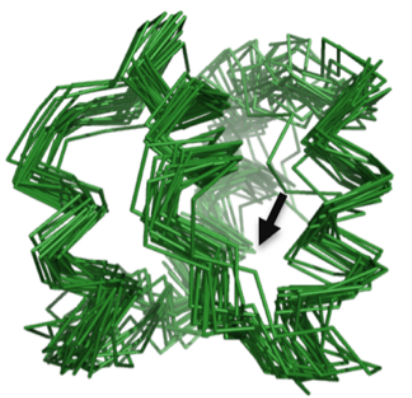


**Figure 2.4. Superimposition of the 20 lowest energy conformers of AcdB.**

The black arrow indicates the N- to C-termini linkage.

Table 2.2 summarizes the structural statistics for the calculation of the structure of AcdB. Briefly, the final calculation utilized 909 NOE crosspeaks consisting of 558 short-range, 296 medium-range, and 55 long-range NOEs. A root-mean-square deviation (RMSD) value of 1.48 Å was obtained, which decreased to 1.26 Å upon excluding the

flexible regions. Lastly, the output Ramachandran data indicate that all  $\phi$  or  $\psi$  backbone angles are within the allowed regions.

**Table 2.2. Structure calculation statistics for AcdB**

<b>NOE restraints</b>	909
short-range, $ i-j  \leq 1$	558
medium-range, $1 <  i-j  < 5$	296
long-range, $ i-j  \geq 5$	55
average target function value ( $\text{\AA}^2$ )	$0.37 \pm 0.06$
<b>RMSD for residues 1-58 (full peptide)</b>	
backbone atoms ( $\text{\AA}$ )	$1.48 \pm 0.47$
heavy atoms ( $\text{\AA}$ )	$1.82 \pm 0.50$
<b>RMSD for the <math>\alpha</math>-helices</b>	
backbone atoms ( $\text{\AA}$ )	$1.26 \pm 0.44$
heavy atoms ( $\text{\AA}$ )	$1.47 \pm 0.50$
<b>Ramachandran plot</b>	
$\Phi/\Psi$ in most favored regions	74.6%
$\Phi/\Psi$ in additionally allowed regions	25.4%
$\Phi/\Psi$ in generously allowed regions	0.0%
$\Phi/\Psi$ in disallowed regions	0.0%

### 2.2.4.3. Structural features

The structure of AcdB is composed of four right-handed  $\alpha$ -helices that are separated by loops composed of three to six residues. Helices 1, 2, 3, and 4 are comprised of Gly15 to Gly27 (13 residues), Gly31 to Val40 (10 residues), Ala44 to Ala52 (9 residues), and Ala56 to Phe8 (11 residues), respectively. The fourth helix bears the N- to C-termini linkage. The helices are folded into a compact globular bundle with a central pore (Figure 2.5).

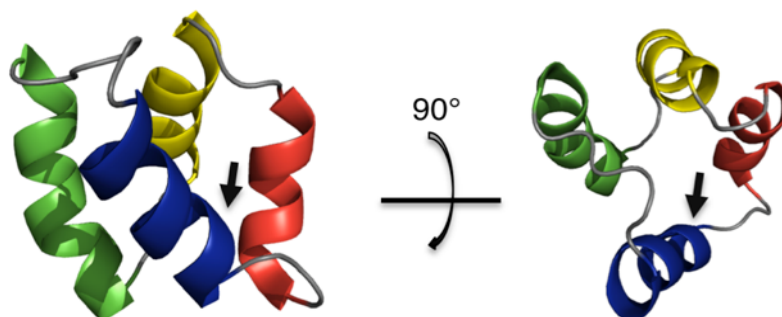


**Figure 2.5. NMR solution structure of AcdB (PDB: 2MWR).**

Helix 1 is shown in blue, helix 2 in green, helix 3 in yellow, and helix 4 in red.  
A black arrow indicates the N- to C-termini linkage.

The PyMOL<sup>235</sup> hydrophobicity analysis function revealed that helices 1, 2, and 4 of AcdB are amphipathic (Figure 2.6A). The hydrophobic residues of these amphipathic helices are buried in the core of the molecule, while the relatively hydrophilic residues are exposed on the surface. Figure 2.6A shows that helix 3 is completely hydrophobic (red color), while helix 1 has the most pronounced amphipathic character as illustrated by a distinct white strip (hydrophilic strip) located at the exposed surface. On the other hand, helices 2 and 4 exhibit only weak amphipathic character.

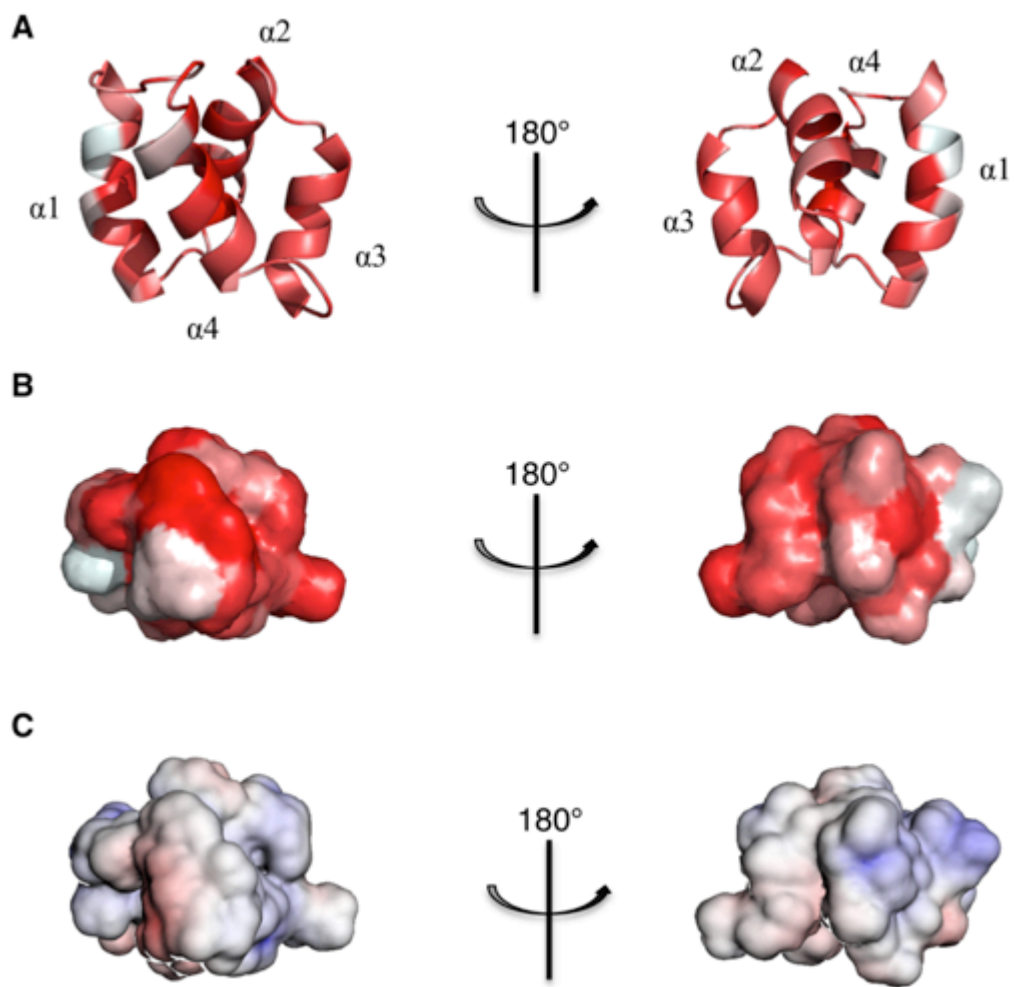


**Figure 2.6. Surface analysis of AcdB.**

(A) 3D structure showing the amphipathicity of the helices, and B) hydrophobic surface map, wherein hydrophobic regions are shown in red, while hydrophilic regions are in white. (C) Electrostatic potential surface map, wherein cationic regions are shown in blue, while anionic regions are in red.

The surface maps (Figures 2.6B and 2.6C) further point out that AcdB is highly hydrophobic. The hydrophobic surface map (Figure 2.6B) shows that the solvent exposed surface is mainly covered with hydrophobic patches (red regions), while the electrostatic potential surface map (Figure 2.6C) shows that the surface is largely uncharged (white regions). This is consistent with the primary sequence of AcdB, which only contains 2 anionic (Asp6 and Asp22) and 3 cationic (His11, Arg18, Lys19) amino acid residues among the 58 total number of residues.

#### **2.2.4.4. Comparison to subgroup I circular bacteriocins**

Structure elucidation is a prerequisite in understanding the properties and the mode of action of antimicrobial peptides. Prior to this work, only two 3D structures of circular bacteriocins have been reported, specifically those of enterocin AS-48 and carnocyclin A.<sup>74,75</sup> More recently, the structure of enterocin NKR-5-3B was also elucidated.<sup>63</sup> These three circular peptides were shown to have localized positive charges on their surfaces, a property that has been implicated with their initial binding to negatively charged phospholipids on the cell membrane of target organisms.<sup>59,236</sup> Mode of action studies demonstrated that enterocin AS-48 causes membrane permeabilization and formation of pores that allow the discharge of ions and low molecular weight substances, while carnocyclin A acts by transporting anions through the membrane.<sup>78,81</sup> Details on the mode of action of enterocin NKR-5-3B have yet to be determined, however, it is important to note that the overall fold of enterocin NKR-5-3B highly resembles those of enterocin AS-48 and carnocyclin A. This suggests that these three peptides could potentially share some similarities in the mechanism by which they interact with target membranes and induce

cell death. Enterocin AS-48, carnocyclin A, and enterocin NKR-5-3B are all members of subgroup I circular bacteriocins, while AcdB belongs to subgroup II. The structure of AcdB is therefore the first representative structure for subgroup II circular bacteriocins.

Subgroup I circular bacteriocins have high pI values (~10) and characteristic cationic surfaces. On the other hand, subgroup II circular bacteriocins have lower pI values and are mainly composed of neutral amino acid residues. These differences in their properties may implicate variations in their structures and modes of action. To further investigate the similarities and differences between the two circular bacteriocin subgroups, the structure of AcdB was compared to a representative member of subgroup I circular bacteriocins. Carnocyclin A was chosen for analysis because its length (60 residues) is most similar to the length of AcdB (58 residues). Enterocin AS-48 is composed of 70 residues and has five  $\alpha$ -helices, while enterocin NKR-5-3B has 64 residues.

Subgroup I circular bacteriocins have been shown to assume a common overall saposin-like fold, despite having low sequence similarity.<sup>63,74,75</sup> It was previously proposed that subgroup II circular bacteriocins may also share the same structural motif. While carnocyclin A and AcdB are both composed of four helices that are separated by short loop segments, their overall fold is not the same. The structural differences may be due to a number of factors, including the solvent systems used. Carnocyclin A was dissolved in water, while AcdB was prepared in a membrane-mimicking SDS micelle system. Several studies have shown that peptides can undergo conformational changes from a free state in water to a membrane-bound form in membrane mimetic solvents.<sup>237–</sup>  
<sup>239</sup> It was not possible to solve the structure of AcdB in water because its solubility in water was below the required concentration for NMR analysis. Hence, it was not feasible

to compare the structures of AcdB and carnocyclin A in the same solvent system. Aside from the solvent systems used, the variations in the overall fold of AcdB and carnocyclin A may also be attributed to the inherent differences of their physical properties. Carnocyclin A, like other subgroup I circular bacteriocins, has several basic residues rendering the surface of the molecule highly cationic.<sup>75</sup> On the other hand, AcdB only contains 3 basic residues. Sequence alignment of carnocyclin A and AcdB using Clustal W<sup>240</sup> further reveals a low sequence identity of 17% (Figure 2.7).

```

Acidocin B      IYWIADQFGIHLATGTARKLLDAVASGASLGTAFPAAILGVTLPAWALAAA--GA---LGATAA--- 58
Carnocyclin A  -----LVAYGIAQGTAEKVVSLINAGLTVGSIISILGGVTVGLSGVFTAVKAAIAKQGIKKAIQL 60
               ..  :*  ***.*:..  :  :*  :::  ::  :  :::  .:  :*  .*  *  .  *

```

**Figure 2.7. Amino acid sequence alignment of AcdB and carnocyclin A.**

The  $\alpha$ -helical regions are highlighted in gray. Conserved, conservative, and semi-conservative substitutions are indicated by an asterisk, colon, and period, respectively.

As a result of the differences in their primary sequences, the four helices of carnocyclin A are distinctly amphipathic, while AcdB only has 1 amphipathic and 2 weakly amphipathic helices. Consequently, their surface properties are also different. AcdB displays a highly uncharged and hydrophobic surface, while carnocyclin A has a prominent positively charged surface (Figure 2.8). Altogether, the structure of AcdB is best described as an  $\alpha$ -helical bundle with a hydrophobic surface, while that of carnocyclin A assumes a saposin-like fold with a cationic surface.

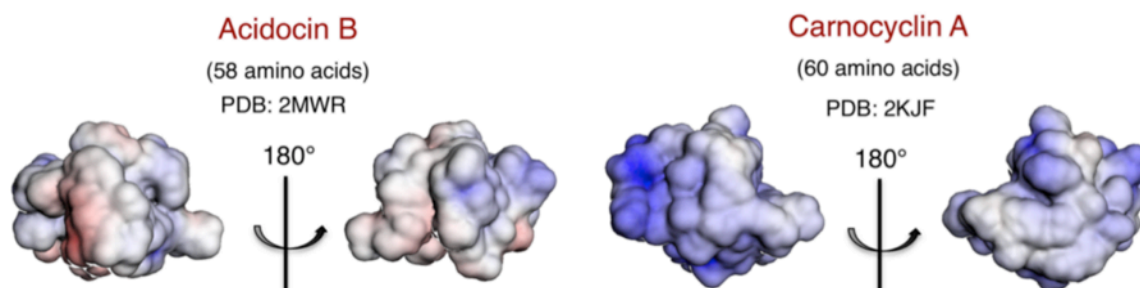


**Figure 2.8. Comparison of electrostatic potential maps of AcdB and carnocyclin A.**

Cationic regions are shown in blue, while anionic regions are in red.

This suggests that while electrostatic interactions with target bacterial membranes are critical for carnocyclin A, hydrophobic interactions appear to play a more important role for AcdB.

#### **2.2.4.5. Homology modeling of the other subgroup II circular bacteriocins**

There are two other known subgroup II circular bacteriocins, namely gassericin A and butyrivibriocin AR10, that are produced by *L. gasseri* LA39 and *Butyrivibrio fibrisolvens* AR10, respectively. *Lactobacillus reuteri* LA6 was previously reported to produce another subgroup II circular bacteriocin named reutericin 6, but it was later proven to be identical to gassericin A.<sup>241</sup> Gassericin A and AcdB share 98% amino acid sequence identity, only varying in residue 24, where AcdB has valine and gassericin A has methionine (Figure 2.9). Butyrivibriocin AR10, on the other hand, shares only 47% identity to the amino acid sequence of AcdB (Figure 2.9).

```

Acidocin B      IYWIADQFGIHLATGTARKLLDAVASGASLGTAFAAILGVTLPAWALAAAGALGATAA 58
Gassericin A   IYWIADQFGIHLATGTARKLLDAMASGASLGTAFAAILGVTLPAWALAAAGALGATAA 58
Butyrvibriocin AR10 IYFIADKMG IQLAPAWYQDIVNWSAGGTLTTGF A I I VGVTVPAWIAEAAA AFGIASA 58
**:*:*:*:*:*:*..  .:..: :*:.* *.* *:*:*:*:*  **:*:* :*:

```

**Figure 2.9. Amino acid sequence alignment of known subgroup II circular bacteriocins.**

Conserved, conservative, and semi-conservative substitutions are indicated by an asterisk, colon, and period, respectively.

The 3D structures of gassericin A and butyrvibriocin AR10 were modeled based on homology to the solved structure of AcdB using the SWISS-MODEL server.<sup>242</sup> The structure and surface properties of gassericin A were found to be very similar to AcdB, which was expected due to the very high amino acid sequence identity between these two peptides (Figure 2.10). Butyrvibriocin AR10 also assumes a similar fold, but slightly different surface properties due to the presence of an additional acidic residue in its primary sequence (Figure 2.10).

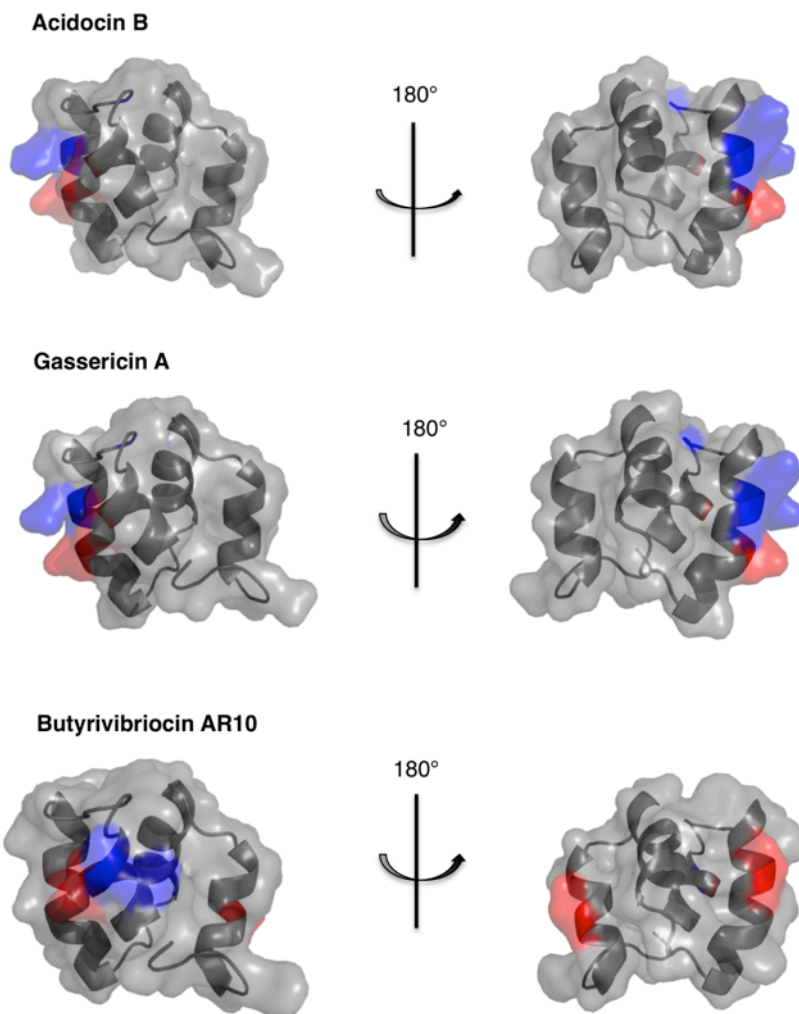


**Figure 2.10. Homology models of gassericin A and butyrivibriocin AR10 as calculated by the SWISS-MODEL server<sup>242</sup>.**

The structure of AcdB was used as template.  
Basic residues are shown in blue; acidic residues are in red.

### 2.2.5. Gene cluster sequencing

Plasmid pCV461 from *L. acidophilus* M46 was previously reported to contain the structural gene for AcdB.<sup>227</sup> Furthermore, a partial nucleotide sequence (2.2 kb) of the AcdB gene cluster has been obtained.<sup>227</sup> With the assistance of Dr. Marco van Belkum, plasmid pCV461 was re-isolated from a culture of *L. acidophilus* M46 and primer walking was performed to completely identify the genes involved in the AcdB biosynthetic machinery. A 3537 bp nucleotide sequence was obtained, which was analyzed and shown to contain the gene cluster *aciBCADITE* (Figure 2.11). This cluster was found to be analogous to that of gassericin A.

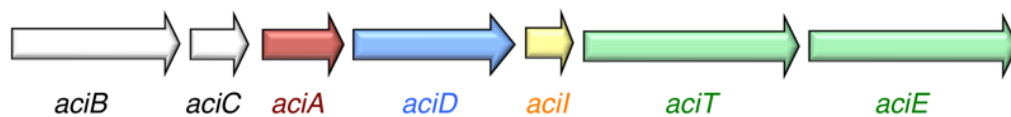


**Figure 2.11. Biosynthetic gene cluster of AcdB.**

The structural bacteriocin gene (*aciA*) is shown in red; DUF95 protein gene (*aciD*) is in blue; immunity protein gene (*aciI*) is in yellow; ATP-binding protein gene (*aciT*) is in green; *aciE* gene encoding a membrane transporter is also in green; and genes *aciB* and *aciC* encoding unknown proteins that contain putative transmembrane domains are in white.

Table 2.3 lists the characteristics of the proteins encoded by the AcdB gene cluster. It also shows a comparison of the amino acid sequences of AciBCADITE to their corresponding homologs in the gassericin A gene cluster. The proteins are highly similar, and sometimes 100% identical, which further supports that AcdB belongs to the group of circular bacteriocins. All of the proteins, except for the ATP-binding protein AciT, contain putative transmembrane segments. AciD was determined to belong to the DUF95 family of membrane proteins based on BLAST results. As mentioned in Chapter 1, the presence

of membrane proteins that belong to the DUF95 family is a characteristic feature of circular bacteriocin gene clusters.<sup>69</sup> The partial sequence of the AcdB gene cluster that was previously reported indicated that AciD is composed of 114 amino acids.<sup>227</sup> However, the more extensive sequencing performed in this study showed that AciD is in fact composed of 162 amino acids. Sequence homology suggests that AciI is likely an immunity protein, while AciTE may be responsible for the secretion of AcdB.<sup>73,243</sup> The functions of AciB and AciC, located upstream AciA, are yet to be determined.

**Table 2.3. Characteristics of predicted proteins encoded by the AcdB gene cluster**

<b>Protein</b>	<b>Size (a.a.)</b>	<b>TM<sup>a</sup></b>	<b>Function</b>	<b>Number of amino acids identical to homologs encoded by gassericin A gene cluster</b>
AciB	174	5	unknown	173/174
AciC	60	2	unknown	60/60
AciA	91	2	acidocin B precursor	88/91
AciD	162	4	unknown, DUF95 family	160/162
AciI	53	1	immunity	53/53
AciT	226	0	ATP-binding protein	225/226
AciE	212	6	membrane transporter	209/212

<sup>a</sup>TM, number of putative transmembrane domains deduced using SOSUI program<sup>244</sup>.

### 2.2.6. Bioinformatics and phylogenetic analysis

Currently, there are only three known members of subgroup II circular bacteriocins, gassericin A, butyrivibriocin AR10, and AcdB. Hence, a BLAST<sup>245</sup> search was done to identify other putative members of this subgroup using a 40% identity threshold relative to the precursor peptide sequence of AcdB. At least seven putative subgroup II circular bacteriocins from various species were identified. The sequences were aligned using



subgroup II circular bacteriocins identified in this work consist of 22 to 42 residues, which are longer than the leader peptides of most subgroup I circular bacteriocins.

Considering the putative cleavage sites indicated in Figure 2.12, the sequences of the mature peptides were used to construct a phylogenetic tree with nisin A as the outgroup (Figure 2.13). Figure 2.13 also indicates the pI values, ranging from 3.9 to 8.7, of each peptide.

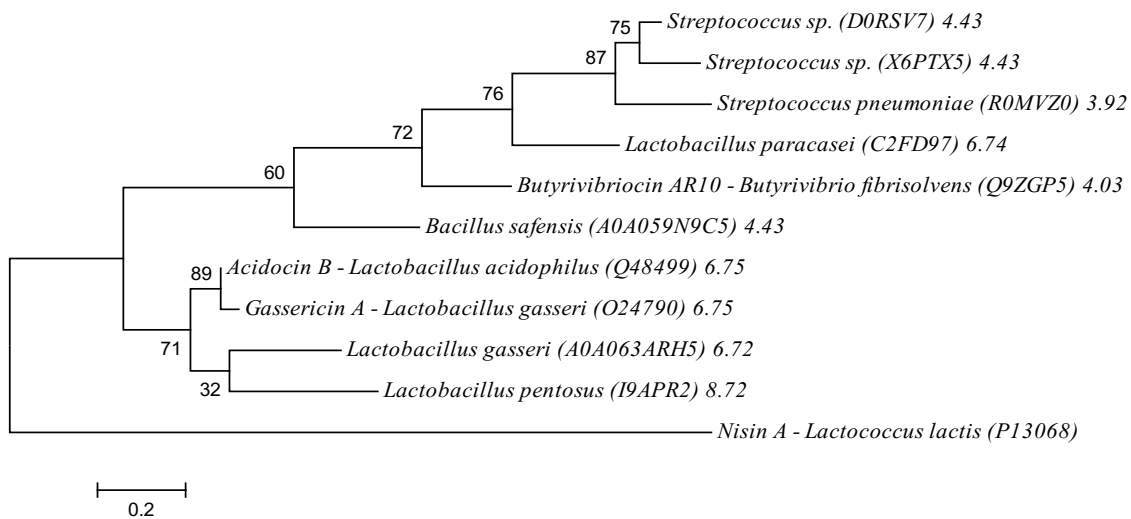


**Figure 2.13. Phylogenetic tree of subgroup II circular bacteriocins with nisin A as outgroup.**

Known members are AcdB, gassericin A, and butyrivibriocin AR10. Putative members identified using BLAST<sup>245</sup> are indicated with their source organism. The isoelectric point of each peptide, as predicted by ExPASy ProtParam tool<sup>246</sup>, is indicated at the end of each name. The evolutionary history was inferred by using the maximum likelihood method based on the JTT matrix-based model<sup>247</sup>. The tree with the highest log likelihood (-827.3975) is shown. The percentage of trees in which the associated taxa clustered together is shown next to the branches. Initial tree(s) for the heuristic search were obtained automatically by applying Neighbor-Join and BioNJ algorithms to a matrix of pairwise distances estimated using a JTT model, and then selecting the topology with superior log likelihood value. The tree is drawn to scale, with branch lengths measured in the number of substitutions per site. The analysis involved 11 amino acid sequences. All positions containing gaps and missing data were eliminated. There were a total of 49 positions in the final dataset. Evolutionary analyses were conducted in MEGA6<sup>248</sup>.

The phylogenetic tree shows that these bacteriocins can be classified into 2 subclades. The first subclade is comprised of circular peptides produced by *Lactobacillus*

spp., including AcdB and gassericin A. The second subclade, on the other hand, is more diverse and is comprised of peptides produced by *Bacillus*, *Lactobacillus*, *Butyrivibrio*, and *Streptococcus* strains. Butyrivibriocin AR10 belongs to the latter subclade.

### **2.3. Conclusions and Future Directions**

AcdB was purified from *L. acidophilus* M46 and its cyclic nature was ascertained by mass spectrometry. Furthermore, AcdB was shown to consist of 58 amino acids, correcting previous reports indicating that it is a linear 59-mer peptide. The solution structure of AcdB in SDS micelles, a membrane-mimicking system, was also elucidated. This is the first reported structure of a subgroup II circular bacteriocin. AcdB was shown to consist of a bundle of four helices that are folded to form a compact, globular molecule. Unlike subgroup I circular bacteriocins, which have highly cationic surfaces, the solvent-exposed surface of AcdB is dominated by hydrophobic and uncharged residues. This implies that hydrophobic interactions may be mainly involved in the binding of AcdB to the cell membrane of target organisms. Homology models of the other known subgroup II circular bacteriocins, gassericin A and butyrivibriocin AR10, were created and were demonstrated to share a similar overall fold with AcdB.

In addition to structural analysis of AcdB, its gene cluster (*aciBCADITE*) was sequenced and shown to be highly similar to that of gassericin A. This further supports that AcdB is a subgroup II circular bacteriocin. BLAST search was then performed to identify other putative members of this subgroup, and at least seven peptides were detected. Sequence alignment of the known and putative members of this subgroup revealed a highly conserved asparagine residue at the cleavage site of the precursor

peptide, suggesting that an asparaginyl endopeptidase may be involved in the maturation of subgroup II circular bacteriocins. Lastly, a phylogenetic tree was constructed using the peptide sequences of AcdB, gassericin A, butyrivibriocin AR10, and other putative members of this subgroup. The results show that the peptides can be divided into two subclades. The first subclade consists of peptides from *Lactobacillus* spp., while the second subclade is comprised of peptides from various strains including *Bacillus*, *Lactobacillus*, *Butyrivibrio*, and *Streptococcus*.

Future studies may focus on uncovering the mode of action of AcdB, relate it to its structural properties, and compare with subgroup I circular bacteriocins. It would be of interest to resolve the conformational changes that AcdB undergoes upon binding to the target membrane, and to determine if a receptor is involved in its interaction with the membrane. Moreover, studies on the biosynthetic machinery of circular bacteriocins in general, specifically on the mechanism by which the peptides are cyclized, have yet to be pursued. Results of the sequence alignment in this study suggest that an asparaginyl endopeptidase may be involved in the leader peptide cleavage and potentially the cyclization of the core peptide. However, the gene cluster of AcdB does not include an asparaginyl endopeptidase, albeit three genes encode proteins that still have unknown functions. It may also be possible that an enzyme that is not associated with the gene cluster is responsible for the leader peptide cleavage and core peptide cyclization. A complete understanding on how these circular bacteriocins are processed may facilitate bioengineering of circular bacteriocins with optimized properties that can be exploited in food preservation and other antimicrobial applications.

# Chapter 3

## Structures of Leaderless Bacteriocins

### Lacticin Q and Aureocin A53

#### 3.1. Project Background

##### 3.1.1. Lacticin Q and aureocin A53

Lacticin Q (LnqQ) and aureocin A53 (AucA) are produced by *Lactococcus lactis* QU 5 and *Staphylococcus aureus* A53, respectively. They share 47% amino acid sequence identity, and are among the longest known leaderless bacteriocins. LnqQ consists of 53 amino acid residues, while AucA has 51 residues (Figure 3.1).

```

LnqQ   MAGFLKVVQLLAKYGSKAVQWAWANKGKILDWLNAGQAIWVVS KIKQILGIK   53
AucA   -MSWLNFLKYIAKYGKKAVSAAWKYKGVLEWLNVGPTLEWVWQK LKKIAGL-  51
      .:*****: :*****.***. **  ***:*:***.* :***** .*:*** *:
```

**Figure 3.1. Amino acid sequence alignment of LnqQ and AucA.**

Conserved, conservative, and semi-conservative substitutions are indicated by an asterisk, colon, and period, respectively.

Aside from the recent work on lactococcal small bacteriocin B (LsbB) and enterocin K1 (EntK1), as described in Chapter 1, most mode of action studies on leaderless bacteriocins have specifically focused on LnqQ and AucA.<sup>102,116,118,249,250</sup> Both peptides are highly cationic, with LnqQ having a net charge of +6 and an isoelectric point (pI) of 10.8, while AucA has a net charge of +8 and pI of 10.7. Both peptides are suggested to

interact with target membranes without having to bind to any specific receptor, and have been found to be active against a broad spectrum of bacterial strains.<sup>116,118,250</sup> In particular, LnqQ is active in nanomolar range against different strains of *Bacillus*, *Enterococcus*, *Lactobacillus*, and *Lactococcus*.<sup>102</sup> On the other hand, AucA was reported to be active against strains of *Listeria*, *Enterococcus*, *Staphylococcus* (including methicillin-resistant strains; MRSA), and *Micrococcus*.<sup>95,116</sup> Previous studies demonstrated that LnqQ acts on target organism by promoting the build-up of detrimental hydroxyl radicals, and through the leakage of cell contents due to the formation of large toroidal pores that are 4.6 to 6.6 nm in diameter.<sup>117,118,250</sup> On the other hand, AucA was suggested to compromise membrane potential and macromolecular synthesis, as well as promote leakage of vital compounds.<sup>116</sup> Unlike LnqQ, AucA was proposed to act through generalized membrane disruption, instead of pore formation.

### **3.1.2. Objectives**

Despite the previous studies on LnqQ and AucA, there has been no report on their 3D structures prior to this work. Hence, this project mainly aimed to elucidate the NMR solution structures of LnqQ and AucA. It was also aimed to compare the structures of LnqQ and AucA to other known 3D structures of relevant bacteriocins, to perform homology modeling of other leaderless bacteriocins, to compare the antimicrobial activities of LnqQ and AucA against a variety of strains, and to test for synergy between LnqQ and AucA.

## **3.2. Results and Discussion**

### **3.2.1. Attempted expression and purification of MBP-lacticin Q**

Dr. Kaitlyn M. Towle and Dr. Christopher T. Lohans previously attempted to chemically synthesize LnqQ and AucA. However, the size of the peptides rendered their synthesis unsuccessful. Isolation from the producer strains was also not possible because the Vederas group has no access to the organisms. Hence, heterologous expression of LnqQ in *Escherichia coli* was attempted, initially through the use of the maltose-binding protein (MBP) fusion system. Cloning of *lnqQ* into the pMAL-c2x vector was accomplished with the assistance of Dr. Marco van Belkum and Dr. Christopher T. Lohans. MBP-LnqQ was then successfully expressed and purified using amylose column chromatography as monitored by SDS-PAGE and MALDI-TOF MS. However, several optimization attempts to cleave the MBP tag using FXa protease (i.e. optimizing temperature and protease concentration, refolding experiments) were unsuccessful.

### **3.2.2. Expression and purification of SUMO-lacticin Q and SUMO-aureocin A53**

Due to failure to isolate LnqQ using the MBP fusion system, the small ubiquitin-like modifier (SUMO) fusion technology was considered. With the assistance of Dr. Marco van Belkum and Dr. Christopher T. Lohans, *lnqQ* and *aucA* were cloned into the pET SUMO vector. The His-tagged SUMO fusion proteins were then expressed and purified by Ni-NTA affinity chromatography. Treatment of the His-tagged SUMO proteins with His-tagged SUMO protease at optimized cleavage conditions successfully removed the tag. The cleavage reaction was monitored using tricine SDS-PAGE and was shown to be

complete after three hours of incubation (Figure 3.2). The cleaved fusion proteins were then purified using a second Ni-NTA affinity chromatography step, followed by RP-HPLC.

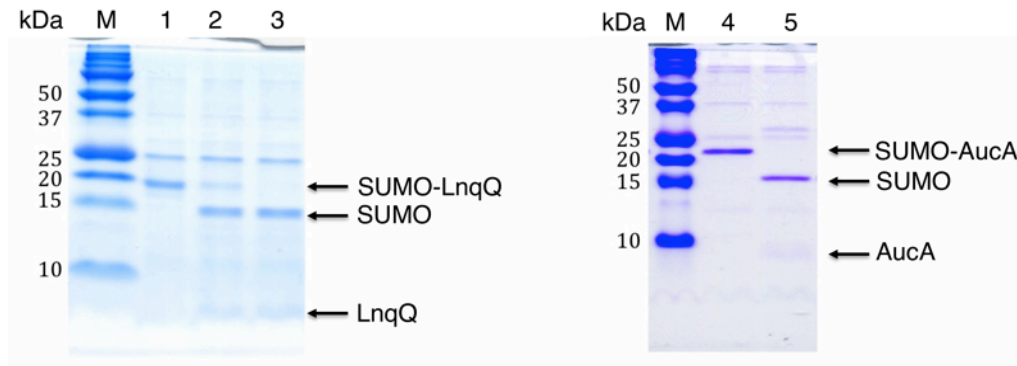


**Figure 3.2. Tricine SDS-PAGE gels of the pilot cleavage trials for (A) SUMO-LnqQ and (B) SUMO-Auca fusion proteins.**

Lanes: M, protein markers; 1, SUMO-LnqQ fusion protein; 2, 1-hr cleavage of SUMO-LnqQ; 3, 3-hr cleavage of SUMO-LnqQ; 4, SUMO-Auca fusion protein; 5, 3-hr cleavage of SUMO-Auca.

Three to five mg of purified peptides were obtained per liter of Terrific Broth culture. MALDI-TOF MS confirmed the identities of LnqQ and AucA, with peaks at 5,898.9 m/z and 5,985.4 m/z for LnqQ and AucA, respectively (Figure 3.3). The N-terminal methionine of the naturally produced LnqQ and AucA is formylated, which is not the case for the recombinant peptides produced in this study. Regardless of the absence of this formyl group, the recombinant LnqQ and AucA were found to be active against carnobacteria, enterococci, lactobacilli, lactococci, and staphylococci based on spot-on-lawn assays.

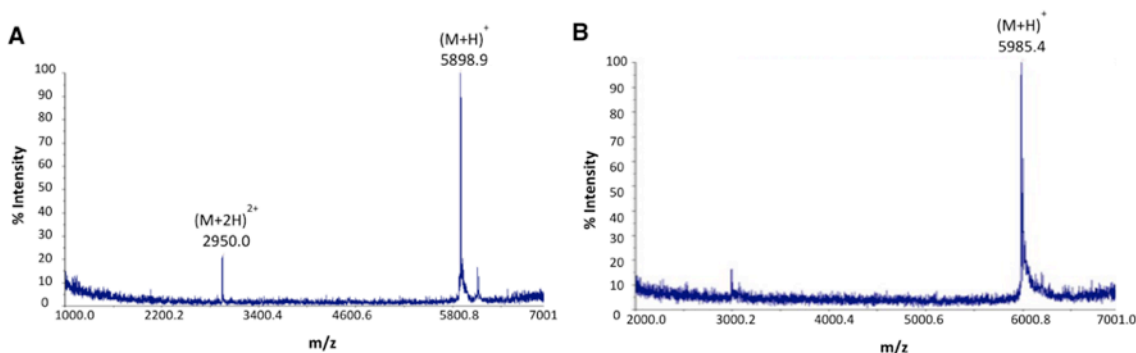


**Figure 3.3. MALDI-TOF MS spectra of (A) LnqQ and (B) AucA.**

### 3.2.3. Circular dichroism spectroscopy

LnqQ and AucA were dissolved in water, 20 mM phosphate buffer (pH 6.0), or 25% trifluoroethanol, and subjected to circular dichroism (CD) analysis in order to identify the solvent in which the peptides have the highest propensity to assume a defined structure. Both peptides were highly  $\alpha$ -helical in all solvent systems, with LnqQ and AucA being most structured in 25% trifluoroethanol and water, respectively (Figure 3.4, Table 3.1). These solvents were consequently used to prepare the samples for NMR data acquisition.

Linear bacteriocins are oftentimes unstructured in aqueous conditions.<sup>105,157,251</sup> This makes LnqQ and AucA distinct, since they are well-folded in water. In fact, the percent  $\alpha$ -helicity of AucA in water is as high as 80%, while a significant value of 48% is the  $\alpha$ -helical content of LnqQ in water. The leaderless bacteriocins, enterocin 7A (Ent7A) and 7B (Ent7B), were also found to be structured in aqueous conditions.<sup>112</sup> This trend was likewise observed for the circular bacteriocins carnocyclin A, enterocin AS-48, and enterocin NKR-5-3B.<sup>63,74,75</sup>

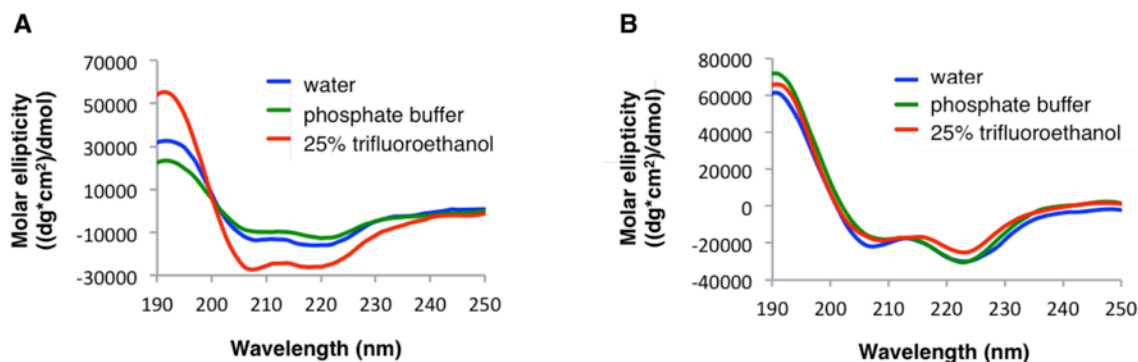


Figure 3.4. CD spectra of (A) LnqQ and (B) AucA in various solvent systems.

Table 3.1. Percentage  $\alpha$ -helicity of LnqQ and AucA in various solvent systems

Solvent	$\alpha$ -Helicity (%)	
	LnqQ	AucA
water	48	80
20 mM phosphate buffer (pH 6.0)	39	78
25% trifluoroethanol	71	64

### 3.2.4. NMR solution structures of lactacin Q and aureocin A53

#### 3.2.4.1. Structure calculations

The structures of LnqQ and AucA were calculated using CYANA 2.1<sup>234</sup> by inputting the chemical shift assignments and a list of nuclear Overhauser effect (NOE) crosspeaks that were derived from the <sup>1</sup>H,<sup>1</sup>H-TOCSY, <sup>1</sup>H,<sup>1</sup>H-NOESY, and <sup>1</sup>H,<sup>1</sup>H-dDQF-COSY data sets. For LnqQ, 856 NOE crosspeaks were used for the final calculation, 508 of which were short-range, 190 medium-range, and 158 long-range (Table 3.2). For AucA, 583 short-range, 364 medium-range, and 334 long-range NOE crosspeaks were used, giving a total of 1281 NOEs. For both cases, the amide proton resonances were well dispersed, signifying that the peptides are well-folded, which corroborates with the earlier

CD data. Furthermore, the percentage  $\alpha$ -helicity of the calculated structures is consistent with the estimated values from the CD experiments. For both peptides, the 20 lowest energy conformers had a low root-mean-square deviation (RMSD), indicating that all 20 structures are very similar (Table 3.2, Figure 3.5C and 3.5D). The Ramachandran plot data indicate that all  $\phi$  or  $\psi$  backbone angles are either in the most favored or additionally allowed regions. The structural statistics are presented in Table 3.2.

**Table 3.2. Structure calculation statistics for LnqQ and AucA**

	<b>LnqQ</b>	<b>AucA</b>
<b>Total NOE peak assignments</b>	856	1281
short-range, $ i-j  \leq 1$	508	583
medium-range, $1 <  i-j  < 5$	190	364
long-range, $ i-j  \geq 5$	158	334
average target function value ( $\text{\AA}^2$ )	$1.53\text{E-}02 \pm 6.94\text{E-}03$	$1.18\text{E-}02 \pm 4.56\text{E-}03$
<b>RMSD for full peptide</b>		
backbone atoms ( $\text{\AA}$ )	$0.56 \pm 0.12$	$0.31 \pm 0.05$
heavy atoms ( $\text{\AA}$ )	$0.98 \pm 0.11$	$0.65 \pm 0.07$
<b>Ramachandran plot</b>		
$\Phi/\Psi$ in most favored regions	78.6%	89.8%
$\Phi/\Psi$ in additionally allowed regions	21.4%	10.2%
$\Phi/\Psi$ in generously allowed regions	0.0%	0.0%
$\Phi/\Psi$ in disallowed regions	0.0%	0.0%

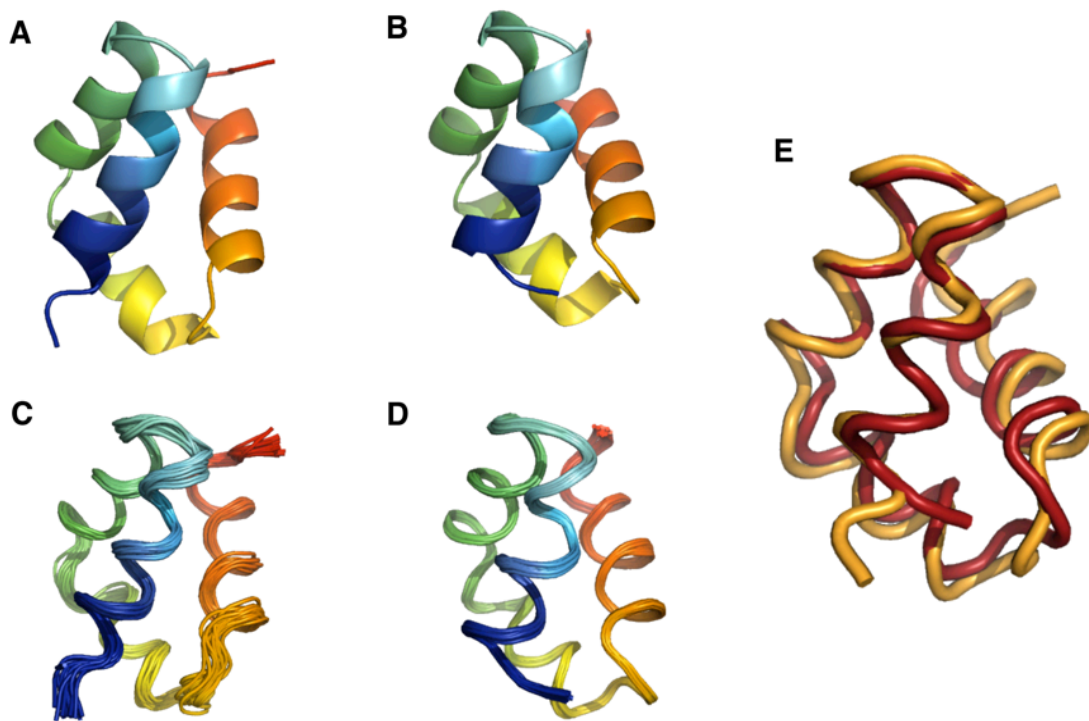


**Figure 3.5. NMR solution structures of LnqQ (PDB: 2N8P) and AucA (PDB:2N8O) in 25% trifluoroethanol and water, respectively.**

Cartoon representation of the solution structures of (A) LnqQ and (B) AucA. The N-terminus is shown in blue, while the C-terminus is in red. Superimposition of the 20 lowest energy conformers of (C) LnqQ and (D) AucA. (E) Superimposition of the structures of LnqQ (orange) and AucA (red).

The calculated structures of LnqQ and AucA have the same overall fold, with an RMSD of 1.691 Å over 611 atoms based on structure alignment in PyMOL<sup>235</sup> (Figure 3.5E). The main difference between the two structures lies at the N- and C- termini. Both peptides are comprised of four  $\alpha$ -helices that form a globular fold, wherein two sets of antiparallel helices (helices 1-2 and helices 3-4) that each assumes a “V” shape are oriented almost perpendicular to each other (Figure 3.5A and 3.5B). Turns that are composed of 1 to 3 amino acid residues connect the helices. For LnqQ, helix 1 has 11 residues (Phe4 to Tyr14); helices 2 and 3 both consist of 10 residues (Ser16 to Asn25 for

helix 2, Gly27 to Gly36 for helix 3); and helix 4 is comprised of Ile39 to Leu50 (12 residues). For AucA, helices 1, 2, 3, and 4 are composed of Trp3 to Tyr13 (11 residues), Lys15 to Tyr24 (10 residues), Gly26 to Gly35 (10 residues), and Leu38 to Ala49 (12 residues), respectively.

An interesting feature of the AucA structure is the significant upfield shift of the resonances of Lys44 protons. In fact, the Lys44  $\beta$  and  $\gamma$  protons have negative values of -0.793 ppm and -0.508 ppm, respectively. A closer look at its structure reveals that Lys44 interacts with two Trp residues (Figure 3.6A). In particular, the side chain of Lys44 lies on top of the aromatic ring of Trp40, significantly shielding it through magnetic anisotropy. Lys44, which is part of helix 4, also interacts with Trp31 of helix 3, thereby bringing helices 3 and 4 in close proximity, and further increasing electron density around Lys44.

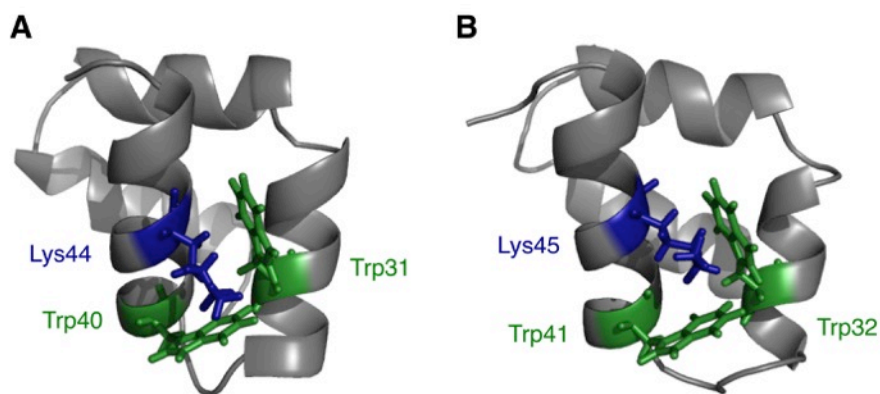


**Figure 3.6. Structures of (A) AucA highlighting the interactions of Lys44 to Trp40 and Trp31, and (B) LnqQ highlighting the interactions of Lys44 to Trp41 and Trp32.**

Several other protons in AucA are significantly shielded due to similar interactions as described above. These include the (a)  $\gamma$  protons of Lys12 (-0.291 ppm) that interact with the aromatic ring of Tyr13, (b)  $\zeta$ 2 proton of Trp3 (4.892 ppm) that interacts with the

aromatic ring of Trp21, (c)  $\gamma$  protons of Lys25 (0.068 ppm),  $\gamma$  (0.523) and  $\delta$  (0.379, 0.110) protons of Leu7 that interact with the aromatic ring of Trp3, and (d)  $\beta$  protons of Lys46 (0.720, 0.154 ppm) that interact with the ring of Trp42. Due to these interactions and other long-range NOEs, the RMSD of AucA is as low as 0.31 Å, indicating an exceptionally defined structure with a consistent confirmation shared among the 20 calculated conformers. The structure of LnqQ (Figure 3.6B) also exhibits a similar trend in shielding of hydrogens although at a lesser extent relative to AucA.

#### **3.2.4.2. Structural features**

Figures 3.7A and 3.7B show distinct white (hydrophilic residues) and red (hydrophobic residues) strips for all the helices of LnqQ and AucA, indicating their amphipathic character. In particular, the hydrophobic residues are oriented towards the core of the molecule, while hydrophilic residues are exposed on the surface. The hydrophobic surface maps (Figures 3.7C and 3.7D) show that the solvent-exposed surface of both peptides has several hydrophilic patches, while the interfaces of the helices have hydrophobic strips.

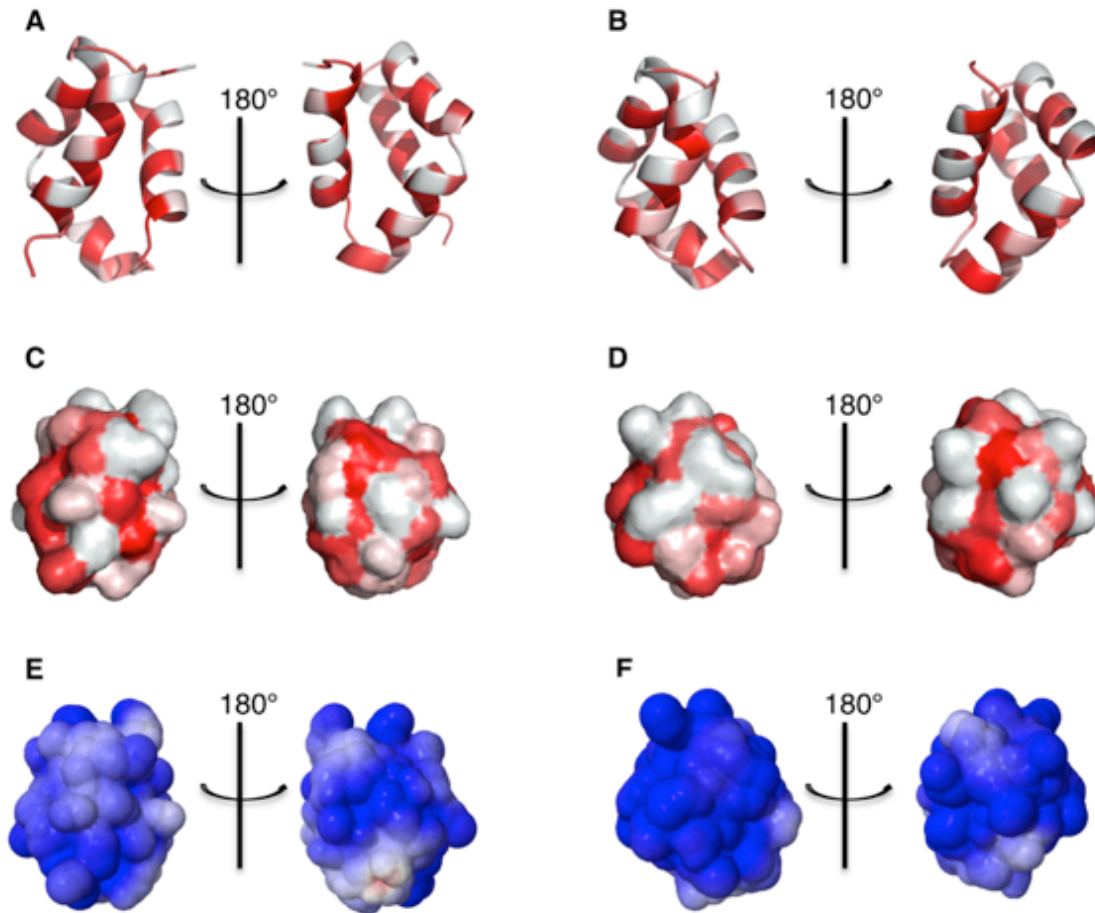


**Figure 3.7. Surface analysis of LnqQ and AucA.**

Amphipathic helices of (A) LnqQ and (B) AucA, where hydrophobic residues are shown in red, while hydrophilic residues are in white. Hydrophobic surface maps of (C) LnqQ and (D) AucA. Electrostatic surface potential maps of (E) LnqQ and (F) AucA, where cationic regions are indicated in blue.

As previously mentioned, LnqQ and AucA are highly cationic peptides. They are specifically composed of 8 and 10 lysine residues, respectively, and these residues are not localized in one region, but are instead well-distributed throughout their primary structures. The electrostatic potential maps (Figures 3.7E and 3.7F) reveal that these lysine residues are all exposed on the surface, giving the surface a vastly cationic character. This property implies that ionic interactions play a crucial role in the binding of LnqQ and AucA to negatively charged bacterial membranes. A previous study, however, showed that AucA interacts stronger with neutral membranes than anionic membranes, suggesting that hydrophobic interactions are likewise important for the initial binding of AucA to bacterial membranes.<sup>116</sup> The hydrophobic surface maps (Figures 3.7C and 3.7D) indeed illustrate that hydrophobic patches are present on the exposed surface.

Aromatic residues are usually involved in maintaining the structures of proteins and peptides, and are therefore normally found buried in the core of structures. This was, however, not the case for AucA and LnqQ. A previous study showed through tryptophan fluorescence spectroscopy that the Trp residues of AucA are mostly exposed on the surface.<sup>95</sup> Examining the elucidated structure of AucA in this study confirms that four out of the five Trp residues are indeed solvent exposed (Figure 3.8B). In particular, Trp3, Trp22, Trp31, and Trp40 are on the surface, while Trp42 is buried in the core of the peptide. As for LnqQ, all of its Trp residues are solvent exposed and exhibit a similar surface pattern with that of AucA (Figure 3.8A and 3.8B). The roles of Trp residues in the interaction of antibiotic peptides with biological membranes have been previously shown to be important. For instance, the activity of a bacteriocin named mesentericin Y105 was reduced by 10,000-fold when a C-terminal Trp residue was removed.<sup>252</sup> For the

antimicrobial cecropin A, on the other hand, Trp residues were found to be the primary anchor site on the membrane.<sup>253</sup> Future work on AucA and LnqQ can therefore be directed towards understanding the function of the solvent-exposed Trp residues.

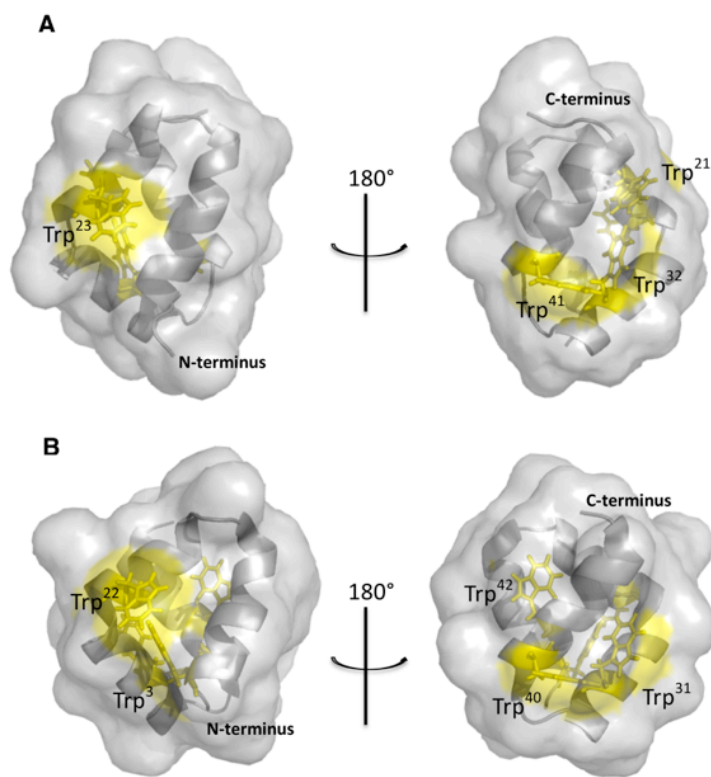


**Figure 3.8. NMR solution structures highlighting the tryptophan residues of (A) LnqQ and (B) AucA.**

### 3.2.4.3. Comparison to enterocin 7A and 7B

The structures of LnqQ and AucA were found to be remarkably similar to those of Ent7A and Ent7B (Figure 3.9A), despite their disparities in length and amino acid composition. LnqQ and AucA are 7 to 10 residues longer than Ent7A and Ent7B. In terms of amino acid sequence identity, Ent7A exhibits 30% and 20% sequence identity with LnqQ and AucA, respectively, while Ent7B only shares 18% sequence identity with both LnqQ and AucA (Figure 3.9B).

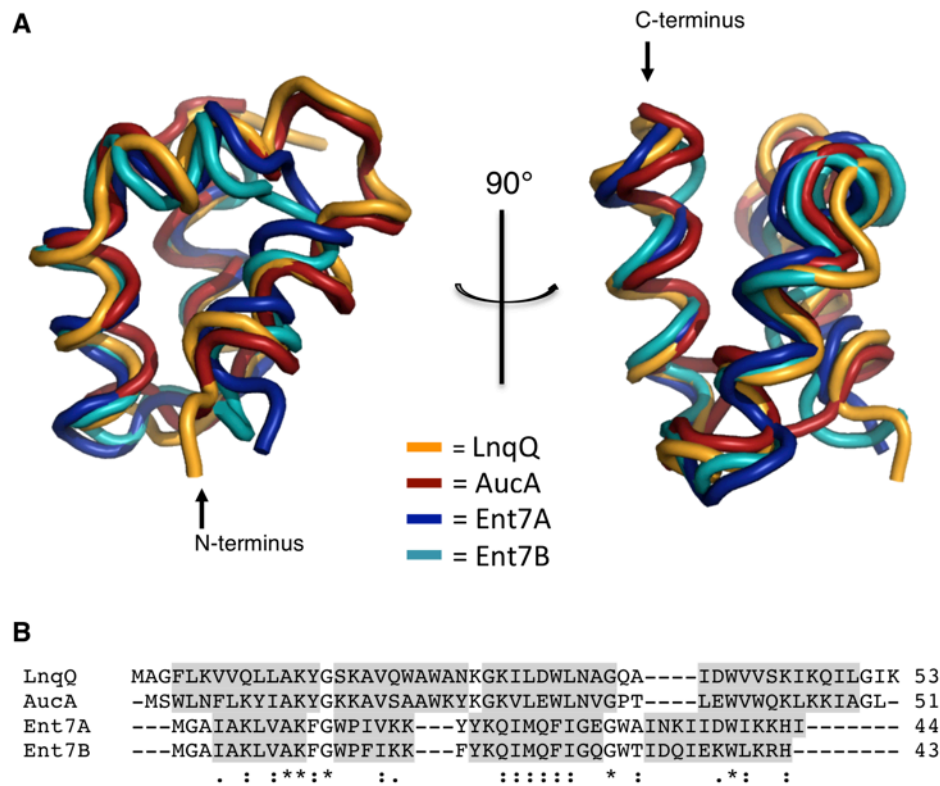


**Figure 3.9. Alignment of the (A) 3D structures and (B) amino acid sequences of LnqQ, AucA, Ent7A (PDB: 2M5Z), and Ent7B (PDB: 2M60).**

The  $\alpha$ -helical regions are highlighted in gray. Conserved, conservative, and semi-conservative substitutions are indicated by an asterisk, colon, and period, respectively.

The main difference among the 3D structures of LnqQ, AucA, Ent7A, and Ent7B is the length of the first two N-terminal helices due to the additional residues in LnqQ and AucA. Despite having an additional three to four residues in helices 1 and 2 of LnqQ and AucA, the overall fold of these segments is still similar to those found in Ent7A and Ent7B. On the other hand, a remarkably good alignment is observed for helices 3 and 4 of all four peptides.

Previously, Ent7A and Ent7B were tested for synergistic activity because of the observed similarity in their 3D structures. They were indeed shown to be more active when both peptides were present.<sup>112</sup> Due to the observed resemblance in the structures of LnqQ and AucA, they were also tested for synergy. With the use of *Carnobacterium divergens* LV13 and *Lactococcus lactis* ATCC 19257 as indicator strains, the activities of LnqQ and AucA were shown to be additive instead of synergistic (Figure 3.10). This result implicates that the two peptides do not interact with each other.

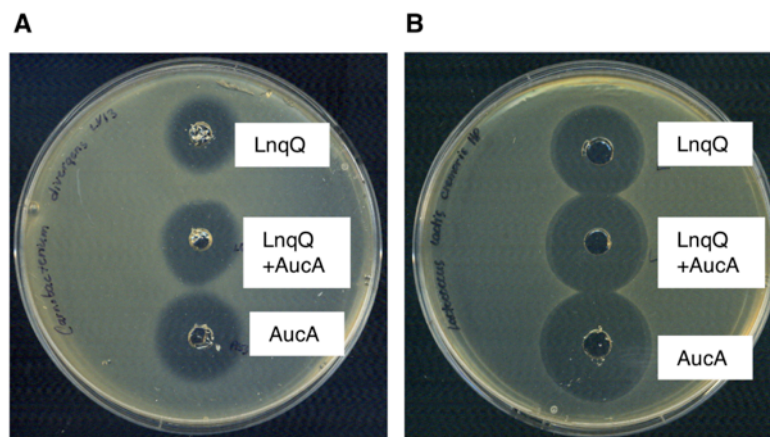


**Figure 3.10. Synergy assay for LnqQ and AucA using (A) *C. divergens* LV13 and (B) *L. lactis* ATCC 19257 as indicator strains.**

In the top and bottom wells, 20  $\mu\text{L}$  of a 50  $\mu\text{M}$  solution of LnqQ or AucA were added. In the middle well, 10  $\mu\text{L}$  of LnqQ (50  $\mu\text{M}$ ) was mixed with 10  $\mu\text{L}$  of AucA (50  $\mu\text{M}$ ), and an additive activity was observed.

#### **3.2.4.4. Homology modeling of broad-spectrum leaderless bacteriocins**

A common theme among LnqQ, AucA, Ent7A, and Ent7B, aside from having the same overall structural fold, is that all these leaderless bacteriocins have broad inhibition spectra. It was therefore hypothesized that the observed common structural motif may also be conserved among other broad-spectrum leaderless bacteriocins. To probe this hypothesis, secondary structure predictions and homology modeling were conducted for the other known broad-spectrum leaderless bacteriocins using JPred v.4 server<sup>254</sup> and SWISS-MODEL server<sup>242</sup>, respectively. The peptides that were analyzed include lacticin Z (LnqZ), epidermicin NI01 (EdcA), EntL50A, EntL50B, weissellicin Y (WelY) and weissellicin M (WelM).<sup>89,103</sup> The amino acid sequences of LnqZ and EdcA are more similar in length to LnqQ and AucA (51 to 53 residues), while those of EntL50A, EntL50B, WelY, and WelM are comparable to Ent7A and Ent7B (42 to 44 residues). Two sets of sequence alignments were therefore done, one for the LnqQ/AucA-like bacteriocins (Figure 3.11A) and the other for the Ent7A/7B-like bacteriocins (Figure 3.11B).

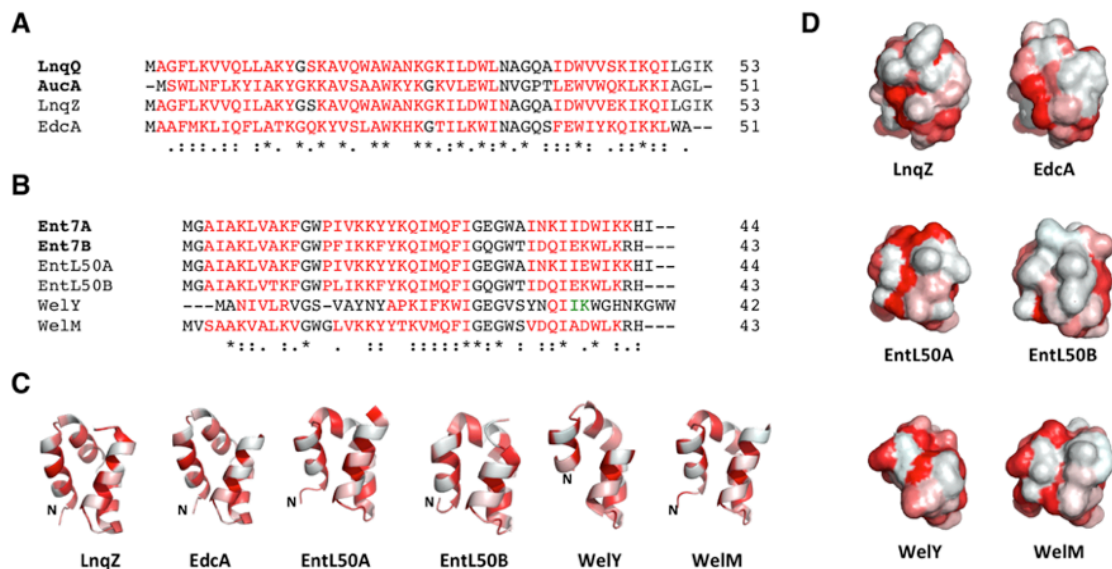


**Figure 3.11. Homology modeling of broad-spectrum leaderless bacteriocins.**

(A) Amino acid sequence alignment of peptides that consist of (A) 51 to 53 residues, and (B) 42 to 44 residues. Conserved, conservative, and semi-conservative substitutions are indicated by an asterisk, colon, and period, respectively. Secondary structure predictions by JPred v.4 server<sup>254</sup> are indicated, wherein helical regions are shown in red, while extended regions are in green. (C) Homology models generated using the SWISS-MODEL server<sup>242</sup>. Hydrophobic residues are shown in red, while hydrophilic residues are in white. LnqQ was used as template for LnqZ and EdcA; Ent7A for EntL50A, Wely and WelM; and Ent7B for EntL50B. (D) Hydrophobic surface maps of the aligned bacteriocins were generated using PyMOL<sup>235</sup>.

LnqZ was found to exhibit 94% and 45% sequence identity with LnqQ and AucA, respectively, while EdcA has 47% and 36% sequence identity with LnqQ and AucA, respectively. Similar to LnqQ and AucA, the predicted secondary structure content of LnqZ and EdcA was predominantly helical. Consequently, the generated homology models for both peptides are comprised of four amphipathic helices consisting of 10 to 12 residues per helix, with a comparable fold to those of LnqQ and AucA (Figure 3.11C). The surfaces of both peptides are mainly hydrophilic with a few hydrophobic patches (Figure 3.11D). The shorter bacteriocins EntL50A, EntL50B, Wely, and WelM share

28% to 98% sequence identity with Ent7A and Ent7B. The secondary structure predictions and homology models were likewise analogous to Ent7A and Ent7B. Overall, these analyses suggest that broad-spectrum leaderless bacteriocins share a common structural motif.

#### **3.2.4.5. Comparison to circular bacteriocins**

The structures of Ent7A and Ent7B were previously reported to display some resemblance to the saposin-like fold of the circular bacteriocins, carnocyclin A and enterocin AS-48.<sup>50,75,112</sup> Structural alignment shows that the same resemblance is observed for LnqQ and AucA. In particular, the two helices near the C-terminus of these leaderless bacteriocins (LnqQ, AucA, Ent7A, and Ent7B) align well with  $\alpha 1$  and  $\alpha 2$  of the circular bacteriocins (carnocyclin A and enterocin AS-48). Aligning these two helical regions with carnocyclin A gave a RMSD of 0.799 Å over 148 atoms, and 1.053 Å over 124 atoms for LnqQ and AucA, respectively (Figure 3.12A and 3.12B). The N-terminal helices of the LnqQ and AucA, however, are folded differently relative to  $\alpha 3$  and  $\alpha 4/\alpha 5$  of carnocyclin A and enterocin AS-48 (Figure 3.12A and 3.12B).

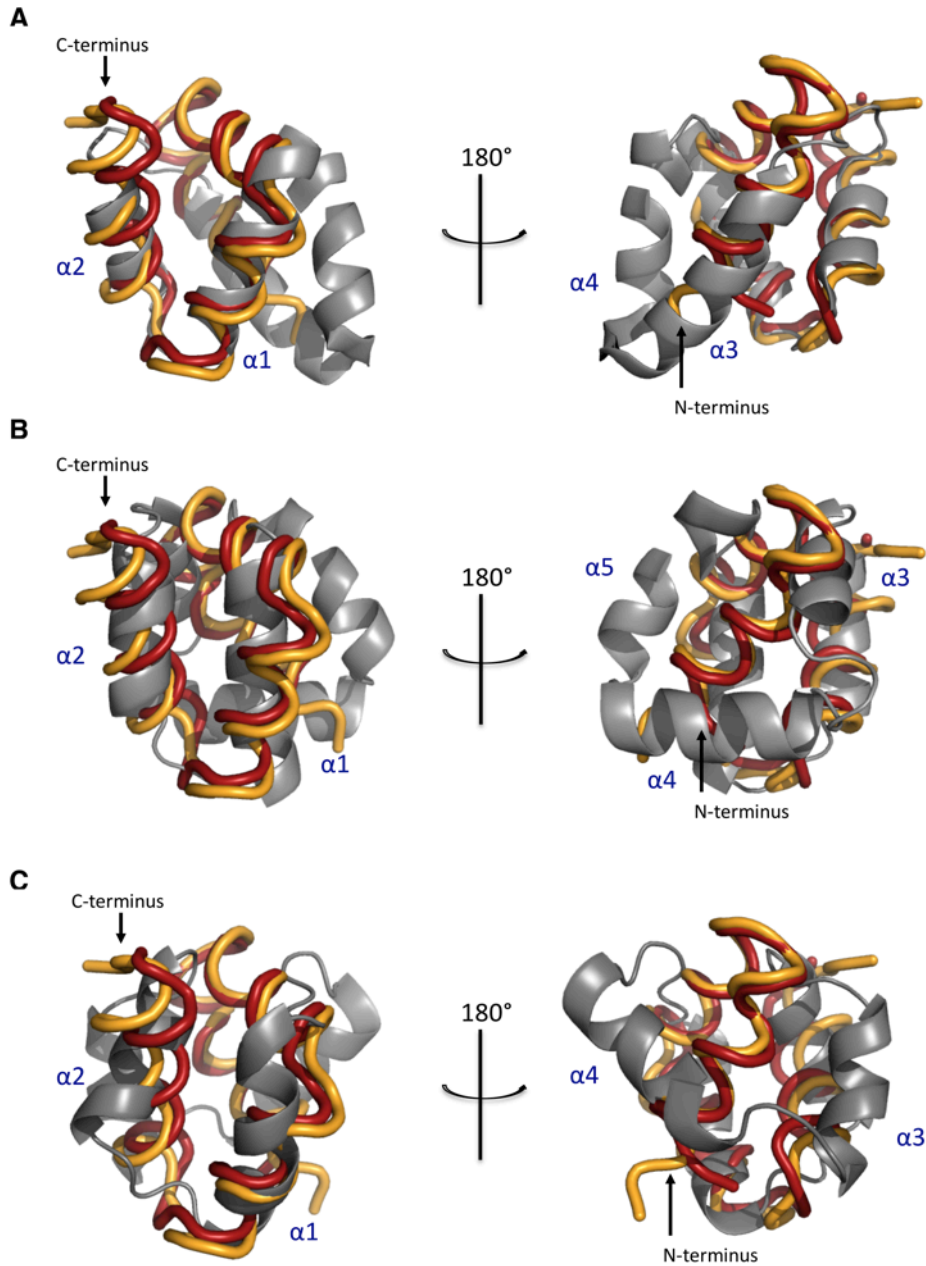


**Figure 3.12. Overlay of the structures of LnqQ and AucA with circular bacteriocins (A) carnocyclin A (PDB: 2KJF), (B) enterocin AS-48 (PDB: 1E68), and (C) acidocin B (PDB: 2MWR).**

LnqQ is in orange, AucA in red, and the circular bacteriocins in gray. The  $\alpha$ -helices of the circular bacteriocins are labelled in blue ( $\alpha 1$  to  $\alpha 4/5$ ). The gap along  $\alpha 4$  or  $\alpha 5$  of the circular bacteriocins indicates the point of N- to C- cyclization.

Circular bacteriocins are categorized into two subgroups. Carnocyclin A and enterocin AS-48 belong to subgroup I, which are characterized by having high isoelectric points. In contrast, subgroup II circular bacteriocins have lower pI values. It has been shown that the overall saposin-like fold is well-conserved for the first subgroup. As presented in Chapter 2, the structure of acidocin B is the first representative for the subgroup II circular bacteriocins, and while it is also composed of four  $\alpha$ -helices, substantial differences are observed in the overall fold of acidocin B relative to members of the subgroup I circular bacteriocins.<sup>51</sup> Interestingly, the C-terminal  $\alpha$ -helices of LnqQ and AucA, also align with  $\alpha$ 1 and  $\alpha$ 2 of acidocin B, although to a lesser extent relative to carnocyclin A and enterocin AS-48 (Figure 3.12C). The N-terminal helices of LnqQ and AucA were likewise folded differently relative to  $\alpha$ 3 and  $\alpha$ 4 of acidocin B. Interestingly, the saposin-like motif is not only observed in circular and leaderless bacteriocins. Our recent work on phenol-soluble modulins (PSMs), the virulence factors of *S. aureus*, revealed that PSM $\beta$ 2 also share a similar structural motif.<sup>255</sup>

### 3.2.5. Antimicrobial activity

With the assistance of Dr. Marco van Belkum, a spot-on-lawn assay was performed to determine the minimum inhibitory concentrations (MICs) of LnqQ and AucA against various Gram-positive indicator strains (Table 3.3). LnqQ was found to be more potent than AucA. It is 4-fold more active against *C. divergens* LV13, *Enterococcus faecium* BFE900, *L. lactis* ATCC 19257, and *S. aureus* 29213, 16-fold more active against *Lactobacillus sakei* UAL1218, and 128-fold more active against *Carnobacterium maltaromaticum* UAL26. The results suggest that the manners by which LnqQ and AucA

kill target strains are different, despite having similar 3D structures. Among the strains tested is *C. maltaromaticum* UAL26 containing plasmid pMG36c-cclBITCDA, which encodes the immunity proteins against carnocyclin A. LnqQ and AucA were found to be less active against this transformant relative to *C. maltaromaticum* UAL26 without the plasmid. This result suggests that carnocyclin A immunity proteins could have recognized LnqQ and AucA resulting in reduced sensitivity against LnqQ and AucA. It will therefore be of interest to investigate details on immunity protein recognition based on the structural similarities of leaderless bacteriocins and circular bacteriocins.

**Table 3.3. Antimicrobial activity of LnqQ and AucA against various strains**

Indicator strain	MIC ( $\mu\text{M}$ ) <sup>a</sup>		Source or Reference <sup>b</sup>
	LnqQ	AucA	
<i>Brochothrix campestris</i> ATCC 43754	2	2	ATCC
<i>Carnobacterium divergens</i> LV13	2	8	256
<i>Carnobacterium maltaromaticum</i> UAL26	1	128	257
<i>C. maltaromaticum</i> UAL26 (pMG36c-cclBITCDA)	16	-	69
<i>Enterococcus faecalis</i> ATCC 7080	32	-	ATCC
<i>E. faecalis</i> 710C	-	-	100
<i>Enterococcus faecium</i> BFE900	4	16	258
<i>Lactobacillus acidophilus</i> M46	0.5	-	229
<i>Lactobacillus sakei</i> UAL1218	0.5	8	Laboratory collection
<i>Lactococcus lactis</i> ATCC 19257	0.06	0.25	ATCC
<i>Staphylococcus aureus</i> ATCC 29213	32	128	ATCC
<i>S. aureus</i> ATCC 6538	8	-	ATCC

<sup>a</sup> -, no inhibition at 128  $\mu\text{M}$  of bacteriocin

<sup>b</sup> ATCC, American Type Culture Collection

### 3.3. Conclusions and Future Directions

This chapter describes the expression, purification, and NMR solution structure elucidation of the leaderless bacteriocins LnqQ and AucA. The calculated structures both consist of four  $\alpha$ -helices with a similar saposin-like globular fold. The elucidated 3D structures resemble those of the two-component leaderless bacteriocins, Ent7A and Ent7B, despite having low sequence identity and disparity in length. Homology modeling results suggest that the observed structural motif is shared among broad-spectrum leaderless bacteriocins. Surface analysis indicates that the surfaces of both peptides are highly cationic, and this property implies that the peptides interact with target membranes mainly through electrostatic interactions. Lastly, LnqQ was found to be more potent than AucA against various Gram-positive strains, suggesting that LnqQ and AucA have different mechanisms of action even though they exhibit similar 3D structures.

The structures of LnqQ and AucA revealed that Trp residues are solvent-exposed, and could potentially play a significant role in target recognition. Future investigations on the function of these Trp residues can therefore be pursued. Mutation of these residues and assessing the effects of such mutations on activity and structure can provide additional insights on peptide-membrane interaction. In addition, the striking similarity in the structural fold of circular and leaderless bacteriocins with broad-spectrum of activity is quite intriguing. Investigation on the significance of the said fold in their mechanisms of action could lead to a better understanding on why these bacteriocins inhibits a wide range of bacteria, unlike most bacteriocins that are only active against closely related strains. Moreover, it would be of interest to determine the impact of the shared structural motif on immunity protein recognition.

## Chapter 4

# Identification and Structure of the Two-Peptide Bacteriocin CbnXY

### 4.1. Project Background

#### 4.1.1. Carnobacteriocin X and Y

One characteristic criterion in predicting bacteriocin-like peptides that are encoded in bacterial genomes is the presence of a double glycine-motif (GG-motif). This motif has been observed to be the leader peptide cleavage site in several bacteriocins.<sup>1</sup> Putative two-peptide bacteriocin precursors encoded by a *cbnXY* gene cluster (Figure 4.1) were previously identified in *Carnobacterium piscicola* LV17B based on the presence of GG-type leaders.<sup>259</sup>

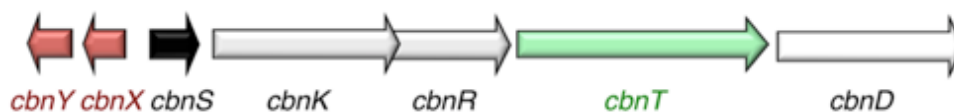


**Figure 4.1. Biosynthetic gene cluster of CbnXY.**

The genes *cbnXY* shown in red encode the two structural bacteriocin genes, *cbnS* in black encodes a putative induction factor; *cbnK* and *cbnR* in gray encode proteins that are homologous to histidine protein kinases and response regulators of bacterial signal transduction systems, respectively; *cbnT* in green encodes an ABC transporter; and *cbnD* in white encodes an accessory protein implicated in bacteriocin secretion.

The gene cluster includes a three-component transcription regulatory system (CbnSKR), an ATP-binding cassette (ABC) transporter (CbnT) that is likely involved in



membranes.<sup>121,261</sup> In addition to a GXXXG motif in CbnY, it also has GXXXG-like motifs, wherein Gly is replaced by Ala (Figure 4.2).

#### **4.1.2. Objectives**

The goals of this project were to confirm that CbnX and CbnY comprise a two-peptide bacteriocin, and to elucidate their NMR solution structures. In addition, it was aimed to investigate the interaction between CbnX and CbnY, and ultimately determine the structure of the CbnX-CbnY complex.

## **4.2. Results and Discussion**

### **4.2.1. Antimicrobial activity**

Spot-on-lawn assays were performed by Dr. Leah A. Martin-Visscher to assess the antimicrobial activity of chemically synthesized CbnX and CbnY, individually and in combination, against *Carnobacterium divergens* LV13 and *C. maltaromaticum* A9b-. Individually, both peptides were found to be inactive even at concentrations as high as 500  $\mu$ M. However, synergistic activity was observed when the peptides were combined at individual peptide concentrations as low as 4  $\mu$ M for *C. divergens* LV13 and 8  $\mu$ M for *C. maltaromaticum* A9b- (Figure 4.3).

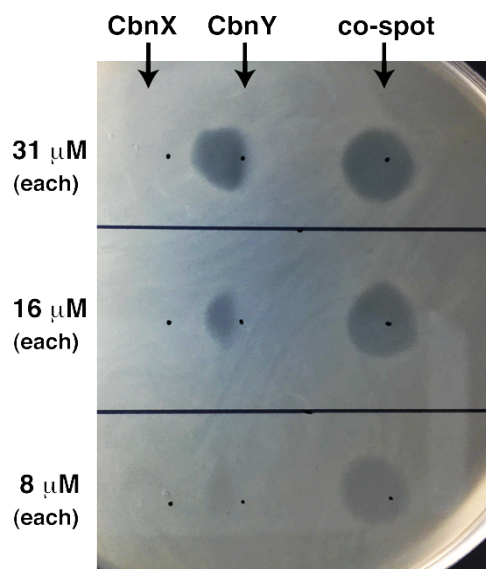


**Figure 4.3. Spot-on-lawn assay showing the synergistic activity of CbnX and CbnY at different concentrations against *C. maltaromaticum* A9b<sup>-</sup>.**

Zones of inhibition were only observed in regions where the peptides overlapped.

The results confirmed that CbnX and CbnY comprise a two-peptide bacteriocin unit, and represent the first confirmed two-peptide bacteriocin from carnobacteria. A previous study showed that CbnX, isolated from cultured cells, was active against *C. maltaromaticum* A9b<sup>-</sup>.<sup>260</sup> It is probable that undetected CbnY or minute amounts of another bacteriocin from the producer strain was present in the sample that caused the observed activity. As a negative control, CbnX and CbnY were also tested against the producer strains, *C. piscicola* LV17B and *C. maltaromaticum* C2. There was no activity observed confirming that the producer strains have immunity proteins that protect them from the antimicrobial effect of CbnXY.

#### 4.2.2. Circular dichroism spectroscopy

The circular dichroism (CD) spectra of CbnX and CbnY in 20 mM sodium phosphate buffer (pH 6.0) or 50% trifluoroethanol were obtained in order to estimate the secondary structure content of the peptides in the aforementioned solvent conditions (Figure 4.4).

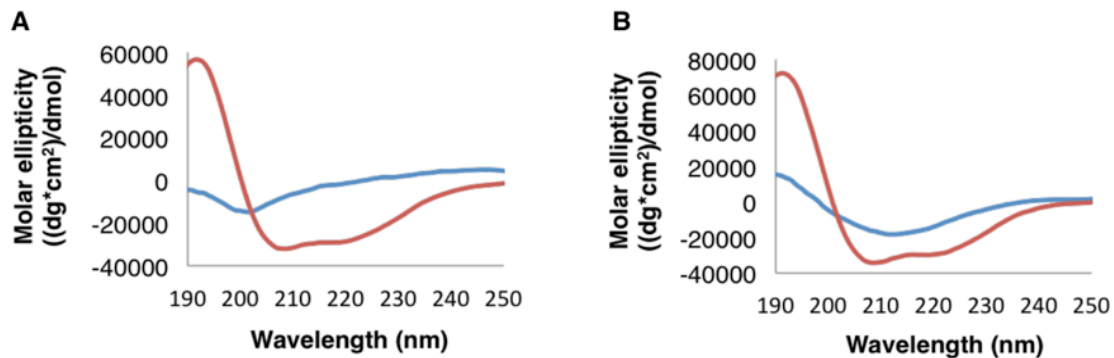


**Figure 4.4. CD profile of (A) CbnX and (B) CbnY in 20 mM sodium phosphate buffer, pH 6.0, (blue) and 50% trifluoroethanol (red).**

In aqueous condition, CbnX was found to be random coiled with a negative minima at 200 nm, while CbnY appeared to have some degree of  $\beta$ -sheet or amyloid formation as indicated by the negative minima at around 215 nm. In the presence of trifluoroethanol, which is a structure-inducing solvent, CbnX exhibits an estimated 78%  $\alpha$ -helicity, while CbnY is 81%  $\alpha$ -helical. The same trend was previously observed in other two-peptide bacteriocins, including lactococcin G (LcnG)<sup>153,156</sup>, plantaricin JK (PlnJK)<sup>155,157</sup>, plantaricin EF (PlnEF)<sup>154,157</sup>, and plantaricin S<sup>161</sup>. All these peptides were found to be unstructured in aqueous conditions, but assume a high degree of helicity when exposed to liposomes, micelles, or trifluoroethanol.

#### 4.2.3. Expression of [ $^{13}\text{C}$ , $^{15}\text{N}$ ]-labelled SUMO-CbnX and SUMO-CbnY

[ $^{13}\text{C}$ ,  $^{15}\text{N}$ ]-Labelled CbnX and CbnY peptides were produced in *Escherichia coli* through overexpression of SUMO (small ubiquitin-like modifier) protein fused to CbnX or CbnY in [ $^{13}\text{C}$ ,  $^{15}\text{N}$ ]-enriched media. The SUMO tag was cleaved using SUMO protease, and the cleaved CbnX and CbnY peptides were purified by RP-HPLC. MALDI-TOF mass spectrometry was used to monitor the incorporation of  $^{13}\text{C}$  and  $^{15}\text{N}$  isotopes. The expected masses for completely labelled CbnX and CbnY are 3,796 m/z and 3,270 m/z, respectively. [ $^{13}\text{C}$ ,  $^{15}\text{N}$ ]-CbnX registered a molecular ion peak of 3,793 m/z, while that of [ $^{13}\text{C}$ ,  $^{15}\text{N}$ ]-CbnY is 3,269 m/z, signifying >95% incorporation of the  $^{13}\text{C}$  and  $^{15}\text{N}$  isotopes (Figure 4.5). A total of 1-1.5 mg of each peptide were obtained and used for NMR data acquisition.

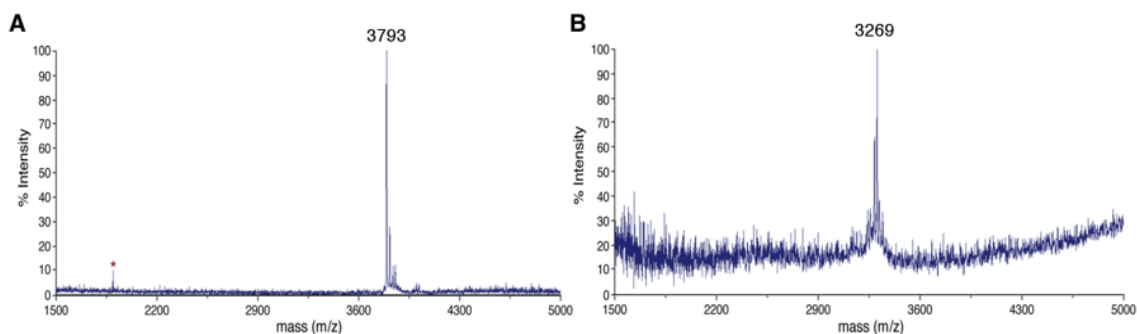


**Figure 4.5. MALDI-TOF mass spectra of (A) [ $^{13}\text{C}$ ,  $^{15}\text{N}$ ]-CbnX and (B) [ $^{13}\text{C}$ ,  $^{15}\text{N}$ ]-CbnY.**

In spectrum A, the doubly charged species is indicated with an asterisk.

## 4.2.4. NMR solution structures of CbnX and CbnY

### 4.2.4.1. Structure calculations

Chemical shifts were assigned using a suite of 2D and 3D experiments, including  $^1\text{H}, ^1\text{H}$ -TOCSY,  $^1\text{H}, ^1\text{H}$ -NOESY,  $^1\text{H}, ^{15}\text{N}$ -HSQC,  $^1\text{H}, ^{13}\text{C}$ -HSQC,  $^1\text{H}, ^{15}\text{N}$ -TOCSY-HSQC,  $^1\text{H}, ^{15}\text{N}$ -NOESY-HSQC, and HCCH-TOCSY. The  $^1\text{H}, ^{15}\text{N}$ -HSQC spectrum of CbnX (Figure 4.6A) shows 30 well-dispersed amide proton signals, indicating a well-defined structure. CbnX is composed of 33 amino acids, two of which are Pro residues, accounting for two of the three missing amide proton signals in the  $^1\text{H}, ^{15}\text{N}$ -HSQC spectrum. The third missing signal corresponds to that of the N-terminal amino group, which is in rapid exchange with the deuterated solvent. As for the  $^1\text{H}, ^{15}\text{N}$ -HSQC spectrum of the 29-mer CbnY (Figure 4.6B), all the backbone amide proton signals except for the N-terminal amino group were observed. The chemical shift peaklist, distance restraints acquired from the NOE experiments, and angle restraints from TALOS<sup>262</sup> were inputted to CYANA 2.1<sup>234</sup> and used for structure calculations. The structure calculation statistics are summarized in Table 4.1.

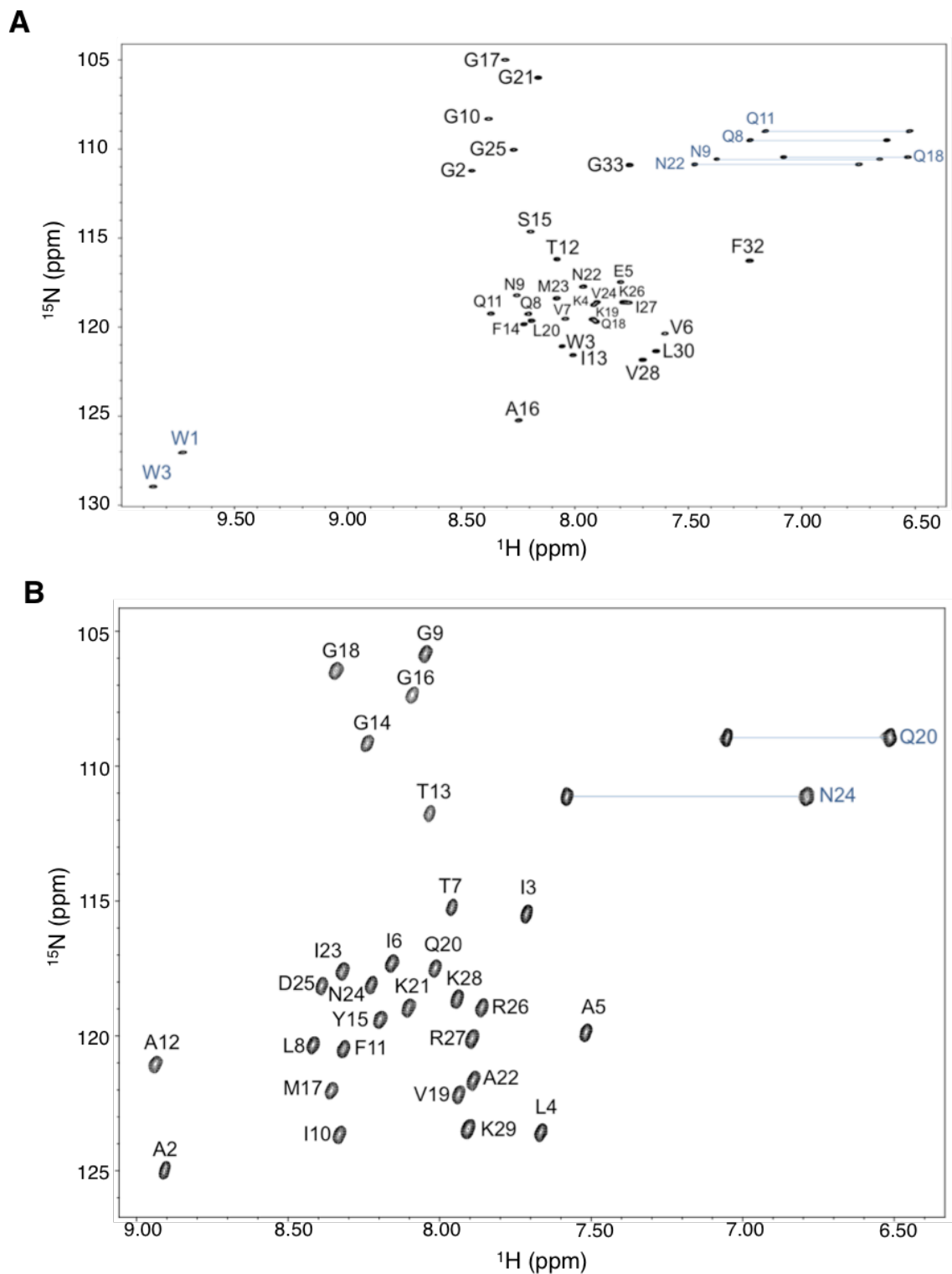


**Figure 4.6.**  $^1\text{H}$ ,  $^{15}\text{N}$ -HSQC spectra of (A) CbnX and (B) CbnY.

Backbone resonances are labelled in black, while side chain signals are indicated in blue.

**Table 4.1. Structure calculation statistics for CbnX and CbnY**

	<b>CbnX</b>	<b>CbnY</b>
<b>Total NOE peak assignments</b>	344	333
short-range, $ i-j  \leq 1$	235	208
medium-range, $1 <  i-j  < 5$	109	118
long-range, $ i-j  \geq 5$	0	7
average target function value ( $\text{\AA}^2$ )	$4.50 \text{ E-}02 \pm 4.06 \text{ E-}03$	$8.94 \text{ E-}03 \pm 9.00 \text{ E-}03$
<b>RMSD</b>	<b>Residues 2-26:</b>	<b>Residues 1-29:</b>
backbone atoms ( $\text{\AA}$ )	$0.82 \pm 0.36$	$0.68 \pm 0.18$
heavy atoms ( $\text{\AA}$ )	$1.37 \pm 0.35$	$1.30 \pm 0.22$
<b>Ramachandran plot</b>		
$\Phi/\Psi$ in most favored regions	91.7%	82.8%
$\Phi/\Psi$ in additionally allowed regions	8.3%	17.0%
$\Phi/\Psi$ in generously allowed regions	0.0%	0.2%
$\Phi/\Psi$ in disallowed regions	0.0%	0.0%

#### 4.2.4.2. Structural features

The calculated structure of CbnX is an extended  $\alpha$ -helix with a flexible C-terminus. The superimposition of the 20 lowest energy conformers is shown in Figure 4.7A, wherein a low root-mean-square deviation (RMSD) of 0.82  $\text{\AA}$  is observed for the backbone atoms of the  $\alpha$ -helical region spanning Gly2 to Lys26. The observed  $\alpha$ -helical region is consistent with the TALOS-predicted  $\alpha$ -helical stretch from Gly2 to Val24. The glycine residues (Gly17, Gly21 and Gly25) of the two consecutive GXXXG motifs in CbnX are all situated on the same side of the  $\alpha$ -helix (Figure 4.7B). The hydrophobic surface map (Figure 4.7C) shows that the  $\alpha$ -helical chain is amphipathic, having hydrophobic patches on one side and hydrophilic patches on the other. The hydrophilic strip is specifically cationic, as revealed by the electrostatic potential surface map (Figure 4.7D). The cationic character is due to the presence of Lys4, Lys19, and Lys26 residues.

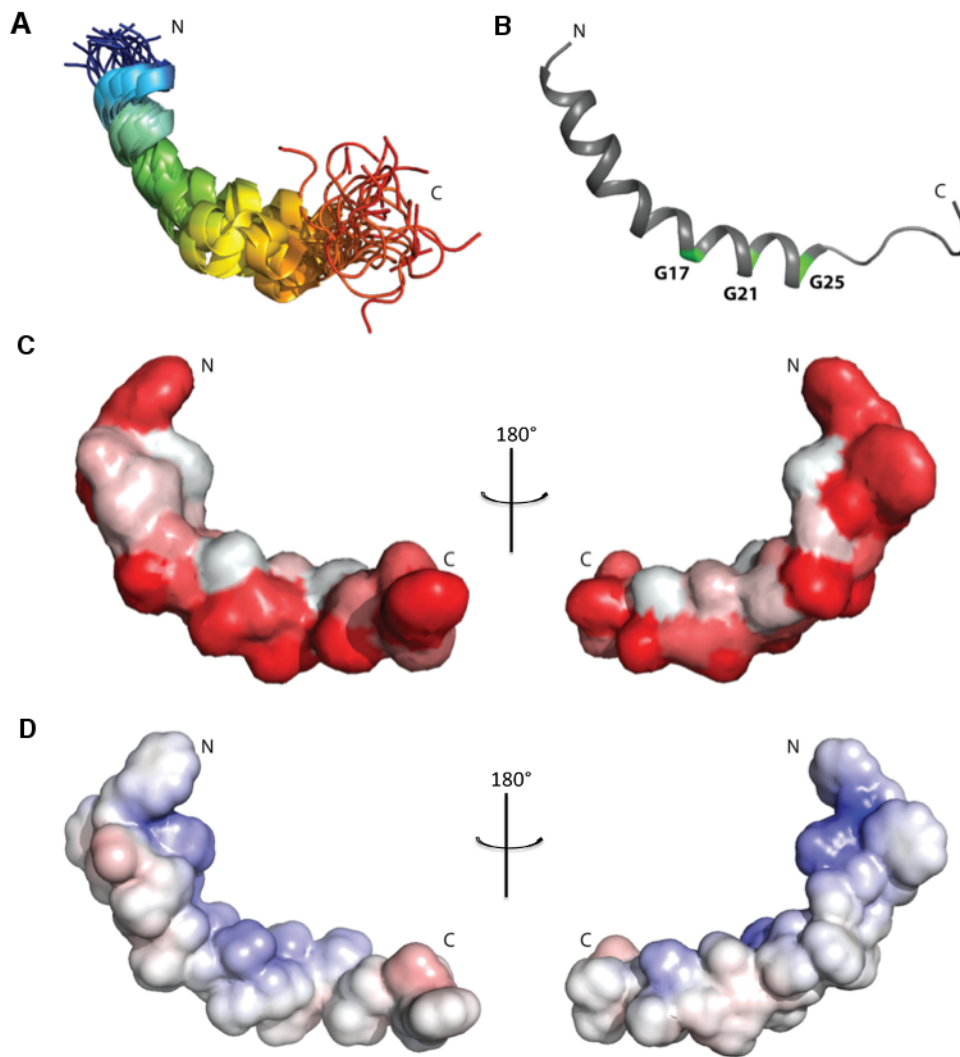


**Figure 4.7. NMR solution structure and surface maps of CbnX (PDB: 5UJR).**

(A) Superimposition of the 20 lowest energy conformers. (B) Cartoon drawing highlighting the two consecutive GXXXG motifs with glycine residues shown in green. (C) Hydrophobic surface map, where red indicates hydrophobic regions and white indicates hydrophilic regions. (D) Electrostatic potential map, where blue and red indicate positive and negative charge, respectively.

The calculated structure of CbnY is comprised of two  $\alpha$ -helices that assume an “L” shape conformation (Figure 4.8A). The N-terminal  $\alpha$ -helix consists of Ala2 to Tyr15 (14 residues), and is connected by a loop to the C-terminal  $\alpha$ -helix that is comprised of Met17 to Arg27 (11 residues). The TALOS-predicted helical segments (Ala2 to Thr13 and Met17

to Arg26) are consistent with the calculated structure. The loop region contains the GXXXG motif, which involves Gly14 and Gly18 (Figure 4.8B). The surface maps show that the N-terminal  $\alpha$ -helix is hydrophobic, while the C-terminal  $\alpha$ -helix is amphipathic, with a highly cationic end that is composed of 4 consecutive basic residues (Figure 4.8C and 4.8D). The rest of the solvent-exposed surface appears to be uncharged.

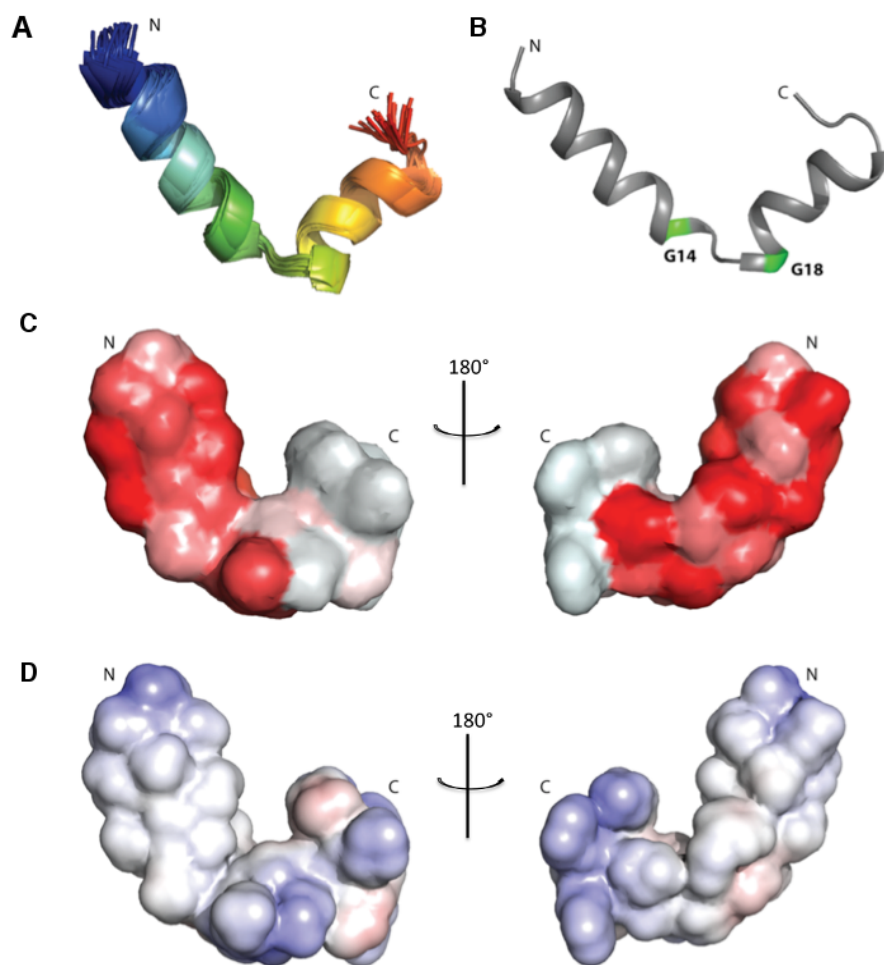


**Figure 4.8. NMR solution structure and surface maps of CbnY (PDB: 5UJQ).**

(A) Superimposition of the 20 lowest energy conformers. (B) Cartoon drawing highlighting the GXXXG motifs with glycine residues shown in green. (C) Hydrophobic surface map, where red indicates hydrophobic regions and white indicates hydrophilic regions. (D) Electrostatic potential map, where blue and red indicate positive and negative charge, respectively.

#### 4.2.4.3. Structural comparison to other two-peptide bacteriocins

Prior to this work, the structures of three other two-peptide bacteriocins have been elucidated. These include LcnG<sup>153</sup> from *Lactococcus lactis* LMG 2081, PlnEF<sup>154</sup> and PlnJK<sup>155</sup>, which are both produced by *Lactobacillus plantarum* C11. The 3D NMR solution structures of CbnX and CbnY were found to resemble the previously reported structures (Figure 4.9). In particular, CbnX shares several features with PlnF of PlnEF, PlnK of PlnJK, and LcnG $\beta$  of LcnG. These peptides consist of an extended amphipathic  $\alpha$ -helix that bears the GXXXG (or GXXXG-like) motifs. This extended helix is, however, disrupted for LcnG $\beta$ , particularly at the segment containing the G<sub>18</sub>XXXG<sub>22</sub> motif. As for CbnY, its structure closely resembles those of PlnE, PlnJ, and LcnG $\alpha$ . These peptides consist of two  $\alpha$ -helices, a longer N-terminal and a shorter C-terminal  $\alpha$ -helix (Figure 4.9). Both helices can either be hydrophobic or amphiphilic. A short flexible loop connects the two helices, and the GXXXG motif is located in or adjacent to the loop. There are several studies on the significance of the GXXXG motifs in two-peptide bacteriocins.<sup>144,155,159–161</sup> This motif has been demonstrated to be involved in helix-helix interactions in transmembrane domains, and has been established to be overrepresented in these domains.<sup>122,123,263</sup> It was therefore proposed that the GXXXG motifs located in the helices of two-peptide bacteriocins facilitate the interaction of complementary peptides to form a transmembrane helix-helix structure.<sup>121,261</sup>

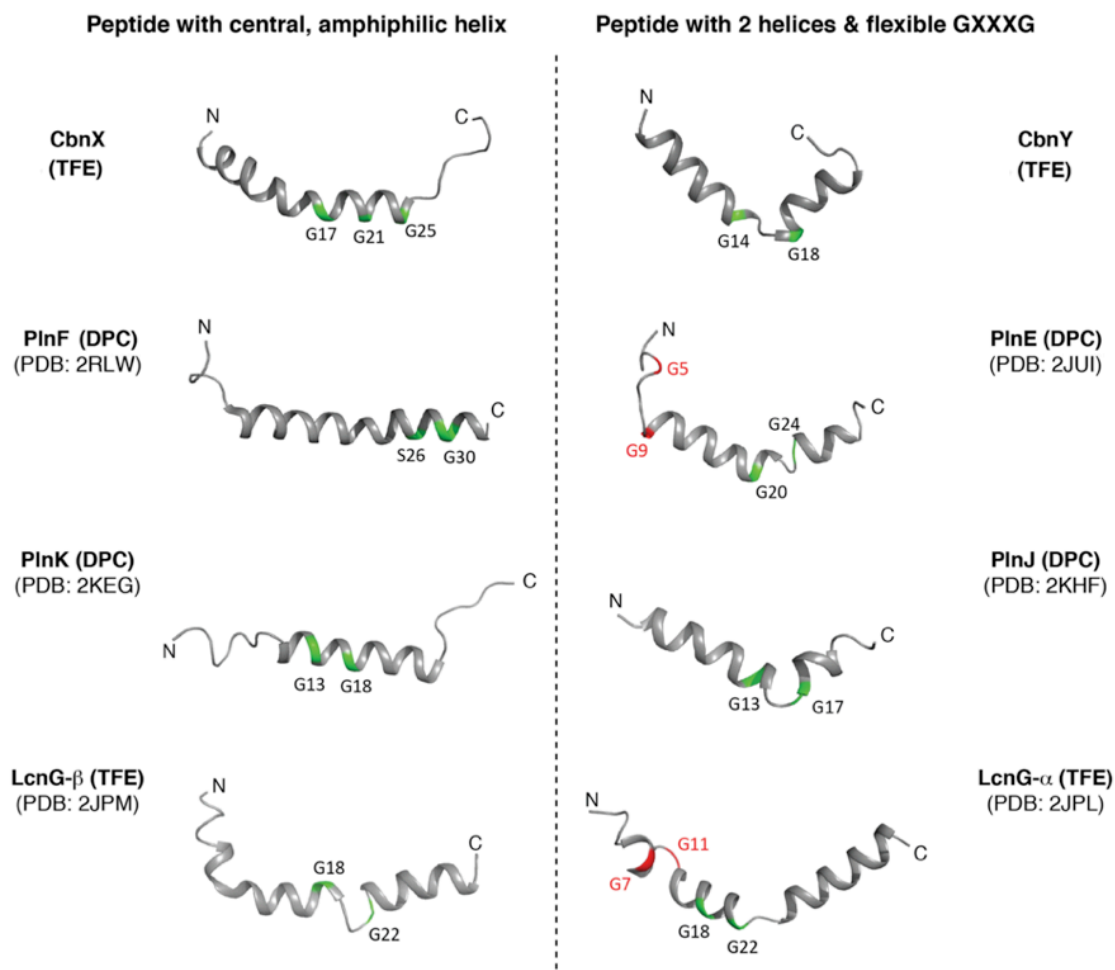


**Figure 4.9. Comparison of the 3D structures of CbnXY to PlnEF, PlnJK, and LcnG.**

The structures of CbnXY and LcnG were solved in the presence of trifluoroethanol (TFE), while those of PlnEF and PlnJK were elucidated in dodecylphosphocholine micelles. Residues involved in the GXXXG (or GXXXG-like) motifs are labelled and highlighted in green. For PlnE<sup>264</sup> and LcnG<sup>259</sup>, additional GXXXG motifs that are considered to be critical for activity are highlighted in red. The N- and C-termini of the peptides are indicated.

## 4.2.5. Binding studies

### 4.2.5.1. Isothermal titration calorimetry

Binding studies were performed by Dr. Kaitlyn M. Towle. Due to the presence of the characteristic GXXXG motifs in CbnX and CbnY, and the propensity of these peptides to form helical structures in structure-inducing conditions, the ability of CbnX and CbnY to form helical structures in structure-inducing conditions, the ability of CbnX and CbnY to form intermolecular contacts was assessed. Binding studies of CbnX and CbnY in 1:1 trifluoroethanol:phosphate buffer (pH 6.9) were performed using isothermal titration calorimetry (ITC). The results showed that the two peptides do not interact in the conditions employed (Figure 4.10). Consequently, elucidation of the NMR solution structure of the CbnXY complex was not feasible.

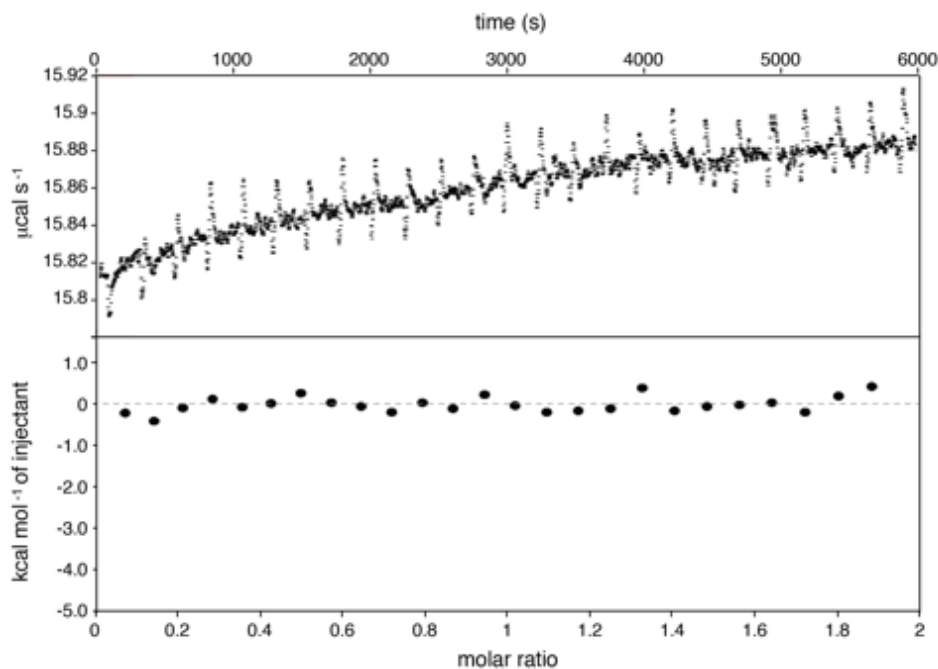


**Figure 4.10. ITC data for the titration of 0.1 mM CbnY into 1 mM CbnX at 25 °C.**

The top panel shows the heat flow as a function of addition of CbnY to the sample cell containing CbnX. The bottom panel shows the binding isotherm (heat change vs. molar ratio of CbnY).

#### 4.2.5.2. Permeability experiments

Two-peptide bacteriocins have been found to interact with membranes and facilitate ion leakage and disruption of membrane potential.<sup>164-167,170,171</sup> Considering this information, the ability of CbnX and CbnY to interact with membrane vesicles was investigated. Individually, both peptides were able to permeate the membrane. However, the effect of using a combination of the peptides was found to be additive rather than synergistic. Taken together, the ITC and permeability assay results strongly support the proposition that a membrane-bound receptor may be needed to serve as anchor for CbnXY to form an active bacteriocin complex. Studies on LcnG<sup>173</sup>, enterocin 1071<sup>173</sup>, and PlnJK<sup>175</sup> have identified specific receptors for these bacteriocins. The receptor for LcnG and enterocin 1071 was found to be undecaprenyl pyrophosphate phosphatase (UppP), a peptidoglycan biosynthetic enzyme. UppP was identified through generation of LcnG/enterocin 1071-resistant mutants and comparison of the genome sequences of the mutants to that of the wild-type strain.<sup>173</sup> The same technique was used for the identification of the PlnJK receptor, which is a putative amino acid-polyamine-organocation transporter.<sup>168,175</sup> A similar strategy may therefore be employed to determine the receptor of CbnXY.

### 4.3. Conclusions and Future Directions

It was previously reported that CbnX is a member of the single-peptide class II d bacteriocins. Based on sequence analysis and synergy assays, this study showed that CbnX, together with CbnY, is in fact part of a two-peptide bacteriocin system that exhibits optimal activity in the presence of both peptides. CbnXY is the first representative two-peptide bacteriocin identified in carnobacteria. [<sup>13</sup>C, <sup>15</sup>N]-Labelled CbnX and CbnY peptides were expressed, purified, and utilized for the elucidation of the 3D NMR solution structures of both peptides. The structures revealed that several features observed in other two-peptide bacteriocins are conserved in CbnX and CbnY. CbnX consists of an extended amphipathic  $\alpha$ -helix, while CbnY is composed of two  $\alpha$ -helices in an “L” shape conformation wherein the N-terminal helix is hydrophobic, while the C-terminal helix is amphipathic. Furthermore, CbnY has a cluster of cationic residues at its C-terminus, which is implicated to be responsible for peptide insertion into negatively charged target bacterial membranes. Two-peptide bacteriocins are suggested to interact with each other in order for them to elicit their synergistic activity. However, binding studies on CbnXY demonstrated that the CbnX and CbnY peptides do not directly interact, suggesting that a receptor may be required to mediate the formation of the CbnXY complex. It was therefore not possible to elucidate the NMR solution structure of the CbnXY complex.

Future work may be directed towards the identification of the CbnXY receptor. A similar approach to what was used for the identification of the receptors of LcnG, enterocin 1071, and PlnJK may be employed. This requires the identification of a CbnXY-sensitive strain, generation of resistant mutants, genome sequence analysis of the mutants to identify a putative membrane-bound receptor, and confirmation of the receptor's

function via heterologous expression. Subsequently, structure-based investigations on the peptide-receptor interaction may be pursued. The derived structural information may in turn serve as basis for the design of more potent peptide antimicrobials. Thus far, the receptors that were identified to be the targets of two-peptide bacteriocins are distinct from those targeted by conventional antibiotics. This therefore suggests that two-peptide bacteriocins, and other bacteriocins with unique receptors, can be used in combination with other antimicrobials without the risk of cross-resistance development.

## Chapter 5

### Characterization of Lanthipeptide Dehydrogenase, PneJ<sub>B</sub>

#### 5.1. Project Background

##### 5.1.1. D-Amino acids in lanthipeptides

The standard amino acids are biosynthesized with an alpha carbon that assumes an L-configuration. However, several ribosomally synthesized natural products from both eukaryotes and prokaryotes contain D-amino acids.<sup>265–270</sup> The presence of these non-canonical residues has been demonstrated to be crucial for bioactivity, stability, and structural conformation.<sup>194,267,268,271–274</sup> The D-amino acids in non-lanthipeptide natural products are usually installed by epimerizing the L-amino acid either via a deprotonation-protonation mechanism<sup>275</sup> or a radical mechanism<sup>276</sup>. In lanthipeptides, this transformation is accomplished by two enzymatic reactions catalyzed by a dehydratase, followed by a dehydrogenase, as previously described in Chapter 1 (Figure 1.12). Briefly, L-Ser and L-Thr residues are initially dehydrated to dehydroalanine (Dha) and dehydrobutyrine (Dhb), respectively, followed by reduction to D-Ala and D-aminobutyrate (D-Abu), respectively. Lanthipeptide dehydrogenases that catalyze the reduction of the dehydro residues are collectively referred to as “LanJ” enzymes.

## 5.1.2. LanJ dehydrogenases

### 5.1.2.1. LanJ<sub>A</sub> enzymes

LanJ enzymes are categorized into two classes, namely the zinc-dependent dehydrogenases (LanJ<sub>A</sub>) and the flavin-dependent dehydrogenases (LanJ<sub>B</sub>).<sup>177,277</sup> As mentioned in Chapter 1, the first characterized LanJ enzyme is LtnJ, which is involved in the biosynthesis of the two-component lantibiotic lactacin 3147 (Figure 5.1).<sup>194</sup> LtnJ is a LanJ<sub>A</sub> enzyme that requires Zn<sup>2+</sup> and NADPH as cofactors in the reduction of Dha to D-Ala. Other known LanJ<sub>A</sub> enzymes include SacJ<sub>A</sub> (involved in the biosynthesis of staphylococcin C55 from *Staphylococcus aureus* C55)<sup>278</sup>, PenJ<sub>A</sub> (originally named as PenN<sup>279</sup>; involved in the biosynthesis of pediocin A from *Pediococcus pentosaceus* FBB61)<sup>280</sup>, and NpnJ<sub>A</sub> (originally named as NstJ<sup>194</sup>; involved in the biosynthesis of six NpnA peptides from the cyanobacterium *Nostoc punctiforme* PCC73102)<sup>277</sup>. The dehydrogenase activities of SacJ<sub>A</sub> and PenJ<sub>A</sub> were demonstrated *in vivo* using lactacin 3147 as substrate. Their respective native peptide products have not yet been structurally characterized.<sup>280</sup> *In silico* analysis suggests that staphylococcin C55 is a putative lanthipeptide, while the identity of pediocin A remains to be determined, since its gene cluster does not include a LanM or LanB/C, which are the key enzymes in lanthipeptide biosynthesis.<sup>177</sup> On the other hand, the gene cluster containing NpnJ<sub>A</sub> includes a LanM enzyme, however, the precursor peptides do not contain Cys residues and are therefore lacking of lanthionine (Lan) and/or methyllanthionine (MeLan) rings. NpnJ<sub>A</sub> is the first LanJ<sub>A</sub> enzyme to be reconstituted *in vitro*.<sup>277</sup> The authors demonstrated that a soluble and active maltose-binding protein (MBP)-NpnJ<sub>A</sub> fusion protein, in the presence of NADPH,



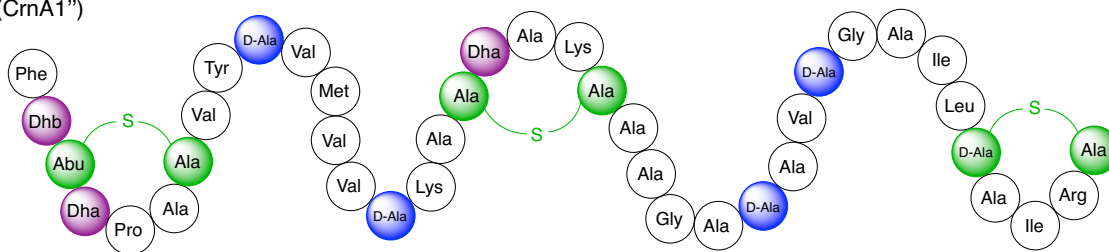
### 5.1.2.2. LanJ<sub>B</sub> enzymes

LanJ<sub>B</sub> enzymes are flavin-dependent oxidoreductases that were shown to reduce not only Dha, but also Dhb.<sup>191,196</sup> Currently, there are two LanJ<sub>B</sub> enzymes that have been characterized, namely CrnJ<sub>B</sub> and BsjJ<sub>B</sub>, which are involved in the biosynthesis of the lantibiotics, carnolysin (from *Carnobacterium maltaromaticum* C2) and bicereucin (from *Bacillus cereus* SJ1), respectively.<sup>191,196</sup> Carnolysin is a two-component lantibiotic that is comprised of carnolysin A1 (CrnA1) and A2 (CrnA2). In contrast to most two-component bacteriocins, their structural genes are not located next to each other. Nonetheless, it was demonstrated that the peptides exhibit synergistic activity. CrnA1 and CrnA2 undergo two proteolytic cleavages during maturation, and the singly cleaved peptides are indicated with a single quote (CrnA1' and CrnA2'), while the doubly cleaved mature peptides are indicated with a double quote (CrnA1'' and CrnA2''). To formally distinguish the different cleaved segments, the translation product is referred to as the prepeptide; the peptide lacking the leader is the propeptide (first cleavage); and the peptide that is obtained after the second cleavage is the mature lantibiotic. CrnA1'' contains four D-Ala, while CrnA2'' contains one D-Ala and one D-Abu (Figure 5.2).<sup>191</sup> It was confirmed *in vivo* through coexpression of CrnJ<sub>B</sub> with CrnA1/CrnA2 and CrnM in *Escherichia coli* that the CrnJ<sub>B</sub> enzyme was indeed responsible for the reduction of Dha and Dhb to D-Ala and D-Abu, respectively. The activity of BsjJ<sub>B</sub>, on the other hand, was confirmed both *in vivo* and *in vitro*.<sup>196</sup> For the *in vivo* assay, a similar heterologous coexpression system to what was used for carnolysin was employed for BsjJ<sub>B</sub>. For the *in vitro* reconstitution, a dehydrated substrate (BsjA1) was treated with an His<sub>6</sub>-BsjJ<sub>B</sub> enzyme together with flavin mononucleotide (FMN) and NADH.<sup>196</sup> Bicereucin is also a two-component system,

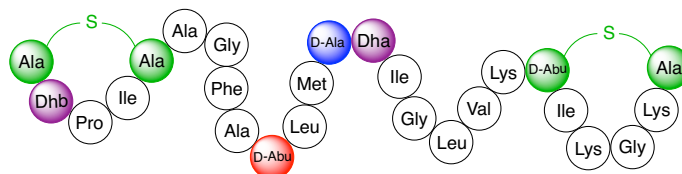
composed of BsjA1 and BsjA2, that undergoes two proteolytic cleavages to yield the mature peptides, named Bsj $\alpha$  and Bsj $\beta$ . Similar to carnolysin, the presence of both peptides is required for optimal activity. The bicereucin system is unique, since only Bsj $\beta$  bears a Lan ring, while Bsj $\alpha$  is simply a linear peptide with dehydro residues and D-amino acids (Figure 5.2). Bsj $\alpha$  contains four D-Ala, while Bsj $\beta$  contains one D-Abu and three D-Ala.

Relative to the LanJ<sub>A</sub> enzymes, the LanJ<sub>B</sub> enzymes were discovered just recently and are therefore not as well-characterized as the former. The substrate specificity of LanJ<sub>B</sub> has not yet been investigated, and while it has been established for LanJ<sub>A</sub> enzymes that the leader peptide is not required for activity, it is not yet known whether this is also the case for LanJ<sub>B</sub> enzymes. It is also unclear why LanJ<sub>B</sub> enzymes can reduce both Dha and Dhb, while the LanJ<sub>A</sub> enzymes are restricted to Dha. Additional insights on their functions may be obtained once crystal structures of LanJ<sub>A</sub> and LanJ<sub>B</sub> enzymes are available, and mutational analysis has been performed to establish the substrate scope of LanJ<sub>B</sub> enzymes.

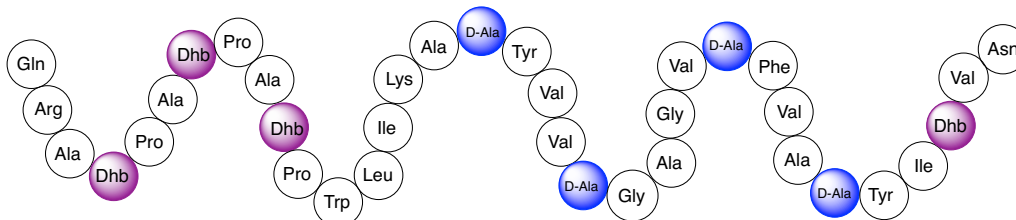
**Carnolysin A1''**  
(CrnA1'')



**Carnolysin A2''**  
(CrnA2'')



**Bicereucin  $\alpha$**   
(Bsj $\alpha$ )



**Bicereucin  $\beta$**   
(Bsj $\beta$ )

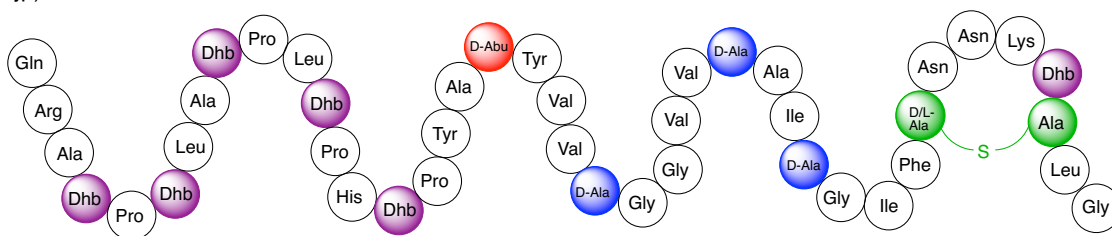


**Figure 5.2. Two-component lantibiotics processed by LanJ<sub>B</sub> enzymes.**

D-Ala residues are shown in blue, and D-aminobutyrate (D-Abu) residues are in red. Dehydroalanine (Dha) and dehydrobutyrine (Dhb) residues are shown in purple. Lanthionine and methyllanthionine rings are indicated in green. For bicereucin  $\beta$ , the lanthionine ring was produced as a mixture of stereoisomers.<sup>196</sup>

### 5.1.3. Pneumococcin and the putative PneJ<sub>B</sub> reductase

#### 5.1.3.1. Biosynthetic gene cluster of pneumococcin

A putative two-component lantibiotic was previously identified in *Streptococcus pneumoniae* R6 and named as pneumococcin A1 (PneA1) and A2 (PneA2).<sup>283</sup> Analysis of the associated biosynthetic gene cluster (Figure 5.3) showed that pneumococcin belongs to class II lanthipeptides, wherein a bifunctional PneM enzyme operates to install Lan and MeLan rings.<sup>283</sup> The gene cluster also includes the gene *pneT*, encoding a putative ATP-binding cassette (ABC) transporter that bears an N-terminal peptidase domain, which is likely involved in the leader peptide cleavage of the prepeptide. Downstream the *pneT* gene is *pneP* that encodes a peptidase that could potentially be involved in the cleavage of the propeptide. PneP in fact exhibits 48% identity to the nisin leader peptidase NisP. The genes *pneF* and *pneE* encode a putative immunity protein and ATP-binding protein, respectively. The gene *lanD* encodes a flavoprotein and will be discussed further in the succeeding sections. Lastly, three other genes in the cluster encode unknown proteins.

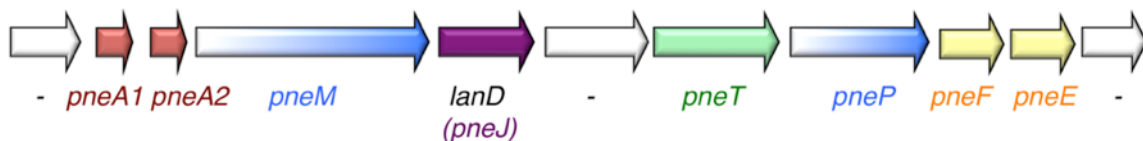


**Figure 5.3. Biosynthetic gene cluster of pneumococcin.**

The genes *pneA1* and *pneA2* shown in red encode the structural bacteriocin genes; genes in gradient blue are modifying enzymes, where *pneM* encodes the bifunctional lanthipeptide synthetase, and *pneP* encodes a serine protease involved in leader peptide cleavage; *lanD* encodes a flavoprotein that was previously predicted to be involved in aminovinylcysteine formation, but is likely a LanJ<sub>B</sub> enzyme (*pneJ<sub>B</sub>*); *pneT* in green encodes an ABC transporter with an N-terminal peptidase domain; *pneF* and *pneE* encode a putative immunity protein and ABC transporter, respectively. Genes in white encode unknown proteins.

PneA1 and PneA2 have not been isolated from the natural producer strain, hence the chemical structures of the native mature peptides have not yet been established. Instead, the precursor peptides were used as substrates for heterologous expression using the nisin machinery composed of NisB dehydratase, NisC cyclase, and NisT ABC transporter.<sup>283</sup> To facilitate recognition by nisin modifying enzymes, the nisin leader was fused to the propeptide of PneA1 and PneA2.<sup>283</sup> In this study, the precursor peptides were successfully dehydrated and cyclized by the nisin enzymes, producing mature peptides with antimicrobial activity, albeit only against *Micrococcus flavus*. It is possible that the weak antimicrobial activity may be due to missing structural features, since only a dehydratase and a cyclase were used in this study, while the pneumococcin gene cluster suggests the presence of another putative modifying enzyme that may be crucial for pneumococcin biosynthesis. Based on *in silico* analysis, the authors proposed that the flavoprotein encoded in the pneumococcin gene cluster is a putative LanD enzyme that is involved in aminovinylcysteine (AviCys) formation. However, with the discovery of CrnJ<sub>B</sub>, the first flavin-dependent lanthipeptide dehydrogenase, we re-evaluated the said proposition. Sequence alignment with known LanD enzymes, including EpiD of epidermin, GdmD of gallidermin, MibD of microbisporicin, and MutD of mutacin 1140, revealed that there is no substantial homology between the proposed pneumococcin LanD and the known LanD enzymes (Figure 5.4). However, sequence alignment with CrnJ<sub>B</sub> and BsjJ<sub>B</sub> revealed that the pneumococcin LanD shares high sequence homology with the aforementioned enzymes (Figure 5.5). Furthermore, alignment of the primary sequences of PneA1 and PneA2 with CrnA1'' and CrnA2'' revealed that the peptides are likewise homologous (Figure 5.6). The pneumococcin LanD will therefore be referred to hereafter as Pnej<sub>B</sub>.

```

PneJ      -----MNKIFIYAGVRN-----HNSKTLEYTK  22
MibD      MTAHSDAGGDPRPPERLLLGVSGSVAALNLPAYIYAFRAAGVARLAVVLTCAAEGFLPAG  60
MutD      -----MEEQNIIEKKILLCLTGSGALLGIAEYITFLT-VRFKHVRVIVSDNAAKMLPVA  52
EpiD      -----MYGKLLICATASINVININHYIVELK-QHFDEVNILFSPSSKNFINTD  47
GdmD      -----MHGKLLICATASINVVNINHYIVELK-QYFEEVNILFSPSSKKFINTD  47
          ::::                               : : .

PneJ      RLSSIISSRNNVDISFRTPFNSELEISNSDSEELFKKIDRQSNADDGGVIKELLES DI  82
MibD      ALRPIVDAVHTE----HDQKGHVVALSRWAQHLLVLPATANLLGCAASG-LAPNFLATVL  115
MutD      AITQLCEKVYTDEVSFDTKQKNHIALTRWADITVVLPATANIIGKVANG-IADNFMTTTL  111
EpiD      VLKLFCDNLYDEI---KDLLNINIVENHEYILVLPASANTINKIANG-ICDNLLTTVC  103
GdmD      VLNLFCDNLYDET---QDLLNHINIVENHEYILVLPASADTINKIASG-ICDNLLTTVC  103
          : : .           . : : . . : . . . * : :: :

PneJ      IIISSPVYLQNVSDTKNFIERIGGWSHLFRLAGKFVVTLTDAESNGSDNVSEYLRDIFS  142
MibD      LAADCPITFVPA-----MNPVMWRKPAVR-----RNVATLRADGHHVVDPLPGAVYE  162
MutD      LSSSKPVLIIYPC-----MNNIMWENPVVQ-----KNVEVLSGTQYKVIVGQESSEFE  158
EpiD      LTGYQKLFIFPN-----MNIRMWGNPFLO-----KNIDLLKNNDVKVYSPDMNKSFE  150
GdmD      LTGYKSLYIFPN-----MNIKMWENPFLO-----KNIDLLKNNSVKVYPPDVNKSFE  150
          : : :           . * :           . :           . :

PneJ      YMGQILHQVSITNSLKDIAEAQLMEATYKIEDVLEGGIKIKYKTTDYQERAYQTLKLILEN  202
MibD      AARSIVEGLAMPR-----PEALVRLGGG  187
MutD      LAGKMKKNIAIPS-----LDELQRVVLEN  183
EpiD      ISSGRYKNNITMPN-----IENVLNFVLNN  175
GdmD      ISSGLYKNSITMPN-----IENVLSFILNS  175
          . . ::::                               . : .

PneJ      YDSEHF EKMYWEKKRLF EANSLEEWYYVENIK-----  234
MibD      DDGSPAGPA-GPVGRAEHV GAVEAVEAVEAVEAVEAAEALA  227
MutD      LQEER-----  188
EpiD      EKRPLD-----  181
GdmD      EKRPLD-----  181
          .

```

**Figure 5.4. Amino acid sequence alignment of PneJ<sub>B</sub> with LanD enzymes.**

PneJ<sub>B</sub> was previously proposed to be a LanD enzyme.<sup>283</sup> LanD enzymes included in the alignment are MibD of microbisporicin, MutD of mutacin 1140, EpiD of epidermin, and GdmD of gallidermin. Conserved, conservative, and semi-conservative substitutions are indicated by an asterisk, colon, and period, respectively.

```

CrnJ      MKKVFVLIGSRKKNNTASFIKSVTRLED---EHYDVEFAPQDYDINFCDGSNDIFID  57
BsjJ      MKHVLAYVGSRNPDSTRKHIERLLQSLSKYKEEISHELLTPNDIQLSPSTGCKNCFKT  60
PneJ      MNKIFIYAGVRNHNSKTLEYTKRLSSIISSRNVDISFRTPFNSELEISNS-DSEELFKK  59
          *:::  * *: ::* .. : : . :.. . . . . : : :. . . : : *

CrnJ      T----DYSLNDELEILQNKILESDIFIIGSPVYVHMSADLKLFIERSAWVHTLRLQGK  113
BsjJ      GKCSLDKVPKDEGELLKRKLEADFIILASPVYSHNVSSDMKMVIDRLSYWAHLFKLVGK  120
PneJ      GID--RQSNADDGGVIKELLESDIIIISSPVYLQNVSDTKNFIERIGGWSHLFRLAGK  117
          *:  :::::***:***:*.**** ::* * * .:* * . * * ::* **

CrnJ      PVIVMSTCGSNGLKTVIEPLSEVITFMGGNVIATANATQIPDRLNDKVIKEISEEITR  173
BsjJ      SGIVLAAAESNGVNFVADYLEKVAYVGLHVVDKIGLMGHQ-ELTDNQLD-FLTESIYNH  178
PneJ      FVVTLDAESNGSDNVSEYLRDIFSYMGGQILHQVSITNSLKDIAEAQLM-EATYKIEDV  176
          :. :. *** . * : * . : : * : : . : : : : : : . *

CrnJ      INTYSELPPMSNKFLEKVFNGSKLNILEQLKLEDKVNTKFGELVYQKTGMINFDNFSSY  233
BsjJ      V--MGIENPYADEKIEATFQALKRSFL-----GYPDHAHEYVYWKESGMFAASSYQEY  229
PneJ      L--EGKIKYKTTDYQERAYQTLKLILE-----NYDSEHFEEKMYWEKKRLFANSLEEW  227
          : . : . * : : * : : . . * :***: . : : . . . :

CrnJ      LEYIQRK----- 240
BsjJ      LDNVLSLRQEIQIAKKINEYSHC 251
PneJ      YYVENI-K----- 234

```

**Figure 5.5. Amino acid sequence alignment of Pnej<sub>B</sub> and the LanJ<sub>B</sub> enzymes, CrnJ<sub>B</sub> and BsjJ<sub>B</sub>.**

Conserved, conservative, and semi-conservative substitutions are indicated by an asterisk, colon, and period, respectively.

```

PneA1      WTPTP----IILKSAAAASSKVCISAASVSGIGGLVSYNNDCLG 38
CrnA1''    FTTPACVYVSMVVS KASSAKCA-AGASAVSGAILSAIRC-- 39
          :*:* * : : *** * *..*:* : *

PneA2      STIICSATLSFIASYLG---SAQTRCGKDNKKK 30
CrnA2''    STPICAGFATLMSS-IGLVKTIKGC----- 25
          ** **:. :*** :* : : *

```

**Figure 5.6. Amino acid sequence alignment of pneumococcin and carnolysin.**

PneA1 and PneA2 are the pneumococcin peptides, while CrnA1'' and CrnA2'' are the carnolysin peptides. Conserved, conservative, and semi-conservative substitutions are indicated by an asterisk, colon, and period, respectively. Thr and Ser residues are highlighted in blue, while Cys residues are shown in red.

### 5.1.3.2. X-ray crystal structure of PneJ<sub>B</sub>

In 2007, the crystal structure of an FMN-dependent enzyme (referred to as SP\_1951) from *S. pneumoniae* was published as part of the structural genomics efforts by the Northeast Structural Genomics Consortium (NESG) sponsored by the Protein Structure Initiative (PSI) at the National Institutes of Health (NIH).<sup>284</sup> Alignment of the amino acid sequence of SP\_1951 to PneJ<sub>B</sub> revealed that the proteins are identical. However, the authors of the structural work did not recognize that SP\_1951 was part of a lanthipeptide cluster and declared the function of the enzyme to be unknown. It is also to be noted that the first FMN-dependent lanthipeptide dehydrogenase was only reported in 2014. Hence, back in 2007, comparison to literature databases only suggested that SP\_1951 is a protein with no definitive function that potentially requires FMN as cofactor. The authors performed high-throughput production and purification of His-tagged proteins, followed by high-throughput crystallization attempts. The final crystallization condition for SP\_1951 was determined to consist of 2  $\mu$ L (10 mg/mL) SP\_1951 dissolved in 5 mM Tris (pH 7.5), 100 mM NaCl, and 5 mM dithiothreitol mixed with 2  $\mu$ L reservoir solution containing 10% polyethylene glycol 3350, 100 mM tartrate, and 200 mM sodium chloride.<sup>284</sup> The crystal structures of SP\_1951 with and without FMN (PDB ID: 1SQS and 2OYS, respectively) both revealed that the enzyme forms a dimer, and that no substantial conformational changes occur upon binding of FMN. Figure 5.7A shows the crystal structure of SP\_1951 with bound FMN. Each monomer is composed of two domains, namely an N-terminal Rossmann-fold domain that consists of five parallel  $\beta$ -strands and six helices, and a C-terminal domain comprised of three helices. The FMN is located at the dimer interface, in particular between the N-terminal domain of one monomer and the C-

terminal domain of the other monomer. It was suggested that the unknown natural substrate of the enzyme is hydrophobic, since the pocket surrounding the flavin moiety of FMN is predominantly hydrophobic. Furthermore, inspection of the residues near the putative active site revealed the presence of Ser109, His110, Tyr143, and Glu209 that are suggested to be involved in catalysis (Figure 5.7B).

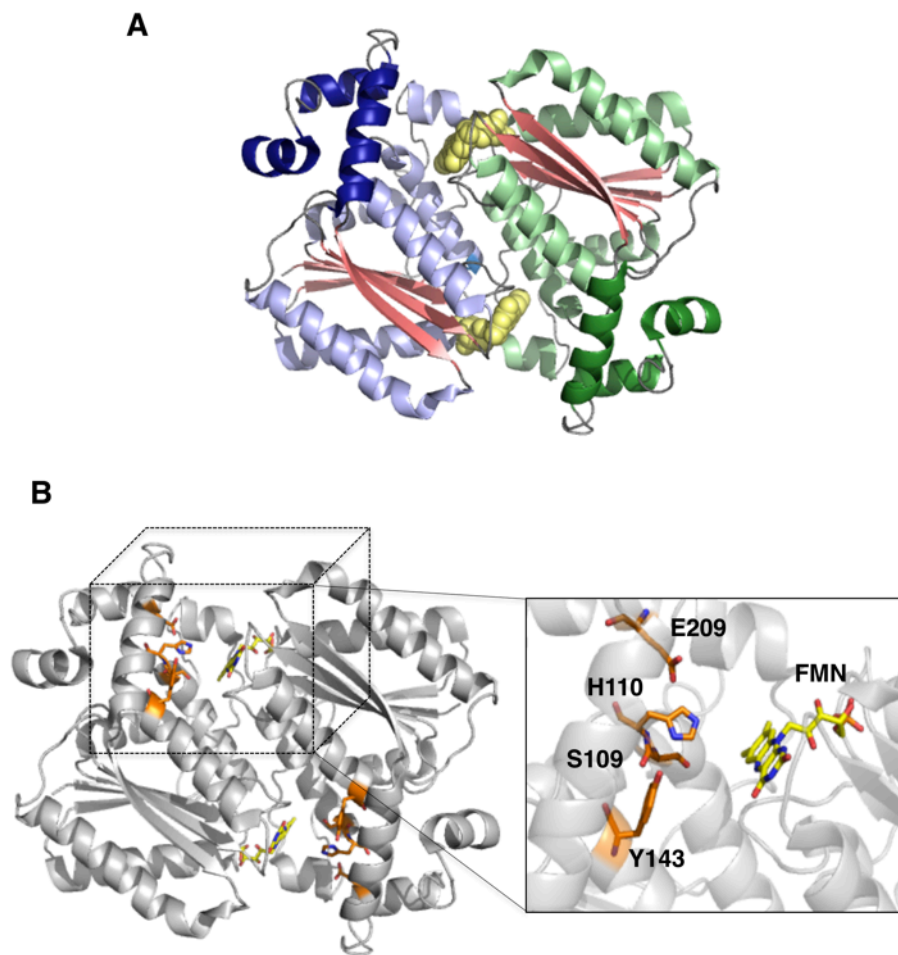


**Figure 5.7. Crystal structure of SP\_1951 dimer (PneJ<sub>B</sub> enzyme).**

(A) Cartoon representation of the SP\_1951 dimer. Monomer one is colored blue, with the N-terminal domain helices shown in light blue and the C-terminal domain shown in dark blue.  $\beta$ -strands of the N-terminal domain in both monomers are shown in salmon red. The second monomer is shown in green, with the N-terminal helices shown in light green and the C-terminal domain helices shown in dark green. FMN cofactors are shown as yellow spheres. (B) The putative active site of SP\_1951. FMN is shown in yellow. The side chain residues that are predicted to be involved in catalysis are shown in orange sticks.

#### **5.1.4. Objectives**

This project was aimed to confirm the reductase activity of Pn<sub>J<sub>B</sub></sub> and characterize the native structures of the mature Pn<sub>A1</sub> and Pn<sub>A2</sub> peptides. This study also aimed to determine the antimicrobial inhibition spectrum of Pn<sub>A1</sub> and Pn<sub>A2</sub>. Lastly, the ultimate objective was to obtain a cocrystal structure of Pn<sub>J<sub>B</sub></sub> with a bound substrate to shed light on the specificity and mechanism of this enzyme.

## **5.2. Results and Discussion**

### **5.2.1. Expression of pneumococcin in *Escherichia coli***

*S. pneumoniae* R6 was grown in brain heart infusion (BHI) broth and in tryptic soy broth (TSB), and the isolation of the prepeptide and/or propeptide was attempted by fractionating the culture supernatant using Amberlite XAD-16 resin (Sigma-Aldrich), C8 solid phase extraction cartridge (Agilent), and RP-HPLC. However, none of the peptides were detected. The absence of activity may be attributed to several reasons, such as inherent low yield or presence of silent genes. Silent lantibiotics refer to peptides with unknown production conditions and are therefore difficult to produce from natural sources. Hence, heterologous expression was pursued to produce recombinant pneumococcin.

#### **5.2.1.1. Cloning and expression of *pneM*, *pneJ<sub>B</sub>*, *pneA1*, and *pneA2***

The activity of the putative reductase Pn<sub>J<sub>B</sub></sub> was investigated via a similar approach to what was employed for Crn<sub>J<sub>B</sub></sub> and Bsj<sub>J<sub>B</sub></sub>.<sup>191,196</sup> In those previous studies, the lantibiotic

precursor peptides were coexpressed with the associated biosynthetic machinery in order to introduce the necessary post-translational modifications. Similarly, in this project, the genes that encode the modifying enzymes, PneM and PneJ<sub>B</sub>, and the precursor peptides, PneA1 and PneA2, were codon-optimized for *E. coli* expression and purchased from BioBasic Inc. As discussed earlier, the PneM enzyme facilitates the dehydration of Ser and Thr residues to Dha and Dhb, respectively, followed by the addition of the Cys thiol group to the dehydro residues to form Lan and MeLan rings. The PneJ<sub>B</sub> enzyme, on the other hand, should theoretically install D-Ala and/or D-Abu residues by reducing select Dha and Dhb residues that are not involved in Lan and MeLan rings. Plasmids pRSFDuet-PneM-PneA1, pRSFDuet-PneM-PneA2, and pETDuet-PneJ<sub>B</sub> were prepared following standard molecular biology techniques.<sup>285</sup> The plasmids were designed such that PneA1 and PneA2 would contain an N-terminal His-tag to facilitate purification by Ni-NTA affinity chromatography. The vector maps of pRSFDuet-1 and pETDuet-1 are shown in Figure 5.8, highlighting the restrictions sites used for cloning.

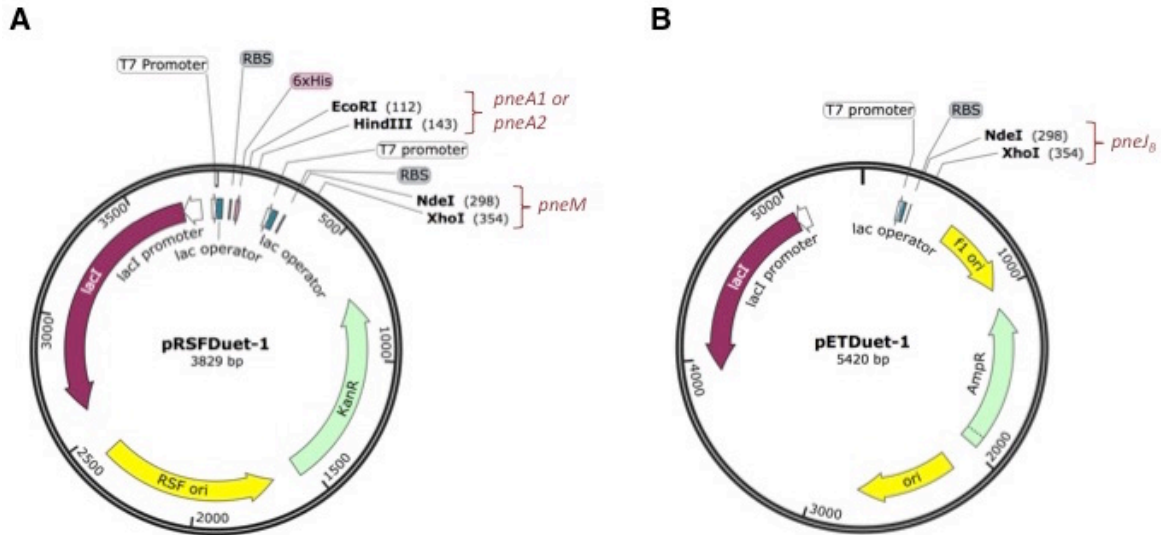


**Figure 5.8. pRSFDuet-1 and pETDuet-1 vector maps.**

The restriction sites utilized for constructing pRSFDuet-PneM-PneA1, pRSFDuet-PneM-PneA2, and pETDuet-PneJ<sub>B</sub> plasmids are indicated in bold. pRSFDuet-1 contains a kanamycin resistance marker, while pETDuet-1 has an ampicillin resistance gene.

*E. coli* BL21 (DE3) was transformed with either pRSFDuet-PneM-PneA1 or pRSFDuet-PneM-PneA2 with and without pETDuet-PneJ<sub>B</sub>. The transformants were grown and induced for protein expression at 18 °C using 0.1 mM isopropyl β-D-1-thiogalactopyranoside (IPTG), which are the same conditions employed for the carnolysin (CrnJ<sub>B</sub>) system.<sup>191</sup> The cultures were lysed and the pneumococcin precursors were purified using Ni-NTA affinity chromatography (Figure 5.9). A strong but diffused band corresponding to the expressed proteins (PneM-PneA1 and PneM-PneA2 with and without PneJ<sub>B</sub>) was observed on the SDS-PAGE gel. Analysis by MALDI-TOF MS revealed a cluster of undistinguishable peaks (Figure 5.10A). Hence, the bands on the SPS-PAGE gel were excised, digested with trypsin, and subjected to tandem mass spectrometry for further analysis. The results showed that the bands from all the expression systems indeed

correspond to the precursor peptides, since the unmodified sequences of the leader peptides were detected. However, results also revealed that the samples consisted of a mixture of partially dehydrated and/or cyclized products. Purification by RP-HPLC was done, however, none of the optimization attempts were successful in separating the different peptide variants.

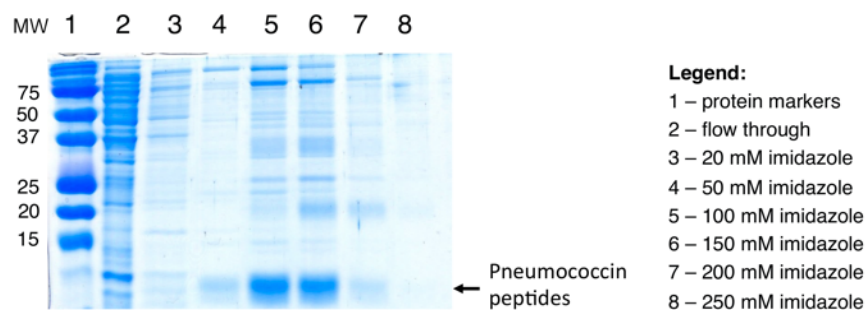


**Figure 5.9. SDS-PAGE gel of Ni-NTA affinity chromatography fractions from the purification of proteins from pRSFDuet-PneM-PneA1 expression.**

A mixture of pneumococcin peptides with different extents of modifications eluted at 100 to 150 mM imidazole. A similar profile was observed for the other expression systems that utilized pRSFDuet-PneM-PneA1 with pETDuet-PneJ<sub>B</sub>, and pRSFDuet-PneM-PneA2 with and without pETDuet-PneJ<sub>B</sub>.

Since the peptides were being expressed in the soluble fraction, expression at a higher temperature (37 °C) was attempted in order to potentially improve the efficiency of the PneM enzyme and facilitate the complete installation of the modifications. Results showed that the PneA1 and PneA2 peptides (with and with PneJ<sub>B</sub>) were still expressed in the soluble fraction. However, after Ni-NTA affinity purification, MALDI-TOF MS (Figure 5.10B) showed that although there was an improvement in the resolution of the signals, there were still numerous peptide variants in the sample that were also not possible to separate by RP-HPLC.

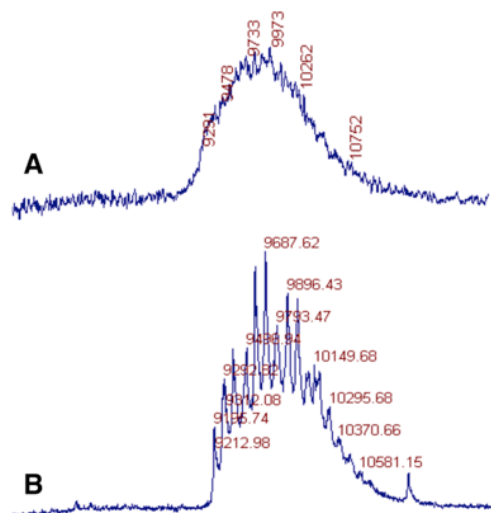


**Figure 5.10. MALDI-TOF mass spectra of PneA1.**

(A) Mass spectrum obtained for the PneA1 precursor peptide coexpressed with PneM, and induced with 0.1 mM IPTG at 18 °C for 20 h, or (B) with 0.5 mM IPTG at 37 °C for 3 h. The same trend was observed for PneA2.

### 5.2.1.2. Cloning and expression of truncated PneA1 and PneA2

Earlier studies have shown that LanJ enzymes are promiscuous and can recognize a variety of substrates.<sup>196,280,281</sup> Hence, truncated versions of PneA1 and PneA2 were designed to simplify the substrates by eliminating other reactive sites (Figure 5.11). The truncated versions of PneA1 and PneA2 were cloned in a similar fashion as was done with the full-length precursor peptides. Expression trials, however, showed that the truncated peptides could not be produced. Hence, chemical synthesis of pneumococcin substrate analogues is currently being pursued by Daniel Engelhart, another graduate student in the Vederas group. The chemically synthesized substrates will in turn be utilized for *in vitro* PneJ<sub>B</sub> activity assay.

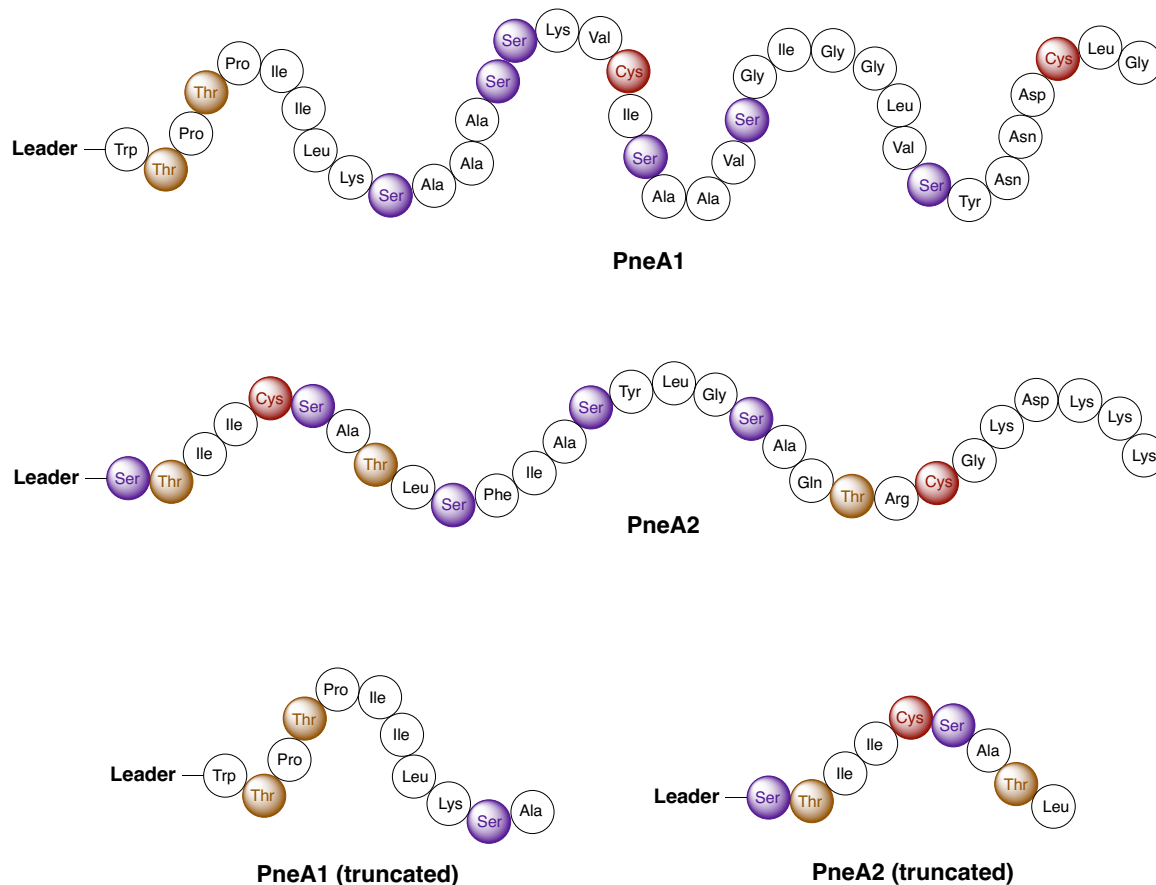


**Figure 5.11. PneA1 and PneA2 precursor peptides and their truncated versions.**

Ser residues are shown in violet; Thr residues are in brown;  
and Cys residues are in maroon.

### 5.2.2. Expression and purification of SUMO-PneJ<sub>B</sub>

Due to the difficulties encountered in the *in vivo* assays, *in vitro* reconstitution of the activity of Pn<sub>B</sub> will be pursued using chemically synthesized substrates. In line with this, a His-tagged SUMO (small ubiquitin-like modifier)–Pn<sub>B</sub> construct was prepared and expressed, wherein 10-20 mg/mL fusion protein was obtained per 400 mL culture (Figure 5.12). This fusion protein can be used for the *in vitro* assays, as well as crystallographic trials with a bound substrate. Several lantibiotic biosynthetic enzymes have been

previously demonstrated to be active even with attached expression tags that are as small as a His<sub>6</sub> tag (~1 kDa) to as large as an MBP tag (~43 kDa).<sup>196,280,286,287</sup> The SUMO tag (~13 kDa) increases yield and solubility, and has also been used for carrier-driven crystallization.<sup>288</sup>

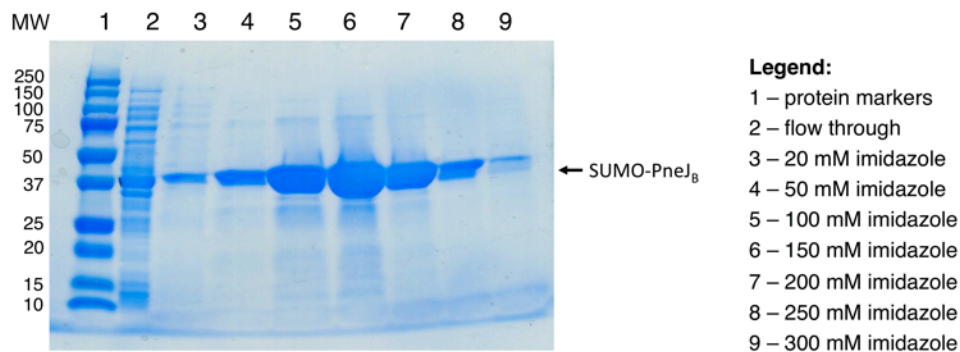


**Figure 5.12. SDS-PAGE gel of SUMO-PneJ<sub>B</sub> Ni-NTA affinity chromatography purification fractions.**

Expressed SUMO-PneJ<sub>B</sub> (~40 kDa) was purified with increasing amounts of imidazole. Majority of the SUMO-PneJ<sub>B</sub> protein eluted at 100 to 150 mM imidazole.

It is also possible to obtain PneJ<sub>B</sub> that is devoid of any tag via treatment of the SUMO-PneJ<sub>B</sub> fusion protein with SUMO protease. A pilot cleavage trial that utilized the recommended protease concentration showed that the SUMO tag can be efficiently removed at 8 °C or 25 °C after 20 h of incubation (Figure 5.13). The cleavage condition for the removal of the SUMO protein normally requires the detergent IGEPAL<sup>®</sup> CA-630 (Sigma-Aldrich), which needs to be removed prior to use in activity assays or protein crystallization. Hence, a cleavage trial without IGEPAL was also set up. The results demonstrated that removal of IGEPAL from the cleavage cocktail reduced the cleavage efficiency by ~50% at room temperature, while minimal cleavage was observed at 8 °C.

Hence, these results showed the importance of incorporating IGEPAL in the cleavage cocktail to obtain higher amounts of cleaved protein. Removal of the detergent may consequently be accomplished by a final purification step such as size exclusion chromatography.

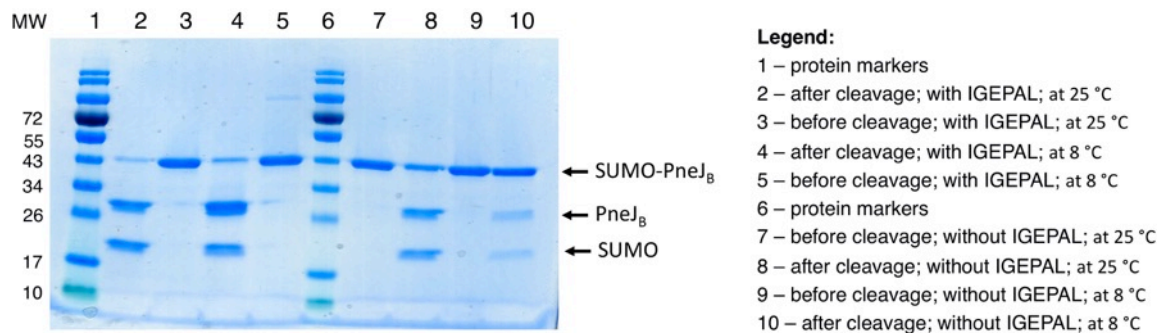


**Figure 5.13. SDS-PAGE gel of SUMO-PneJ<sub>B</sub> pilot cleavage trials.**

Overnight SUMO protease treatment of SUMO-PneJ<sub>B</sub> protein at 8 °C or 25 °C with or without the detergent, IGEPAL.

### 5.3. Conclusions and Future Directions

The role of the putative reductase, PneJ<sub>B</sub>, in the formation of D-Ala and D-Abu in pneumococcin was investigated through the heterologous expression of pneumococcin biosynthetic proteins in *E. coli*. Coexpression of the precursor peptides, PneA1 and PneA2, with PneM (with and without PneJ<sub>B</sub>) produced a mixture of partially modified substrates that could not be separated by RP-HPLC. In order to simplify the precursor peptides, other reactive sites were eliminated by truncating the precursor peptides. However, the truncated peptides could not be expressed. Chemical synthesis of substrate analogues is therefore currently being pursued. The substrate analogues will consequently

be used for *in vitro* PneJ<sub>B</sub> activity assays. In line with this, PneJ<sub>B</sub> was expressed and purified as a SUMO fusion protein. It was further demonstrated that the SUMO tag could be readily cleaved to afford the PneJ<sub>B</sub> enzyme that is devoid of any tag.

Future work may be directed towards the use of an expression vector with a stronger promoter for the PneM enzyme, or a low copy number plasmid for the precursor peptides. This may result in the complete installation of the modifications in PneA1 and PneA2, and will provide the native substrates of PneJ<sub>B</sub>. Alternatively, PneM and the precursor peptides could be expressed and purified separately, and consequently used in an *in vitro* assay where the concentrations of each component can be controlled. Given the optimal concentrations of PneM and the substrate, it is envisioned that a PneM-catalyzed reactions will proceed to completion. Another approach would be to perform alanine mutations of select reactive sites on the precursor peptides via site-directed mutagenesis in order to produce substrate analogues for PneJ<sub>B</sub>. Once the function of PneJ<sub>B</sub> is confirmed, the substrate scope of PneJ<sub>B</sub>, and the role of the leader peptide on the activity of the enzyme may be investigated. If the native substrates were accessed, it would be of interest to establish the structures and stereochemistry of the mature PneA1 and PneA2 peptides, and the antimicrobial activity spectrum of the bacteriocin. Lastly, crystallographic trials of PneJ<sub>B</sub> bound with PneA1 or PneA2 may be pursued. It is worth noting that PneJ<sub>B</sub> has already been crystallized.<sup>284</sup> Therefore, there is a high probability of recrystallizing the enzyme, but this time with a bound substrate. A detailed understanding on the enzyme's specificity and mechanism is essential in developing PneJ<sub>B</sub> as a tool in synthetic biology to obtain peptides with D-amino acids.

## Chapter 6

### Summary and Conclusions

This thesis presented the structural characterization of the circular bacteriocin acidocin B (AcdB)<sup>51</sup>, the leaderless bacteriocins lacticin Q (LnqQ) and aureocin A53 (AucA)<sup>225</sup>, and the two-peptide bacteriocin carnobacteriocin XY (CbnXY)<sup>226</sup>. It also described the investigation of the lanthipeptide dehydrogenase PneJ<sub>B</sub>, which is involved in the biosynthesis of pneumococin.

In the first study, AcdB from *Lactobacillus acidophilus* M46 was purified and shown to be a circular bacteriocin that is composed of 58 amino acid residues based on MALDI-TOF MS and MS/MS sequencing. This corrects the earlier report indicating that AcdB is a linear peptide consisting of 59 residues.<sup>227</sup> Consequently, the NMR solution structure of AcdB in sodium dodecyl sulfate micelles was elucidated, showing that AcdB consists of four  $\alpha$ -helices that are folded to form a compact, globular bundle with a central pore. The three-dimensional (3D) structure of AcdB is the first representative structure for subgroup II circular bacteriocins, which are characterized by having low isoelectric points (pI ~7 or lower) relative to members of subgroup I (pI ~10). The structure of AcdB was compared to that of carnocyclin A, a subgroup I circular bacteriocin. The results revealed variations in their overall fold and surface properties. Carnocyclin A has a highly cationic surface, while AcdB has a vastly hydrophobic surface, signifying that hydrophobic instead of electrostatic interactions may be mainly involved in the binding of AcdB to the cell membrane of target organisms. There are currently only two other known subgroup II circular bacteriocins, namely gassericin A and butyrvibriocin AR10. Homology models

of the said bacteriocins were created and were shown to share a similar overall fold with AcdB. BLAST search identified at least 7 other putative subgroup II circular bacteriocins, and sequence alignment of the known and putative subgroup II circular bacteriocins revealed a highly conserved asparagine residue at the leader peptide cleavage site, suggesting that an asparagine endopeptidase might be involved in the cyclization of the precursor peptide and/or removal of the leader peptide during the maturation of subgroup II circular bacteriocins. The biosynthetic gene cluster of AcdB was sequenced and shown to be highly similar to that of gassericin A, further indicating that AcdB is a circular bacteriocin. Lastly, a phylogenetic tree that was constructed using the peptide sequences of AcdB, gassericin A, butyrivibriocin AR10, and the putative members of this subgroup showed that the peptides can be divided into two subclades. The first subclade consists of peptides from *Lactobacillus* spp., while the second subclade is comprised of peptides from various genera including *Bacillus*, *Lactobacillus*, *Butyrivibrio*, and *Streptococcus*.

In the second study, the leaderless bacteriocins lacticin Q (LnqQ) and aureocin A53 (AucA) from *Lactococcus lactis* QU 5 and *Staphylococcus aureus* A53, respectively, were expressed and purified using the SUMO fusion technology. CD analysis showed that both peptides are highly helical in aqueous conditions unlike most linear peptides. Their NMR solution structures were then determined, revealing that both peptides are composed of four  $\alpha$ -helices that assume a saposin-like fold with a highly cationic surface and a hydrophobic core. The cationic character of their surface suggests that electrostatic interactions facilitate their binding to negatively charged bacterial membranes. The saposin-like fold observed in LnqQ and AucA was strikingly similar to the overall fold of the two-component leaderless bacteriocin enterocin 7 that is composed of Ent7A and

Ent7B, despite their differences in amino acid sequence and peptide length. LnqQ, AucA, Ent7A, and Ent7B have all been shown to have wide inhibition spectra. Consequently, homology modeling showed that other broad-spectrum leaderless bacteriocins share the same structural motif. The structures of LnqQ and AucA also exhibit certain similarities to those of the circular bacteriocins, which are also active against a broad spectrum of organisms. Activity assays were performed and results revealed that LnqQ and AucA are not synergistic, and that LnqQ is more potent than AucA against various Gram-positive strains. These findings suggest that despite the similar 3D structures of LnqQ and AucA, their mechanisms of action are different.

In the third study, carnobacteriocin X (CbnX), which was originally reported to be a single-peptide bacteriocin (class IId), was shown to comprise a two-peptide bacteriocin (class IIb) with CbnY as its partner. This was confirmed by sequence analysis and synergy assays. Gene cluster analysis showed that the genes *cbnX* and *cbnY* are located next to each other, while amino acid analysis showed that both peptides contain GXXXG motifs. Synergy assay revealed that CbnX and CbnY are not active individually, but exhibit antimicrobial activity against closely related strains when combined. These properties are characteristic of two-peptide bacteriocins. CbnXY is the first representative two-peptide bacteriocin identified in *Carnobacteria* spp. CD analysis showed that CbnX and CbnY are unstructured in water but assume a helical conformation in the presence of the structure-inducing solvent, trifluoroethanol. [<sup>13</sup>C, <sup>15</sup>N]-Labelled CbnX and CbnY peptides were then expressed in *Escherichia coli*, purified, and used for NMR data acquisition for the elucidation of their solution structures. The structures of both peptides share several features to those of other two-peptide bacteriocins (i.e. LcnG, PlnEF, PlnJK). CbnX has an

extended amphipathic  $\alpha$ -helix, while CbnY is composed of two  $\alpha$ -helices in an “L” shape conformation, wherein the N-terminal helix is hydrophobic, while the C-terminal helix is amphipathic. The last four residues at the C-terminus of CbnY are cationic residues, which are suggested to facilitate peptide insertion into negatively charged target bacterial membranes. It has been previously proposed that two-peptide bacteriocins interact with each other in order to elicit synergistic activity. However, there was no significant interaction observed between CbnX and CbnY, suggesting that a receptor may be required to mediate the formation of the CbnXY complex.

In the fourth project, the activity of the putative flavin-dependent lanthipeptide reductase, PneJ<sub>B</sub>, was investigated. Sequence analysis suggests that PneJ<sub>B</sub> is likely involved in the installation of D-Ala and D-Abu residues in the two-component lantibiotic from *Streptococcus pneumoniae* R6, named pneumococcin, which is comprised of PneA1 and PneA2. The pneumococcin precursor peptides (PneA1 and PneA2) and the lantibiotic synthetase (PneM) were coexpressed with and without PneJ<sub>B</sub> to monitor the activity of PneJ<sub>B</sub>. However, a mixture of partially modified substrates was produced and could not be further purified. To potentially address this problem, truncated precursor peptides were designed and cloned. However, the truncated peptides could not be successfully produced in *E. coli*. Hence, chemical synthesis of substrate analogues is currently being pursued. The substrates will consequently be used for *in vitro* PneJ<sub>B</sub> activity assays using a PneJ<sub>B</sub> enzyme that was expressed in *E. coli* and purified as a SUMO fusion protein. The SUMO tag of the fusion protein could be readily cleaved, and the resulting enzyme may also be tested for activity.

In summary, this thesis covered the structure elucidation of different types of bacteriocins and the investigation of a bacteriocin biosynthetic enzyme. Structure characterization of antimicrobial peptides is essential in understanding their properties and modes of action, and in the design of peptide analogues with improved biological attributes. Moreover, a detailed understanding on the mechanism of the enzymes involved in the biosynthesis of antimicrobial peptides could open avenues for bioengineering to design antimicrobials with superior properties.

## Chapter 7

### Experimental Procedures

#### 7.1. General Experimental Details

##### 7.1.1. Media and bacterial strains

###### 7.1.1.1. Media preparation

All media were purchased from Becton Dickinson and Company (BD, Franklin Lakes, NJ, USA), and prepared based on the manufacturer's instructions. Soft agar contained 0.75% (w/v) agar dissolved in the desired broth. Five mL of the molten soft agar solution was placed per test tube prior to autoclaving. Agar plates contained 1.5% (w/v) agar dissolved in the desired broth. The agar solution was autoclaved and allowed to cool prior to adding any antibiotic. Twenty mL of the solution was poured in each sterile Petri dish in a laminar flow cabinet. Once the agar solidified, the plates were stored at 4 – 8 °C.

###### 7.1.1.2. Glycerol stocks

Bacterial strains were stored at -80 °C as 20% glycerol stocks, except for *Escherichia coli* BL21 strains, which were maintained in 8% glycerol. A sterile 80% glycerol solution was used to prepare the glycerol stocks by mixing the bacterial culture with the appropriate volume of the glycerol solution to give the desired final concentration, with a final volume of 1 mL. For inoculating fresh cultures, a small amount

of the frozen glycerol stock was transferred into the broth using a sterile pipet tip under aseptic conditions. Thawing the glycerol stocks was avoided.

### 7.1.1.3. Growth conditions for indicator strains

Table 7.1 lists the different indicator strains that were used in the various chapters of this thesis along with the media and culture conditions employed for each strain.

**Table 7.1. Indicator strains and corresponding growth conditions**

Indicator strain	Media <sup>a</sup>	Conditions
<i>Brochothrix campestris</i> ATCC 43754	APT	RT, 0 rpm
<i>Carnobacterium divergens</i> LV13	APT/BHI	RT, 0 rpm
<i>Carnobacterium maltaromaticum</i> UAL26	APT	16 °C, 0 rpm
<i>C. maltaromaticum</i> UAL26 (pMG36c-cclBITCDA)	APT	16 °C, 0 rpm
<i>C. maltaromaticum</i> A9b-	BHI	RT, 0 rpm
<i>Enterococcus faecalis</i> ATCC 7080	APT	RT, 0 rpm
<i>E. faecalis</i> 710C	APT	RT, 0 rpm
<i>Enterococcus faecium</i> BFE900	APT	RT, 0 rpm
<i>Lactobacillus acidophilus</i> M46	MRS	RT, 0 rpm
<i>Lactobacillus sakei</i> UAL1218	APT	RT, 0 rpm
<i>Lactococcus lactis</i> ATCC 19257	APT	RT, 0 rpm
<i>Staphylococcus aureus</i> ATCC 29213	TSB	RT, 0 rpm
<i>S. aureus</i> ATCC 6538	TSB	RT, 0 rpm

<sup>a</sup> APT, all-purpose tween; BHI, brain heart infusion; MRS, de Man, Rogosa and Sharpe; TSB, tryptic soy broth

## 7.1.2. Antimicrobial activity assays

### 7.1.2.1. Deferred inhibition assay

An agar plate with appropriate media was stabbed with a sterile toothpick that was dipped into the desired bacterial colony or culture broth. The plate was incubated overnight at the optimal temperature for bacterial growth. At the same time, the indicator strain was grown in the appropriate broth overnight. Once the test bacteria had grown on

the plate, and the indicator culture in the broth, a 5 mL molten soft agar was inoculated with 100  $\mu$ L of the indicator strain culture, vortexed, and poured over the stabbed agar plate. The plate was incubated at the optimal temperature for the indicator strain for 20 h, and observed for zones of clearing.

#### **7.1.2.2. Spot-on-lawn assay**

The indicator strain was grown overnight in 5 mL of appropriate broth. A 5 mL molten soft agar was inoculated with 100  $\mu$ L of the overnight indicator strain culture, vortexed, and poured over an agar plate (20 mL/plate). The soft agar was dried and 10  $\mu$ L test samples were pipetted on top of the bacterial lawn. The samples were dried, incubated overnight at the optimal temperature for the indicator strain, and observed for zones of clearing.

### **7.1.3. General molecular biology techniques**

#### **7.1.3.1. Plasmid isolation**

*E. coli* DH5 $\alpha$  transformed with the desired plasmid was grown overnight at 37  $^{\circ}$ C, 225 rpm, in 5 mL Luria-Bertani (LB) broth containing the appropriate antibiotic. Plasmids were isolated using either a GeneJET Plasmid Miniprep Kit (Fermentas Canada Inc., Burlington, ON, Canada) or a QIAprep Spin Miniprep Kit (Qiagen, Mississauga, ON, Canada) according to the manufacturer's instructions. The plasmids were eluted in Tris-ethylenediaminetetraacetic acid (EDTA; TE) buffer and stored at -20  $^{\circ}$ C.

#### **7.1.3.2. Polymerase chain reaction**

DNA was amplified by polymerase chain reaction (PCR) using a Techgene Thermal Cycler (Techne Inc., Burlington, NJ, USA). Either Taq polymerase or Platinum<sup>®</sup> Taq High Fidelity from Invitrogen (Carlsbad, CA, USA) were used according to the manufacturer's instructions. When applicable, PCR products were purified either by using a QIAquick PCR Purification Kit (Qiagen) or a QIAquick Gel Extraction Kit (Qiagen).

#### **7.1.3.3. Restriction enzyme digestion**

FastDigest restriction enzymes from Thermo Scientific (Waltham, MA, USA) were used according to the manufacturer's instructions. Digests were cleaned-up either by using a QIAquick PCR Purification Kit (Qiagen) or a QIAquick Gel Extraction Kit (Qiagen).

#### **7.1.3.4. Agarose gel electrophoresis**

Agarose gels (1 – 2 % w/v, depending on PCR product size) were prepared using Ultra-Pure Agarose (Invitrogen) in either Tris-acetate-EDTA (TAE) or Tris-borate-EDTA (TBE) buffer, and were stained with SYBR<sup>®</sup> Safe DNA gel stain (Life Technologies; 1/10,000 dilution in DMSO). Sample buffer (6x; Thermo Scientific) was added to DNA samples prior to loading into the gel. Gels were run at 90 – 110 V and visualized using a Dark Reader Transilluminator (Clare Chemical Research, Dolores, CO, USA) or an ImageQuant RT ECL Imager (GE Healthcare Life Sciences, Little Chalfont, Buckinghamshire, UK).

#### **7.1.3.5. DNA quantification**

DNA concentrations were measured using an Implen NanoPhotometer P360 (Implen Inc., Westlake Village, CA, USA), specifically using the absorbance at 260 nm. Purity from protein contaminants was assessed based on the 260/280 nm absorbance ratio.

#### **7.1.3.6. Ligation reactions**

T4 DNA ligase (Invitrogen) was used for the ligation reactions according to the manufacturer's instructions, following a 3:1 insert:vector molar ratio. Ligation reactions were transformed into chemically competent *E. coli* DH5 $\alpha$  or *E. coli* Mach1 strains from Invitrogen.

#### **7.1.3.7. Transformation of chemically competent *Escherichia coli***

A 50  $\mu$ L aliquot of chemically competent *E. coli* cells (Invitrogen or New England Biolabs; Ipswich, MA, USA) was thawed on ice bath, and the DNA sample (1 to 5  $\mu$ L) was added, stirred gently with a pipette tip, and incubated on ice for 30 min. The cells were heat-shocked at 42 °C for 30 s, placed back on ice for 2 min, and added with 950  $\mu$ L LB broth. The mixture was incubated at 37 °C, 225 rpm, for 1 h. The cells (20 to 100  $\mu$ L) were spread on LB agar plates containing the appropriate antibiotic(s), and incubated overnight at 37 °C.

#### **7.1.3.8. DNA sequencing**

DNA sequencing was done at the University of Alberta Molecular Biology Service Unit using a BigDye Terminator v3.1 Cycle Sequencing Kit (Applied Biosystems, Foster City, CA, USA) and an ABI 3730 DNA Analyzer (Applied Biosystems).

#### **7.1.4. Heterologous expression of proteins**

##### **7.1.4.1. Cell lysis**

Bacterial cells were lysed mostly using a TS Series Bench Top Cell Disruptor (Constant Systems Ltd., Low March, UK). In cases when the cell disruptor was unavailable, cell lysis was accomplished through sonication using a Branson Sonifier 450 (Branson Ultrasonics Corp., Danbury, CT, USA), or treatment with B-PER Bacterial Protein Extraction Reagent (Thermo Scientific) according to the manufacturer's instructions. Bacterial suspensions in lysis buffer were added with 5 mg lysozyme and 20 U DNase (Invitrogen) per 30 mL buffer prior to cell lysis to lower sample viscosity. The lysis buffer components are specified in the subsequent relevant sections. For the cell disruptor, the instrument was first washed with 20 mL of the lysis buffer at 10 kpsi. The bacterial suspension was then passed through the system at 20 – 25 kpsi, followed with 10 – 20 mL lysis buffer for washing at the same operating pressure. For the sonication procedure, the bacterial suspension was transferred into a 50 mL falcon tube, and the cells were lysed by 3 cycles of 10 s sonication followed by 30 s on ice. In both cases, the lysate was centrifuged ( $23,700 \times g$ , 30 min, 4 °C), and the supernatant was collected.

#### **7.1.4.2. Tris-glycine SDS-PAGE**

Protein samples were analyzed using 10% or 15% (w/v) acrylamide SDS-PAGE (sodium dodecyl sulfate-polyacrylamide gel electrophoresis) resolving gel with 4% stacking gel, or using a commercial 12% or 4 – 20 % Mini-PROTEAN TGX precast gel (Bio-Rad, Hercules, CA, USA). Protein samples were mixed with 2x Laemmli Sample Buffer (Bio-Rad) and boiled at 100 °C for 5 min. Prepared samples and protein standards (Bio-Rad) were loaded into the gels, and were run at 70 V for 15 min to compress the bands, and 120 – 180 V until the dye reached the bottom of the gel. Gels were visualized with either coomassie stain (0.1% w/v coomassie R-250, 40% ethanol, 10% acetic acid), followed by destaining (10% ethanol, 7.5% acetic acid), or GelCode Blue stain (Pierce, Rockford, IL, USA) and destained with water.

#### **7.1.4.3. Tris-tricine SDS-PAGE**

Small peptides (<10 kDa) were resolved on 16% (w/v) acrylamide Tris-Tricine polyacrylamide gels with 4% stacking gels. Samples were prepared in Tris-Tricine Sample Buffer (Bio-Rad) and heated to 100 °C for 5 min. Prepared samples and protein standards (Bio-Rad) were loaded into the gels, and electrophoresis was run at 70 V for 15 min to compress the bands, followed by 100 – 120 V until the dye reached the bottom of the gel. The gels were fixed with a solution containing 50% methanol, 40% water, and 10% glacial acetic acid for 1 h. The gels were then visualized the same way as with Tris-Glycine SDS-PAGE gels.

## **7.1.5. Purification of peptides and proteins**

### **7.1.5.1. Amberlite XAD-16**

Amberlite XAD-16 resin (Sigma-Aldrich, St. Louis, MO, USA) was used to purify culture supernatants based on hydrophobic interaction with the resin. The resin (40 – 80 g) was soaked in isopropanol (IPA) for 30 min and loaded into a glass column fitted at the base with Miracloth (EMD Millipore, Billerica, MA, USA). The resin was washed with 250 mL of 0.1% trifluoroacetic acid (TFA) per 40 g resin at 10 mL/min using a peristaltic pump (Econo Pump, Bio-Rad). The solvent fractions that were used are described later in the subsequent relevant sections. Spot-on-lawn assays were performed on all fractions to identify the bacteriocin-containing fractions.

### **7.1.5.2. C8 and C18 solid-phase extraction**

Bond Elut C8 10 g, 60 mL cartridge (Agilent, Mississauga, ON, Canada) and Strata C18-E (Phenomenex, Torrance, CA, USA) were used. The cartridge was first activated by washing with 50 mL methanol and 100 mL Milli-Q water at 10 mL/min. The samples and solvents used (described later in the subsequent relevant sections) were passed through the cartridge at 5 mL/min using a peristaltic pump (Econo Pump, Bio-Rad).

### **7.1.5.3. RP-HPLC**

Reverse-phase high-performance liquid chromatography (RP-HPLC) was performed on Beckman System Gold units (analytical and preparative), a Varian Prostar Model 210 system (analytical), and Gilson systems with a model 322 HPLC pump (analytical and

preparative). HPLC grade solvents were filtered through a Millipore filter under vacuum prior to use. Details on the columns, solvents, and methods used are described in the subsequent relevant sections.

#### **7.1.5.4. Ni-NTA affinity chromatography**

Ni-NTA (nickel-nitrilotriacetic acid) Superflow resin (Qiagen) was used to purify His-tagged proteins. Typically, 2 mL of slurry (50% suspension in 30% ethanol) was used for every 40 mL cell free lysate. Samples and buffers were allowed to pass through by gravity. Details on the buffers used are described in the subsequent relevant sections.

#### **7.1.6. SUMO protease digestion**

For every 200  $\mu$ L cleavage cocktail containing 20  $\mu$ g fusion protein, 1 – 10 U of the His-tagged SUMO (small ubiquitin-like modifier) protease (McLab, South San Francisco, CA, USA) was used, together with 20  $\mu$ L of 10x SUMO protease buffer (500 mM Tris-HCl pH 8.0, 2% IGEPAL<sup>®</sup> CA-630 (Sigma-Aldrich), 10 mM dithiothreitol) and 150 mM NaCl. Details on the amount of protease and time required to complete cleavage are described in the subsequent relevant sections.

#### **7.1.7. Protein quantification**

##### **7.1.7.1. Spectrophotometric quantification**

Protein concentrations were determined by measuring absorbance at 280 nm using an Implen NanoPhotometer P360 (Implen Inc.). Molar extinction coefficients were

calculated using the ProtParam program<sup>289</sup> in the ExPASy Proteomics server. Protein concentration was then calculated using Beer's Law:  $c = A/b\epsilon$ ; where  $c$  is the concentration (mol/L),  $A$  is the UV absorbance at 280 nm,  $b$  is the path length (cm), and  $\epsilon$  is the molar extinction coefficient (L/mol-cm).

#### **7.1.7.2. BCA colorimetric analysis**

A Pierce BCA (bicinchoninic acid) Protein Micro Assay Kit (Thermo Scientific) was used according to the manufacturer's instructions. Bovine serum albumin was used as protein standard. Samples were prepared in 96-well plates and absorbance at 562 nm was measured using a SpectraMax<sup>®</sup> i3x Plate Reader (Molecular Devices, Sunnyvale, CA, USA).

#### **7.1.8. Circular dichroism spectroscopy**

Circular dichroism (CD) data were acquired using an OLIS DSM 17 CD spectrophotometer using a 0.2 mm quartz cuvette. Five scans were run for each sample at 1 nm increments from 185 to 250 nm. Baseline spectra of solvent reference samples were subtracted from the respective peptide samples, and the percent  $\alpha$ -helicity was estimated using the equation,  $\% \alpha\text{-helicity} = (3000 - \theta_{222})/39000$ .<sup>290</sup> Details on the temperature and solutions used are described in the subsequent relevant sections.

## **7.1.9. Mass spectrometry**

### **7.1.9.1. MALDI-TOF MS**

Matrix-assisted laser desorption ionization-time of flight mass spectrometry (MALDI-TOF MS) was performed on an AB Sciex Voyager Elite system (Foster City, CA, USA) in positive reflectron mode with delayed extraction, using either 3,5-dimethoxy-4-hydroxycinnamic acid (sinapinic acid) or 4-hydroxy- $\alpha$ -cyanocinnamic acid as matrix. A two-layer sample preparation method was employed.<sup>291</sup> Prior to data acquisition, samples were acidified, and whenever applicable, samples were cleaned-up either by rinsing with 0.1% TFA or with ZipTip pipette tips (C4 or C18, EMD Millipore) according to the manufacturer's instructions.

### **7.1.9.2. LC-MS/MS**

Liquid chromatography-tandem mass spectrometry (LC-MS/MS) was performed using a nanoAcquity column (100 Å pore size, 75  $\mu$ m x 15 cm, 3  $\mu$ m Atlantis dC18; Waters, MA) on a nanoAcquity ultra performance liquid chromatography (Waters, MA). Quadrupole-time of flight Premier MS (Micromass, UK) was used to collect MS/MS data, which were processed using PEAKS 5.1 software (Bioinformatics Solutions, Waterloo, ON, Canada).<sup>292</sup> Details on the solvent gradient and flow rate used are described in the subsequent relevant sections.

#### **7.1.10. NMR spectroscopy**

Nuclear magnetic resonance (NMR) data were acquired on a Varian Inova 600 MHz spectrometer (equipped with a triple-resonance HCN probe) or a Varian VNMRS 700 MHz spectrometer (equipped with a triple-resonance HCN cold probe and z-axis pulsed-field gradients) at the Department of Chemistry of the University of Alberta. Experimental details are described in the subsequent relevant sections.

#### **7.1.11. Bioinformatics and structural programs**

The NCBI-BLAST<sup>245</sup> (National Center for Biotechnology Information-Basic Local Alignment Search Tool) was used for genome mining. Clustal W<sup>240</sup> and Clustal Omega<sup>293</sup> were used for sequence alignment. NMRPipe<sup>232</sup> was used to process NMR data, while NMRView<sup>233</sup> was used for data analysis. Angle restraints were obtained using TALOS<sup>262</sup> (Torsion Angle Likelihood Obtained from Shift and Sequence Similarity). Structural calculations were performed using CYANA 2.1<sup>234</sup> (Combined Assignment and Dynamics Algorithm for NMR Applications). PyMOL<sup>235</sup> was used to generate the 3D structures and hydrophobic surface maps, while the APBS<sup>294</sup> (Adaptive Poisson-Boltzmann Solver) was used for the electrostatic surface calculations. Structure homology modeling was done using the SWISS-MODEL<sup>242</sup> server, while secondary structure predictions were obtained using the JPred v.4 server<sup>254</sup>.

## **7.2. Experimental Procedures for the Structural Studies of Acidocin B**

### **7.2.1. Bacterial strains and culture conditions**

*Lactobacillus acidophilus* M46, producer strain of acidocin B (AcdB), was grown in MRS (de Man, Rogosa and Sharpe) broth containing twice the recommended amount of MRS powder per liter of media and further supplemented with 20 g/L dextrose. The strain was grown overnight at 37 °C without shaking. The indicator strain for the activity assays was *Carnobacterium divergens* LV13, which was grown at 25 °C in APT (all-purpose Tween) broth.

### **7.2.2. Plasmid isolation and sequencing**

GeneJET Plasmid Miniprep Kit (Fermentas) was used to isolate plasmid DNA as described by the manufacturer with modification. Specifically, prior to the cell lysis step, 5 mg of lysozyme per mL was added. The sample was then incubated for 1 h at 37 °C. The gene cluster of AcdB on plasmid pCV461 was sequenced by primer walking using ABI BigDye version 3.1 Terminator Sequencing Kit (Applied Biosystems) and an ABI 3730 DNA Analyzer (Applied Biosystems).

### **7.2.3. Isolation of acidocin B**

*L. acidophilus* M46 (1% v/v inoculum) was grown for 24 h at 37 °C in 1 L of the modified MRS broth. The cells were harvested (10,000 × g, 10 min, 4 °C) and the supernatant was loaded into a column containing 80 g of activated Amberlite XAD-16 resin (Sigma-Aldrich), which was subsequently washed with 500 mL deionized water, 500

mL 20% IPA, 750 mL 40% IPA, and 500 mL 80% IPA with 0.1% TFA. The flow rate was maintained at 10 mL/min. Based on activity assay results, AcdB eluted in the last fraction, which was consequently concentrated to 100 mL and passed through a Bond Elut C8 10 g, 60 mL cartridge (Agilent). Prior to sample loading, the cartridge was activated by washing with 50 mL methanol and 100 mL deionized water. After applying the sample into the cartridge, the silica was washed with 50 mL each of 30% ethanol, 30% acetonitrile, 20% IPA, and 100 mL 40% IPA. AcdB was then eluted with 50 mL 80% IPA with 0.1% TFA. The flow rate was set at 5 mL/min. The active fraction was concentrated to 15 mL and further purified by RP-HPLC using a C4 Protein column (10 µm particle size, 300 Å pore size, 22 mm x 250 mm, Vydac 214TP1022). A two-solvent system was employed with water-0.1% TFA as solvent A, and acetonitrile-0.1% TFA as solvent B. Solvent B was programmed to increase from 10% to 40% for 5 min, sustained at 40% for 8 min, ramped up to 86% over the course of 30 min, increased to 95% for 2 min, and held at 95% for another 2 min. The detector and flow rate were set at 220 nm and 8 mL/min, respectively. Five mL of sample was injected per run. The active fraction containing AcdB eluted at 44 min and was concentrated *in vacuo*, lyophilized, and stored at -20 °C. The molecular weight of AcdB was determined using MALDI-TOF MS.

#### **7.2.4. LC-MS/MS**

AcdB was dissolved in 0.1 M ammonium bicarbonate to a final concentration of 60 mM (100 µL). Trypsin (sequencing grade; Promega, Madison, WI, USA) was then added (1:20 enzyme:peptide molar ratio) and the sample was incubated at 37 °C overnight. One microliter of a 0.5 µg/µL solution of chymotrypsin (Roche, Indianapolis, IN, USA) was

added to 20  $\mu\text{L}$  of the overnight digest, and the sample was incubated further for 3 h at 37  $^{\circ}\text{C}$ . LC-MS/MS was then performed by Jing Zheng using a nanoAcquity column (100  $\text{\AA}$  pore size, 75  $\mu\text{m}$  x 15 cm, 3  $\mu\text{m}$  Atlantis dC18) on a nanoAcquity ultra performance liquid chromatography (Waters) to separate fragments obtained from the trypsin-chymotrypsin digestion. A linear water-acetonitrile gradient (both with 0.1% formic acid) was employed with the flow rate set at 350 nL/min. Quadrupole-time of flight Premier MS (Micromass) was used to collect MS/MS data, which were processed using PEAKS 5.1 software (Bioinformatics Solutions).<sup>292</sup>

#### **7.2.5. Circular dichroism spectroscopy**

Solutions of AcdB (100  $\mu\text{L}$ ; 0.4 mg/mL) in 6 mM sodium dodecyl sulfate (SDS) or 6 mM dodecylphosphocholine (DPC) were prepared and loaded into a quartz cell (0.2 mm path length). CD data were acquired at 20  $^{\circ}\text{C}$  using an OLIS DSM 17 CD spectrophotometer (OLIS).

#### **7.2.6. NMR spectroscopy**

AcdB was dissolved in 80 mM deuterated SDS (9:1  $\text{H}_2\text{O}:\text{D}_2\text{O}$ ) to a final concentration of  $\sim 1$  mM (pH 6). DSS (4,4-dimethyl-4-silapentane-1-sulfonic acid) was added as reference standard (0.01% w/v). The resulting solution (350  $\mu\text{L}$ ) was then transferred into a 5 mm  $\text{D}_2\text{O}$ -matched Shigemi tube (Shigemi Inc., PA USA). One-dimensional  $^1\text{H}$  NMR, and two-dimensional (2D)  $^1\text{H},^1\text{H}$ -TOCSY (total correlation spectroscopy), and  $^1\text{H},^1\text{H}$ -NOESY (nuclear Overhauser effect spectroscopy) experiments were run at 27  $^{\circ}\text{C}$  on a Varian VNMRS 700 MHz spectrometer fitted with a triple

resonance HCN cryoprobe, z-axis pulsed-field gradients, and VNMRJ 3.2 as host control. The sweep width was set to 10,000 Hz and the mixing time to 80 ms. The complex points for the indirectly detected dimension was 512, and the real and imaginary points for the directly detected dimension was 4,882. The cumulative scans for each point of acquisition was 32 and 64 for TOCSY and NOESY, respectively. Presaturation during the relaxation delay was performed to suppress the water signal. NMR data were processed in NMRPipe<sup>232</sup> and analyzed using NMRView<sup>233</sup>. Manual assignments of chemical shifts (Table 7.2) was accomplished following previously described procedure.<sup>295,296</sup> The chemical shift assignments were deposited in the Biological Magnetic Resonance Data Bank (accession number 25352).

#### **7.2.7. Structure calculations**

The chemical shift assignments, along with a combination of manually and automatically assigned nuclear Overhauser effect (NOE) crosspeaks, were inputted into CYANA 2.1<sup>234</sup> for structure calculations, wherein seven cycles were done with 10,000 steps per cycle. Simulated annealing calculated 100 conformers and produced 20 lowest energy conformers that were used for further analysis, including root-mean-square deviation (RMSD) and target function calculations, and generation of Ramachandran plot. The coordinates of the calculated structure were deposited in the Protein Data Bank (PDB accession number 2MWR).

### **7.2.8. Topology prediction, homology modeling, and phylogenetic tree construction**

The SOSUI<sup>244</sup> program was used to determine the number of putative transmembrane domains of proteins encoded by the AcdB gene cluster. The nucleotide sequence of the AcdB gene cluster was deposited in GenBank (accession number KP728900). SWISS-MODEL server<sup>242</sup> was used to create 3D structure homology models of gassericin A and butyrivibriocin AR10 based on the structure of AcdB. BLAST<sup>245</sup> was used to mine for other putative subgroup II circular bacteriocins using the sequence of the AcdB precursor peptide as the query, and a threshold of 40% identity. Phylogenetic tree was constructed using the maximum likelihood method of the MEGA6 software<sup>248</sup>.

**Table 7.2. <sup>1</sup>H Chemical shift assignments for AcdB in 80 mM SDS**

	HN	H $\alpha$	H $\beta$	Others
Ile-1	7.95	3.81	1.95	$\alpha$ CH <sub>3</sub> 0.81, $\beta$ CH <sub>2</sub> 1.25, 1.54, $\gamma$ CH <sub>3</sub> 0.83
Tyr-2	7.75	4.27	3.26, 3.09	$\beta$ CH 7.20, $\alpha$ CH 6.83
Trp-3	8.24	4.31	3.63, 3.44	$\alpha$ CH 7.36, $\beta$ NH 10.04, $\zeta_2$ CH 7.43, $\eta_2$ CH 7.10, $\zeta_3$ CH 6.94, $\epsilon_3$ CH 7.50
Ile-4	8.50	3.56	2.12	$\alpha$ CH <sub>3</sub> 1.01, $\beta$ CH <sub>2</sub> 1.33, 2.21, $\gamma$ CH <sub>3</sub> 0.98
Ala-5	8.06	4.21	1.53	
Asp-6	8.08	4.37	2.75, 2.63	
Gln-7	8.06	3.72	1.36	$\gamma$ CH <sub>2</sub> 1.00, 1.57, $\epsilon$ NH <sub>2</sub> 6.39, 6.33
Phe-8	7.83	4.55	3.34, 2.83	$\delta$ CH 7.33, $\epsilon$ CH 7.23, $\zeta$ CH 7.19
Gly-9	7.86	3.98, 3.85		
Ile-10	7.62	4.09	1.68	$\alpha$ CH <sub>3</sub> 0.76, $\beta$ CH <sub>2</sub> 1.10, 1.42, $\gamma$ CH <sub>3</sub> 0.79
His-11	8.20		3.25, 3.07	
Leu-12	8.12	4.45	1.67	$\beta$ CH 1.55, $\alpha$ CH <sub>3</sub> 0.88
Ala-13	8.26	4.43	1.45	
Thr-14	8.54	3.99	4.25	$\alpha$ CH <sub>3</sub> 1.27
Gly-15	8.30	4.25		
Thr-16	7.98	3.90	4.17	$\alpha$ CH <sub>3</sub> 1.47
Ala-17	8.54	3.99	1.47	
Arg-18	7.91	3.93	1.91	$\beta$ CH <sub>2</sub> 1.78, 1.68, $\alpha$ CH <sub>2</sub> 3.22, 3.30, $\beta$ NH 7.20
Lys-19	7.75	4.13	1.98	$\beta$ CH <sub>2</sub> 1.45, $\alpha$ CH <sub>2</sub> 1.61, 1.73, $\gamma$ CH <sub>2</sub> 2.99
Leu-20	7.93	4.13	1.86, 1.82	$\beta$ CH 1.64, $\alpha$ CH <sub>3</sub> 0.92, 0.89
Leu-21	8.17	3.99	1.76, 1.69	$\beta$ CH 1.56, $\alpha$ CH <sub>3</sub> 0.90, 0.88
Asp-22	8.36	4.41	2.85, 2.71	
Ala-23	7.77	4.23	1.60	
Val-24	7.99	3.96	2.24	$\alpha$ CH <sub>3</sub> 0.98, 1.07
Ala-25	8.31	4.28	1.49	
Ser-26	7.92	4.39	4.00, 4.04	
Gly-27	8.23	4.03, 3.96		
Ala-28	8.04	4.37	1.43	
Ser-29	8.21	4.52	3.95	
Leu-30	8.23	4.24	1.76, 1.70	$\beta$ CH 1.56, $\alpha$ CH <sub>3</sub> 0.91, 0.86
Gly-31	8.40	4.01, 3.90		
Thr-32	7.95	4.11	4.28	$\alpha$ CH <sub>3</sub> 1.26
Ala-33	8.06	4.20	1.42	
Phe-34	8.24	4.34	3.17	$\delta$ CH 7.21, $\epsilon$ CH 7.23, $\zeta$ CH 7.16
Ala-35	7.95	3.99	1.49	
Ala-36	7.80	4.17	1.52	
Ile-37	7.98	3.92	1.96	$\alpha$ CH <sub>3</sub> 0.93, $\beta$ CH <sub>2</sub> 1.69, 1.25, $\gamma$ CH <sub>3</sub> 0.86
Leu-38	7.64	4.14	1.68, 1.63	$\beta$ CH 1.52, $\alpha$ CH <sub>3</sub> 0.80, 0.78
Gly-39	7.84	4.06, 3.85		
Val-40	7.35	4.24	2.18	$\alpha$ CH <sub>3</sub> 0.93, 0.97
Thr-41	7.98	4.39	4.04	$\alpha$ CH <sub>3</sub> 1.16
Leu-42	8.32	4.31	1.61	$\alpha$ CH <sub>3</sub> 0.82, 0.74
Pro-43		4.38	2.25, 1.91	$\gamma$ CH <sub>2</sub> 1.23, 1.01, $\delta$ CH <sub>2</sub> 3.77, 3.01
Ala-44	8.65	3.99	1.53	
Trp-45	7.59	4.47	3.48, 3.34	$\alpha$ CH 7.55, $\beta$ NH 10.31, $\zeta_2$ CH 7.44, $\eta_2$ CH 7.04, $\zeta_3$ CH 6.88, $\epsilon_3$ CH 7.27
Ala-46	6.72	3.89	0.79	
Leu-47	7.31	3.98	1.71	$\beta$ CH 1.58, $\alpha$ CH <sub>3</sub> 0.84, 0.88
Ala-48	7.95	4.18	1.54	
Ala-49	8.05	4.18	1.60	
Ala-50	8.11	4.01	1.48	
Gly-51	8.13	3.94		
Ala-52	7.92	4.01	1.49	
Gly-54	8.23	4.05, 3.95		
Ala-55	8.04	4.22	1.86	
Thr-56	7.89	4.12	4.32	$\alpha$ CH <sub>3</sub> 1.34
Ala-57	8.16	4.38	1.57	
Ala-58	8.23	4.31	1.50	

## **7.3. Experimental Procedures for the Structural Studies of Lacticin Q and Aureocin A53**

### **7.3.1. Construction of pET SUMO-lacticin Q and pET SUMO-aureocin A53**

Lacticin Q (LnqQ) and aureocin A53 (AucA) gene sequences that were codon-optimized for *E. coli* expression were purchased from BioBasic Inc. (Markham, ON, Canada), and amplified through PCR using primers MVB264 (5'-ATGGCAGGTTTCCTGAAGGT-3') and MVB265 (5'-TTATTTGATGCCCAGAATCTG-3') for *lnqQ*, and MVB266 (5'-ATGTCTTGGCTGAACTTCCT-3') and MVB267 (5'-TTACAGGCCCGCAATTTTTTTT-3') for *aucA*. The amplified genes were then cloned into the pET SUMO expression vector as suggested by the manufacturer (Invitrogen). Clones from transformants were sequenced to ensure that the sequences were correct and in frame with the His-tagged SUMO fusion protein. Plasmids of pET SUMO-LnqQ and pET SUMO-AucA were made by Dr. Marco van Belkum and Dr. Christopher T. Lohans, respectively. The pET SUMO-LnqQ and pET SUMO-AucA plasmids were transformed into competent *E. coli* BL21 (DE3) cells according to the manufacturer's instructions.

### **7.3.2. Expression of SUMO-lacticin Q and SUMO-aureocin A53**

Terrific Broth (12 g tryptone, 24 g yeast extract, 4 mL glycerol, 2.31 g potassium dihydrogen phosphate, 12.64 g potassium hydrogen phosphate, pH 7.4, per 1 L) was used for the expression of both fusion proteins. A liter of Terrific Broth containing 50 µg/ml kanamycin was inoculated with an overnight starter culture (1% v/v) and grown at 37 °C with shaking at 225 rpm to an optical density (OD<sub>600</sub>) of 0.8 – 1.0. The OD was measured

using an 8451A Diode Array Spectrophotometer (Hewlett Packard, Palo Alto, CA, USA). The cultures were cooled in an ice bath for 20 min, added with 1 mM isopropyl- $\beta$ -D-1-thiogalactopyranoside (IPTG), and incubated at 30 °C for 24 h at 225 rpm. The cultures were centrifuged ( $5,000 \times g$ , 15 min, 4 °C), and the cells were resuspended in 10 mL lysis buffer (50 mM  $\text{NaH}_2\text{PO}_4$ , 500 mM NaCl, 10 mM imidazole, 1% glycerol, pH 8.0) per 1 g pellet, and passed once through a Constant Systems Cell Disruptor (Constant Systems Ltd.) operated at 20 kpsi. The lysate was centrifuged ( $15,000 \times g$ , 30 min, 4 °C) and the supernatant was collected for the subsequent Ni-NTA affinity chromatography.

### **7.3.3. Purification of SUMO-lacticin Q and SUMO-aureocin A53**

Ni-NTA (Qiagen) resin (2.5 mL) was added into each of the supernatant containing His-tagged SUMO-LnqQ or SUMO-AucA. The mixture was shaken (50 rpm) for 1 h at 8 °C, and then loaded into a fritted column and allowed to flow by gravity. The resin was washed with 25 mL buffer A (50 mM  $\text{NaH}_2\text{PO}_4$ , 500 mM NaCl, 20 mM imidazole, pH 8.0) and 12.5 mL buffer B (50 mM  $\text{NaH}_2\text{PO}_4$ , 500 mM NaCl, 50 mM imidazole, pH 8.0). The fusion protein was eluted using 7.5 mL buffer C (50 mM  $\text{NaH}_2\text{PO}_4$ , 500 mM NaCl, 400 mM imidazole, pH 8.0), and dialyzed against 3 L 20 mM Tris-HCl buffer (pH 8.0) with 150 mM NaCl for 4 h at 8 °C. The fractions were run on an SDS-PAGE gel to confirm elution of the desired protein.

### **7.3.4. SUMO protease digestion**

The SUMO tag on the fusion proteins was removed by treatment with His-tagged SUMO protease (McLab) using 10 U protease per 20  $\mu\text{g}$  fusion protein and following the

buffer conditions indicated in section 7.1.6. Complete cleavage was attained at 25 °C after 3 h incubation as monitored by tricine SDS-PAGE. The cleaved His-tagged SUMO and His-tagged SUMO protease were then removed by treatment with 1 mL Ni-NTA (Qiagen) resin for 1 h, and collecting the supernatant.

### **7.3.5. Purification of lacticin Q by RP-HPLC**

A C8 column (10 µm particle size, 300 Å pore size, 10 mm x 250 mm, Vydac 208TP1010) was used to further purify LnqQ. Ten mL of the sample from the previous step was injected per run. Solvent A (water with 0.1% TFA) and solvent B (acetonitrile with 0.1% TFA) were used at a flow rate of 5 mL/min. Solvent B was set at 30% for 15 min, slowly increased to 70% for 30 min, kept at 70% for 1 min, and ramped up to 95% for 4 min. The detector was set at 220 nm, where LnqQ was detected at 36 min. The identity of LnqQ was confirmed by MALDI-TOF MS. The LnqQ fractions were combined, concentrated *in vacuo*, lyophilized, and stored at -20 °C.

### **7.3.6. Purification of aureocin A53 by RP-HPLC**

A C18(2) LUNA AXIA column (5 µm particle size, 100 Å pore size, 21.2 mm x 250 mm) was used for the purification of AucA. Ten mL sample was injected to the column per run. The same solvent system as with LnqQ purification was used. Solvent B was initially set at 30% for 10 min, gradually increased to 80% for 25 min, and ramped up to 95% for 5 min at a flow rate of 10 mL/min. The detector was set at 220 nm. AucA eluted at 28 min based on MALDI-TOF MS. The AucA fractions were combined, concentrated *in vacuo*, lyophilized, and stored at -20 °C.

### 7.3.7. Circular dichroism spectroscopy

Solutions of LnqQ and AucA (100)  $\mu\text{L}$  were prepared in water, 20 mM sodium phosphate buffer (pH 6.0), or 25% trifluoroethanol at a concentration of 0.4 mg/mL and 0.2 mg/mL for LnqQ and AucA, respectively. CD spectra were acquired on an OLIS DSM 17 CD spectrophotometer at 25 °C in a 0.2 mm quartz cell.

### 7.3.8. NMR spectroscopy

Solutions of LnqQ (0.8 mM, 600  $\mu\text{L}$ ) in 1:3 2,2,2-trifluoroethanol- $\text{d}_3$ : $\text{H}_2\text{O}$  (pH 6), and AucA (1.5 mM, 350  $\mu\text{L}$ ) in 9:1  $\text{H}_2\text{O}$ : $\text{D}_2\text{O}$  were prepared. DSS (0.01% w/v) was added in both samples for referencing. LnqQ was loaded into a standard 5 mm NMR tube, while AucA was loaded into a 5-mm  $\text{D}_2\text{O}$ -matched Shigemi tube (Shigemi Inc.). One-dimensional  $^1\text{H}$  NMR, and 2D  $^1\text{H}$ , $^1\text{H}$ -TOCSY,  $^1\text{H}$ , $^1\text{H}$ -NOESY, and  $^1\text{H}$ , $^1\text{H}$ -gDQF-COSY (gradient double-quantum filter correlation spectroscopy) spectra were acquired at 27 °C on a triple resonance HCN cryoprobe-equipped Varian VNMRS 700 MHz spectrometer with z-axis pulsed-field gradients and VNMRJ 4.2A as host control. The water signal was suppressed either by presaturation during the relaxation delay or water gradient tailored excitation.<sup>297</sup> The experimental details are summarized in Table 7.3.

**Table 7.3. NMR data acquisition parameters for LnqQ and AucA**

Sample	Experiment	Sweep width (Hz) (t2, t1)	ni	np	nt	Mix time (ms)
LnqQ	<sup>1</sup> H, <sup>1</sup> H-NOESY	10000, 10000	512	8192	64	100
	<sup>1</sup> H, <sup>1</sup> H-TOCSY	10000, 10000	512	8192	48	70
	<sup>1</sup> H, <sup>1</sup> H-gDQF-COSY	10000, 10000	256	9764	80	
AucA	<sup>1</sup> H, <sup>1</sup> H-NOESY	10000, 10000	512	8192	32	100
	<sup>1</sup> H, <sup>1</sup> H-TOCSY	10000, 10000	512	8192	32	70
	<sup>1</sup> H, <sup>1</sup> H-gDQF-COSY	10000, 10000	512	8192	96	

t2 = directly detected dimension

t1 = indirectly detected dimension

ni = number of complex points collected for the indirectly detected dimension

np = number of real + imaginary points for the directly detected dimension

nt = number of cumulative scans collected for each point of acquisition

The spectra were processed using NMRPipe<sup>232</sup> and analyzed in NMRView<sup>233</sup>. Chemical shifts were manually assigned based on a previously described procedure.<sup>295,296</sup> The chemical shift assignments are presented in Tables 7.4 and 7.5, and have been deposited in the Biological Magnetic Resonance Data Bank (accession numbers 25858 and 25857 for LnqQ and AucA, respectively).

### 7.3.9. Structure calculations

CYANA 2.1<sup>234</sup> was used to calculate the structures of LnqQ and AucA. A combination of automatically and manually assigned NOE crosspeaks were inputted into the software and were used for seven cycles of calculations with 10,000 steps per cycle. Simulated annealing calculated 100 conformers and produced 20 lowest energy conformers that were used for further analysis, including root-mean-square deviation (RMSD) and target function calculations, and generation of Ramachandran plots. The coordinates for the calculated structures of LnqQ and AucA were deposited in the Protein Data Bank (accession numbers 2N8P for LnqQ, and 2N8O for AucA).

### **7.3.10. Homology modeling and secondary structure predictions**

Homology models of the 3D structures of other known leaderless bacteriocins were generated using the SWISS-MODEL server<sup>242</sup>. The structures of enterocin 7A (Ent7A), enterocin 7B (Ent7B), LnqQ, or AucA were used as templates. Each of the target bacteriocins was aligned with Ent7A, Ent7B, LnqQ, and AucA using Clustal Omega<sup>293</sup>, and the peptide to which it exhibits the highest amino acid sequence identity with was chosen as template for homology modeling. Secondary structure predictions were obtained using the JPred v.4 server<sup>254</sup>.

**Table 7.4. <sup>1</sup>H Chemical shift assignments for LnqQ in 25% trifluoroethanol**

	HN	H $\alpha$	H $\beta$	Others
Met-1		4.181	2.251, 2.201	[CH <sub>2</sub> 2.692, 2.633
Ala-2	8.777	4.449	1.535	
Gly-3	8.640	3.983, 3.883		
Phe-4	8.309	4.047	3.152, 2.902	[CH 6.975, [CH 6.839, $\zeta$ CH 6.625
Leu-5	7.522	3.912	1.842, 1.615	[CH 1.771, [CH <sub>3</sub> 1.055, 0.996
Lys-6	7.552	3.960	2.185	[CH <sub>2</sub> 2.130, 2.452
Val-7	7.549	3.447	2.308	$\gamma$ CH <sub>3</sub> 0.884, 1.138
Val-8	7.619	3.337	2.003	$\gamma$ CH <sub>3</sub> 0.514, 0.882
Gln-9	8.052	3.903	2.280, 2.138	[CH <sub>2</sub> 2.592, 2.262
Leu-10	7.922	4.153	2.054, 1.546	[CH 1.909, [CH <sub>3</sub> 0.925, 0.889
Leu-11	8.219	4.312	1.984	[CH 1.466, [CH <sub>3</sub> 0.905, 0.941
Ala-12	8.047	3.914	1.462	
Lys-13	7.493	3.986	1.532	[CH <sub>2</sub> 0.846, 1.059, [CH <sub>2</sub> 1.629, 1.445, [CH <sub>3</sub> 2.875
Tyr-14	8.152	4.608	3.366, 2.852	[CH 7.205, [CH 6.750
Gly-15	8.450	3.673, 3.604		
Ser-16	8.447	4.087	3.983	
Lys-17	8.472	4.212	1.983, 1.894	[CH <sub>2</sub> 1.524, 1.653, [CH <sub>2</sub> 1.785, [CH <sub>2</sub> 3.054
Ala-18	7.483	4.194	1.507	
Val-19	7.332	3.625	2.181	[CH <sub>3</sub> 1.044, 1.069
Gln-20	8.600	4.145	2.322, 2.232	[CH <sub>2</sub> 2.651, 2.425, $\epsilon$ NH <sub>2</sub> 7.131, 6.711
Trp-21	8.327	4.030	3.416, 3.621	[ $\alpha$ ]CH 7.219, [NH 9.982, $\zeta_2$ CH 7.407, $\eta_2$ CH 7.032, $\zeta_3$ CH 6.894, $\epsilon_3$ CH 7.298
Ala-22	8.318	3.986	1.531	
Trp-23	8.327	4.407	3.410, 3.331	[ $\alpha$ ]CH 7.298, [NH 9.562, $\zeta_2$ CH 7.480, $\eta_2$ CH 7.253, $\zeta_3$ CH 7.122, $\epsilon_3$ CH 7.642
Ala-24	8.293	4.079	1.392	
Asn-25	7.596	4.612	2.065, 1.260	[NH <sub>2</sub> 6.011, 5.936
Lys-26	7.553	4.109	1.994, 1.953	[CH <sub>2</sub> 1.528, 1.532, [CH <sub>2</sub> 1.782, 1.654, [CH <sub>2</sub> 2.972
Gly-27	7.912	4.214, 4.093		
Lys-28	7.400		2.484, 2.385	[CH <sub>2</sub> 1.231, 1.071
Ile-29	7.261	3.781	2.056	[CH <sub>2</sub> 1.832, [CH <sub>3</sub> 1.217, [CH <sub>3</sub> 1.171
Leu-30	8.592	4.089	1.806, 1.456	[CH 1.702, [CH <sub>3</sub> 0.872, 0.734
Asp-31	7.846	4.470	3.013, 2818	
Trp-32	8.162	4.626	3.800, 3.145	[ $\alpha$ ]CH 7.260, [NH 10.089, $\zeta_2$ CH 7.518, $\eta_2$ CH 7.102, $\zeta_3$ CH 7.037, $\epsilon_3$ CH 7.716
Leu-33	8.709	4.380	2.051, 2.133	[CH 1.640, [CH <sub>3</sub> 0.970
Asn-34	9.055	4.605	3.008, 2.884	[NH <sub>2</sub> 7.600, 6.679
Ala-35	7.860	4.408	1.626	
Gly-36	7.914	4.213, 3.746		
Gln-37	7.806	4.153	1.626, 1.786	[CH <sub>2</sub> 2.072
Ala-38	8.269	4.368	1.603	
Ile-39	8.617	3.708	1.913	[CH <sub>2</sub> 1.290, 0.973, [CH <sub>3</sub> 0.907, [CH <sub>3</sub> 1.729
Asp-40	8.600	4.317	2.836	
Trp-41	7.478	4.100	3.722, 3.303	[ $\alpha$ ]CH 7.219, [NH 9.907, $\zeta_2$ CH 7.268, $\eta_2$ CH 6.565, $\zeta_3$ CH 5.912, $\epsilon_3$ CH 7.202
Val-42	8.353	3.369	2.547	$\gamma$ CH <sub>3</sub> 1.411, 1.330
Val-43	8.561	3.478	2.113	$\gamma$ CH <sub>3</sub> 1.169, 0.939
Ser-44	7.797	3.958	3.902, 3.756	
Lys-45	8.027	3.716	1.288	
Ile-46	8.172	3.266	1.828	[CH <sub>3</sub> 1.093
Lys-47	8.265	3.505	1.715	[CH <sub>2</sub> 0.662, [CH <sub>2</sub> 1.663, 1.963
Gln-48	7.551	3.961	2.130	[CH <sub>2</sub> 2.452, 2.183, $\epsilon$ NH <sub>2</sub> 6.638, 7.236
Ile-49	8.209	3.548	1.659	[CH <sub>2</sub> 1.052, 1.755, [CH <sub>3</sub> 0.756, [CH <sub>3</sub> 0.888
Leu-50	7.914	4.095	1.518, 1.396	[CH 1.304, [CH <sub>3</sub> 0.547, 0.446
Gly-51	7.738	3.931, 3.772		
Ile-52	8.177	3.942	1.376	[CH <sub>2</sub> 0.899, [CH <sub>3</sub> 0.634, [CH <sub>3</sub> 0.592
Lys-53	8.013	4.129	1.719	[CH <sub>2</sub> 1.425, [CH <sub>2</sub> 1.827, [CH <sub>2</sub> 2.990

**Table 7.5. <sup>1</sup>H Chemical shift assignments for AucA in water**

	HN	H $\alpha$	H $\beta$	Others
Met-1		4.250	2.289, 2.126	[CH <sub>2</sub> 2.579, 2.698
Ser-2	8.773	4.885	3.984, 4.374	
Trp-3	8.966	4.458	3.199, 3.276	[CH 7.100, [NH 9.093, $\zeta_2$ CH 4.892, $\eta_2$ CH 6.293, $\zeta_3$ CH 6.748, $\epsilon_3$ CH 7.221
Leu-4	8.336	3.816	1.760, 1.516	[CH 1.848, [CH <sub>3</sub> 1.032, 0.980
Asn-5	7.815	4.515	3.032, 2.765	[NH <sub>2</sub> 7.749, 7.122
Phe-6	8.504	4.297	3.241, 3.202	
Leu-7	8.111	3.463	1.466, 1.071	[CH 0.523, [CH <sub>3</sub> 0.379, 0.110
Lys-8	7.390	3.884	1.856	[CH <sub>2</sub> 1.574, 1.394, [CH <sub>2</sub> 1.674, [CH <sub>2</sub> 2.948
Tyr-9	7.784	4.010	3.181, 3.097	[CH 6.940, [CH 6.837
Ile-10	7.673	3.679	1.565	[CH <sub>2</sub> 0.944, 0.814, [CH <sub>3</sub> 0.403, [CH <sub>3</sub> 0.471
Ala-11	7.013	3.645	1.312	
Lys-12	7.100	3.925	1.299, 1.401	[CH <sub>2</sub> 0.574, -0.291, [CH <sub>2</sub> 1.091, [CH <sub>2</sub> 2.501, 2.264
Tyr-13	7.715	4.540	3.114, 2.208	[CH 6.224, [CH 6.073
Gly-14	7.472	4.581, 3.881		
Lys-15	8.496	3.998	1.900	[CH <sub>2</sub> 1.526, 1.596, [CH <sub>2</sub> 1.732, [CH <sub>2</sub> 3.024
Lys-16	8.805	4.206	2.004, 1.905	[CH <sub>2</sub> 1.655, 1.529, [CH <sub>2</sub> 1.793, [CH <sub>2</sub> 3.072
Ala-17	7.441	4.240	1.516	
Val-18	7.286	3.528	2.167	$\gamma$ CH <sub>3</sub> 1.169, 0.934
Ser-19	8.527	4.512	4.087, 4.062	
Ala-20	8.049	4.484	1.772	
Ala-21	8.301	4.212	1.611	
Trp-22	7.714	4.525	3.521, 3.375	[CH 7.693, [NH 10.272, $\zeta_2$ CH 7.731, $\eta_2$ CH 7.547, $\zeta_3$ CH 7.226, $\epsilon_3$ CH 7.891
Lys-23	8.308	4.051	1.922	[CH <sub>2</sub> 1.160, 0.532, [CH <sub>2</sub> 1.632, 1.565, [CH <sub>2</sub> 2.902, 2.852
Tyr-24	8.186	4.809	3.371, 2.639	[CH 7.352, [CH 6.822
Lys-25	6.963	3.875	1.987, 1.619	[CH <sub>2</sub> 0.702, 0.068, [CH <sub>2</sub> 0.945, 1.298
Gly-26	8.529	3.750, 3.570		
Lys-27	7.331	3.589	1.421, 1.419	[CH <sub>2</sub> 1.142, 0.391, [CH <sub>2</sub> 1.457, [CH <sub>2</sub> 2.904
Val-28	8.195	3.611	2.414	$\gamma$ CH <sub>3</sub> 1.297, 0.882
Leu-29	8.818	4.003	1.763, 1.376	[CH 1.675, [CH <sub>3</sub> 0.722, 0.606
Glu-30	6.932	4.207	2.051	[CH <sub>2</sub> 2.411, 2.547
Trp-31	8.426	4.885	3.702, 3.428	[CH 7.282, [NH 10.194, $\zeta_2$ CH 7.349, $\eta_2$ CH 6.759, $\zeta_3$ CH 6.475, $\epsilon_3$ CH 7.273
Leu-32	9.254	4.034	2.015, 1.603	[CH 1.838, [CH <sub>3</sub> 0.942, 0.776
Asn-33	7.589	4.810	3.002	[NH <sub>2</sub> 7.551, 6.911
Val-34	7.416	4.508	2.273	$\gamma$ CH <sub>3</sub> 1.167, 1.025
Gly-35	8.295	2.908, 2.987		
Pro-36		4.391	2.064, 1.924	$\gamma$ CH <sub>2</sub> 1.777, 1.994, $\delta$ CH <sub>2</sub> 2.593
Thr-37	6.595	4.721	4.638	[CH <sub>3</sub> 1.234
Leu-38	8.748	4.065	1.111, 0.965	[CH 1.852, [CH <sub>3</sub> 0.815, 0.776
Glu-39	8.099	4.511	1.992, 2.440	[CH <sub>2</sub> 2.545, 2.700
Trp-40	8.285	4.038	3.423, 3.357	[CH 7.324, [NH 10.193, $\zeta_2$ CH 7.453, $\eta_2$ CH 7.134, $\zeta_3$ CH 7.025, $\epsilon_3$ CH 7.279
Val-41	7.539	3.296	2.514	[CH <sub>3</sub> 1.326, 0.810
Trp-42	8.814	5.052	3.819, 3.627	[CH 7.382, [NH 9.276, $\eta_2$ CH 6.825, $\zeta_3$ CH 6.712, $\epsilon_3$ CH 7.577
Gln-43	8.466	3.061	1.811, 1.751	$\gamma$ CH <sub>2</sub> 2.415, 2.474, $\epsilon$ NH <sub>2</sub> 7.618, 6.773
Lys-44	6.845	3.189	0.567, -0.793	[CH <sub>2</sub> -0.508, [CH <sub>2</sub> 0.044, 0.132, [CH <sub>2</sub> 1.676, 1.931
Leu-45	7.932	4.118	2.394	[CH 1.620, [CH <sub>3</sub> 1.080, 1.505
Lys-46	8.741	3.091	0.720, 0.154	[CH <sub>2</sub> 0.505, 0.657, [CH <sub>2</sub> 1.088, 1.018, [CH <sub>2</sub> 2.783, 2.676
Lys-47	6.766	3.980	1.724, 1.607	[CH <sub>2</sub> 1.287, [CH <sub>2</sub> 1.530, [CH <sub>2</sub> 2.860
Ile-48	7.634	3.995	1.767	[CH <sub>3</sub> 0.667, [CH <sub>2</sub> 1.437, 1.119 [CH <sub>3</sub> 0.816
Ala-49	8.047	4.475	1.438	
Gly-50	7.514	3.907		
Leu-51	7.885	4.286	1.770	[CH 1.491, [CH <sub>3</sub> 0.956, 0.890

### 7.3.11. MIC testing

A spot-on-lawn assay was used to determine the minimum inhibitory concentrations (MICs) of LnqQ and AucA against various indicator strains, which were all grown at 25 °C in APT broth, except for the *Staphylococcus* strains and *L. acidophilus* M46, which were grown in tryptic soy broth (TSB) and MRS broth, respectively. LnqQ and AucA solutions were prepared from 128 µM stock solutions that were serially diluted 2-fold. Ten µL of each solution was spotted onto the indicator lawn and allowed to dry. The plates were incubated overnight at the appropriate temperature for the indicator strains, and examined for zones of inhibition. The MIC recorded was the lowest bacteriocin concentration that caused a clear zone of growth inhibition.

### 7.3.12. Synergy assay

Synergy of LnqQ and AucA was tested using a well-diffusion assay with *C. divergens* LV13 and *L. lactis* ATCC 19257 as indicator strains. Wells (~6 mm diameter) were bored on solidified agar that was previously inoculated with the indicator strain (100 µL overnight culture per 20 mL 1.5% agar solution). Twenty µL LnqQ and AucA solutions (50 µM) were added into separate wells. To test for synergy, 10 µL of each of the LnqQ and AucA solutions was added into the same well. After overnight incubation at 25 °C, the plates were examined for zones of clearing.

## **7.4. Experimental Procedures for the Structural Studies of CbnXY**

### **7.4.1. Unlabelled CbnX and CbnY**

Unlabelled carnobacteriocin X and Y (CbnX and CbnY) of >98% purity were purchased from GenScript (NJ, USA). The peptides were used for activity testing, CD analysis, and interaction studies.

### **7.4.2. Antimicrobial activity assay**

This section was performed by Dr. Leah A. Martin-Visscher. Stock solutions of CbnX and CbnY (1 mM) were prepared in 20 mM sodium phosphate buffer (pH 7.5), and were serially diluted 2-fold each time. Spot-on-lawn assays were performed to test the activity of CbnX and CbnY individually and when combined. For the combined samples, 10  $\mu$ L of each peptide (equimolar) was co-spotted, or spotted such that the spots for CbnX and CbnY overlapped. Prior to adding the second spot, the first spot was first dried. The plates were incubated overnight at 25 °C and examined for zones of inhibition. The indicator strains used were *C. divergens* LV13 and *C. maltaromaticum* A9b<sup>-</sup>. *C. piscicola* LV17B and *C. maltaromaticum* C2 were used as negative controls. All strains were grown at 25 °C in BHI (brain heart infusion) broth.

### **7.4.3. Circular dichroism spectroscopy**

CbnX and CbnY solutions (100  $\mu$ L) were prepared in either 20 mM sodium phosphate buffer (pH 6.0) or 50% trifluoroethanol to a final concentration of 0.25 mg/mL for CbnX and 0.22 mg/mL for CbnY. CD data were acquired at 27 °C using an OLIS

DSM 17 CD spectrophotometer (OLIS).

#### **7.4.4. Construction of pET SUMO-CbnX and pET SUMO-CbnY**

The expression plasmids were prepared by Dr. Christopher T. Lohans. Briefly, codon-optimized *cbnX* and *cbnY* genes that were intended for *E. coli* expression were purchased from BioBasic Inc. The primers CTL72 (5'-TGGGGTTGGAAAGAAGTGGTTCAGAATGG-3') and CTL73 (5'-TTAGCCAAACGGCAGCGGCAC-3') for *cbnX*, and CTL76 (5'-TCTGCAATCCTGGCTATCACTCTGG-3') and CTL98 (5'-TTACTTTTTGCGACGGTCGTTAATGGC-3') for *cbnY* were used to amplify the genes through PCR. The PCR products were each cloned into the pET SUMO expression vector based on the manufacturer's instructions (Invitrogen). A QIAprep Spin Miniprep Kit (Qiagen) was used to isolate plasmids from transformants. The plasmids were sequenced to confirm that the genes were correct and in frame with the DNA encoding the His-tagged SUMO protein. The resulting pET SUMO-CbnX and pET SUMO-CbnY plasmids were stored at -20 °C.

#### **7.4.5. Expression of [<sup>13</sup>C, <sup>15</sup>N]-labelled SUMO-CbnX and SUMO-CbnY**

The pET SUMO-CbnX and pET SUMO-CbnY plasmids were transformed into *E. coli* BL21 (DE3) cells according to manufacturer's instructions. Transformants were used for protein expression in [<sup>13</sup>C, <sup>15</sup>N]-labelled BioExpress Cell Growth Media (Cambridge Isotope Laboratories Inc., Tewksbury, MA, USA). An overnight starter culture containing 50 µg/mL kanamycin was grown at 37 °C with shaking at 225 rpm. This was used to inoculate larger cultures at 1% v/v. Two liters of labelled media was used for SUMO-CbnX, while 1 L was used for SUMO-CbnY. The cultures were grown at 37 °C with

shaking at 225 rpm to an OD<sub>600</sub> of 0.8 – 1.0. After placing on ice for 20 min, the cultures were induced with 0.5 mM IPTG, and incubated for 24 h at 25 °C with shaking (225 rpm). The cells were harvested (5,000 × g, 15 min, 4 °C) and stored at -80 °C.

#### **7.4.6. Purification of [<sup>13</sup>C,<sup>15</sup>N]-labelled SUMO-CbnX and SUMO-CbnY**

Cell pellets were resuspended in 30 mL lysis buffer (50 mM NaH<sub>2</sub>PO<sub>4</sub>, 500 mM NaCl, 10 mM imidazole, 1% glycerol, pH 8.0), passed through a Constant Systems Cell Disruptor (Constant Systems Ltd.) at 20 kpsi, and centrifuged (15,000 × g, 30 min, 4 °C). Ni-NTA (Qiagen) resin (1-2 mL) was added to the supernatant, and the mixture was shaken at 50 rpm for 1 h at 8 °C. The mixtures were transferred into a column with frit and allowed to flow by gravity. The resin was washed with buffer (50 mM NaH<sub>2</sub>PO<sub>4</sub>, 500 mM NaCl, 25 mM imidazole, pH 8.0), followed by increasing amounts of imidazole in the same buffer (up to 1 M). SDS-PAGE was used to monitor the purification. The fractions containing the desired protein were pooled and diluted to a final concentration of 50 mM imidazole and 150 mM NaCl.

#### **7.4.7. SUMO protease digestion**

Fifty μL of 100 U/μL SUMO protease (McLab) and SUMO protease buffer (50 mM Tris-HCl pH 8.0, 2% IGEPAL<sup>®</sup> CA-630 (Sigma-Aldrich), 1 mM dithiothreitol) was added to the sample from section 7.4.6. The cleavage cocktail was incubated at 25 °C for 20 h, and monitored by SDS-PAGE. SUMO-CbnY was cleaved completely, but SUMO-CbnX was only cleaved with ~70% efficiency. It could not be further cleaved by increasing the protease concentration and incubation time. The cleaved His-tagged SUMO, His-tagged

SUMO protease, and any uncleaved fusion protein were then removed by treatment with 1 mL Ni-NTA (Qiagen) resin for 1 h, and collecting the supernatant.

#### 7.4.8. Purification of [ $^{13}\text{C}$ , $^{15}\text{N}$ ]-labelled CbnX and CbnY

RP-HPLC using a C18(2) LUNA AXIA column (5  $\mu\text{m}$  particle size, 100  $\text{\AA}$  pore size, 21.2 mm x 250 mm) was performed to further purify CbnX and CbnY. Water and acetonitrile, both containing 0.1% TFA, were used as solvents A and B, respectively. Solvent B was initially set at 30% for 10 min, and ramped up to 95% over 30 min. The flow rate was set at 8 mL/min, and detector at 220 nm. CbnX eluted at 27 min, while CbnY eluted at 25 min. Fractions containing CbnX or CbnY were pooled, concentrated *in vacuo*, lyophilized, and stored at  $-20\text{ }^{\circ}\text{C}$ . A yield of 1-1.5 mg each of [ $^{13}\text{C}$ ,  $^{15}\text{N}$ ]-CbnX and [ $^{13}\text{C}$ ,  $^{15}\text{N}$ ]-CbnY were obtained.

#### 7.4.9. NMR spectroscopy

[ $^{13}\text{C}$ ,  $^{15}\text{N}$ ]-CbnX and [ $^{13}\text{C}$ ,  $^{15}\text{N}$ ]-CbnY were each dissolved in 350  $\mu\text{L}$  1:1 2,2,2-trifluoroethanol- $\text{d}_3$ :water (pH 6) to a final concentration of  $\sim 1\text{ mM}$ . DSS was added as reference standard at 0.01% w/v. The samples were each transferred into a 5 mm  $\text{D}_2\text{O}$ -matched Shigemi tube (Shigemi Inc.). 2D and 3D NMR experiments were performed at  $27\text{ }^{\circ}\text{C}$  using a Varian VNMRS 700 MHz spectrometer and a triple resonance HCN-coldprobe with z-axis pulsed-field gradients, and VNMRJ 4.2A as host control. The 2D experiments included  $^1\text{H}$ ,  $^1\text{H}$ -TOCSY,  $^1\text{H}$ ,  $^1\text{H}$ -NOESY,  $^1\text{H}$ ,  $^{15}\text{N}$ -HSQC (heteronuclear single quantum correlation), and  $^1\text{H}$ ,  $^{13}\text{C}$ -HSQC, while 3D experiments included  $^1\text{H}$ ,  $^{15}\text{N}$ -TOCSY-HSQC,  $^1\text{H}$ ,  $^{15}\text{N}$ -NOESY-HSQC, and HCCH-TOCSY. The experimental

parameters are summarized in Table 7.6. The water signal was suppressed either by presaturation during the relaxation delay or via water gradient tailored excitation.<sup>297</sup> The spectra were processed in NMRPipe<sup>232</sup> and analyzed in NMRView<sup>233</sup>. Chemical shift assignments are listed in Tables 7.7 to 7.10, and have been deposited in the Biological Magnetic Resonance Data Bank with accession numbers 30236 and 30235 for CbnX and CbnY, respectively.

**Table 7.6. NMR data acquisition parameters for CbnX and CbnY**

Sample	Experiment	x-sw <sup>a</sup>	y-sw	z-sw	x-pts	y-pts	z-pts	Mixing time (ms)
CbnX	<sup>1</sup> H, <sup>1</sup> H-TOCSY	10000	10000	-	893	512	-	100
	<sup>1</sup> H, <sup>1</sup> H-NOESY	10000	10000	-	893	512	-	175
	<sup>1</sup> H, <sup>15</sup> N-HSQC	11468	2500	-	1024	128	-	-
	<sup>1</sup> H, <sup>13</sup> C-HSQC	10000	30000	-	893	256	-	-
	<sup>1</sup> H, <sup>15</sup> N-TOCSY-HSQC	11468	11468	2000	1024	64	32	80
	<sup>1</sup> H, <sup>15</sup> N-NOESY-HSQC	11468	11468	2000	1024	116	32	150
	HCCH-TOCSY	10000	8389	14080	610	128	32	14
CbnY	<sup>1</sup> H, <sup>1</sup> H-TOCSY	7184	7184	-	1024	512	-	100
	<sup>1</sup> H, <sup>1</sup> H-NOESY	10000	11468	-	893	512	-	175
	<sup>1</sup> H, <sup>15</sup> N-HSQC	8389	3545	-	839	128	-	-
	<sup>1</sup> H, <sup>13</sup> C-HSQC	11468	24638	-	1024	256	-	-
	<sup>1</sup> H, <sup>15</sup> N-TOCSY-HSQC	11468	11468	2000	1024	64	32	80
	<sup>1</sup> H, <sup>15</sup> N-NOESY-HSQC	11468	11468	2000	1024	116	32	150
	HCCH-TOCSY	8013	8013	12070	512	128	32	14

<sup>a</sup> x,y,z-pts and sw are the number of complex points and sweep width in each respective dimension (x is the directly detected dimension).

**Table 7.7. <sup>1</sup>H Chemical shift assignments for CbnX in 50% trifluoroethanol**

	HN	H $\alpha$	H $\beta$	Others
<b>Trp-1</b>		4.280	3.392	$\alpha$ CH 7.268, $\alpha$ NH 9.728, $\zeta_2$ CH 7.092, $\eta_2$ CH 7.205, $\zeta_3$ CH 7.454, $\epsilon_3$ CH 7.581
<b>Gly-2</b>	8.511	4.077		
<b>Trp-3</b>	8.066	4.441	3.362, 3.259	$\alpha$ CH 7.263, $\alpha$ NH 9.857, $\zeta_2$ CH 7.105, $\eta_2$ CH 7.208, $\zeta_3$ CH 7.452, $\epsilon_3$ CH 7.522
<b>Lys-4</b>	7.924	3.729	1.548, 1.591	$\alpha$ CH <sub>2</sub> 1.056, 1.090, $\beta$ CH <sub>2</sub> 1.588, $\gamma$ CH <sub>2</sub> 2.926
<b>Glu-5</b>	7.827	4.022	2.082, 1.840	$\alpha$ CH <sub>2</sub> 2.363, 2.502
<b>Val-6</b>	7.604	3.690	2.247	$\gamma$ CH <sub>3</sub> 0.950, 1.049
<b>Val-7</b>	8.059	3.758	2.061	$\gamma$ CH <sub>3</sub> 0.927
<b>Gln-8</b>	8.203	4.290	2.165, 2.122	$\alpha$ CH <sub>2</sub> 2.592, 2.262, $\epsilon$ NH <sub>2</sub> 7.277, 6.632
<b>Asn-9</b>	8.247	4.668	2.923, 2.838	$\alpha$ NH <sub>2</sub> 7.378, 6.664
<b>Gly-10</b>	8.374	3.948, 3.896		
<b>Gln-11</b>	8.370	4.272	2.236	$\alpha$ CH <sub>2</sub> 2.555, 2.440, $\epsilon$ NH <sub>2</sub> 7.161, 6.526
<b>Thr-12</b>	8.072	4.143	4.441	$\alpha$ CH <sub>3</sub> 1.301
<b>Ile-13</b>	8.008	3.857	1.870	$\alpha$ CH <sub>2</sub> 1.562, 1.147, $\beta$ CH <sub>3</sub> 0.835, $\gamma$ CH <sub>3</sub> 0.844
<b>Phe-14</b>	8.222	4.437	3.243, 3.181	$\alpha$ CH 7.278, $\beta$ CH 7.329, $\zeta$ CH 7.225
<b>Ser-15</b>	8.190	4.298	4.144, 4.044	
<b>Ala-16</b>	8.244	4.204	1.531	
<b>Gly-17</b>	8.305	3.906, 3.868		
<b>Gln-18</b>	7.907	4.144	2.117, 2.140	$\alpha$ CH <sub>2</sub> 2.328, 2.262, $\epsilon$ NH <sub>2</sub> 7.084, 6.538
<b>Lys-19</b>	7.920	4.206	1.964, 1.966	$\alpha$ CH <sub>2</sub> 1.496, 1.612, $\beta$ CH <sub>2</sub> 1.731, $\gamma$ CH <sub>2</sub> 3.015
<b>Leu-20</b>	8.190	4.289	1.658, 1.772	$\alpha$ CH 1.744, $\beta$ CH <sub>3</sub> 0.932, 0.908
<b>Gly-21</b>	8.158	3.930, 3.895		
<b>Asn-22</b>	7.968	4.698	2.881	$\alpha$ NH <sub>2</sub> 7.473, 6.750
<b>Met-23</b>	8.080	4.480	2.226	$\alpha$ CH <sub>2</sub> 2.709, 2.590, $\beta$ CH <sub>3</sub> 2.101
<b>Val-24</b>	7.894	3.981	2.184	$\gamma$ CH <sub>3</sub> 0.993, 1.053
<b>Gly-25</b>	8.70	4.051, 3.918		
<b>Lys-26</b>	7.789	4.461	1.916, 1.841	$\alpha$ CH <sub>2</sub> 1.436, 1.511, $\beta$ CH <sub>2</sub> 1.734, $\gamma$ CH <sub>2</sub> 3.040
<b>Ile-27</b>	7.769	4.233	1.913	$\alpha$ CH <sub>2</sub> 1.215, 1.560, $\beta$ CH <sub>3</sub> 0.922, $\gamma$ CH <sub>3</sub> 0.891
<b>Val-28</b>	7.701	4.536	2.104	$\gamma$ CH <sub>3</sub> 0.964, 0.984
<b>Pro-29</b>		4.482	2.027	$\gamma$ CH <sub>2</sub> 1.989, 2.151, $\delta$ CH <sub>2</sub> 3.823, 3.656
<b>Leu-30</b>	7.648	4.629	1.551, 1.317	$\alpha$ CH 1.678, $\beta$ CH <sub>3</sub> 0.976, 0.937
<b>Pro-31</b>		4.384	2.101	$\gamma$ CH <sub>2</sub> 1.945, 1.843, $\delta$ CH <sub>2</sub> 3.435, 3.694
<b>Phe-32</b>	7.246	4.700	3.217, 3.062	
<b>Gly-33</b>	7.727	3.912, 3.856		

**Table 7.8. Nitrogen and carbon chemical shift assignments for CbnX**

	N	C $\alpha$	C $\beta$	Others
<b>Trp-1</b>		56.643	29.497	$\epsilon_3$ C 120.058, $\epsilon$ N 127.043
<b>Gly-2</b>	111.229	45.028		
<b>Trp-3</b>	121.074	59.917	28.778	$\epsilon_3$ C 120.066, $\epsilon$ N 128.949
<b>Lys-4</b>	118.748	59.350	28.989	$\alpha$ C 24.251, $\beta$ C 31.693, $\gamma$ C 41.727
<b>Glu-5</b>	117.477	59.343	28.275	$\alpha$ C 36.142
<b>Val-6</b>	120.362	65.702	31.524	$\gamma$ C 21.075, 21.446
<b>Val-7</b>	119.535	65.412	31.510	$\gamma$ C 20.273, 20.308
<b>Gln-8</b>	119.260	56.405	30.699	$\alpha$ C 33.745, $\epsilon$ N 109.509
<b>Asn-9</b>	118.211	54.265	38.564	$\alpha$ N 110.569
<b>Gly-10</b>	108.305	46.296		
<b>Gln-11</b>	119.243	57.998	28.322	$\alpha$ C 33.635, $\epsilon$ N 108.983
<b>Thr-12</b>	116.188	65.130	69.054	$\alpha$ C 20.837
<b>Ile-13</b>	121.566	64.083	37.805	$\alpha$ C 16.290, $\beta$ C 27.831, $\gamma$ C 12.068
<b>Phe-14</b>	119.839	59.442	38.749	$\alpha$ C 131.308, 131.265
<b>Ser-15</b>	114.637	60.698	63.096	
<b>Ala-16</b>	125.230	54.614	17.430	
<b>Gly-17</b>	104.998	44.547		
<b>Gln-18</b>	119.695	57.581	28.455	$\alpha$ C 33.483, $\epsilon$ N 110.456
<b>Lys-19</b>	119.570	58.060	32.229	$\alpha$ C 24.424, $\beta$ C 28.636, $\gamma$ C 41.727
<b>Leu-20</b>	119.651	56.405	41.998	$\alpha$ C 26.705, $\beta$ C 23.756, 22.604
<b>Gly-21</b>	106.007	46.296		
<b>Asn-22</b>	117.737	56.386	38.564	$\alpha$ N 110.868
<b>Met-23</b>	118.387	56.666	32.684	$\alpha$ C 31.738, $\beta$ C 15.931
<b>Val-24</b>	118.610	63.986	31.696	$\gamma$ C 20.395, 20.457
<b>Gly-25</b>	110.051	44.797		
<b>Lys-26</b>	118.604	55.881	32.985	$\alpha$ C 24.599, $\beta$ C 28.636, $\gamma$ C 42.005
<b>Ile-27</b>	118.632	61.127	38.833	$\alpha$ C 16.664, $\beta$ C 26.883, $\gamma$ C 11.976
<b>Val-28</b>	121.843	58.938	32.871	$\gamma$ C 19.556, 19.453
<b>Pro-29</b>		62.522	30.748	$\gamma$ C 26.557, $\delta$ C 50.207
<b>Leu-30</b>	121.353	52.425	42.378	$\alpha$ C 26.711, $\beta$ C 24.446, 22.439
<b>Pro-31</b>		63.314	30.635	$\gamma$ C 26.481, $\delta$ C 49.721
<b>Phe-32</b>	116.271	55.050	39.100	
<b>Gly-33</b>	110.901	46.296		

**Table 7.9. <sup>1</sup>H Chemical shift assignments for CbnY in 50% trifluoroethanol**

	HN	H $\alpha$	H $\beta$	Others
<b>Ser-1</b>		4.291	4.230, 4.106	
<b>Ala-2</b>	8.909	4.396	1.500	
<b>Ile-3</b>	7.712	4.020	1.847	$\alpha$ CH <sub>2</sub> 1.514, 1.321, $\beta$ CH <sub>3</sub> 0.947, $\gamma$ CH <sub>3</sub> 0.933
<b>Leu-4</b>	7.666	4.191	1.656, 1.752	$\alpha$ CH 0.943, $\beta$ CH <sub>3</sub> 0.884
<b>Ala-5</b>	7.517	4.078	1.525	
<b>Ile-6</b>	8.158	3.846	1.899	$\alpha$ CH <sub>2</sub> 1.767, 1.174, $\beta$ CH <sub>3</sub> 0.925, $\gamma$ CH <sub>3</sub> 0.867
<b>Thr-7</b>	7.960	3.887	4.356	$\beta$ CH <sub>3</sub> 1.211
<b>Leu-8</b>	8.417	4.263	1.879, 1.621	$\alpha$ CH 0.911, $\beta$ CH <sub>3</sub> 0.898, 0.884
<b>Gly-9</b>	8.045	3.929		
<b>Ile-10</b>	8.330	3.872	2.035	$\alpha$ CH <sub>2</sub> 1.811, 1.126, $\beta$ CH <sub>3</sub> 0.853, $\gamma$ CH <sub>3</sub> 0.850
<b>Phe-11</b>	8.319	4.380	3.288	
<b>Ala-12</b>	8.937	4.165	1.616	
<b>Thr-13</b>	8.033	4.153	4.388	$\beta$ CH <sub>3</sub> 1.327
<b>Gly-14</b>	8.239	3.912		
<b>Tyr-15</b>	8.198	4.331	2.694, 2.194	
<b>Gly-16</b>	8.090	3.891		
<b>Met-17</b>	8.356	4.268		$\beta$ CH <sub>3</sub> 2.091
<b>Gly-18</b>	8.343	3.863		
<b>Val-19</b>	7.935	3.736	2.113	$\gamma$ CH <sub>3</sub> 0.889
<b>Gln-20</b>	8.014	3.955	2.165	$\alpha$ CH <sub>2</sub> 2.497, 2.386, $\epsilon$ NH <sub>2</sub> 7.052, 6.512
<b>Lys-21</b>	8.104	4.024	1.961	$\alpha$ CH <sub>2</sub> 1.492, $\beta$ CH <sub>2</sub> 1.740, $\gamma$ CH <sub>2</sub> 3.023
<b>Ala-22</b>	7.888	4.153	1.544	
<b>Ile-23</b>	7.789	4.461	1.916, 1.841	$\alpha$ CH <sub>2</sub> 1.767, 1.174, $\beta$ CH <sub>3</sub> 0.925, $\gamma$ CH <sub>3</sub> 0.867
<b>Asn-24</b>	8.226	4.508	2.860, 2.922	$\alpha$ NH <sub>2</sub> 7.581, 6.788
<b>Asp-25</b>	8.391	4.592	2.908, 3.017	
<b>Arg-26</b>	7.861	4.281	1.968	$\alpha$ CH <sub>2</sub> 1.821, 1.839, $\beta$ CH <sub>2</sub> 3.237
<b>Arg-27</b>	7.894	4.318	1.894	$\alpha$ CH <sub>2</sub> 1.527, $\beta$ CH <sub>2</sub> 3.020
<b>Lys-28</b>	7.940	4.292	1.975	$\alpha$ CH <sub>2</sub> 1.742, $\beta$ CH <sub>2</sub> 1.839, $\gamma$ CH <sub>2</sub> 3.228
<b>Lys-29</b>	7.906	4.338	1.836, 1.956	$\alpha$ CH <sub>2</sub> 1.505, 1.602, $\beta$ CH <sub>2</sub> 1.740, $\gamma$ CH <sub>2</sub> 3.039

**Table 7.10. Nitrogen and carbon chemical shift assignments for CbnY**

	N	C $\alpha$	C $\beta$	Others
<b>Ser-1</b>		56.675	63.272	
<b>Ala-2</b>	124.972	54.063	17.799	
<b>Ile-3</b>	115.450	63.085	37.903	$\alpha$ C 28.285, $\beta$ C 16.608, $\gamma$ C 11.956
<b>Leu-4</b>	123.558	57.821	41.638	$\alpha$ C 23.782, $\beta$ C 22.002
<b>Ala-5</b>	119.876	55.272	17.556	
<b>Ile-6</b>	117.295	65.046	38.196	$\alpha$ C 28.908, $\beta$ C 11.955, $\gamma$ C 12.176
<b>Thr-7</b>	115.236	67.028	69.012	$\alpha$ C 20.559
<b>Leu-8</b>	120.305	57.922	41.464	$\alpha$ C 24.116, $\beta$ C 23.099, 21.962
<b>Gly-9</b>	105.812	46.736		
<b>Ile-10</b>	123.652	64.445	37.866	$\alpha$ C 28.355, $\beta$ C 16.306, $\gamma$ C 12.569
<b>Phe-11</b>	120.524	60.797	38.571	
<b>Ala-12</b>	121.021	54.990	17.911	
<b>Thr-13</b>	111.768	65.185	69.240	$\alpha$ C 20.645
<b>Gly-14</b>	109.143	46.736		
<b>Tyr-15</b>	119.399	57.859	32.131	
<b>Gly-16</b>	107.357	46.639		
<b>Met-17</b>	122.025	60.634		$\alpha$ C 16.085
<b>Gly-18</b>	106.464	46.639		
<b>Val-19</b>	122.128	66.083	31.866	$\gamma$ C 20.452
<b>Gln-20</b>	117.500	59.107	28.178	$\alpha$ C 33.871, $\epsilon$ N 108.950
<b>Lys-21</b>	118.950	59.250	32.283	$\alpha$ C 24.564, $\beta$ C 28.834, $\gamma$ C 42.130
<b>Ala-22</b>	121.627	54.990	17.322	
<b>Ile-23</b>	117.558	64.554	38.196	$\alpha$ C 28.389, $\beta$ C 12.190, $\gamma$ C 12.390
<b>Asn-24</b>	118.098	55.863	38.609	$\beta$ N 111.143
<b>Asp-25</b>	118.158	55.127	38.463	
<b>Arg-26</b>	118.925	56.795	30.311	$\alpha$ C 27.054, $\beta$ C 43.215
<b>Arg-27</b>	120.113	56.852	32.936	$\alpha$ C 24.557, $\beta$ C 42.130
<b>Lys-28</b>	118.605	56.746	30.311	$\alpha$ C 27.071, $\beta$ C 28.908, $\gamma$ C 43.215
<b>Lys-29</b>	123.445	56.357	32.972	$\alpha$ C 24.785, $\beta$ C 28.908, $\gamma$ C 42.130

#### 7.4.10. Structure calculations

CYANA 2.1<sup>234</sup> was the software used to calculate the structures of CbnX and CbnY, utilizing a combination of automatically and manually assigned NOE restraints from the <sup>1</sup>H,<sup>1</sup>H-NOESY and <sup>1</sup>H,<sup>15</sup>N-NOESY-HSQC spectra, and angle restraints obtained from TALOS<sup>262</sup>. Seven cycles with 10,000 steps per cycle were run for each calculation. Simulated annealing calculated 100 conformers, and the 20 lowest energy conformers were used for further analysis. Coordinates for CbnX and CbnY were deposited in the Protein Data Bank with accession numbers 5UJR and 5UJQ, respectively.

#### 7.4.11. Isothermal titration calorimetry

Dr. Kaitlyn M. Towle conducted the isothermal titration calorimetry and permeability experiments. An MCS isothermal titration calorimeter (Microcal, Northampton, MA, USA) was used to study the binding interaction of CbnX and CbnY. Solutions of CbnX (1 mM) and CbnY (0.1 mM) were prepared in 1:1 trifluoroethanol:phosphate buffer (pH 6.9). The solutions were degassed by stirring *in vacuo* for 5 min. The microcalorimetric cell was filled with the CbnX solution, and the cell temperature was equilibrated to 25 °C. Ten μL aliquots of CbnY were then titrated into the cell every 5 min with constant stirring. The change in heat per injection was measured. Origin<sup>®</sup>7 software was used to process the data.

## **7.4.12. Permeability experiments**

### **7.4.12.1. Vesicle preparation**

Vesicles were made by dissolving 16 mg 1,2-dioleoyl-sn-glycero-3-phosphoethanolamine (DOPE) and 4 mg 1,2-dioleoyl-sn-glycero-3-phospho-(1'-rac-glycerol) (DOPG) in 2 mL chloroform. The solution was vortexed until it turned cloudy and opaque. The solvent was then removed under reduced pressure. The sample was desiccated under high vacuum for 2 h and suspended in 2 mL 50 mM sodium phosphate buffer (pH 8). Ten microliters of a 2 mM 2',7'-bis-(2-carboxyethyl)-5-(and-6)-carboxyfluorescein acid (BCECF) solution was added under reduced light, and the resulting solution was vortexed and placed into a cryovial. The sample was freeze-thawed five times by submerging in liquid nitrogen and thawing at 37 °C, with thorough shaking (vortex) in between each cycle. An Avanti Mini-Extruder (Avanti Polar Lipids Inc., Alabaster, AL, USA) with gastight syringes was used to extrude the sample through a 100 nm pore filter. Extrusion was done twenty times. The sample was passed through a G-50 size-exclusion column to remove excess BCECF dye using 50 mM sodium phosphate buffer (pH 8) as eluent. The vesicles were eluted in the dead volume of the column and were stored at 4 °C. Fluorescence studies were performed within one week of preparation of the vesicles.

#### **7.4.12.2. Fluorescence spectroscopy**

A 75 XE PTI fluorescence spectrophotometer was used for fluorescence measurements. The excitation wavelength was set at 500 nm, while the emission was at 525 nm. All slits on the instrument were opened to 1 mm and measurements were collected every second. Felix32 software facilitated real-time observation of results, which were exported and analyzed using Microsoft Excel. The prepared vesicles were added to 2 mL of potassium phosphate buffer (50 mM, pH 6) and equilibrated with stirring. Once the fluorescence reading was stable, the peptide samples were added, and the fluorescence was recorded until it was once again stable. After which, fluorescence was quenched by adding 50  $\mu$ L of a 5% Triton X-100 solution. Decreased fluorescence upon addition of the peptide solution indicates that protons are able to permeate the membrane and quench the BCECF acid dye, signifying vesicle disruption. The peptide solutions that were tested are 16  $\mu$ M, 8  $\mu$ M, 4  $\mu$ M and 2  $\mu$ M of CbnX and CbnY separately and combined.

## **7.5. Experimental Procedures for the Biosynthetic Studies of PneJ<sub>B</sub>**

### **7.5.1. Construction of pRSFDuet-PneM-PneA1 and pRSFDuet-PneM-PneA2**

Synthetic genes of PneM, PneA1, and PneA2 that were codon-optimized for *E. coli* expression were purchased from BioBasic Inc. and obtained as pUC57 derivatives, pUC57-PneM, pUC57-PneA1, and pUC57-PneA2, respectively. The pRSFDuet-1 expression vector was purchased from Novagen (EMD Millipore). Each of the constructs was transformed in chemically competent *E. coli* DH5 $\alpha$ , and transformants were stored in 20% glycerol at -80 °C. For plasmid isolation, a 5 mL LB broth was inoculated with the glycerol stock and grown at 37 °C with shaking at 225 rpm. Ampicillin (100  $\mu$ g/mL) was used for selective pressure for the pUC57 plasmids, while kanamycin (50  $\mu$ g/mL) was used for pRSFDuet-1. Plasmids were isolated using the QIAprep Spin Miniprep Kit (Qiagen).

The pUC57-PneM and pRSFDuet-1 plasmids were digested with FastDigest NdeI and XhoI (Thermo Scientific) restriction enzymes. The digests were purified by agarose gel electrophoresis, and the desired bands were extracted using QIAquick Gel Extraction Kit (Qiagen). The cut *pneM* insert was ligated to the cut pRSFDuet-1 vector using T4 DNA ligase (Invitrogen). The ligation mixture was transformed into chemically competent *E. coli* DH5 $\alpha$ , and plasmids from transformants were sequenced to screen for the desired pRSFDuet-PneM plasmid.

The isolated pRSFDuet-PneM plasmid, and the purchased pUC57-PneA1 and pUC57-PneA2 plasmids were digested with FastDigest EcoRI and HindIII (Thermo Scientific), and ran on an agarose gel. The desired bands were extracted using QIAquick

Gel Extraction Kit (Qiagen). The cut *pneA1* and *pneA2* genes were each ligated to the cut pRSFDuet-PneM vector using T4 DNA ligase (Invitrogen). The ligation mixture was transformed into chemically competent *E. coli* DH5 $\alpha$ , and transformants were sequenced to screen for the desired pRSFDuet-PneM-PneA1 and pRSFDuet-PneM-PneA2 plasmids. The resulting constructs introduced an N-terminal His-tag to PneA1 or PneA2, but not to PneM.

### **7.5.2. Construction of pETDuet-PneJ<sub>B</sub>**

The synthetic gene of PneJ<sub>B</sub> that was codon-optimized for *E. coli* expression was purchased from BioBasic Inc. and obtained as a pUC57 derivative, pUC57-PneJ<sub>B</sub>. Plasmids pETDuet-1 and pUC57-PneJ<sub>B</sub> were transformed in chemically competent *E. coli* DH5 $\alpha$  and transformants were stored in 20% glycerol at -80 °C. A 5 mL LB broth (with 100  $\mu$ g/mL ampicillin) was inoculated with the glycerol stock and grown at 37 °C with shaking at 225 rpm. Plasmids were then isolated from the overnight culture using the QIAprep Spin Miniprep Kit (Qiagen). Both constructs were digested using FastDigest NdeI and XhoI (Thermo Scientific). The digests were separated by agarose gel electrophoresis, and the desired bands were extracted using QIAquick Gel Extraction Kit (Qiagen). The *pneJ<sub>B</sub>* insert was ligated to the digested pETDuet-1 vector using T4 DNA ligase (Invitrogen), and the ligation mixture was transformed into chemically competent *E. coli* DH5 $\alpha$ . The transformants were sequenced to screen for the desired pETDuet-PneJ<sub>B</sub> plasmid.

### **7.5.3. Expression of PneMA1 and PneMA2 with and without PneJ<sub>B</sub>**

Chemically competent *E. coli* BL21 (DE3) was transformed with either pRSFDuet-PneM-PneA1 or pRSFDuet-PneM-PneA2 with and without pETDuet-PneJ<sub>B</sub>. For all expression systems, the isolated transformants were inoculated into 50 mL LB broth containing the appropriate antibiotic(s) (50 µg/mL kanamycin for the pRSFDuet vector, and 100 µg/mL ampicillin for pETDuet), and grown at 37 °C, 225 rpm, overnight. A liter of LB broth with the appropriate antibiotic(s) was inoculated with 1% (v/v) of the starter culture, and incubated at 37 °C, 225 rpm, until the OD<sub>600</sub> of the culture reached 0.5–0.6. Two induction conditions were tested for gene expression. For cultures induced with 0.1 mM IPTG, the samples were first cooled on ice for 30 min prior to addition of IPTG. Induction was done at 18 °C for 20 h. For cultures induced with 0.5 mM IPTG, induction was done at 37 °C for 3 h. The induced cultures were then centrifuged (5,000 × g, 10 min, 4 °C) and the supernatant was decanted.

### **7.5.4. Purification of expressed PneMA1 and PneMA2**

The cell pellet obtained from protein expression was resuspended in 30 mL lysis buffer (50 mM NaH<sub>2</sub>PO<sub>4</sub>, 500 mM NaCl, 10 mM imidazole, pH 8.0), passed once through a Constant Systems Cell Disruptor (Constant Systems Ltd.) operated at 23 kpsi, and centrifuged (23,700 × g, 30 min, 4 °C). Based on SDS-PAGE, the peptides with the expected molecular weight were found in the soluble fraction. Hence, the supernatant from the lysate was purified by Ni-NTA affinity chromatography. One mL Ni-NTA (Qiagen) resin was added, and the mixture was shaken at 50 rpm for 1 h at 8 °C. The sample was then loaded into a fritted column and allowed to flow by gravity. The resin

was washed with increasing amounts of imidazole in a buffer containing 50 mM sodium phosphate (pH 7.4) and 500 mM NaCl. The fractions were run on an SDS-PAGE gel to confirm elution of the desired peptide. The band at the expected molecular weight was excised, subjected to in-gel trypsin digestion, and submitted to Jing Zheng for tandem mass spectrometric analysis. Ni-NTA-purified fractions were subjected to RP-HPLC using C8 and C18 columns, and water-acetonitrile (both with 0.1% TFA) as solvent system. The solvents were programmed using both isocratic and gradient methods; however, there was no success in resolving the mixture of precursor peptides that were modified incompletely at various extents. HPLC fractions were analyzed by MALDI-TOF MS, and fractions containing peptides within the expected molecular weight range were submitted to Jing Zheng for high resolution MALDI-TOF MS analysis.

#### **7.5.5. Construction of truncated pRSFDuet-PneM-PneA1 and pRSFDuet-PneM-PneA2**

To address the problem on the inseparable mixture of precursor peptides with varying extents of modifications, truncated versions of the precursor peptides that eliminate other sites of modifications were designed. The genes for the truncated precursor peptides were amplified using primers JZA07 (5'-GAATTCAATGACGAACTTCAACAGCAACG-3') and JZA08 (5'-AAGCTTTTAAGCAGATTTTCAGGATAATCGGGG -3') for pUCSP-PneA1, and JZA09 (5'-GAATTCAATGAAAACGACTTCGTGATCGG-3') and JZA10 (5'- AAGCTTTTACAGCGTAGCAGAACAGATAATGG -3') for pUCSP-PneA2. The PCR products were run on an agarose gel, and purified using QIAquick Gel Extraction Kit (Qiagen). The pRSFDuet-PneM plasmid and the PCR products were

digested with FastDigest EcoRI and HindIII (Thermo Scientific), ran on an agarose gel, and the desired bands were extracted with QIAquick Gel Extraction Kit (Qiagen). The cut *pneA1*(truncated) and *pneA2*(truncated) genes were each ligated to the cut pRSFDuet-PneM vector using T4 DNA ligase (Invitrogen). The ligation mixture was transformed into chemically competent *E. coli* DH5 $\alpha$ , and plasmids from transformants were sequenced to screen for the desired pRSFDuet-PneM-PneA1(truncated) and pRSFDuet-PneM-PneA2(truncated) plasmids.

#### **7.5.6. Expression and purification of truncated PneMA1 and PneMA2**

Chemically competent *E. coli* BL21 (DE3) was transformed with either pRSFDuet-PneM-PneA1(truncated) or pRSFDuet-PneM-PneA2(truncated). The isolated transformants were inoculated into 50 mL LB broth containing 50  $\mu$ g/mL kanamycin, and grown overnight at 37 °C, 225 rpm. LB broth (400 mL) with 50  $\mu$ g/mL kanamycin was inoculated with 1% of the starter culture, and incubated at 37 °C, 225 rpm until the OD<sub>600</sub> of the culture reached 0.5 – 0.6. The culture was cooled on ice for 30 min and added with 0.5 mM IPTG. Induction was done at 25 °C for 20 h. Protein expression was monitored using SDS-PAGE, and no significant band at the desired molecular weight was observed in both the soluble and insoluble fractions. To further confirm this, the pellet was lysed and purified by Ni-NTA chromatography as in section 7.5.3, and monitored using SDS-PAGE and MALDI-TOF MS after clean-up with a C18 ZipTip.

#### **7.5.7. Construction of pET SUMO-PneJ<sub>B</sub>**

Instead of TA cloning, the EcoRI and HindIII restriction sites on the cyclized pET

SUMO vector (Invitrogen) were utilized for cloning. SUMO-PneJ<sub>B</sub> gene that was codon-optimized for *E. coli* expression was purchased from BioBasic Inc. The plasmid was transformed in chemically competent *E. coli* DH5 $\alpha$  and transformants were stored in 20% glycerol at -80 °C. Plasmid pUC57-SUMO-PneJ<sub>B</sub> was isolated using the QIAprep Spin Miniprep Kit (Qiagen) from an overnight culture of 5 mL LB broth (with 50  $\mu$ g/mL kanamycin) that was inoculated with the glycerol stock, and grown at 37 °C with shaking at 225 rpm. A cyclized pET SUMO vector and pUC57-SUMO-PneJ<sub>B</sub> were digested using FastDigest EcoRI and HindIII (Thermo Scientific). The digests were separated by agarose gel electrophoresis, and the desired bands were extracted using QIAquick Gel Extraction Kit (Qiagen). The SUMO-PneJ<sub>B</sub> insert was ligated to the digested pET SUMO vector using T4 DNA ligase (Invitrogen). The ligation mixture was transformed into chemically competent *E. coli* Mach1, and plasmids from transformants were sequenced to screen for the desired pET SUMO-PneJ<sub>B</sub> plasmid. The resulting pET SUMO-PneJ<sub>B</sub> plasmid was transformed into competent *E. coli* BL21 (DE3) for protein expression.

#### **7.5.8. Expression of SUMO-PneJ<sub>B</sub>**

LB broth (400 mL) containing 50  $\mu$ g/ml kanamycin was inoculated with an overnight starter culture (1% v/v), and grown at 37 °C with shaking at 225 rpm to an OD<sub>600</sub> of 0.6 – 0.8. The cultures were cooled on ice for 20 min, added with 0.5 mM IPTG, and incubated at 25 °C for 24 h at 225 rpm. The cultures were centrifuged (5,000  $\times$  g, 15 min, 4 °C), and the cells were resuspended in 30 mL lysis buffer (50 mM NaH<sub>2</sub>PO<sub>4</sub>, 500 mM NaCl, 10 mM imidazole, pH 7.4) and passed once through a Constant Systems Cell Disruptor (Constant Systems Ltd.) operated at 23 kpsi. The lysate was centrifuged (23,700

× g, 30 min, 4 °C) and the supernatant was collected for the subsequent Ni-NTA affinity chromatography.

#### **7.5.9. Purification of SUMO-PneJ<sub>B</sub>**

Ni-NTA (Qiagen) resin (1 mL) was added into the supernatant containing His-tagged SUMO-PneJ<sub>B</sub>. The mixture was shaken (50 rpm) for 1 h at 8 °C, and then loaded into a fritted column and allowed to flow by gravity. The resin was washed with 50 mL buffer A (50 mM NaH<sub>2</sub>PO<sub>4</sub>, 500 mM NaCl, pH 7.4) containing 20 mM imidazole, 25 mL of 50 mM imidazole in buffer A, and 5 mL each of 100 mM, 150 mM, 200 mM, 250 mM, and 300 mM imidazole in buffer A. The fractions were run on an SDS-PAGE gel to confirm elution of the desired protein. The fraction containing SUMO-PneJ<sub>B</sub> was dialyzed against 3 L of water overnight at 8 °C. Protein sample that was not used for SUMO protease digestion was concentrated using an Amicon Ultra-15 Centrifugal Filter Unit (EMD Millipore), and stored at -80 °C in 18% glycerol.

#### **7.5.10. SUMO protease digestion**

The SUMO tag on the fusion proteins was removed by treatment with His-tagged SUMO protease (McLab) using 10 U protease per 20 µg fusion protein and following the buffer conditions indicated in section 7.1.6. Overnight cleavage trials were performed with or without the detergent IGEPAL<sup>®</sup> CA-630 (Sigma-Aldrich) either at 8 °C or 25 °C, and monitored using SDS-PAGE. The cleaved His-tagged SUMO protein and His-tagged SUMO protease were then removed by treatment with 0.5 mL Ni-NTA (Qiagen) resin for 1 h, and collecting the supernatant.

## References

1. Cotter, P.D.; Hill, C.; Ross, R.P. Bacteriocins: Developing Innate Immunity for Food. *Nat. Rev. Microbiol.* **2005**, *3*, 777–788.
2. Tagg, J.R.; Dajani, A.S.; Wannamaker, L.W. Bacteriocins of Gram-positive Bacteria. *Bacteriol. Rev.* **1976**, *40*, 722–756.
3. Klaenhammer, T.R. Bacteriocins of Lactic Acid Bacteria. *Biochimie.* **1988**, *70*, 337–349.
4. Gillor, O.; Etzion, A.; Riley, M.A. The Dual Role of Bacteriocins as Anti- and Probiotics. *Appl. Microbiol. Biotechnol.* **2008**, *81*, 591–606.
5. Gratia, A. Sur Un Remarquable Exemple D'Antagonisme Entre Deux Souches De Coillbacille. *CR Seances. Soc. Biol. Fil.* **1925**, *93*, 1040–1041.
6. Hammami, R.; Zouhir, A.; Le Lay, C.; Ben Hamida, J.; Fliss, I. BACTIBASE Second Release: a Database and Tool Platform for Bacteriocin Characterization. *BMC Microbiol.* **2010**, *10*, 22.
7. van Belkum, M.J.; Stiles, M.E. Nonantibiotic Antibacterial Peptides From Lactic Acid Bacteria. *Nat. Prod. Rep.* **2000**, *17*, 323–335.
8. Wood, B.J.B.; Holzapfel, W.H.N. *The Genera of Lactic Acid Bacteria*. Springer Science & Business Media: Heidelberg, Germany, 1995; pp 398.
9. Alvarez-Sieiro, P.; Montalbán-López, M.; Mu, D.; Kuipers, O.P. Bacteriocins of Lactic Acid Bacteria: Extending the Family. *Appl. Microbiol. Biotechnol.* **2016**, *100*, 2939–2951.
10. Abriouel, H.; Franz, C.M.A.P.; Ben Omar, N.; Gálvez, A. Diversity and

- Applications of *Bacillus* Bacteriocins. *FEMS Microbiol. Rev.* **2011**, *35*, 201–232.
11. Cochrane, S.A.; Vederas, J.C. Lipopeptides From *Bacillus* and *Paenibacillus* spp.: a Gold Mine of Antibiotic Candidates. *Med. Res. Rev.* **2016**, *36*, 4–31.
  12. Cochrane, S.A.; Findlay, B.; Bakhtiary, A.; Acedo, J.Z.; Rodriguez-Lopez, E.M.; Mercier, P.; Vederas, J.C. Antimicrobial Lipopeptide Tridecaptin A1 Selectively Binds to Gram-negative Lipid II. *Proc. Natl. Acad. Sci. USA.* **2016**, *113*, 11561–11566.
  13. Daas, M.S.; Rosana, A.R.R.; Acedo, J.Z.; Nateche, F.; Kebbouche-Gana, S.; Vederas, J.C.; Case, R.J. Draft Genome Sequences of *Bacillus cereus* E41 and *Bacillus anthracis* F34 Isolated From Algerian Salt Lakes. *Genome Announc.* **2017**, *5*, e00383–17.
  14. Nascimento, J.S.; Ceotto, H.; Nascimento, S.B.; Giambiagi-Demarval, M.; Santos, K.R.; Bastos, M.C. Bacteriocins as Alternative Agents for Control of Multiresistant Staphylococcal Strains. *Lett. Appl. Microbiol.* **2006**, *42*, 215–221.
  15. Ahmad, V.; Khan, M.S.; Jamal, Q.M.; Alzohairy, M.A.; Al Karaawi, M.A.; Siddiqui, M.U. Antimicrobial Potential of Bacteriocins: In Therapy, Agriculture, and Food Preservation. *Int. J. Antimicrob. Agents.* **2017**, *49*, 1–11.
  16. Chen, H.; Hoover, D.G. Bacteriocins and Their Food Applications. *Compr. Rev. Food Sci. Food Saf.* **2003**, *2*, 82–100.
  17. Deegan, L.H.; Cotter, P.D.; Hill, C.; Ross, P. Bacteriocins: Biological Tools for Bio-preservation and Shelf-life Extension. *Int. Dairy J.* **2006**, *16*, 1058–1071.
  18. Lee, N.K.; Paik, H.D. Status, Antimicrobial Mechanism, and Regulation of Natural Preservatives in Livestock Food Systems. *Korean J. Food. Sci. Anim. Resour.* **2016**,

- 36, 547–557.
19. Lubelski, J.; Rink, R.; Khusainov, R.; Moll, G.N.; Kuipers, O.P. Biosynthesis, Immunity, Regulation, Mode of Action, and Engineering of the Model Lantibiotic Nisin. *Cell Mol. Life Sci.* **2008**, *65*, 455–476.
  20. Kuipers, O.P.; Beerthuyzen, M.M.; Siezen, R.J.; de Vos, W.M. Characterization of the Nisin Gene Cluster *nisABTCIPR* of *Lactococcus lactis*. Requirement of Expression of the *nisA* and *nisI* Genes for Development of Immunity. *Eur. J. Biochem.* **1993**, *216*, 281–291.
  21. Settanni, L.; Corsetti, A. Application of Bacteriocins in Vegetable Food Biopreservation. *Int. J. Food. Microbiol.* **2008**, *121*, 123–138.
  22. Mahendra, R. *Natural Antimicrobials in Food Safety and Quality*. CABI: Wallingford, Oxfordshire, England, 2011; pp 384.
  23. López-Cuellar, M.D.R.; Rodríguez-Hernández, A.I.; Chavarría-Hernández, N. LAB Bacteriocin Applications in the Last Decade. *Biotechnol. Biotechnol. Equip.* **2016**, *30*, 1039–1050.
  24. Grande, M.; Lucas, R.; Abriouel, H.; Valdivia, E.; Ben Omar, N.; Maqueda, M.; Martínez-Cañamero, M.; Gálvez, A. Inhibition of *Bacillus licheniformis* LMG 19409 From Ropy Cider by Enterocin AS-48. *J. Appl. Microbiol.* **2006**, *101*, 422–428.
  25. Lauková, A.; Czikková, S. The Use of Enterocin CCM 4231 in Soy Milk to Control the Growth of *Listeria monocytogenes* and *Staphylococcus aureus*. *J. Appl. Microbiol.* **1999**, *87*, 182–186.
  26. García, M.; Lucas, R.; Abriouel, H.; Omar, N.B.; Pérez, R.; Grande, M.; Martínez-Cañamero, M.; Gálvez, A. Antimicrobial Activity of Enterocin EJ97 Against

- 'Bacillus macroides/Bacillus maroccanus'* Isolated From Zucchini Purée. *J. Appl. Microbiol.* **2004**, *97*, 731–737.
27. Cotter, P.D.; Ross, R.P.; Hill, C. Bacteriocins - a Viable Alternative to Antibiotics. *Nat. Rev. Microbiol.* **2013**, *11*, 95–105.
  28. Grinter, R.; Milner, J.; Walker, D. Bacteriocins Active Against Plant Pathogenic Bacteria. *Biochem. Soc. Trans.* **2012**, *40*, 1498–1502.
  29. Coelho, M.L.V.; Nascimento, J.S.; Fagundes, P.C.; Madureira, D.J.; Oliveira, S.S.; Vasconcelos de Paiva Brito, M.A.; Bastos, M.C. Activity of Staphylococcal Bacteriocins Against *Staphylococcus aureus* and *Streptococcus agalactiae* Involved in Bovine Mastitis. *Res. Microbiol.* **2007**, *158*, 625–630.
  30. Ongey, E.L.; Yassi, H.; Pflugmacher, S.; Neubauer, P. Pharmacological and Pharmacokinetic Properties of Lanthipeptides Undergoing Clinical Studies. *Biotechnol. Lett.* **2017**, *39*, 473–482.
  31. Sandiford, S.K. Perspectives on Lantibiotic Discovery - Where Have We Failed and What Improvements Are Required. *Expert Opin. Drug. Discov.* **2015**, *10*, 315–320.
  32. Gillor, O.; Kirkup, B.C.; Riley, M.A. Colicins and Microcins: The Next Generation Antimicrobials. *Adv. Appl. Microbiol.* **2004**, *54*, 129–146.
  33. Ghequire, M.G.; De Mot, R. Ribosomally Encoded Antibacterial Proteins and Peptides From *Pseudomonas*. *FEMS Microbiol. Rev.* **2014**, *38*, 523–568.
  34. Rebuffat, S. Bacteriocins From Gram-negative bacteria: a classification. In *Prokaryotic Antimicrobial Peptides: From Genes to Applications*, Drider, D.; Rebuffat, S., Ed.; Springer: New York City, New York, USA, 2011; pp 55-72.
  35. Michel-Briand, Y.; Baysse, C. The Pyocins of *Pseudomonas aeruginosa*. *Biochimie.*

- 2002**, *84*, 499–510.
36. Morales-Soto, N.; Gaudriault, S.; Ogier, J.-C.; Thappeta, K.R.V.; Forst, S.  
Comparative Analysis of P2-type Remnant Prophage Loci in *Xenorhabdus bovienii*  
and *Xenorhabdus nematophila* Required for Xenorhabdicolin Production. *FEMS  
Microbiol. Lett.* **2012**, *333*, 69–76.
  37. Liu, J.; Chen, P.; Zheng, C.; Huang, Y.P. Characterization of Maltocin P28, a Novel  
Phage Tail-like Bacteriocin From *Stenotrophomonas maltophilia*. *Appl. Environ.  
Microbiol.* **2013**, *79*, 5593–5600.
  38. Yao, G.W.; Duarte, I.; Le, T.T.; Carmody, L.; LiPuma, J.J.; Young, R.; Gonzalez, C.  
A Broad-host-range Tailocin From *Burkholderia cenocepacia*. *Appl. Environ.  
Microbiol.* **2017**, *83*, e03414–16.
  39. Ghequire, M.G.K.; De Mot, R. The Tailocin Tale: Peeling Off Phage Tails. *Trends  
Microbiol.* **2015**, *23*, 587–590.
  40. Gebhart, D.; Lok, S.; Clare, S.; Tomas, M.; Stares, M.; Scholl, D.; Donskey, C.J.;  
Lawley, T.D.; Govoni, G.R. A Modified R-type Bacteriocin Specifically Targeting  
*Clostridium difficile* Prevents Colonization of Mice Without Affecting Gut  
Microbiota Diversity. *MBio.* **2015**, *6*, e02368–14.
  41. Klaenhammer, T.R. Genetics of Bacteriocins Produced by Lactic Acid Bacteria.  
*FEMS Microbiol. Rev.* **1993**, *12*, 39–85.
  42. Oman, T.J.; van der Donk, W.A. Follow the Leader: The Use of Leader Peptides to  
Guide Natural Product Biosynthesis. *Nat. Chem. Biol.* **2010**, *6*, 9–18.
  43. van Belkum, M.J.; Martin-Visscher, L.A.; Vederas, J.C. Structure and Genetics of  
Circular Bacteriocins. *Trends Microbiol.* **2011**, *19*, 411–418.

44. Gabrielsen, C.; Brede, D.A.; Nes, I.F.; Diep, D.B. Circular Bacteriocins: Biosynthesis and Mode of Action. *Appl. Environ. Microbiol.* **2014**, *80*, 6854–6862.
45. Gálvez, A.; Abriouel, H.; Lopez, R.L.; Ben Omar, N. Bacteriocin-based Strategies for Food Biopreservation. *Int. J. Food. Microbiol.* **2007**, *120*, 51–70.
46. Sawa, N.; Zendo, T.; Kiyofuji, J.; Fujita, K.; Himeno, K.; Nakayama, J.; Sonomoto, K. Identification and Characterization of Lactocyclicin Q, a Novel Cyclic Bacteriocin Produced by *Lactococcus* sp. Strain QU 12. *Appl. Environ. Microbiol.* **2009**, *75*, 1552–1558.
47. Masuda, Y.; Ono, H.; Kitagawa, H.; Ito, H.; Mu, F.; Sawa, N.; Zendo, T.; Sonomoto, K. Identification and Characterization of Leucocyclicin Q, a Novel Cyclic Bacteriocin Produced by *Leuconostoc mesenteroides* TK41401. *Appl. Environ. Microbiol.* **2011**, *77*, 8164–8170.
48. Gálvez, A.; Maqueda, M.; Martínez-Bueno, M.; Valdivia, E. Bactericidal and Bacteriolytic Action of Peptide Antibiotic AS-48 Against Gram-positive and Gram-negative Bacteria and Other Organisms. *Res. Microbiol.* **1989**, *140*, 57–68.
49. Martin-Visscher, L.A.; Yoganathan, S.; Sit, C.S.; Lohans, C.T.; Vederas, J.C. The Activity of Bacteriocins From *Carnobacterium maltaromaticum* UAL307 Against Gram-negative Bacteria in Combination With EDTA Treatment. *FEMS Microbiol. Lett.* **2011**, *317*, 152–159.
50. Samyn, B.; Martínez-Bueno, M.; Devreese, B.; Maqueda, M.; Gálvez, A.; Valdivia, E.; Coyette, J.; Van Beeumen, J. The Cyclic Structure of the Enterococcal Peptide Antibiotic AS-48. *FEBS Lett.* **1994**, *352*, 87–90.
51. Acedo, J.Z.; van Belkum, M.J.; Lohans, C.T.; McKay, R.T.; Miskolzie, M.; Vederas,

- J.C. Solution Structure of Acidocin B, a Circular Bacteriocin Produced by *Lactobacillus acidophilus* M46. *Appl. Environ. Microbiol.* **2015**, *81*, 2910–2918.
52. Babasaki, K.; Takao, T.; Shimonishi, Y.; Kurahashi, K. Subtilosin A, a New Antibiotic Peptide Produced by *Bacillus subtilis* 168: Isolation, Structural Analysis, and Biogenesis. *J. Biochem.* **1985**, *98*, 585–603.
53. Murphy, K.; O’Sullivan, O.; Rea, M.C.; Cotter, P.D.; Ross, R.P.; Hill, C. Genome Mining for Radical SAM Protein Determinants Reveals Multiple Sactibiotic-like Gene Clusters. *PLoS One.* **2011**, *6*, e20852.
54. Arnison, P.G.; Bibb, M.J.; Bierbaum, G.; Bowers, A.A.; Bugni, T.S.; Bulaj, G.; Camarero, J.A.; Campopiano, D.J.; Challis, G.L.; Clardy, J.; Cotter, P.D.; Craik, D.J.; Dawson, M.; Dittmann, E.; Donadio, S.; Dorrestein, P.C.; Entian, K.D.; Fischbach, M.A.; Garavelli, J.S.; Göransson, U.; Gruber, C.W.; Haft, D.H.; Hemscheidt, T.K.; Hertweck, C.; Hill, C.; Horswill, A.R.; Jaspars, M.; Kelly, W.L.; Klinman, J.P.; Kuipers, O.P.; Link, A.J.; Liu, W.; Marahiel, M.A.; Mitchell, D.A.; Moll, G.N.; Moore, B.S.; Müller, R.; Nair, S.K.; Nes, I.F.; Norris, G.E.; Olivera, B.M.; Onaka, H.; Patchett, M.L.; Piel, J.; Reaney, M.J.; Rebuffat, S.; Ross, R.P.; Sahl, H.G.; Schmidt, E.W.; Selsted, M.E.; Severinov, K.; Shen, B.; Sivonen, K.; Smith, L.; Stein, T.; Süßmuth, R.D.; Tagg, J.R.; Tang, G.L.; Truman, A.W.; Vederas, J.C.; Walsh, C.T.; Walton, J.D.; Wenzel, S.C.; Willey, J.M.; van der Donk, W.A. Ribosomally Synthesized and Post-translationally Modified Peptide Natural Products: Overview and Recommendations for a Universal Nomenclature. *Nat. Prod. Rep.* **2013**, *30*, 108–160.
55. Kawai, Y.; Saito, T.; Kitazawa, H.; Itoh, T. Gassericin A; an Uncommon Cyclic

- Bacteriocin Produced by *Lactobacillus gasseri* LA39 Linked at N- and C-terminal Ends. *Biosci. Biotechnol. Biochem.* **1998**, *62*, 2438–2440.
56. Kalmokoff, M.L.; Cyr, T.D.; Hefford, M.A.; Whitford, M.F.; Teather, R.M. Butyrivibriocin AR10, a New Cyclic Bacteriocin Produced by the Ruminal Anaerobe *Butyrivibrio fibrisolvens* AR10: Characterization of the Gene and Peptide. *Can. J. Microbiol.* **2003**, *49*, 763–773.
57. Kemperman, R.; Kuipers, A.; Karsens, H.; Nauta, A.; Kuipers, O.; Kok, J. Identification and Characterization of Two Novel Clostridial Bacteriocins, Circularin A and Closticin 574. *Appl. Environ. Microbiol.* **2003**, *69*, 1589–1597.
58. Wirawan, R.E.; Swanson, K.M.; Kleffmann, T.; Jack, R.W.; Tagg, J.R. Uberolysin: a Novel Cyclic Bacteriocin Produced by *Streptococcus uberis*. *Microbiology.* **2007**, *153*, 1619–1630.
59. Martin-Visscher, L.A.; van Belkum, M.J.; Garneau-Tsodikova, S.; Whittall, R.M.; Zheng, J.; McMullen, L.M.; Vederas, J.C. Isolation and Characterization of Carnocyclin A, a Novel Circular Bacteriocin Produced by *Carnobacterium maltaromaticum* UAL307. *Appl. Environ. Microbiol.* **2008**, *74*, 4756–4763.
60. Borrero, J.; Brede, D.A.; Skaugen, M.; Diep, D.B.; Herranz, C.; Nes, I.F.; Cintas, L.M.; Hernández, P.E. Characterization of Garvicin ML, a Novel Circular Bacteriocin Produced by *Lactococcus garvieae* DCC43, Isolated From Mallard Ducks (*Anas platyrhynchos*). *Appl. Environ. Microbiol.* **2011**, *77*, 369–373.
61. Scholz, R.; Vater, J.; Budiharjo, A.; Wang, Z.; He, Y.; Dietel, K.; Schwecke, T.; Herfort, S.; Lasch, P.; Borriss, R. Amylocyclicin, a Novel Circular Bacteriocin Produced by *Bacillus amyloliquefaciens* FZB42. *J. Bacteriol.* **2014**, *196*, 1842–1852.

62. Potter, A.; Ceotto, H.; Coelho, M.L.; Guimarães, A.J.; Bastos, M.C. The Gene Cluster of Aureocyclacin 4185: the First Cyclic Bacteriocin of *Staphylococcus aureus*. *Microbiology*. **2014**, *160*, 917–928.
63. Himeno, K.; Rosengren, K.J.; Inoue, T.; Perez, R.H.; Colgrave, M.L.; Lee, H.S.; Chan, L.Y.; Henriques, S.T.; Fujita, K.; Ishibashi, N.; Zendo, T.; Wilaipun, P.; Nakayama, J.; Leelawatcharamas, V.; Jikuya, H.; Craik, D.J.; Sonomoto, K. Identification, Characterization, and Three-dimensional Structure of the Novel Circular Bacteriocin, Enterocin NKR-5-3B, From *Enterococcus faecium*. *Biochemistry*. **2015**, *54*, 4863–4876.
64. Bogaardt, C.; Tonder, A.J.; Brueggemann, A.B. Genomic Analyses of Pneumococci Reveal a Wide Diversity of Bacteriocins—Including Pneumocyclacin, a Novel Circular Bacteriocin. *BMC Genomics*. **2015**, *16*, 554.
65. van Heel, A.J.; Montalbán-López, M.; Quentin, O.; Kuipers, O.P. Genome-guided Identification of Novel Head-to-tail Cyclized Antimicrobial Peptides, Exemplified by the Discovery of Pumilarin. *Microbial Genomics*. **2017**, *3*, DOI 10.1099/mgen.0.000134.
66. Martínez-Bueno, M.; Valdivia, E.; Gálvez, A.; Coyette, J.; Maqueda, M. Analysis of the Gene Cluster Involved in Production and Immunity of the Peptide Antibiotic AS-48 in *Enterococcus faecalis*. *Mol. Microbiol.* **1998**, *27*, 347–358.
67. Diaz, M.; Valdivia, E.; Martínez-Bueno, M.; Fernández, M.; Soler-González, A.S.; Ramírez-Rodrigo, H.; Maqueda, M. Characterization of a New Operon, *as-48EFGH*, From the AS-48 Gene Cluster Involved in Immunity to Enterocin AS-48. *Appl. Environ. Microbiol.* **2003**, *69*, 1229–1236.

68. Mu, F.; Masuda, Y.; Zendo, T.; Ono, H.; Kitagawa, H.; Ito, H.; Nakayama, J.; Sonomoto, K. Biological Function of a DUF95 Superfamily Protein Involved in the Biosynthesis of a Circular Bacteriocin, Leucocyclicin Q. *J. Biosci. Bioeng.* **2014**, *117*, 158–164.
69. van Belkum, M.J.; Martin-Visscher, L.A.; Vederas, J.C. Cloning and Characterization of the Gene Cluster Involved in the Production of the Circular Bacteriocin Carnocyclin A. *Probiotics Antimicrob. Proteins.* **2010**, *2*, 218–225.
70. Kemperman, R.; Jonker, M.; Nauta, A.; Kuipers, O.P.; Kok, J. Functional Analysis of the Gene Cluster Involved in Production of the Bacteriocin Circularin A by *Clostridium beijerinckii* ATCC 25752. *Appl. Environ. Microbiol.* **2003**, *69*, 5839–5848.
71. Perez, R.H.; Ishibashi, N.; Inoue, T.; Himeno, K.; Masuda, Y.; Sawa, N.; Zendo, T.; Wilaipun, P.; Leelawatcharamas, V.; Nakayama, J.; Sonomoto, K. Functional Analysis of Genes Involved in the Biosynthesis of Enterocin NKR-5-3B, a Novel Circular Bacteriocin. *J. Bacteriol.* **2016**, *198*, 291–300.
72. Gabrielsen, C.; Brede, D.A.; Salehian, Z.; Nes, I.F.; Diep, D.B. Functional Genetic Analysis of the GarML Gene Cluster in *Lactococcus garvieae* DCC43 Gives New Insights into Circular Bacteriocin Biosynthesis. *J. Bacteriol.* **2014**, *196*, 911–919.
73. Kawai, Y.; Kusnadi, J.; Kemperman, R.; Kok, J.; Ito, Y.; Endo, M.; Arakawa, K.; Uchida, H.; Nishimura, J.; Kitazawa, H.; Saito, T. DNA Sequencing and Homologous Expression of a Small Peptide Conferring Immunity to Gassericin A, a Circular Bacteriocin Produced by *Lactobacillus gasseri* LA39. *Appl. Environ. Microbiol.* **2009**, *75*, 1324–1330.

74. González, C.; Langdon, G.M.; Bruix, M.; Gálvez, A.; Valdivia, E.; Maqueda, M.; Rico, M. Bacteriocin AS-48, a Microbial Cyclic Polypeptide Structurally and Functionally Related to Mammalian NK-lysin. *Proc. Natl. Acad. Sci. USA*. **2000**, *97*, 11221–11226.
75. Martin-Visscher, L.A.; Gong, X.; Duszyk, M.; Vederas, J.C. The Three-dimensional Structure of Carnocyclin A Reveals That Many Circular Bacteriocins Share a Common Structural Motif. *J. Biol. Chem.* **2009**, *284*, 28674–28681.
76. Vaccaro, A.M.; Salvioli, R.; Tatti, M.; Ciaffoni, F. Saposins and their Interaction With Lipids. *Neurochem. Res.* **1999**, *24*, 307–314.
77. Bruhn, H. A Short Guided Tour through Functional and Structural Features of Saposin-like Proteins. *Biochem. J.* **2005**, *389*, 249–257.
78. Gálvez, A.; Maqueda, M.; Martínez-Bueno, M.; Valdivia, E. Permeation of Bacterial Cells, Permeation of Cytoplasmic, and Artificial Membrane Vesicles, and Channel Formation on Lipid Bilayers by Peptide Antibiotic AS-48. *J. Bacteriol.* **1991**, *173*, 886–892.
79. Sánchez-Barrena, M.J.; Martínez-Ripoll, M.; Gálvez, A.; Valdivia, E.; Maqueda, M.; Cruz, V.; Albert, A. Structure of Bacteriocin AS-48: From Soluble State to Membrane Bound State. *J. Mol. Biol.* **2003**, *334*, 541–549.
80. Cruz, V.L.; Ramos, J.; Melo, M.N.; Martínez-Salazar, J. Bacteriocin AS-48 Binding to Model Membranes and Pore Formation as Revealed by Coarse-grained Simulations. *Biochim. Biophys. Acta.* **2013**, *1828*, 2524–2531.
81. Gong, X.; Martin-Visscher, L.A.; Nahirney, D.; Vederas, J.C.; Duszyk, M. The Circular Bacteriocin, Carnocyclin A, Forms Anion-Selective Channels in Lipid

- Bilayers. *Biochim. Biophys. Acta.* **2009**, *1788*, 1797–1803.
82. Kawai, Y.; Ishii, Y.; Arakawa, K.; Uemura, K.; Saitoh, B.; Nishimura, J.; Kitazawa, H.; Yamazaki, Y.; Tateno, Y.; Itoh, T.; Saito, T. Structural and Functional Differences in Two Cyclic Bacteriocins With the Same Sequences Produced by Lactobacilli. *Appl. Environ. Microbiol.* **2004**, *70*, 2906–2911.
83. Gabrielsen, C.; Brede, D.A.; Hernández, P.E.; Nes, I.F.; Diep, D.B. The Maltose ABC Transporter in *Lactococcus lactis* Facilitates High-level Sensitivity to the Circular Bacteriocin Garvicin ML. *Antimicrob. Agents Chemother.* **2012**, *56*, 2908–2915.
84. Masuda, Y.; Zendo, T.; Sonomoto, K. New Type Non-lantibiotic Bacteriocins: Circular and Leaderless Bacteriocins. *Benef. Microbes.* **2012**, *3*, 3–12.
85. Abba, K. *Handbook of Biologically Active Peptides*. Academic Press: San Diego, CA, USA, 2013; pp 1978.
86. Sherman, F.; Stewart, J.W.; Tsunasawa, S. Methionine or Not Methionine at the Beginning of a Protein. *Bioessays.* **1985**, *3*, 27–31.
87. Cintas, L.M.; Casaus, P.; Holo, H.; Hernandez, P.E.; Nes, I.F.; Håvarstein, L.S. Enterocins L50A and L50B, Two Novel Bacteriocins From *Enterococcus faecium* L50, Are Related to Staphylococcal Hemolysins. *J. Bacteriol.* **1998**, *180*, 1988–1994.
88. Hanchi, H.; Hammami, R.; Fernandez, B.; Kourda, R.; Ben Hamida, J.; Fliss, I. Simultaneous Production of Formylated and Nonformylated Enterocins L50A and L50B as well as 61A, a New Glycosylated Durancin, by *Enterococcus durans* 61A, a Strain Isolated From Artisanal Fermented Milk in Tunisia. *J. Agric. Food Chem.*

- 2016**, *64*, 3584–3590.
89. Masuda, Y.; Zendo, T.; Sawa, N.; Perez, R.H.; Nakayama, J.; Sonomoto, K. Characterization and Identification of Weissellicin Y and Weissellicin M, Novel Bacteriocins Produced by *Weissella hellenica* QU 13. *J. Appl. Microbiol.* **2012**, *112*, 99–108.
  90. Ovchinnikov, K.V.; Chi, H.; Mehmeti, I.; Holo, H.; Nes, I.F.; Diep, D.B. Novel Group of Leaderless Muropeptide Bacteriocins From Gram-positive Bacteria. *Appl. Environ. Microbiol.* **2016**, *82*, 5216–5224.
  91. Netz, D.J.; Sahl, H.G.; Marcolino, R.; Nascimento, J.S.; De Oliveira, S.S.; Soares, M.B.; Bastos, M.C. Molecular Characterization of Aureocin A70, a Multi-peptide Bacteriocin Isolated From *Staphylococcus aureus*. *J. Mol. Biol.* **2001**, *311*, 939–949.
  92. Singh, P.K.; Chittipurna; Ashish; Sharma, V.; Patil, P.B.; Korpole, S. Identification, Purification, and Characterization of Laterosporulin, a Novel Bacteriocin Produced by *Brevibacillus* sp. strain GI-9. *PLoS One.* **2012**, *7*, e31498.
  93. Baidara, P.; Singh, N.; Ranjan, M.; Nallabelli, N.; Chaudhry, V.; Pathania, G.L.; Sharma, N.; Kumar, A.; Patil, P.B.; Korpole, S. Laterosporulin10: a Novel Defensin-like Class IId Bacteriocin From *Brevibacillus* sp. strain SKDU10 With Inhibitory Activity Against Microbial Pathogens. *Microbiology.* **2016**, *162*, 1286–1299.
  94. Cintas, L.M.; Casaus, P.; Herranz, C.; Håvarstein, L.S.; Holo, H.; Hernández, P.E.; Nes, I.F. Biochemical and Genetic Evidence That *Enterococcus faecium* L50 Produces Enterocins L50A and L50B, the Sec-dependent Enterocin P, and a Novel Bacteriocin Secreted Without an N-terminal Extension Termed Enterocin Q. *J. Bacteriol.* **2000**, *182*, 6806–6814.

95. Netz, D.J.; Pohl, R.; Beck-Sickinger, A.G.; Selmer, T.; Pierik, A.J.; Bastos, M.C.; Sahl, H.G. Biochemical Characterization and Genetic Analysis of Aureocin A53, a New, Atypical Bacteriocin From *Staphylococcus aureus*. *J. Mol. Biol.* **2002**, *319*, 745–756.
96. Sánchez-Hidalgo, M.; Maqueda, M.; Gálvez, A.; Abriouel, H.; Valdivia, E.; Martínez-Bueno, M. The Genes Coding for Enterocin EJ97 Production by *Enterococcus faecalis* EJ97 Are Located on a Conjugative Plasmid. *Appl. Environ. Microbiol.* **2003**, *69*, 1633–1641.
97. Gajic, O.; Buist, G.; Kojic, M.; Topisirovic, L.; Kuipers, O.P.; Kok, J. Novel Mechanism of Bacteriocin Secretion and Immunity Carried Out by Lactococcal Multidrug Resistance Proteins. *J. Biol. Chem.* **2003**, *278*, 34291–34298.
98. Hyink, O.; Balakrishnan, M.; Tagg, J.R. *Streptococcus rattus* strain BHT Produces Both a Class I Two-component Lantibiotic and a Class II Bacteriocin. *FEMS Microbiol. Lett.* **2005**, *252*, 235–241.
99. Martín-Platero, A.M.; Valdivia, E.; Ruíz-Rodríguez, M.; Soler, J.J.; Martín-Vivaldi, M.; Maqueda, M.; Martínez-Bueno, M. Characterization of Antimicrobial Substances Produced by *Enterococcus faecalis* MRR 10-3, Isolated From the Uropygial Gland of the Hoopoe (*Upupa epops*). *Appl. Environ. Microbiol.* **2006**, *72*, 4245–4249.
100. Liu, X.; Vederas, J.C.; Whittal, R.M.; Zheng, J.; Stiles, M.E.; Carlson, D.; Franz, C.M.A.P.; McMullen, L.M.; van Belkum, M.J. Identification of an N-terminal Formylated, Two-peptide Bacteriocin From *Enterococcus faecalis* 710C. *J. Agric. Food. Chem.* **2011**, *59*, 5602–5608.

101. Caly, D.L.; Chevalier, M.; Flahaut, C.; Cudennec, B.; Al Atya, A.K.; Chataigné, G.; D’Inca, R.; Auclair, E.; Drider, D. The Safe Enterocin DD14 Is a Leaderless Two-peptide Bacteriocin With Anti-*Clostridium perfringens* Activity. *Int. J. Antimicrob. Agents*. **2017**, *49*, 282–289.
102. Fujita, K.; Ichimasa, S.; Zendo, T.; Koga, S.; Yoneyama, F.; Nakayama, J.; Sonomoto, K. Structural Analysis and Characterization of Lacticin Q, a Novel Bacteriocin Belonging to a New Family of Unmodified Bacteriocins of Gram-positive Bacteria. *Appl. Environ. Microbiol.* **2007**, *73*, 2871–2877.
103. Iwatani, S.; Zendo, T.; Yoneyama, F.; Nakayama, J.; Sonomoto, K. Characterization and Structure Analysis of a Novel Bacteriocin, Lacticin Z, Produced by *Lactococcus lactis* QU 14. *Biosci. Biotechnol. Biochem.* **2007**, *71*, 1984–1992.
104. Sandiford, S.; Upton, M. Identification, Characterization, and Recombinant Expression of Epidermicin NI01, a Novel Unmodified Bacteriocin Produced by *Staphylococcus epidermidis* That Displays Potent Activity Against Staphylococci. *Antimicrob. Agents Chemother.* **2012**, *56*, 1539–1547.
105. Ovchinnikov, K.V.; Kristiansen, P.E.; Uzelac, G.; Topisirovic, L.; Kojic, M.; Nissen-Meyer, J.; Nes, I.F.; Diep, D.B. Defining the Structure and Receptor Binding Domain of the Leaderless Bacteriocin LsbB. *J. Biol. Chem.* **2014**, *289*, 23838–23845.
106. Du, L.; Liu, F.; Zhao, P.; Zhao, T.; Doyle, M.P. Characterization of *Enterococcus durans* 152 Bacteriocins and their Inhibition of *Listeria monocytogenes* in Ham. *Food Microbiol.* **2017**, *68*, 97–103.
107. Lozo, J.; Mirkovic, N.; O’Connor, P.M.; Malesevic, M.; Miljkovic, M.; Polovic, N.;

- Jovcic, B.; Cotter, P.D.; Kojic, M. Lactolisterin BU, a Novel Class II Broad Spectrum Bacteriocin From *Lactococcus lactis* subsp. *lactis* bv. diacetylactis BGBU1-4. *Appl. Environ. Microbiol.* **2017**, DOI: 10.1128/AEM.01519-17.
108. Criado, R.; Diep, D.B.; Aakra, A.; Gutiérrez, J.; Nes, I.F.; Hernández, P.E.; Cintas, L.M. Complete Sequence of the Enterocin Q-encoding Plasmid pCIZ2 From the Multiple Bacteriocin Producer *Enterococcus faecium* L50 and Genetic Characterization of Enterocin Q Production and Immunity. *Appl. Environ. Microbiol.* **2006**, *72*, 6653–6666.
109. Nascimento, J.S.; Coelho, M.L.; Ceotto, H.; Potter, A.; Fleming, L.R.; Salehian, Z.; Nes, I.F.; Bastos, M.C. Genes Involved in Immunity to and Secretion of Aureocin A53, an Atypical Class II Bacteriocin Produced by *Staphylococcus aureus* A53. *J. Bacteriol.* **2012**, *194*, 875–883.
110. Iwatani, S.; Horikiri, Y.; Zendo, T.; Nakayama, J.; Sonomoto, K. Bifunctional Gene Cluster *lnqBCDEF* Mediates Bacteriocin Production and Immunity With Differential Genetic Requirements. *Appl. Environ. Microbiol.* **2013**, *79*, 2446–2449.
111. Iwatani, S.; Ishibashi, N.; Flores, F.P.; Zendo, T.; Nakayama, J.; Sonomoto, K. LnqR, a Tetr-family Transcriptional Regulator, Positively Regulates Lactacin Q Production in *Lactococcus lactis* QU 5. *FEMS Microbiol. Lett.* **2016**, *363*, fnw200.
112. Lohans, C.T.; Towle, K.M.; Miskolzie, M.; McKay, R.T.; van Belkum, M.J.; McMullen, L.M.; Vederas, J.C. Solution Structures of the Linear Leaderless Bacteriocins Enterocin 7A and 7B Resemble Carnocyclin A, a Circular Antimicrobial Peptide. *Biochemistry.* **2013**, *52*, 3987–3994.
113. Towle, K.M.; Vederas, J.C. Structural Features of Many Circular and Leaderless

- Bacteriocins Are Similar to Those in Saposins and Saposin-like Peptides. *Med. Chem. Commun.* **2017**, *8*, 276–285.
114. Ovchinnikov, K.V.; Kristiansen, P.E.; Straume, D.; Jensen, M.S.; Aleksandrak-Piekarczyk, T.; Nes, I.F.; Diep, D.B. The Leaderless Bacteriocin Enterocin K1 Is Highly Potent Against *Enterococcus faecium*: a Study on Structure, Target, Spectrum, and Receptor. *Front. Microbiol.* **2017**, *8*, 774.
115. Singh, P.K.; Solanki, V.; Sharma, S.; Thakur, K.G.; Krishnan, B.; Korpole, S. The Intramolecular Disulfide-stapled Structure of Laterosporulin, a Class IId Bacteriocin, Conceals a Human Defensin-like Structural Module. *FEBS J.* **2015**, *282*, 203–214.
116. Netz, D.J.; Bastos, M.C.; Sahl, H.G. Mode of Action of the Antimicrobial Peptide Aureocin A53 From *Staphylococcus aureus*. *Appl. Environ. Microbiol.* **2002**, *68*, 5274–5280.
117. Yoneyama, F.; Imura, Y.; Ohno, K.; Zendo, T.; Nakayama, J.; Matsuzaki, K.; Sonomoto, K. Peptide-Lipid Huge Toroidal Pore, a New Antimicrobial Mechanism Mediated by a Lactococcal Bacteriocin, Lacticin Q. *Antimicrob. Agents Chemother.* **2009**, *53*, 3211–3217.
118. Yoneyama, F.; Imura, Y.; Ichimasa, S.; Fujita, K.; Zendo, T.; Nakayama, J.; Matsuzaki, K.; Sonomoto, K. Lacticin Q, a Lactococcal Bacteriocin, Causes High-level Membrane Permeability in the Absence of Specific Receptors. *Appl. Environ. Microbiol.* **2009**, *75*, 538–541.
119. Uzelac, G.; Kojic, M.; Lozo, J.; Aleksandrak-Piekarczyk, T.; Gabrielsen, C.; Kristensen, T.; Nes, I.F.; Diep, D.B.; Topisirovic, L. A Zn-Dependent Metallopeptidase Is Responsible for Sensitivity to LsbB, a Class II Leaderless

- Bacteriocin of *Lactococcus lactis* subsp. *lactis* BGMN1-5. *J. Bacteriol.* **2013**, *195*, 5614–5621.
120. Miljkovic, M.; Uzelac, G.; Mirkovic, N.; Devescovi, G.; Diep, D.B.; Venturi, V.; Kojic, M. LsbB Bacteriocin Interacts With the Third Transmembrane Domain of the YvjB Receptor. *Appl. Environ. Microbiol.* **2016**, *82*, 5364–5374.
121. Nissen-Meyer, J.; Oppegård, C.; Rogne, P.; Haugen, H.S.; Kristiansen, P.E. Structure and Mode-of-action of the Two-peptide (Class-IIb) Bacteriocins. *Probiotics Antimicrob. Proteins.* **2010**, *2*, 52–60.
122. Senes, A.; Engel, D.E.; DeGrado, W.F. Folding of Helical Membrane Proteins: the Role of Polar, GXXXG-like and Proline Motifs. *Curr. Opin. Struct. Biol.* **2004**, *14*, 465–479.
123. Senes, A.; Gerstein, M.; Engelman, D.M. Statistical Analysis of Amino Acid Patterns in Transmembrane Helices: the GXXXG Motif Occurs Frequently and in Association With Beta-branched Residues at Neighboring Positions. *J. Mol. Biol.* **2000**, *296*, 921–936.
124. Nissen-Meyer, J.; Holo, H.; Håvarstein, L.S.; Sletten, K.; Nes, I.F. A Novel Lactococcal Bacteriocin Whose Activity Depends on the Complementary Action of Two Peptides. *J. Bacteriol.* **1992**, *174*, 5686–5692.
125. Blom, H.; Katla, T.; Holck, A.; Sletten, K.; Axelsson, L.; Holo, H. Characterization, Production, and Purification of Leucocin H, a Two-peptide Bacteriocin From *Leuconostoc* MF215B. *Curr. Microbiol.* **1999**, *39*, 43–48.
126. van Belkum, M.J.; Hayema, B.J.; Jeeninga, R.E.; Kok, J.; Venema, G. Organization and Nucleotide Sequences of Two Lactococcal Bacteriocin Operons. *Appl. Environ.*

- Microbiol.* **1991**, *57*, 492–498.
127. Ghrairi, T.; Frère, J.; Berjeaud, J.M.; Manai, M. Lactococcin MMT24, a Novel Two-peptide Bacteriocin Produced by *Lactococcus lactis* Isolated From Rigouta Cheese. *Int. J. Food Microbiol.* **2005**, *105*, 389–398.
128. Fremaux, C.; Ahn, C.; Klaenhammer, T.R. Molecular Analysis of the Lactacin F Operon. *Appl. Environ. Microbiol.* **1993**, *59*, 3906–3915.
129. Jiménez-Díaz, R.; Ruiz-Barba, J.L.; Cathcart, D.P.; Holo, H.; Nes, I.F.; Sletten, K.H.; Warner, P.J. Purification and Partial Amino Acid Sequence of Plantaricin S, a Bacteriocin Produced by *Lactobacillus plantarum* LPCO10, the Activity of which Depends on the Complementary Action of Two Peptides. *Appl. Environ. Microbiol.* **1995**, *61*, 4459–4463.
130. Stephens, S.K.; Floriano, B.; Cathcart, D.P.; Bayley, S.A.; Witt, V.F.; Jiménez-Díaz, R.; Warner, P.J.; Ruiz-Barba, J.L. Molecular Analysis of the Locus Responsible for Production of Plantaricin S, a Two-peptide Bacteriocin Produced by *Lactobacillus plantarum* LPCO10. *Appl. Environ. Microbiol.* **1998**, *64*, 1871–1877.
131. Marciset, O.; Jeronimus-Stratingh, M.C.; Mollet, B.; Poolman, B. Thermophilin 13, a Nontypical Antilisterial Poration Complex Bacteriocin, That Functions Without a Receptor. *J. Biol. Chem.* **1997**, *272*, 14277–14284.
132. McCormick, J.K.; Poon, A.; Sailer, M.; Gao, Y.; Roy, K.L.; McMullen, L.M.; Vederas, J.C.; Stiles, M.E.; van Belkum, M.J. Genetic Characterization and Heterologous Expression of Brochocin-C, an Antibotulinal, Two-peptide Bacteriocin Produced by *Brochothrix campestris* ATCC 43754. *Appl. Environ. Microbiol.* **1998**, *64*, 4757–4766.

133. Anderssen, E.L.; Diep, D.B.; Nes, I.F.; Eijsink, V.G.; Nissen-Meyer, J. Antagonistic Activity of *Lactobacillus plantarum* C11: Two New Two-peptide Bacteriocins, Plantaricins EF and JK, and the Induction Factor Plantaricin A. *Appl. Environ. Microbiol.* **1998**, *64*, 2269–2272.
134. Balla, E.; Dicks, L.M.; Du Toit, M.; van der Merwe, M.J.; Holzapfel, W.H. Characterization and Cloning of the Genes Encoding Enterocin 1071A and Enterocin 1071B, Two Antimicrobial Peptides Produced by *Enterococcus faecalis* BFE 1071. *Appl. Environ. Microbiol.* **2000**, *66*, 1298–1304.
135. Cuozzo, S.A.; Sesma, F.; Palacios, J.M.; de Ruíz Holgado, A.P.; Raya, R.R. Identification and Nucleotide Sequence of Genes Involved in the Synthesis of Lactocin 705, a Two-peptide Bacteriocin From *Lactobacillus casei* CRL 705. *FEMS Microbiol. Lett.* **2000**, *185*, 157–161.
136. Qi, F.; Chen, P.; Caufield, P.W. The Group I Strain of *Streptococcus mutans*, UA140, Produces Both the Lantibiotic Mutacin I and a Nonlantibiotic Bacteriocin, Mutacin IV. *Appl. Environ. Microbiol.* **2001**, *67*, 15–21.
137. Flynn, S.; van Sinderen, D.; Thornton, G.M.; Holo, H.; Nes, I.F.; Collins, J.K. Characterization of the Genetic Locus Responsible for the Production of ABP-118, a Novel Bacteriocin Produced by the Probiotic Bacterium *Lactobacillus salivarius* subsp. *salivarius* UCC118. *Microbiology.* **2002**, *148*, 973–984.
138. Maldonado, A.; Ruiz-Barba, J.L.; Jiménez-Díaz, R. Purification and Genetic Characterization of Plantaricin NC8, a Novel Coculture-inducible Two-peptide Bacteriocin From *Lactobacillus plantarum* NC8. *Appl. Environ. Microbiol.* **2003**, *69*, 383–389.

139. Zendo, T.; Koga, S.; Shigeri, Y.; Nakayama, J.; Sonomoto, K. Lactococcin Q, a Novel Two-peptide Bacteriocin Produced by *Lactococcus lactis* QU 4. *Appl. Environ. Microbiol.* **2006**, *72*, 3383–3389.
140. Barrett, E.; Hayes, M.; O'Connor, P.; Gardiner, G.; Fitzgerald, G.F.; Stanton, C.; Ross, R.P.; Hill, C. Salivaricin P, One of a Family of Two-component Antilisterial Bacteriocins Produced by Intestinal Isolates of *Lactobacillus salivarius*. *Appl. Environ. Microbiol.* **2007**, *73*, 3719–3723.
141. Maldonado-Barragán, A.; Caballero-Guerrero, B.; Jiménez, E.; Jiménez-Díaz, R.; Ruiz-Barba, J.L.; Rodríguez, J.M. Enterocin C, a Class IIb Bacteriocin Produced by *E. faecalis* C901, a Strain Isolated From Human Colostrum. *Int. J. Food Microbiol.* **2009**, *133*, 105–112.
142. Hu, C.B.; Malaphan, W.; Zendo, T.; Nakayama, J.; Sonomoto, K. Enterocin X, a Novel Two-peptide Bacteriocin From *Enterococcus faecium* KU-B5, has an Antibacterial Spectrum Entirely Different From Those of Its Component Peptides. *Appl. Environ. Microbiol.* **2010**, *76*, 4542–4545.
143. O'Shea, E.F.; O'Connor, P.M.; Raftis, E.J.; O'Toole, P.W.; Stanton, C.; Cotter, P.D.; Ross, R.P.; Hill, C. Production of Multiple Bacteriocins From a Single Locus by Gastrointestinal Strains of *Lactobacillus salivarius*. *J. Bacteriol.* **2011**, *193*, 6973–6982.
144. Noda, M.; Miyauchi, R.; Danshiitsoodol, N.; Higashikawa, F.; Kumagai, T.; Matoba, Y.; Sugiyama, M. Characterization and Mutational Analysis of a Two-polypeptide Bacteriocin Produced by Citrus Iyo-derived *Lactobacillus brevis* 174A. *Biol. Pharm. Bull.* **2015**, *38*, 1902–1909.

145. Armstrong, B.D.; Herfst, C.A.; Tonial, N.C.; Wakabayashi, A.T.; Zeppa, J.J.; McCormick, J.K. Identification of a Two-component Class IIb Bacteriocin in *Streptococcus pyogenes* by Recombinase-based *In Vivo* Expression Technology. *Sci. Rep.* **2016**, *6*, 36233.
146. Oppegård, C.; Emanuelsen, L.; Thorbek, L.; Fimland, G.; Nissen-Meyer, J. The Lactococcin G Immunity Protein Recognizes Specific Regions in Both Peptides Constituting the Two-peptide Bacteriocin Lactococcin G. *Appl. Environ. Microbiol.* **2010**, *76*, 1267–1273.
147. Nissen-Meyer, J.; Oppegård, C.; Rogne, P.; Haugen, H.S.; Kristiansen, P.E. The two-peptide (class-IIb) bacteriocins: genetics, biosynthesis, structure, and mode of action. In *Prokaryotic Antimicrobial Peptides: From Genes to Applications*, Drider, D.; Rebuffat, S., Ed.; Springer: New York City, New York, USA, 2011; pp 197-212.
148. van Belkum, M.J.; Worobo, R.W.; Stiles, M.E. Double-glycine-type Leader Peptides Direct Secretion of Bacteriocins by ABC Transporters: Colicin V Secretion in *Lactococcus lactis*. *Mol. Microbiol.* **1997**, *23*, 1293–1301.
149. Håvarstein, L.S.; Diep, D.B.; Nes, I.F. A Family of Bacteriocin ABC Transporters Carry Out Proteolytic Processing of their Substrates Concomitant With Export. *Mol. Microbiol.* **1995**, *16*, 229–240.
150. Ishibashi, N.; Zendo, T.; Koga, S.; Shigeri, Y.; Sonomoto, K. Molecular Characterization of the Genes Involved in the Secretion and Immunity of Lactococcin Q, a Two-peptide Bacteriocin Produced by *Lactococcus lactis* QU 4. *Microbiology.* **2015**, *161*, 2069–2078.
151. Kleerebezem, M.; Quadri, L.E. Peptide Pheromone-dependent Regulation of

- Antimicrobial Peptide Production in Gram-positive Bacteria: a Case of Multicellular Behavior. *Peptides*. **2001**, *22*, 1579–1596.
152. Diep, D.B.; Myhre, R.; Johnsborg, O.; Aakra, A.; Nes, I.F. Inducible Bacteriocin Production in *Lactobacillus* Is Regulated by Differential Expression of the *pln* Operons and by Two Antagonizing Response Regulators, the Activity of Which Is Enhanced Upon Phosphorylation. *Mol. Microbiol.* **2003**, *47*, 483–494.
153. Rogne, P.; Fimland, G.; Nissen-Meyer, J.; Kristiansen, P.E. Three-dimensional Structure of the Two Peptides That Constitute the Two-peptide Bacteriocin Lactococcin G. *Biochim. Biophys. Acta.* **2008**, *1784*, 543–554.
154. Fimland, N.; Rogne, P.; Fimland, G.; Nissen-Meyer, J.; Kristiansen, P.E. Three-dimensional Structure of the Two Peptides That Constitute the Two-peptide Bacteriocin Plantaricin EF. *Biochim. Biophys. Acta.* **2008**, *1784*, 1711–1719.
155. Rogne, P.; Haugen, C.; Fimland, G.; Nissen-Meyer, J.; Kristiansen, P.E. Three-dimensional Structure of the Two-peptide Bacteriocin Plantaricin JK. *Peptides*. **2009**, *30*, 1613–1621.
156. Hauge, H.H.; Nissen-Meyer, J.; Nes, I.F.; VG, E. Amphiphilic  $\alpha$ -Helices Are Important Structural Motifs in the A and B Peptides That Constitute the Bacteriocin Lactococcin G. *FEBS J.* **1998**, *251*, 565–572.
157. Hauge, H.H.; Mantzilas, D.; Eijssink, V.G.; Nissen-Meyer, J. Membrane-mimicking Entities Induce Structuring of the Two-peptide Bacteriocins Plantaricin E/F and Plantaricin J/K. *J. Bacteriol.* **1999**, *181*, 740–747.
158. Senes, A.; Ubarretxena-Belandia, I.; Engelman, D.M. The C $\alpha$ —h $\cdots$  O Hydrogen Bond: a Determinant of Stability and Specificity in Transmembrane Helix

- Interactions. *Proc. Natl. Acad. Sci. USA*. **2001**, *98*, 9056–9061.
159. Oppegård, C.; Schmidt, J.; Kristiansen, P.E.; Nissen-Meyer, J. Mutational Analysis of Putative Helix-Helix Interacting GXXXG-Motifs and Tryptophan Residues in the Two-peptide Bacteriocin Lactococcin G. *Biochemistry*. **2008**, *47*, 5242–5249.
160. Ekblad, B.; Kyriakou, P.K.; Oppegård, C.; Nissen-Meyer, J.; Kaznessis, Y.N.; Kristiansen, P.E. Structure–Function Analysis of the Two-peptide Bacteriocin Plantaricin EF. *Biochemistry*. **2016**, *55*, 5106–5116.
161. Soliman, W.; Wang, L.; Bhattacharjee, S.; Kaur, K. Structure-Activity Relationships of an Antimicrobial Peptide Plantaricin S From Two-peptide Class IIb Bacteriocins. *J. Med. Chem.* **2011**, *54*, 2399–2408.
162. Kyriakou, P.K.; Ekblad, B.; Kristiansen, P.E.; Kaznessis, Y.N. Interactions of a Class IIb Bacteriocin With a Model Lipid Bilayer, Investigated Through Molecular Dynamics Simulations. *Biochim. Biophys. Acta*. **2016**, *1858*, 824–835.
163. Nissen-Meyer, J.; Rogne, P.; Oppegård, C.; Haugen, H.S.; Kristiansen, P.E. Structure-Function Relationships of the Non-lanthionine-containing Peptide (Class II) Bacteriocins Produced by Gram-positive Bacteria. *Curr. Pharm. Biotechnol.* **2009**, *10*, 19–37.
164. Moll, G.; Ubbink-Kok, T.; Hildeng-Hauge, H.; Nissen-Meyer, J.; Nes, I.F.; Konings, W.N.; Driessen, A.J. Lactococcin G Is a Potassium Ion-conducting, Two-component Bacteriocin. *J. Bacteriol.* **1996**, *178*, 600–605.
165. Moll, G.; Hildeng-Hauge, H.; Nissen-Meyer, J.; Nes, I.F.; Konings, W.N.; Driessen, A.J. Mechanistic Properties of the Two-component Bacteriocin Lactococcin G. *J. Bacteriol.* **1998**, *180*, 96–99.

166. Moll, G.N.; van den Akker, E.; Hauge, H.H.; Nissen-Meyer, J.; Nes, I.F.; Konings, W.N.; Driessen, A.J. Complementary and Overlapping Selectivity of the Two-peptide Bacteriocins Plantaricin EF and JK. *J. Bacteriol.* **1999**, *181*, 4848–4852.
167. Zhang, X.; Wang, Y.; Liu, L.; Wei, Y.; Shang, N.; Zhang, X.; Li, P. Two-peptide Bacteriocin PlnEF Causes Cell Membrane Damage to *Lactobacillus plantarum*. *Biochim. Biophys. Acta.* **2016**, *1858*, 274–280.
168. Ekblad, B.; Nissen-Meyer, J.; Kristensen, T. Whole-genome Sequencing of Mutants With Increased Resistance Against the Two-peptide Bacteriocin Plantaricin JK Reveals a Putative Receptor and Potential Docking Site. *PLoS One.* **2017**, *12*, e0185279.
169. Abee, T.; Klaenhammer, T.R.; Letellier, L. Kinetic Studies of the Action of Lactacin F, a Bacteriocin Produced by *Lactobacillus johnsonii* That Forms Poration Complexes in the Cytoplasmic Membrane. *Appl. Environ. Microbiol.* **1994**, *60*, 1006–1013.
170. Castellano, P.; Raya, R.; Vignolo, G. Mode of Action of Lactocin 705, a Two-component Bacteriocin From *Lactobacillus casei* CRL705. *Int. J. Food Microbiol.* **2003**, *85*, 35–43.
171. Cuozzo, S.A.; Castellano, P.; Sesma, F.J.M.; Vignolo, G.M.; Raya, R.R. Differential Roles of the Two-component Peptides of Lactocin 705 in Antimicrobial Activity. *Curr. Microbiol.* **2003**, *46*, 180–183.
172. Cotter, P.D. An ‘Upp’-Turn in Bacteriocin Receptor Identification. *Mol. Microbiol.* **2014**, *92*, 1159–1163.
173. Kjos, M.; Oppegård, C.; Diep, D.B.; Nes, I.F.; Veening, J.W.; Nissen-Meyer, J.;

- Kristensen, T. Sensitivity to the Two-peptide Bacteriocin Lactococcin G Is Dependent on UppP, an Enzyme Involved in Cell-wall Synthesis. *Mol. Microbiol.* **2014**, *92*, 1177–1187.
174. Bickford, J.S.; Nick, H.S. Conservation of the PTEN Catalytic Motif in the Bacterial Undecaprenyl Pyrophosphate Phosphatase, BacA/UppP. *Microbiology*. **2013**, *159*, 2444–2455.
175. Oppegård, C.; Kjos, M.; Veening, J.W.; Nissen-Meyer, J.; Kristensen, T. A Putative Amino Acid Transporter Determines Sensitivity to the Two-peptide Bacteriocin Plantaricin JK. *MicrobiologyOpen*. **2016**, *5*, 700–708.
176. Knerr, P.J.; van der Donk, W.A. Discovery, Biosynthesis, and Engineering of Lantipeptides. *Annu. Rev. Biochem.* **2012**, *81*, 479–505.
177. Repka, L.M.; Chekan, J.R.; Nair, S.K.; van der Donk, W.A. Mechanistic Understanding of Lanthipeptide Biosynthetic Enzymes. *Chem. Rev.* **2017**, *117*, 5457–5520.
178. Doroghazi, J.R.; Albright, J.C.; Goering, A.W.; Ju, K.S.; Haines, R.R.; Tchalukov, K.A.; Labeda, D.P.; Kelleher, N.L.; Metcalf, W.W. A Roadmap for Natural Product Discovery Based on Large-scale Genomics and Metabolomics. *Nat. Chem. Biol.* **2014**, *10*, 963–968.
179. Cimermancic, P.; Medema, M.H.; Claesen, J.; Kurita, K.; Wieland Brown, L.C.; Mavrommatis, K.; Pati, A.; Godfrey, P.A.; Koehrsen, M.; Clardy, J.; Birren, B.W.; Takano, E.; Sali, A.; Linington, R.G.; Fischbach, M.A. Insights into Secondary Metabolism From a Global Analysis of Prokaryotic Biosynthetic Gene Clusters. *Cell*. **2014**, *158*, 412–421.

180. Walsh, C.J.; Guinane, C.M.; Hill, C.; Ross, R.P.; O'Toole, P.W.; Cotter, P.D. *In Silico* Identification of Bacteriocin Gene Clusters in the Gastrointestinal Tract, Based on the Human Microbiome Project's Reference Genome Database. *BMC Microbiol.* **2015**, *15*, 183.
181. Skinnider, M.A.; Johnston, C.W.; Edgar, R.E.; Dejong, C.A.; Merwin, N.J.; Rees, P.N.; Magarvey, N.A. Genomic Charting of Ribosomally Synthesized Natural Product Chemical Space Facilitates Targeted Mining. *Proc. Natl. Acad. Sci. USA.* **2016**, *113*, E6343–E6351.
182. Zhang, Q.; Doroghazi, J.R.; Zhao, X.; Walker, M.C.; van der Donk, W.A. Expanded Natural Product Diversity Revealed by Analysis of Lanthipeptide-like Gene Clusters in Actinobacteria. *Appl. Environ. Microbiol.* **2015**, *81*, 4339–4350.
183. Marsh, A.J.; O'Sullivan, O.; Ross, R.P.; Cotter, P.D.; Hill, C. *In Silico* Analysis Highlights the Frequency and Diversity of Type 1 Lantibiotic Gene Clusters in Genome Sequenced Bacteria. *BMC Genomics.* **2010**, *11*, 679.
184. Férir, G.; Petrova, M.I.; Andrei, G.; Huskens, D.; Hoorelbeke, B.; Snoeck, R.; Vanderleyden, J.; Balzarini, J.; Bartoschek, S.; Brönstrup, M.; Süssmuth, R.D.; Schols, D. The Lantibiotic Peptide Labyrinthopeptin A1 Demonstrates Broad Anti-HIV and Anti-HSV Activity With Potential for Microbicidal Applications. *PLoS One.* **2013**, *8*, e64010.
185. Mohr, K.I.; Volz, C.; Jansen, R.; Wray, V.; Hoffmann, J.; Bernecker, S.; Wink, J.; Gerth, K.; Stadler, M.; Müller, R. Pinensins: The First Antifungal Lantibiotics. *Angew. Chem. Int. Ed. Engl.* **2015**, *54*, 11254–11258.
186. Iorio, M.; Sasso, O.; Maffioli, S.I.; Bertorelli, R.; Monciardini, P.; Sosio, M.;

- Bonezzi, F.; Summa, M.; Brunati, C.; Bordoni, R.; Corti, G.; Tarozzo, G.; Piomelli, D.; Reggiani, A.; Donadio, S. A Glycosylated, Labionin-containing Lanthipeptide With Marked Antinociceptive Activity. *ACS Chem. Biol.* **2014**, *9*, 398–404.
187. Kodani, S.; Hudson, M.E.; Durrant, M.C.; Buttner, M.J.; Nodwell, J.R.; Willey, J.M. The SapB Morphogen Is a Lantibiotic-like Peptide Derived From the Product of the Developmental Gene *ramS* in *Streptomyces coelicolor*. *Proc. Natl. Acad. Sci. USA.* **2004**, *101*, 11448–11453.
188. Kodani, S.; Lodato, M.A.; Durrant, M.C.; Picart, F.; Willey, J.M. Sapt, a Lanthionine-containing Peptide Involved in Aerial Hyphae Formation in the Streptomycetes. *Mol. Microbiol.* **2005**, *58*, 1368–1380.
189. Meindl, K.; Schmiederer, T.; Schneider, K.; Reicke, A.; Butz, D.; Keller, S.; Gühring, H.; Vértesy, L.; Wink, J.; Hoffmann, H.; Brönstrup, M.; Sheldrick, G.M.; Süssmuth, R.D. Labyrinthopeptins: a New Class of Carbacyclic Lantibiotics. *Angew. Chem. Int. Ed. Engl.* **2010**, *49*, 1151–1154.
190. Tang, W.; van der Donk, W.A. The Sequence of the Enterococcal Cytolysin Imparts Unusual Lanthionine Stereochemistry. *Nat. Chem. Biol.* **2013**, *9*, 157–159.
191. Lohans, C.T.; Li, J.L.; Vederas, J.C. Structure and Biosynthesis of Carnolysin, a Homologue of Enterococcal Cytolysin With D-Amino Acids. *J. Am. Chem. Soc.* **2014**, *136*, 13150–13153.
192. Allgaier, H.; Jung, G.; Werner, R.G.; Schneider, U.; Zähler, H. Elucidation of the Structure of Epidermin, a Ribosomally Synthesized, Tetracyclic Heterodetic Polypeptide Antibiotic. *Angew. Chem. Int. Ed. Engl.* **1985**, *24*, 1051–1053.
193. Skaugen, M.; Nissen-Meyer, J.; Jung, G.; StevanoVic, S.; Sletten, K.; Inger, C.;

- Abildgaard, M.; Nes, I.F. *In Vivo* Conversion of L-Serine to D-Alanine in a Ribosomally Synthesized Polypeptide. *J. Biol. Chem.* **1994**, *269*, 27183–27185.
194. Cotter, P.D.; O'Connor, P.M.; Draper, L.A.; Lawton, E.M.; Deegan, L.H.; Hill, C.; Ross, R.P. Posttranslational Conversion of L-Serines to D-Alanines Is Vital for Optimal Production and Activity of the Lantibiotic Lacticin 3147. *Proc. Natl. Acad. Sci. USA.* **2005**, *102*, 18584–18589.
195. Suda, S.; Cotter, P.D.; Hill, C.; Ross, R.P. Lacticin 3147 - Biosynthesis, Molecular Analysis, Immunity, Bioengineering, and Applications. *Curr. Protein Pept. Sci.* **2012**, *13*, 193–204.
196. Huo, L.; van der Donk, W.A. Discovery and Characterization of Bicerucin, an Unusual D-Amino Acid-Containing Mixed Two-component Lantibiotic. *J. Am. Chem. Soc.* **2016**, *138*, 5254–5257.
197. Kupke, T.; Stevanović, S.; Sahl, H.G.; Götz, F. Purification and Characterization of EpiD, a Flavoprotein Involved in the Biosynthesis of the Lantibiotic Epidermin. *J. Bacteriol.* **1992**, *174*, 5354–5361.
198. Kupke, T.; Uebele, M.; Schmid, D.; Jung, G.; Blaesse, M.; Steinbacher, S. Molecular Characterization of Lantibiotic-synthesizing Enzyme EpiD Reveals a Function for Bacterial Dfp Proteins in Coenzyme A Biosynthesis. *J. Biol. Chem.* **2000**, *275*, 31838–31846.
199. Blaesse, M.; Kupke, T.; Huber, R.; Steinbacher, S. Crystal Structure of the Peptidyl-Cysteine Decarboxylase EpiD Complexed With a Pentapeptide Substrate. *EMBO J.* **2000**, *19*, 6299–6310.
200. Goto, Y.; Okesli, A.; van der Donk, W.A. Mechanistic Studies of Ser/Thr

- Dehydration Catalyzed by a Member of the LanL Lanthionine Synthetase Family. *Biochemistry*. **2011**, *50*, 891–898.
201. Goto, Y.; Li, B.; Claesen, J.; Shi, Y.; Bibb, M.J.; van der Donk, W.A. Discovery of Unique Lanthionine Synthetases Reveals New Mechanistic and Evolutionary Insights. *PLoS Biol.* **2010**, *8*, e1000339.
202. Garg, N.; Salazar-Ocampo, L.M.; van der Donk, W.A. *In Vitro* Activity of the Nisin Dehydratase NisB. *Proc. Natl. Acad. Sci. USA*. **2013**, *110*, 7258–7263.
203. Ortega, M.A.; Hao, Y.; Zhang, Q.; Walker, M.C.; van der Donk, W.A.; Nair, S.K. Structure and Mechanism of the tRNA-dependent Lantibiotic Dehydratase NisB. *Nature*. **2015**, *517*, 509–512.
204. Yang, X.; van der Donk, W.A. Michael-type Cyclizations in Lantibiotic Biosynthesis Are Reversible. *ACS Chem. Biol.* **2015**, *10*, 1234–1238.
205. Xie, L.; Miller, L.M.; Chatterjee, C.; Averin, O.; Kelleher, N.L.; van der Donk, W.A. Lacticin 481: *In Vitro* Reconstitution of Lantibiotic Synthetase Activity. *Science*. **2004**, *303*, 679–681.
206. Chatterjee, C.; Miller, L.M.; Leung, Y.L.; Xie, L.; Yi, M.; Kelleher, N.L.; van der Donk, W.A. Lacticin 481 Synthetase Phosphorylates Its Substrate During Lantibiotic Production. *J. Am. Chem. Soc.* **2005**, *127*, 15332–15333.
207. Dougherty, B.A.; Hill, C.; Weidman, J.F.; Richardson, D.R.; Venter, J.C.; Ross, R.P. Sequence and Analysis of the 60 kb Conjugative, Bacteriocin-producing Plasmid pMRC01 From *Lactococcus lactis* DPC3147. *Mol. Microbiol.* **1998**, *29*, 1029–1038.
208. Gilmore, M.S.; Segarra, R.A.; Booth, M.C.; Bogie, C.P.; Hall, L.R.; Clewell, D.B. Genetic Structure of the *Enterococcus faecalis* Plasmid pAD1-encoded Cytolytic

- Toxin System and Its Relationship to Lantibiotic Determinants. *J. Bacteriol.* **1994**, *176*, 7335–7344.
209. Müller, W.M.; Schmiederer, T.; Ensle, P.; Süssmuth, R.D. *In Vitro* Biosynthesis of the Prepeptide of Type-III Lantibiotic Labyrinthopeptin A2 Including Formation of a C-C Bond as a Post-translational Modification. *Angew. Chem. Int. Ed. Engl.* **2010**, *49*, 2436–2440.
210. Krawczyk, B.; Völler, G.H.; Völler, J.; Ensle, P.; Süssmuth, R.D. Curvopeptin: a New Lanthionine-Containing Class III Lantibiotic and Its Co-substrate Promiscuous Synthetase. *Chembiochem.* **2012**, *13*, 2065–2071.
211. van der Meer, J.R.; Polman, J.; Beerthuyzen, M.M.; Siezen, R.J.; Kuipers, O.P.; de Vos, W.M. Characterization of the *Lactococcus lactis* Nisin A Operon Genes *nisP*, Encoding a Subtilisin-like Serine Protease Involved in Precursor Processing, and *nisR*, Encoding a Regulatory Protein Involved in Nisin Biosynthesis. *J. Bacteriol.* **1993**, *175*, 2578–2588.
212. Corvey, C.; Stein, T.; Düsterhus, S.; Karas, M.; Entian, K.D. Activation of Subtilin Precursors by *Bacillus subtilis* Extracellular Serine Proteases Subtilisin (AprE), WprA, and Vpr. *Biochem. Biophys. Res. Commun.* **2003**, *304*, 48–54.
213. Koponen, O.; Takala, T.M.; Saarela, U.; Qiao, M.; Saris, P.E. Distribution of the NisI Immunity Protein and Enhancement of Nisin Activity by the Lipid-free NisI. *FEMS Microbiol. Lett.* **2004**, *231*, 85–90.
214. Immonen, T.; Saris, P.E. Characterization of the *nisFEG* Operon of the Nisin Z Producing *Lactococcus lactis* subsp. *lactis* N8 Strain. *DNA Seq.* **1998**, *9*, 263–274.
215. Hsu, S.T.; Breukink, E.; Tischenko, E.; Lutters, M.A.; de Kruijff, B.; Kaptein, R.;

- Bonvin, A.M.; van Nuland, N.A. The Nisin-Lipid II Complex Reveals a Pyrophosphate Cage That Provides a Blueprint for Novel Antibiotics. *Nat. Struct. Mol. Biol.* **2004**, *11*, 963–967.
216. Breukink, E.; Wiedemann, I.; van Kraaij, C.; Kuipers, O.P.; Sahl, H.G.; de Kruijff, B. Use of the Cell Wall Precursor Lipid II by a Pore-forming Peptide Antibiotic. *Science*. **1999**, *286*, 2361–2364.
217. Hasper, H.E.; de Kruijff, B.; Breukink, E. Assembly and Stability of Nisin-Lipid II Pores. *Biochemistry*. **2004**, *43*, 11567–11575.
218. Brötz, H.; Bierbaum, G.; Markus, A.; Molitor, E.; Sahl, H.G. Mode of Action of the Lantibiotic Mersacidin: Inhibition of Peptidoglycan Biosynthesis Via a Novel Mechanism. *Antimicrob. Agents Chemother.* **1995**, *39*, 714–719.
219. Brötz, H.; Bierbaum, G.; Reynolds, P.E.; Sahl, H.G. The Lantibiotic Mersacidin Inhibits Peptidoglycan Biosynthesis at the Level of Transglycosylation. *FEBS J.* **1997**, *246*, 193–199.
220. Brötz, H.; Bierbaum, G.; Leopold, K.; Reynolds, P.E.; Sahl, H.G. The Lantibiotic Mersacidin Inhibits Peptidoglycan Synthesis by Targeting Lipid II. *Antimicrob. Agents Chemother.* **1998**, *42*, 154–160.
221. Wiedemann, I.; Böttiger, T.; Bonelli, R.R.; Wiese, A.; Hagge, S.O.; Gutschmann, T.; Seydel, U.; Deegan, L.; Hill, C.; Ross, P.; Sahl, H.G. The Mode of Action of the Lantibiotic Lacticin 3147 - a Complex Mechanism Involving Specific Interaction of Two Peptides and the Cell Wall Precursor Lipid II. *Mol. Microbiol.* **2006**, *61*, 285–296.
222. Oman, T.J.; van der Donk, W.A. Insights into the Mode of Action of the Two-

- peptide Lantibiotic Haloduracin. *ACS Chem. Biol.* **2009**, *4*, 865–874.
223. Wiedemann, I.; Böttiger, T.; Bonelli, R.R.; Schneider, T.; Sahl, H.G.; Martínez, B. Lipid II-based Antimicrobial Activity of the Lantibiotic Plantaricin C. *Appl. Environ. Microbiol.* **2006**, *72*, 2809–2814.
224. Arthur, T.D.; Cavera, V.L.; Chikindas, M.L. On Bacteriocin Delivery Systems and Potential Applications. *Future Microbiol.* **2014**, *9*, 235–248.
225. Acedo, J.Z.; van Belkum, M.J.; Lohans, C.T.; Towle, K.M.; Miskolzie, M.; Vederas, J.C. Nuclear Magnetic Resonance Solution Structures of Lacticin Q and Aureocin A53 Reveal a Structural Motif Conserved Among Leaderless Bacteriocins With Broad-Spectrum Activity. *Biochemistry.* **2016**, *55*, 733–742.
226. Acedo, J.Z.; Towle, K.M.; Lohans, C.T.; Miskolzie, M.; McKay, R.T.; Doerksen, T.A.; Vederas, J.C.; Martin-Visscher, L.A. Identification and Three-dimensional Structure of Carnobacteriocin XY, a Class IIb Bacteriocin Produced by Carnobacteria. *FEBS Lett.* **2017**, *591*, 1349–1359.
227. Leer, R.J.; van der Vossen, J.M.; van Giezen, M.; van Noort, J.M.; Pouwels, P.H. Genetic Analysis of Acidocin B, a Novel Bacteriocin Produced by *Lactobacillus acidophilus*. *Microbiology.* **1995**, *141*, 1629–1635.
228. van der Vossen, J.M.; van Herwijnen, M.H.M.; Leer, R.J.; ten Brink, B.; Pouwels, P.H.; Huis in't Veld, J.H.J. Production of Acidocin B, a Bacteriocin of *Lactobacillus acidophilus* M46 Is a Plasmid-encoded Trait: Plasmid Curing, Genetic Marking by *In Vivo* Plasmid Integration, and Gene Transfer. *FEMS Microbiol. Lett.* **1994**, *116*, 333–340.
229. ten Brink, B.; Minekus, M.; van der Vossen, J.M.; Leer, R.J.; Huis in't Veld, J.H.

- Antimicrobial Activity of Lactobacilli: Preliminary Characterization and Optimization of Production of Acidocin B, a Novel Bacteriocin Produced by *Lactobacillus acidophilus* M46. *J. Appl. Bacteriol.* **1994**, *77*, 140–148.
230. Strandberg, E.; Ulrich, A.S. NMR Methods for Studying Membrane-active Antimicrobial Peptides. *Concepts. Magn. Reson.* **2004**, *23*, 89–120.
231. Wutzke, K.D.; Oetjens, I. <sup>13</sup>C- and <sup>15</sup>N-Incorporation of Doubly Stable Isotope Labelled *Lactobacillus johnsonii* in Humans. *Eur. J. Clin. Nutr.* **2005**, *59*, 1167–1172.
232. Delaglio, F.; Grzesiek, S.; Vuister, G.W.; Zhu, G.; Pfeifer, J.; Bax, A. NMRPipe: a Multidimensional Spectral Processing System Based on Unix Pipes. *J. Biomol. NMR.* **1995**, *6*, 277–293.
233. Johnson, B.A. Using NMRView to Visualize and Analyze the NMR Spectra of Macromolecules. *Methods Mol. Biol.* **2004**, *278*, 313–352.
234. Guntert, P.; Mumenthaler, C.; Wuthrich, K. Torsion Angle Dynamics for NMR Structure Calculation With the New Program DYANA. *J. Mol. Biol.* **1997**, *273*, 283–298.
235. DeLano, W.L. The PyMol Molecular Graphics System. *DeLano Scientific*. San Carlos, CA, USA. 2002.
236. Maqueda, M.; Gálvez, A.; Bueno, M.M.; Sánchez-Barrena, M.J.; González, C.; Albert, A.; Rico, M.; Valdivia, E. Peptide AS-48: Prototype of a New Class of Cyclic Bacteriocins. *Curr. Protein Pept. Sci.* **2004**, *5*, 399–416.
237. Bandyopadhyay, S.; Junjie, R.L.; Lim, B.; Sanjeev, R.; Xin, W.Y.; Yee, C.K.; Hui Melodies, S.M.; Yow, N.; Sivaraman, J.; Chatterjee, C. Solution Structures and

- Model Membrane Interactions of Ctriporin, an Anti-methicillin-resistant *Staphylococcus aureus* Peptide From Scorpion Venom. *Biopolymers*. **2014**, *101*, 1143–1153.
238. Bandyopadhyay, S.; Ng, B.Y.; Chong, C.; Lim, M.Z.; Gill, S.K.; Lee, K.H.; Sivaraman, J.; Chatterjee, C. Micelle Bound Structure and DNA Interaction of Brevinin-2-related Peptide, an Antimicrobial Peptide Derived From Frog Skin. *J. Pept. Sci.* **2014**, *20*, 811–821.
239. Barbosa, S.C.; Cilli, E.M.; Dias, L.G.; Fuzo, C.A.; Degève, L.; Stabeli, R.G.; Itri, R.; Ciancaglini, P.; Barber, J.D.; Barton, G.J. Interaction of Cyclic and Linear Labaditin Peptides With Anionic and Zwitterionic Micelles. *J. Colloid. Interface. Sci.* **2014**, *438*, 39–46.
240. Larkin, M.; Blackshields, G.; Brown, N.P.; Chenna, R.; McGettigan, P.A.; McWilliam, H.; Valentin, F.; Wallace, I.M.; Wilm, A.; Lopez, R. Clustal W and Clustal X Version 2.0. *Bioinformatics*. **2007**, *23*, 2947–2948.
241. Arakawa, K.; Kawai, Y.; Ito, Y.; Nakamura, K.; Chujo, T.; Nishimura, J.; Kitazawa, H.; Saito, T. HPLC Purification and Re-evaluation of Chemical Identity of Two Circular Bacteriocins, Gassericin A and Reutericin 6. *Lett. Appl. Microbiol.* **2010**, *50*, 406–411.
242. Arnold, K.; Bordoli, L.; Kopp, J.; Schwede, T. The SWISS-Model Workspace: a Web-based Environment for Protein Structure Homology Modelling. *Bioinformatics*. **2006**, *22*, 195–201.
243. Ito, Y.; Kawai, Y.; Arakawa, K.; Honme, Y.; Sasaki, T.; Saito, T. Conjugative Plasmid From *Lactobacillus gasseri* LA39 That Carries Genes for Production of and

- Immunity to the Circular Bacteriocin Gassericin A. *Appl. Environ. Microbiol.* **2009**, 75, 6340–6351.
244. Hirokawa, T.; Boon-Chieng, S.; Mitaku, S. Sosui: Classification and Secondary Structure Prediction System for Membrane Proteins. *Bioinformatics.* **1998**, 14, 378–379.
245. Altschul, S.F.; Gish, W.; Miller, W.; Myers, E.W.; Lipman, D.J. Basic Local Alignment Search Tool. *J. Mol. Biol.* **1990**, 215, 403–410.
246. Walker, J.M. *The Proteomics Protocols Handbook*. Springer: New York City, New York, USA, 2005; pp 607.
247. Jones, D.T.; Taylor, W.R.; Thornton, J.M. The Rapid Generation of Mutation Data Matrices From Protein Sequences. *Comput. Appl. Biosci.* **1992**, 8, 275–282.
248. Tamura, K.; Stecher, G.; Peterson, D.; Filipski, A.; Kumar, S. MEGA6: Molecular Evolutionary Genetics Analysis Version 6.0. *Mol. Biol. Evol.* **2013**, 30, 2725–2729.
249. Yoneyama, F.; Shioya, K.; Zendo, T.; Nakayama, J.; Sonomoto, K. Effect of a Negatively Charged Lipid on Membrane-Lacticin Q Interaction and Resulting Pore Formation. *Biosci. Biotechnol. Biochem.* **2010**, 74, 218–221.
250. Li, M.; Yoneyama, F.; Toshimitsu, N.; Zendo, T.; Nakayama, J.; Sonomoto, K. Lethal Hydroxyl Radical Accumulation by a Lactococcal Bacteriocin, Lacticin Q. *Antimicrob. Agents Chemother.* **2013**, 57, 3897–3902.
251. Fregeau Gallagher, N.L.; Sailer, M.; Niemczura, W.P.; Nakashima, T.T.; Stiles, M.E.; Vederas, J.C. Three-dimensional Structure of Leucocin A in Trifluoroethanol and Dodecylphosphocholine Micelles: Spatial Location of Residues Critical for Biological Activity in Type IIa Bacteriocins From Lactic Acid Bacteria.

- Biochemistry*. **1997**, *36*, 15062–15072.
252. Fleury, Y.; Dayem, M.A.; Montagne, J.J.; Chaboisseau, E.; Le Caer, J.P.; Nicolas, P.; Delfour, A. Covalent Structure, Synthesis, and Structure-Function Studies of Mesentericin Y 105(37), a Defensive Peptide From Gram-positive Bacteria *Leuconostoc mesenteroides*. *J. Biol. Chem.* **1996**, *271*, 14421–14429.
253. Kourie, J.I.; Shorthouse, A.A. Properties of Cytotoxic Peptide-formed Ion Channels. *Am. J. Physiol. Cell Physiol.* **2000**, *278*, C1063–87.
254. Drozdetskiy, A.; Cole, C.; Procter, J.; Barton, G.J. JPred4: a Protein Secondary Structure Prediction Server. *Nucleic Acids Res.* **2015**, *43*, W389–94.
255. Towle, K.M.; Lohans, C.T.; Miskolzie, M.; Acedo, J.Z.; van Belkum, M.J.; Vederas, J.C. Solution Structures of Phenol-soluble Modulins A1, A3, and B2, Virulence Factors From *Staphylococcus aureus*. *Biochemistry*. **2016**, *55*, 4798–4806.
256. Worobo, R.W.; van Belkum, M.J.; Sailer, M.; Roy, K.L.; Vederas, J.C.; Stiles, M.E. A Signal Peptide Secretion-dependent Bacteriocin From *Carnobacterium divergens*. *J. Bacteriol.* **1995**, *177*, 3143–3149.
257. Gursky, L.J.; Martin, N.I.; Derksen, D.J.; van Belkum, M.J.; Kaur, K.; Vederas, J.C.; Stiles, M.E.; McMullen, L.M. Production of Piscicolin 126 by *Carnobacterium maltaromaticum* UAL26 Is Controlled by Temperature and Induction Peptide Concentration. *Arch. Microbiol.* **2006**, *186*, 317–325.
258. Franz, C.M.A.P.; Worobo, R.W.; Quadri, L.E.; Schillinger, U.; Holzapfel, W.H.; Vederas, J.C.; Stiles, M.E. Atypical Genetic Locus Associated With Constitutive Production of Enterocin B by *Enterococcus faecium* BFE 900. *Appl. Environ. Microbiol.* **1999**, *65*, 2170–2178.

259. Quadri, L.E.; Kleerebezem, M.; Kuipers, O.P.; de Vos, W.M.; Roy, K.L.; Vederas, J.C.; Stiles, M.E. Characterization of a Locus From *Carnobacterium piscicola* LV17B Involved in Bacteriocin Production and Immunity: Evidence for Global Inducer-mediated Transcriptional Regulation. *J. Bacteriol.* **1997**, *179*, 6163–6171.
260. Tulini, F.L.; Lohans, C.T.; Bordon, K.C.; Zheng, J.; Arantes, E.C.; Vederas, J.C.; De Martinis, E.C. Purification and Characterization of Antimicrobial Peptides From Fish Isolate *Carnobacterium maltaromaticum* C2: Carnobacteriocin X and Carnolysins A1 and A2. *Int. J. Food Microbiol.* **2014**, *173*, 81–88.
261. Oppegård, C.; Rogne, P.; Emanuelsen, L.; Kristiansen, P.E.; Fimland, G.; Nissen-Meyer, J. The Two-peptide Class II Bacteriocins: Structure, Production, and Mode of Action. *J. Mol. Microbiol. Biotechnol.* **2007**, *13*, 210–219.
262. Cornilescu, G.; Delaglio, F.; Bax, A. Protein Backbone Angle Restraints From Searching a Database for Chemical Shift and Sequence Homology. *J. Biomol. NMR.* **1999**, *13*, 289–302.
263. Russ, W.P.; Engelman, D.M. The GXXXG Motif: a Framework for Transmembrane Helix-Helix Association. *J. Mol. Biol.* **2000**, *296*, 911–919.
264. Iwatani, S.; Zendo, T.; Sonomoto, K. Class II d or linear and non-pediocin-like bacteriocins. In *Prokaryotic Antimicrobial Peptides: From Genes to Applications*, Drider, D.; Rebuffat, S., Ed.; Springer: New York City, New York, USA, 2011; pp 237-252.
265. Freeman, M.F.; Gurgui, C.; Helf, M.J.; Morinaka, B.I.; Uria, A.R.; Oldham, N.J.; Sahl, H.G.; Matsunaga, S.; Piel, J. Metagenome Mining Reveals Polytheonamides as Posttranslationally Modified Ribosomal Peptides. *Science.* **2012**, *338*, 387–390.

266. Kreil, G. D-Amino Acids in Animal Peptides. *Annu. Rev. Biochem.* **1997**, *66*, 337–345.
267. Kreil, G. Peptides Containing a D-Amino Acid From Frogs and Molluscs. *J. Biol. Chem.* **1994**, *269*, 10967–10970.
268. Heck, S.D.; Siok, C.J.; Krapcho, K.J.; Kelbaugh, P.R.; Thadeio, P.F.; Welch, M.J.; Williams, R.D.; Ganong, A.H.; Kelly, M.E.; Lanzetti, A.J. Functional Consequences of Posttranslational Isomerization of Ser46 in a Calcium Channel Toxin. *Science*. **1994**, *266*, 1065–1068.
269. Jilek, A.; Mollay, C.; Tippelt, C.; Grassi, J.; Mignogna, G.; Müllegger, J.; Sander, V.; Fehrer, C.; Barra, D.; Kreil, G. Biosynthesis of a D-Amino Acid in Peptide Linkage by an Enzyme From Frog Skin Secretions. *Proc. Natl. Acad. Sci. USA*. **2005**, *102*, 4235–4239.
270. Shikata, Y.; Watanabe, T.; Teramoto, T.; Inoue, A.; Kawakami, Y.; Nishizawa, Y.; Katayama, K.; Kuwada, M. Isolation and Characterization of a Peptide Isomerase From Funnel Web Spider Venom. *J. Biol. Chem.* **1995**, *270*, 16719–16723.
271. Rink, R.; Arkema-Meter, A.; Baudoin, I.; Post, E.; Kuipers, A.; Nelemans, S.A.; Akanbi, M.H.; Moll, G.N. To Protect Peptide Pharmaceuticals Against Peptidases. *J. Pharmacol. Toxicol. Methods*. **2010**, *61*, 210–218.
272. Jungheim, L.N.; Shepherd, T.A.; Baxter, A.J.; Burgess, J.; Hatch, S.D.; Lubbehusen, P.; Wiskerchen, M.; Muesing, M.A. Potent Human Immunodeficiency Virus Type 1 Protease Inhibitors That Utilize Noncoded D-Amino Acids as P2/P3 Ligands. *J. Med. Chem.* **1996**, *39*, 96–108.
273. Tugyi, R.; Uray, K.; Iván, D.; Fellingner, E.; Perkins, A.; Hudecz, F. Partial D-Amino

- Acid Substitution: Improved Enzymatic Stability and Preserved Ab Recognition of a MUC2 Epitope Peptide. *Proc. Natl. Acad. Sci. USA*. **2005**, *102*, 413–418.
274. Chatterjee, S.; Gu, Z.Q.; Dunn, D.; Tao, M.; Josef, K.; Tripathy, R.; Bihovsky, R.; Senadhi, S.E.; O’Kane, T.M.; McKenna, B.A.; Mallya, S.; Ator, M.A.; Bozyczko-Coyne, D.; Siman, R.; Mallamo, J.P. D-Amino Acid Containing, High-affinity Inhibitors of Recombinant Human Calpain I. *J. Med. Chem.* **1998**, *41*, 2663–2666.
275. Heck, S.D.; Faraci, W.S.; Kelbaugh, P.R.; Saccomano, N.A.; Thadeio, P.F.; Volkmann, R.A. Posttranslational Amino Acid Epimerization: Enzyme-catalyzed Isomerization of Amino Acid Residues in Peptide Chains. *Proc. Natl. Acad. Sci. USA*. **1996**, *93*, 4036–4039.
276. Morinaka, B.I.; Vagstad, A.L.; Helf, M.J.; Gugger, M.; Kegler, C.; Freeman, M.F.; Bode, H.B.; Piel, J. Radical S-Adenosyl Methionine Epimerases: Regioselective Introduction of Diverse D-Amino Acid Patterns into Peptide Natural Products. *Angew. Chem. Int. Ed. Engl.* **2014**, *53*, 8503–8507.
277. Yang, X.; van der Donk, W.A. Post-translational Introduction of D-Alanine into Ribosomally Synthesized Peptides by the Dehydroalanine Reductase NpnJ. *J. Am. Chem. Soc.* **2015**, *137*, 12426–12429.
278. Navaratna, M.A.; Sahl, H.G.; Tagg, J.R. Two-component Anti-*Staphylococcus aureus* Lantibiotic Activity Produced by *Staphylococcus aureus* C55. *Appl. Environ. Microbiol.* **1998**, *64*, 4803–4808.
279. Giacomini, A.; Squartini, A.; Nuti, M.P. Nucleotide Sequence and Analysis of Plasmid pMD136 From *Pediococcus pentosaceus* FBB61 (ATCC43200) Involved in Pediocin A Production. *Plasmid*. **2000**, *43*, 111–122.

280. Suda, S.; Lawton, E.M.; Wistuba, D.; Cotter, P.D.; Hill, C.; Ross, R.P. Homologues and Bioengineered Derivatives of LtnJ Vary in Ability to Form D-Alanine in the Lantibiotic Lactacin 3147. *J. Bacteriol.* **2012**, *194*, 708–714.
281. van Heel, A.J.; Mu, D.; Montalbán-López, M.; Hendriks, D.; Kuipers, O.P. Designing and Producing Modified, New-to-nature Peptides With Antimicrobial Activity by Use of a Combination of Various Lantibiotic Modification Enzymes. *ACS Synth. Biol.* **2013**, *2*, 397–404.
282. Mu, D.; Montalbán-López, M.; Deng, J.; Kuipers, O.P. Lantibiotic Reductase LtnJ Substrate Selectivity Assessed With a Collection of Nisin Derivatives as Substrates. *Appl. Environ. Microbiol.* **2015**, *81*, 3679–3687.
283. Majchrzykiewicz, J.A.; Lubelski, J.; Moll, G.N.; Kuipers, A.; Bijlsma, J.J.; Kuipers, O.P.; Rink, R. Production of a Class II Two-component Lantibiotic of *Streptococcus pneumoniae* Using the Class I Nisin Synthetic Machinery and Leader Sequence. *Antimicrob. Agents Chemother.* **2010**, *54*, 1498–1505.
284. Forouhar, F.; Kuzin, A.; Seetharaman, J.; Lee, I.; Zhou, W.; Abashidze, M.; Chen, Y.; Yong, W.; Janjua, H.; Fang, Y.; Wang, D.; Cunningham, K.; Xiao, R.; Acton, T.B.; Pichersky, E.; Klessig, D.F.; Porter, C.W.; Montelione, G.T.; Tong, L. Functional Insights From Structural Genomics. *J. Struct. Funct. Genomics.* **2007**, *8*, 37–44.
285. Sambrook, J.; Russell, D.W. Directional Cloning into Plasmid Vectors. *CSH Protoc.* **2006**, *2006*, pdb.prot3919.
286. Oman, T.J.; Knerr, P.J.; Bindman, N.A.; Velásquez, J.E.; van der Donk, W.A. An Engineered Lantibiotic Synthetase That Does Not Require a Leader Peptide on Its

- Substrate. *J. Am. Chem. Soc.* **2012**, *134*, 6952–6955.
287. McClerren, A.L.; Cooper, L.E.; Quan, C.; Thomas, P.M.; Kelleher, N.L.; van der Donk, W.A. Discovery and *In Vitro* Biosynthesis of Haloduracin, a Two-component Lantibiotic. *Proc. Natl. Acad. Sci. USA.* **2006**, *103*, 17243–17248.
288. Bell, M.R.; Engleka, M.J.; Malik, A.; Strickler, J.E. To Fuse or Not to Fuse: What Is Your Purpose. *Protein Sci.* **2013**, *22*, 1466–1477.
289. Gasteiger, E.; Hoogland, C.; Gattiker, A.; Duvaud, S.; Wilkins, M.R.; Appel, R.D.; Bairoch, A. Protein identification and analysis tools on the ExPASy server. In *The Proteomics Protocols Handbook*, Walker, J.M., Ed.; Humana Press: New York City, New York, USA, 2005; pp 571-607.
290. Morrow, J.A.; Segall, M.L.; Lund-Katz, S.; Phillips, M.C.; Knapp, M.; Rupp, B.; Weisgraber, K.H. Differences in Stability Among the Human Apolipoprotein E Isoforms Determined by the Amino-terminal Domain. *Biochemistry.* **2000**, *39*, 11657–11666.
291. Dai, Y.; Whittal, R.M.; Li, L. Two-layer Sample Preparation: a Method for MALDI-MS Analysis of Complex Peptide and Protein Mixtures. *Anal. Chem.* **1999**, *71*, 1087–1091.
292. Ma, B.; Zhang, K.; Hendrie, C.; Liang, C.; Li, M.; Doherty-Kirby, A.; Lajoie, G. Peaks: Powerful Software for Peptide *De Novo* Sequencing by Tandem Mass Spectrometry. *Rapid Commun. Mass Spectrom.* **2003**, *17*, 2337–2342.
293. Sievers, F.; Higgins, D.G. Clustal Omega. *Curr. Protoc. Bioinformatics.* **2014**, *48*, 3.13.1–3.13.16.
294. Dolinsky, T.J.; Nielsen, J.E.; McCammon, J.A.; Baker, N.A. PDB2PQR: an

Automated Pipeline for the Setup of Poisson Boltzmann Electrostatics Calculations.  
*Nucleic Acids Res.* **2004**, *32*, W665–W667.

295. Wider, G.; Macura, S.; Kumar, A.; Ernst, R.R.; Wüthrich, K. Homonuclear Two-dimensional  $^1\text{H}$  NMR of Proteins. Experimental Procedures. *J. Magn. Reson.* **1984**, *56*, 207–234.
296. Wüthrich, K. Nmr of Proteins and Nucleic Acids. *The George Fisher Baker non-resident lectureship in chemistry at Cornell University (USA)*. 1986.
297. Hwang, T.L.; Shaka, A.J. Water Suppression That Works. Excitation Sculpting Using Arbitrary Wave-forms and Pulsed-field Gradients. *J. Magn. Reson.* **1995**, *112*, 275–279.